School of Chemical Engineering

Synergistic Interactions of Plasticizers and Nanoclays in Hydrophilic Starch Based Bionanocomposites

HuiHua LIU

This thesis is presented for the Degree of

Doctor of Philosophy

Of

Curtin University

April 2011

To my parents and sisters……..

DECLARATION

To the best of my knowledge and belief this thesis contains no material previously published by any other person except where due acknowledgement had been made.

This thesis contains no material which has been accepted for the award of any other degree or diploma in any University.

Signature: _____

Date: _____

ABSTRACT

Depletion of non-renewable resources and exorbitant levels of carbon dioxide emissions have questioned the further usage of traditional plastics. The imbalance in global sustainability has necessitated the development and use of biodegradable polymers. This research work set sights on understanding the synergistic interactions of plasticizer, starch and Na^+-montmorillonite (MMT). Having a clear view of the molecular behavior within this ternary system ameliorates the performance of the end product and fabrication of the tailored-property biodegradable polymers. Conversely, the explicit information of the synergistic Interactions of Plasticizers and MMT in hydrophilic starch is still vague. Hence a great degree of work and effort has been put forward through this work to understand the fundamental principles of competitive interaction.

The study emphasizes on modelling the kinetics of various components in the system such as crystallisation of the long chain starch, water diffusion from the polymer matrix and the interaction between the MMT molecules and the water molecules. It was observed that the interactions between MMT and plasticiser were enhanced upon increasing the MMT loading. The high hydrophilicity of plasticizer ensured a stronger interaction of plasticizer/MMT which overtook the MMT/MMT interaction causing a dimensional increase in *basal spacing* in the high plasticiser loading samples.

GAB model based on the multi-layer kinetics has been applied in the current work to understand the isotherm behaviour. Small Angle X-ray Scattering (SAXS) was employed to determine the diffraction pattern and intensity of the samples at the micro/nano structural level and thereby fathom the orientation of the crystalline domains. Differential Scanning Calorimetry was carried out to indicate the changes in T_g/T_m values of various samples and the corresponding degree of plasticization. The obtained results were then interpreted with Avrami equation to reach solid conclusions.

The crystallization ability and intermolecular hydrogen bond strength of the applied plasticizer were the key parameters that affected the crystallisation process. The crystallisation mechanism in xylitol-plasticized samples differed from that of

glycerol/sorbitol-plasticized samples. It was also determined that the molecular size of the plasticizer was another significant element that influenced the crystalline domain formation. The interaction process was defined into three stages based on the concentration of plasticizer used. The plasticizer concentration for the formation of a *loosen-soft* polymeric network and *tighten-firm* polymeric network was categorised. Correspondingly, the 'threshold' value for glycerol, xylitol and sorbitol-plasticized systems was characterised to be 5%, 10% and 5%, respectively. Morphological observations such as Wide Angle X-ray Diffraction (WAXD) and Transmission electron microscopy (TEM) has been utilised to examine the morphology formed in all nanocomposite samples.

A relatively unsaturated *loosen-soft* polymeric network was formed and the starch/plasticizer interaction and starch/MMT interaction transpired without interfering each other within the threshold limits. Nonetheless, beyond the threshold, a relatively saturated *tighten-firm* polymeric network was observed as confirmed by x-ray scattering results, the molecular dynamic modelling results and Positron Annihilation Lifetime Spectroscopy (PALS) measurements from representative samples. Plasticizer/plasticizer interactions significantly altered the MMT exfoliation process and crystallization behaviour of the corresponding sample.

The complex interactions existing in the polymeric system were found to be dependent on several main factors including type of the plasticizer and the relative ratio of plasticizer and MMT. These factors have been kept in mind whilst designing the modes of experiment and understanding the related outcomes. The incidence of excess moisture successfully modified the interactions amongst starch/ MMT/plasticizer. Water molecules behaved like a typical plasticizer and occupied most of the small voids between the starch polymers throughout the polymeric network.

ACKNOWLEDGEMENTS

God will look after you, my faith being the invisible strength for my whole study; my gratitude to him is beyond words. So is to my beloved parents and sisters.

Upon completing my research work, I would like to convey my gigantic appreciation to my paramount supervisor Dr. Deeptangshu Shekhar Chaudhary and co-supervisor Prof. Moses Oludayo Tadé for their kind and countless guidance and help during my PhD study.

I would like to thank Curtin University for offering the Curtin International Research Tuition Scholarships (CIRTS) so that I could finish my study smoothly. I would like to say thanks to all the kind staff in Chemical Engineering, especially Prof. Ming Ang, Jann Bolton, Naomi Mockford and Tammy Atkins.

My research would not have been completed without the enormous help from the technical staffs in the Chemical Engineering Department. I would also like to extend my sincere gratitude to Karen Haynes, Zhezi Zhang, Jason Wright, Veronica Wisniewski and Ann Carroll. The inspirational discussions from my colleagues were important for my research life. I would like to send my earnest appreciation to my colleagues (but not limited to)Shariff Ibrahim, Pradeep Kumar Shukla, Yash Boyjoo, and Joseph John. Furthermore, the innovative academic insights from A/Prof. Ricardo Mancera and Neha Gandhi have been the valuable merits for this study.

The fortunate opportunity to visit Japan was a big leap in my research progress and I would like to thank University of Hyogo for offering me the scholarship (HUMAP) to study in Japan. All the kind help that I received during my stay are important for my life. I would like to thank those persons who brought wonderful experience to me. This includes (but not limited to) Prof. Mikio Ouchi, A/Prof. Shin-ichi Yusa, A/Prof. Kouji Maeda, Dr. Kyuya Nakagawa, Dr. Yusuke Asakuma, Dr. Yusuke Daiko and Kio Matsuoka.

Last, but certainly not the least, I cannot help to mention again the invaluable aid and support from my beloved family. Catherine, my gorgeous niece, has always lifted up my spirits when things were not going good. Best wishes to my best friends, MiXue-Zheng and Ling-Zhang, for those silent and warm encouragements.

BIOGRAPHY AND PUBLICATIONS

BIOGRAPHY

HuiHua LIU received her Bachelor of Engineering in 2005 from ChongQing JiaoTong University and Master of Safety Engineering in 2008 from South China University of Technology. Then she commenced her PhD study at Department of Chemical Engineering August 2008 under Curtin International Research Tuition Scholarships (CIRTS). From March 2010 to September 2010, she obtained the sponsorship, Hyogo University Mobility in Asia and Pacific (HUMAP), to undertake research work at the University of Hyogo, Japan.

Her general areas of interest and research activities have covered a broad range of subject areas, including Biodegradable Polymer, Nanomaterial, Freeze-dried Porous Materials, Molecular Dynamic Modelling and Enzyme Encapsulation. Her specific interests and expertise are in Starch-based biaonancomposites analyses, Freeze-dried Porous Materials and Atomistic Molecular Dynamic Modelling.

PRIZE

STUDENT Prize

Conference Name: *40th symposium for Separation Process and technology*

Venue: *June 2-4 2010, MeiJi University, Tokyo, Japan,*

JOURNALS

1. Liu, H. and D. Chaudhary, *The Moisture Migration Behavior of Plasticized Starch Biopolymer*. Drying Technology, 2011. **29**(3): p. 278-285.
2. Liu, H., et al., *Interactions of hydrophilic plasticizer molecules with amorphous starch biopolymer- an investigation into the glass transition and the water activity behaviour*. Journal of Polymer Science Part B: Polymer Physics, 2011. **In press**.
3. Liu, H., et al., *Glycerol/starch/Na+-montmorillonite nanocomposites: A XRD; FTIR; DSC and 1H NMR study*. Carbohydrate Polymers, 2011. **83**(4): p. 1591-1597.
4. Liu, H., D. Chaudhary, and M.O. Tadé *Preparation and characterization of sorbitol modified nanoclay with high amylose bionanocomposites*. Carbohydrate Polymers, 2011. **85**(1): p. 97-104.

5. Liu, H., et al., Morphological investigation into starch bionanocomposites via synchrotron radiation and differential scanning calorimetry. Journal of Nanotechnology, 2011. **accepted**.
6. Liu, H., et al., *Enzyme Encapsulation in Freeze-dried Bionanocomposites Prepared from Chitosan and Xanthan Gum Blend.* Materials Chemistry and Physics, 2011. **In Press**.
7. Liu, H., et al., *Freeze-dried Macroporous Foam Prepared from Chitosan/ Xanthan Gum/ Montmorillonite Nanocomposites.* Chemical Engineering Research and Design, 2011. **In Press**.
8. Chaudhary, D. and H. Liu, *Influence of high temperature and high acidic conditions on geopolymeric composite material for steel pickling tanks.* Journal of Materials Science, 2009. **44**(16): p. 4472-4481.

CONFERENCES

1. Liu, H., D.S. Chaudhary, B. Adhikari and M.O. Tadé. *Reduced RH influence on starch structure with different Plasticizer for biodegradable packaging*. in *International Symposium on Recent Developments and Applications in Polymer Nanostructured-Materials*. 2009. Melbourne, Australia.

2. Liu, H., D.S. Chaudhary and M.O. Tadé, *^{13}C NMR study of Extruded Starch-Based Na^{+}-MMT Nanocomposite Plasticized by Sorbitol*, in *CHEMECA* 2010: Adelaide, Australia.

3. Liu, H., D.S. Chaudhary and M.O. Tadé, *Atomistic dynamic modelling of starch fragments with different hydration and glycerol concentration: Equilibrium behaviour and T_g estimation,* in *CHEMECA* 2011: Adelaide, Australia.

4. Liu, H., D.S. Chaudhary and M.O. Tadé, *Effect of nanoclay and sorbitol on structure relaxation of extruded high-starch bionanocomposite via synchrotron radiation,* in *CHEMECA* 2011: Sydney, Australia.

5. Liu, H., K. Nakagawa, D. Chaudhary and M.O. Tadé. *Investigation on microstructure of freeze-dried macroporous foam prepared from biopolymeric materials*. in *40th symposium for Separation Process and technology*. 2010. Tokyo, Japan.

6. Liu, H., D.S. Chaudhary, K. Nakagawa and M.O. Tadé, *Investigation on microstructure of freeze-dried macroporous foam prepared from biopolymeric materials*, in *CHEMECA* 2010: Adelaide, Australia.

7. Chaudhary, D.S., H. Liu and B. Adhikari, *Influence of Branching and Plasticiser on Water Activity in Starch Biopolymer*, in *30th Australasian Polymer* 2008: Melbourne, Victoria, Australia. p. 151.

8. Chaudhary, D.S. and H. Liu, *Understanding the Relationship Between Water Activity and Plasticized Biopolymer Type*, in *CHEMECA* 2009: Perth , Australia.

TABLE OF CONTENTS

LIST OF FIGURES

LIST OF TABLES

ABBREVIATIONS, NOMENCLATURES and NOTATIONS

TPS	Thermoplastic Starch
MMT	Na^+-Montmorillonite
DOE	Design of Experiments
MCM	Moisture Content Measurement
WAXD	Wide Angle X-ray Diffraction
TEM	Transmission Electron Microscopy
SAXS	Small Angle X-ray Scattering
FTIR	Fourier Transform Infrared Spectroscopy
NMR	Nuclear Magnetic Resonance
DSC	Differential Scanning Calorimetry
PALS	Positron Annihilation Lifetimes Spectroscopy
$wt\%$:	Weight percentage
$m\%$:	Moisture content
GAB Model:	Evaluation Model for sorption isotherm.
w_m:	Parameter calculated from GAB Model analyses; denotes the moisture content value that corresponds to a 'monomolecular layer' of water to cover the whole polymer surface.
C:	Parameter calculated from GAB Model analyses; depend on the corresponding molar sorption enthalpies.
K:	Parameter calculated from GAB Model analyses; depend on the temperature.
Bragg's Law:	The relationship of angles for coherent and incoherent scattering from a crystal lattice, $\lambda = 2d \sin\theta$.
Basal spacing (d):	Spacing between the planes in the atomic lattice of MMT.
λ:	The Wavelength of incident wave in *Bragg's Law.*
θ:	The angle between the incident ray and the scattering planes.

Δd:	$\Delta d = d_{-samples} - d_{-pristineMMT}$
IGOR:	Statistics software for crystallinity calculation.
$X_c\%$:	Crystallinity
T_g:	Glass-transition temperature
T_m:	Melting temperature
Avrami equation:	Equation for modelling the crystallization process.
n:	Parameter calculated from Avrami equation analyses; denotes the nucleation mechanism and form of crystal formation.
k:	Parameter calculated from Avrami equation analyses; denotes the crystal growth rate.
$DMSO-d_6$:	[($^2H_3$)methylsulfinyl]($^2H_3$)methane
I_{starch}:	Characteristic peak from NMR spectrum of starch.
$I_{glycerol}$:	Characteristic peak from NMR spectrum of glycerol.
$I_{sorbitol}$:	Characteristic peak from NMR spectrum of sorbitol.
ΔI:	$\Delta I = I_{-starch} / I_{-sorbitol}$.
NIKA:	2D to 1D SAXS data reduction macros for IGOR software by Jan Ilavsky.
Q:	Scattering Vector in SAXS; $Q = 4\pi \sin\theta / \lambda$.
P_{starch}:	Characteristic peak of starch in the 1-D SAXS profiles.
P_{MMT}:	Characteristic peak of MMT in the 1-D SAXS profiles.
d_{SAXS}:	Basal spacing of MMT evaluated from SAXS results.
INERA:	Domain size distribution evaluation macros for IGOR software by Jan Ilavsky.
MEM:	Maximum Entropy Method; an algorithm for crystalline domain size distribution calculation put forward in Potton *et al.'s publication.*
$\bar{d}_1$:	Scatter diameter of crystalline domain one.
$\bar{d}_2$:	Scatter diameter of crystalline domain two.

$\bar{d}_{1-hm}$: Scatter diameter of crystalline domain one for high moisture content sample.

CAMFIT V2.1: An in-house developed program for PALS data evaluation developed by Jason Robert (Centre for Antimatter-Matter Studies).

Material Studio 4.0: Software for simulating and modelling materials developed and distributed by Accelrys (US).

Chapter 1

Introduction

1.1 Background

In current years, biopolymers have been attracting increasingly high interest in public and media in the field of packaging, such as waste bags and food packaging. Though oil-based plastics have lots of advantages like lightness, strength and durability, their disadvantages are obvious. Oil-based plastics are produced from the fossil fuel, a non-renewable resource, and emit millions of tons of carbon dioxide in the process of production which deteriorates the global greenhouse. Also, due to plastic's non-biodegradability, inappropriately disposed plastic products lead to serious environmental problems. Compared with those disadvantages of oil-based plastics, biopolymer that are made from renewable resources such as food crops or biomass show some advantages like degradability, eco-friendliness, renewability and low emission of carbon dioxide. Using biopolymer as an alternative to oil-based plastic will become a future trend. Many companies and institutes take a high interest in developing biopolymer and have announced investments in expanding the production capacities of biopolymer within the upcoming years. It is estimated that the global production capacity will dramatically increase from 262 kton in 2007 to approximately 1,502 kton in 2012. According to the latest issue of EL (Environmental Leader) Insights, the global market for bioplastic in 2010 achieved sales of $2.74 billion and it is expected to surpass a value of $11billion by 2015.

Why biodegradable? Some convincing answers have been put forward in terms of both environmental issues and economic prospects as shown below:

1. The fundamental advantage is the degradability which plays an important role in releasing the universal environmental problems related to the usage of non-degradable materials.
2. The outstanding characteristics of recently developed biodegradable polymer/ layered-silicate nanocomposite ensure that the biodegradable material will become the paramount equivalent for most petrol-based derivatives, and balanced the dependence of the plastic market on fossil fuels.

3. Moreover, the benefit of widely applied biodegradable materials rather than traditional ones could be further evidenced from its positive impact in reducing CO_2 emission and biodiversity protection.

'Biodegradable polymers are defined as those that undergo microbial induced chain scission leading to the mineralization under specific conditions in terms of pH, humidity, oxygenation and the presence of some metals '. According to their resources, biodegradable polymers could be grouped into two main categories; bio-resources based polymer and oil-based polymers. The former candidate is generally obtained from bio-sources (starches, wood cellulose, etc.) or synthesized by bacteria from small molecules like Polyhydroxybutyrate (PHB) and Polyvinyl alcohol (PVA). On the other hand, oil-based polymers are usually modified polymer derived from petroleum sources or mixed sources of biomass and petroleum.

1.1.1 Starch

Flexible packaging for food articles, where the packaging material itself is biodegradable, is receiving a significant push from consumer and manufacturers alike. Being the most abundant polysaccharide on the earth, starch exists in diverse plants, such as cereal grains, corns as well as tubers (potato). Starch is made up of two main components, namely, amylose and amylopectin. Amylose and amylopectin are arranged in granules (as semi-crystalline and amorphous layer) with different size, 2 μm to 100 μm, based on the resources. The semi-crystalline native granules could be divided as the crystalline lamellae formed by ordered amylopectin branches and the amorphous region composed of mainly amylose. Properties and features for studied starch and its corresponding product are significantly influenced by amylose/amylopectin ratio as confirmed in many publications [1]. Native starch can be transferred into thermoplastic starch (a rather uniform amorphous phase), TPS, via adding of suitable plasticizer (polyols and water) under specific conditions, like melt-extrusion or melt-blending.

1.1.2 Starch-based Na^+-montmorillonite (MMT) nanocomposite

The drawbacks of poor moisture sensitivity and rather weak mechanical properties compared to conventional synthetic polymer pose the biggest hindrance for the widespread utilization of biopolymers. Since 1970, scientists started to examine different strategies for conquering these weaknesses, which mainly included

chemical modification of starch and incorporating other compounds to develop new classes of materials, ranging from macro-TPS-biocomposite, nano-TPS-biocomposite and macro/nano multi-phases TPS-biocomposite [2-7]. The widely reported successful cases about properties enhancements of starch polymer materials by addition of nanofillers in to pristine polymer (nano reinforcement) enlighten the idea to all the addressed defects of TPS. Na^{+}-Montmorillonite (MMT) is hydrophilic clay with a high surface area [8, 9]. Researches on using MMT as the reinforcing phase due to their very high aspect ratio (100) and versatility [10-15] have been widely carried out. This is because montmorillonite crystal lattice consists of 1nm thin layers with an octahedral alumina sheet sandwiched between two tetrahedral silica sheets, which can accommodate various polymeric groups for greater stability. The stacking of the platelet leads to a Van der Waals gap or gallery between the layers. Thus biodegradable TPS/MMT is undoubtedly the pioneer in the next generation of materials. As mentioned above, significant enhancements have been confirmed by lots of researchers, and these improvements are considered to be strongly related to the dispersion degree of incorporated MMT [16-19].

Starch /MMT nanocomposite is a promising material that combines the advantage of TPS (fully degradable, industrial proceeding availability, abundant and low-cost) and polymer/layered-silicate nanocomposites (excellent mechanical properties, barrier characteristic, and water permeability etc.), Figure 1-1.

Figure 1-1 Schematic drawing of Starch /MMT nanocomposite.

Most studies are focused on the examinations of the properties, mechanisms, and aiming for fabrication of properties-tailored materials via introducing different plasticizers. Benefits from the availability of polymer/clay intercalation via hydroxyl interaction and the extra advantages of shear force and powerful mixing capacity results from extrusion processing. Starch/MMT nanocomposites can be produced by incorporating suitable plasticizer in to the native starch matrices under a condition

consisting of strong enough shear force and powerful mixing, such as extrusion cooking.

1.2 Motivation for this work

1.2.1 Knowledge gap in starch-based nanocomposites

The high *Glass-transition temperature (Tg)*, low flexibility and the time-dependent changes on starch/MMT nanocomposite's properties etc., led to a great negative effect on its utilization. Furthermore, the current knowledge gap in understanding how plasticizers and MMT interact in a starch biopolymer has led to limited applications and frustrated the processing of such bionanocomposites. All these issues are rising from the situation that the synergistic interactions from this complex system are still vague. Due to the weakness recognized upon the studies about TPS polymer, scientists are moving on to the investigations concerning its interaction mechanisms. However, to date, although large quantities of experimental studies have been done concerning the properties of end products, the synergistic interactions in the starch/MMT nanocomposite are still poorly understood. This is because of the difficulties associated with identifying the interactions of different components within the complex system. This includes the starch-MMT interaction, starch-plasticizer interaction, starch-water interaction, plasticizer-water interaction, water-MMT interaction, plasticizer-MMT interaction and the interaction of same components (starch-starch interaction and plasticizer-plasticizer interaction). Moreover, the interactions co-existing in the system are dependent on other components and will influence mutually. For instance, measurement of crystallinity due to plasticizers is not only related to its concentration, but plasticizer-water interaction within the biopolymer. It is still unclear how such interactions are affected by plasticizer type or its concentration.

The importance of filling the knowledge gap lies on the potential of fabrication tailored-properties smart materials. A good understanding can provide solid and correct method in producing materials that can meet various requirements. For example, it had been proved that addition of plasticizer increased the flexibility of the product but induced certain decrease in the strength. To overcome this, incorporation of MMT as an enforcement phase at a certain concentration will be a promising solution. However, the quantitative relationship and the preference of

interactions orientation have not been developed yet. The quantitative properties of prepared products are still out of control.

Therefore, such knowledge can serve as an important benchmark for further investigation on obtaining materials with the quantitative required characteristics.

1.2.2 Significance of current study

Several practical approaches are available for interpreting the mechanism for reinforcement generated from MMT/polymer nanocomposite including [20-22]. However most of them are based on synthetic polymers rather than bio-resources polymer. Although, it was possible in some cases, the theory for synthetic polymers can be applied to starch-based nanocomposite; starch-based nanocomposites have their unique features which are not comparable to other polymers. A well-constructed map of the role of water, plasticizer, MMT starch chains and their correlated interactions is necessary for solving the disadvantages of a starch-MMT product as a flexible packaging material.

This project is aiming to explore the synergistic interactions within the starch/MMT/ plasticizer system and obtain necessary knowledge for fabrication of tailored-functional starch-MMT biodegradable nanocomposite to take upon the blooming demands for creating a ‘green world’.

1.3 Research methodology

This thesis entailed the development of fundamental understanding of interplay of the relevant hydrophilic interactions within starch/plasticizer/MMT ternary system on the basis of various characterization results from designed experiments. To achieve this, the following studies were carried out:

- Selection of targeted plasticizer and MMT.
- Design of sample preparation sheet based on selected plasticizer and comprehensive characterizations on the obtained samples.
- Data analysis:
    - Samples prepared from same plasticizer (glycerol, xylitol or sorbitol): to investigate the effect of the plasticizer and MMT (at different ratio) on the synergistic interactions.

- Samples with same formula but from different plasticizer: to investigate the influence of plasticizer type on the synergistic interactions.

The detailed research methodologies are briefly outlined as follows.

1.3.1 Materials selection

The most-commonly used plasticizers for starch-based nanocomposite preparation lies in the polyol family such as glycerol and it had been proven that the hydrophilicity of incorporated polyol turned out to be the dominant factor affecting the molecular interactions within the corresponding system. Thus, in the current study three different plasticizers (glycerol, xylitol and sorbitol) with different number of hydroxyl groups are used based on their hydrophilicities so as to study the importance of the hydrophilicity of plasticizer and its relevant behaviour. Meanwhile, considering the fact that the interactions within a nanocomposite were component concentration-dependent, the plasticizer will be applied at different levels ranging from 5%-20% at an interval of 5%. Unmodified montmorillonite was chosen as the nanofiller in this study due to its raw natural hydrophilicity which showed good compatibility with the hydrophilic starches/polyols and high aspect ratio which was strongly related to the property of the prepared nanocomposite. Similarly, the influence of MMT concentration was studied via applying MMT at four levels ranging from 1-4 wt% at an interval of 1 %.

1.3.2 Sample preparation and characterizations

The samples were prepared by using a Lab-Scale Twin-screw co-rotating Extruder with optimized process parameters according to a design of experiments (DOE). The DOE was determined by using Minitab version 3.2 statistical software which took into account of the influence of both plasticizer loading and MMT concentration (Mixture design with constrained surfaces (extreme vertices design) at full degree). One of the unique aspects of the current study was the pre-treatment of the plasticizer and MMT before extrusion (the plasticizer was mixed with the MMT at known concentrations and this mixture was sonicated for required duration to achieve MMT intercalation with plasticizer) which will be described in detail in the methodology Chapter (*Chapter 3*). High amylose starch was mixed with the pre-treated

plasticizer/MMT slurry using a bench-top twin-hook mixer and kept in plastic bag overnight to allow sufficient equilibration before extrusion processing.

Comprehensive characterizations on the prepared starch/MMT/plasticizer nanocomposite had been conducted including: Wide Angle X-ray diffraction (WAXD), Transmission Electron Microscopy (TEM), Fourier transform infrared spectroscopy (FTIR), Differential Scanning Calorimetry (DSC), Small Angle X-ray Scattering (SAXS) via synchrotron radiation. Moisture content measurement and other supplement experiments where necessary such as Nuclear magnetic resonance (NMR) and Positron Annihilation Lifetimes Spectroscopy (PALS) had been carried out on selected samples so as to gain a better understanding of the interaction mechanism.

1.3.3 Data Analyses

As mentioned above, three plasticizers were chosen in the current study at different level, the analysis of obtained data were arranged in the manner as described below. First, discussions based on the samples with same plasticizer but at different level (both plasticizer and MMT) were illustrated in *Chapter 4* (Glycerol), *Chapter 5* (Xylitol) and *Chapter 6* (Sorbitol); second, the *Integrity Analysis Chapter* (*Chapter* 7) was focussed on identifying the difference of the samples prepared from different plasticizer at a fix formula so as to explore the effect of different plasticizer.

a) Within each discussion Chapter (samples from same plasticizer): the discussions on the data obtained were organised with the aim to efficiently interpret the influence of the plasticizer and MMT on the morphology or structure of the nanocomposites. Thus, the binary composite, which consisted of only starch and either plasticizer or MMT, is discussed, followed by a more comprehensive analysis on the complicated ternary composites (starch+plasticizer+MMT). More specifically, the morphology and crystallinity development of these bionanocomposites was studied by WAXD, FTIR, SAXS and DSC. Based on the SAXS results, the scattering patterns were analysed in detail, and the size distribution profiles of the crystalline domain were examined using the Maximum Entropy Method [23]. Calorimetry data were further analysed for the nucleation and growth kinetics through the Avrami model [24]. The ‘role of water’ was also discussed by

studying the distinctness of two sets of samples with different moisture content via SAXS and crystalline domain size distribution discusses.

b) In Integrity Analysis Chapter: What is the main dominating factors affecting the interactions? This Chapter was divided into three major parts referring to the suggested factor. These factors included physical factors of different plasticizers (molecular size of the plasticizer, molecular structure of the plasticizer), intrinsic chemistry of the plasticizer (hydrophilicity-number of hydroxyl groups, crystal features), and the role of water molecules. Finally a clear interaction map was put forward at the end of the integrity analyses chapter.

1.4 Research contributions

This thesis makes significant contributions to the understanding of the synergistic interactions within the hydrophilic starch/MMT/plasticizer (glycerol, xylitol and sorbitol) system in terms of interpreting the dependency of such interactions on the plasticizer type/loading, the MMT loading and the moisture available within the relevant environment. The main contributions are briefly summarized below:

1. A new method of preparing designated plasticizer (based on number of –OH presented) modified MMT via ultra-sonic treatment for nanocomposites fabrication was proposed. Furthermore, the characterization results on plasticizer modified MMT clearly suggested the interaction mode between MMT and plasticizer which provided important clues for identifying the interaction mechanism for the complex starch/MMT/plasticizer system.

2. The investigations of xylitol-plasticized nanocomposites at different xylitol: MMT ratio provided important information about the influence of intrinsic chemistry of the applied plasticizer on the synergistic interactions. This induced the attention of taking the crystallization ability and the strength of intermolecular hydrogen bonds of the employed plasticizer into consideration when choosing the proper plasticizer.

3. Clearly mapped out the preferential route/scenario of the formation of highly intercalated or exfoliated morphology within the nanocomposites according to the main factors: plasticizer loading which turned out to result in the

competing interactions between plasticizer/starch and plasticizer/plasticizer. The existence of 'threshold' for MMT's gallery expansion was found in all the studied system and is a result of the interplay of the plasticizer chosen (type and concentration) and the MMT loading.

4. The hypothesised synergistic interaction map was directly evidenced, for the first time, by the Positron Annihilation Lifetimes Spectroscopy (PALS) results where obvious uniformed voids distribution was found in low-plasticizer loading sample (loosen-soft polymeric network) and two types of voids was observed in high-plasticizer loading sample (tighten-firm polymeric network) , Chapter 7.

5. The success on applying molecular modelling to interpret the antiplasticization phenomenon in glycerol/water/starch system which served as a solid evidence in explaining the low domain packing density (broaden WAXD characteristic peak) in the low-glycerol loading samples.

1.5 Thesis outline

The primary objectives of the investigation were: (1) To clarify the dominant factors which impact each interaction process in different experimental system; (2) To explore the extent of that factor which influence the interaction process; (3) To figure out the relationship between different factors; (4) To establish a clear map of the inter-effected interactions in starch/plasticizer/ MMT. The structure of the thesis is summarized in Figure 1-2.

The thesis is organized into eight chapters as outlined below:

Chapter 1 provides introductory information about the project which includes the background and progress in this area; existing knowledge gap and the significance of the study. Brief research methodology and the key contribution are outlined. *Chapter 2* covers the literature on development, current finding and knowledge gaps in the starch-based nanocomposites field.

Detailed research methodology has been illustrated in *Chapter 3*, which includes the design of experimental sheet, sample fabrication (dry materials preparation, processing parameters optimization and sample storage), and characterizations

techniques (WAXD, FTIR, DSC, SAXS, NMR, PALS, Moisture Content Measurement) used.

Discussion of the influence of multi-competing interactions which depend on the ratio of the plasticizer and MMT was put forward in designated nanocomposites systems. These include glycerol-plasticized nanocomposite (*Chapter 4*), xylitol-plasticized nanocomposite (*Chapter 5*) and sorbitol-plasticized nanocomposite (*Chapter 6*). Specifically, the corresponding analyses included the intermolecular interactions, morphology observations, and crystallization behaviour in material.

Integrity analysis, *Chapter 7*, investigates the influence of the suggested factors on the systems' interactions by comparing the characterization results from selected samples (same formula but different plasticizer). That interplay of those factors induced the achievable *basal spacing* of MMT and the appearance of different crystallization behaviours (crystalline domains size and crystal growth rate). Furthermore, an attempt was made to employ molecular dynamic as an efficient tool to elaborate the fundamental interaction process from a molecular level. Based on the integrity analyses, the interactions map was drawn at the end of the chapter.

Finally, major conclusions and several recommendations for future work are summarized in *Chapter 8*.

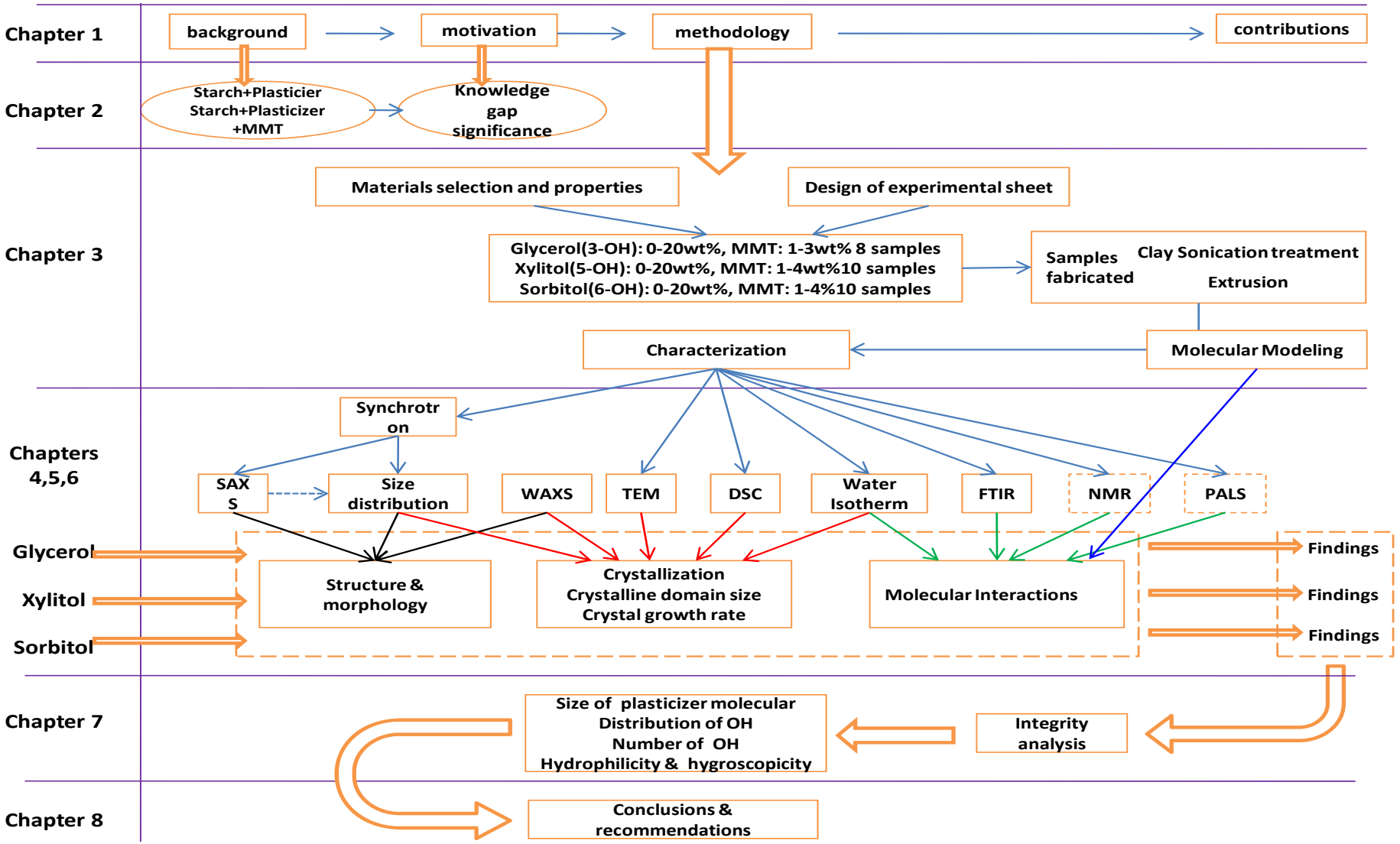

Figure 1-2 The structure of the thesis.

Chapter 2

Literature reviews

2.1 Starch

Starch is the most economical and plentiful food biopolymer on earth. It can be found in many botanical sources such as potato, wheat and maize. Starch, either in native or processed form, exist in diverse applications ranging from breakfast cereals, snacks and thickeners in the food industry to binders for drug delivery systems, packaging, paper and adhesives in the non-food industry.

2.1.1 Molecular composition of starch Granules and its main properties

Green plants synthesize starch granules for energy requirements. They are generally packed as a dense semicrystalline structure with a density of 1.5 g/cm^3 [25]. Starch granules are not water-soluble at ambient temperature due to their stable semicrystalline structure. Native starch contains starch and amylopectin, Figure 2-1, which are initially mixed with amylose mainly in amorphous form dispersed within the semi-crystalline amylopectin network.

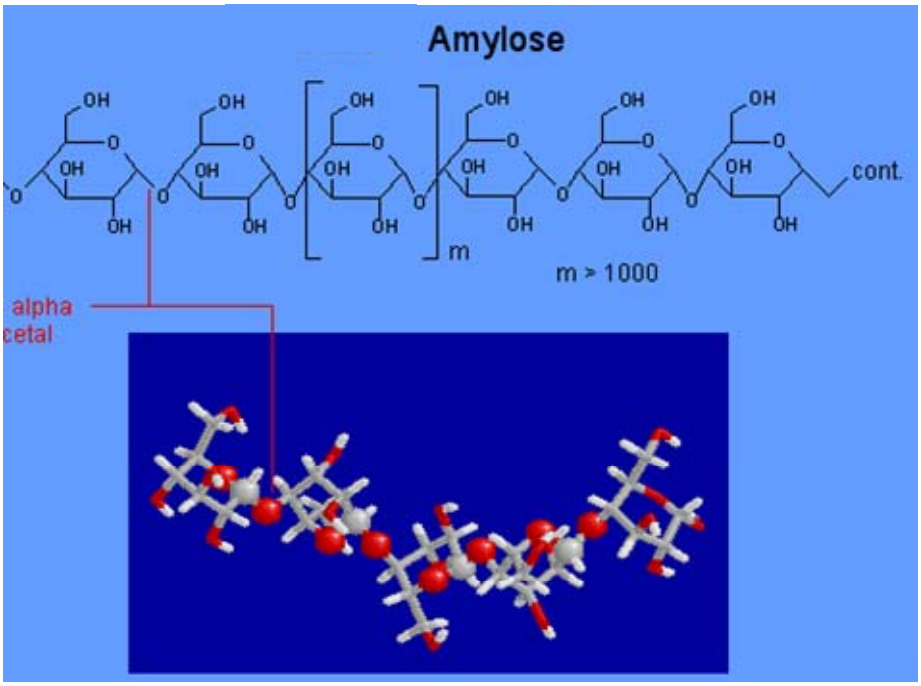

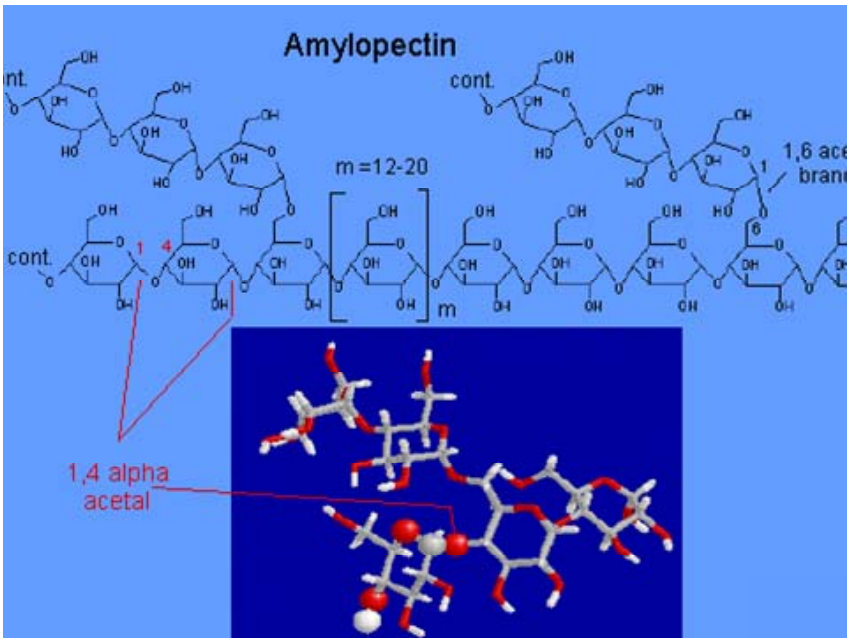

Figure 2-1Molecular structures for amylose and amylopectin. Reproduced from [26].

As revealed from the studies of WAXD, three well-recognized polymorphs of long-range ordering, crystallinity of starch granules are A,B and C (combination of A and B-type) type [27, 28]. The A pattern is typical for cereal starches, while type B comes from tuber plants as well as high amylose starch and retrograded starches [29]. In addition, V-type crystallinity is generally associated with starch fraction which complexes with aliphatic alcohols and monacyl lipids .

Several key properties of starch are listed as follows:

a) Glass Transition Behaviour

The glass transition temperature (T_g) of starch polymer is perhaps one of the most important parameters to understand the interactions that occur at the molecular scale.

Glass transition is a reversible transition in the amorphous region of a semicrystalline polymer, which experiences the transformation from rigid glassy state to rubbery state. Below the T_g, molecular chains are frozen and stay in the glassy state, showing glassy and stiff status. In this state, molecular chains do not have any segmental motion but only slightly vibrate. When the polymer is heated above the T_g by applying a force, the molecular chains transfer to rubbery state and wiggle, showing a rubber-like status. In this state,

the molecular chains have a segmental motion; exhibiting great deformation under a force and return to the initial form when the force is removed.

Glass transition has a great influence on polymer properties, such as elasticity moduli, density and viscosity. The viscosity drops dramatically as the system transforms from the glassy state to the rubbery state. As a consequence, the polymer chain and reactant mobility are facilitated. An increase in free volume, which is devoid of any polymer chains, is also observed. The T_g values are frequently used in relationships that characterize the glass-forming ability of polymers or the stability of the amorphous state during heating. The rubbery state is also accompanied by higher rotational and protons mobility. Hence, investigating glass transition is necessary and helpful to understand some of polymer properties and behaviour.

A couple of theoretical approaches have been developed for interpreting the complex phenomenon including free volume theories, thermodynamic theories and kinetic theories [30, 31]. The most popular method to modify T_g is to introduce proper additives which efficiently facilitate the mobility of the corresponding polymer; this behaviour is termed as plasticization [10]. Several theories have been developed to explain this phenomenon including the classical theories (the lubricity theory, the gel theory [32], the Moorshead's empirical approach [33]) and the most widely accepted free volume theory [34]. Based on the well-known free volume theory of plasticization [35], there are two factors that contribute to the decrease of T_g; first, the intrinsic lower T_g of incorporated smaller plasticizer molecules, and secondly, the addition of those small plasticizer molecules which induces extra free volume to the system. Consequently, several factors such as molecular weight, molecular structure and molecular size are associated with the ability of the plasticizer to subordinate the T_g. It can be stated that a highly-branched plasticizer with smaller molecular weight could exhibit superior plasticization effect since it generates a relatively greater free volume to the system. Concerning the importance of glass transition phenomenon, a method to control the T_g is of great importance in material engineering. And based on the free volume theory, a study of T_g is a study to control the free volume via different strategies.

b) Gelatinization

The unique characteristic of starch is their ability to gel in aqueous environment under certain conditions [36]. When starch gelatinizes and swells, which is primarily a property of the amylopectin order crystallites, double helices in crystalline region uncoil and dissociate as hydrogen bonds are broken [37]. The relative significance of double helix versus crystallites dissociation in starch granules during gelatinization has been discussed in detail by Cooke and Gidley [38]. They concluded that double helix dissociation was the dominant contributing factor to the enthalpy of gelatinization rather than the separation of double helices located within starch crystallites. The irreversible process, gelatinization, can be divided into two stages [39, 40]. During the first stage, the starch crystallites, melt down forming a rearranged polymer network and during the second stage this network is broken down further and eventually a molecular solution is formed [41, 42]. The narrowing and shifting of the gelatinization temperature can be explained by a recrystallisation of the defect crystallites. The real melting point of the native starch should be higher than the original gelatinization range.

Each starch has its own characteristic gelatinization properties. This is associated with a temperature dependent swelling profile where the volume expansion of a given starch when heated in water at different temperature is the characteristic of that starch [32]. Generally, several factors contribute to the unique characteristic of different starch including amylopectin structure, starch composition, starch resources and granular architecture.

c) Retrogradation

Retrogradation, the common name for all the changes that happen during storage of a freshly gelatinization starch, is considered to be another factor that profoundly influences the starch product quality. The retrogradation can be described as the changes which occur in a starch paste or gel on ageing. Solutions of low concentration (~2% or less) become increasingly cloudy due to the progressive association of starch molecules into larger particles. Spontaneous precipitation of starch from solution took place and it was because the precipitated starch appeared to be reverting to its original

condition of cold-water insolubility through the process of retrogradation. Retrogradation can be detected by changes in the WAXD patterns as it is principally a crystallization process [43]. This involves strong hydrogen-bond formation between hydroxyl groups on adjacent starch molecules.

Retrogradation includes flocculation of a starch solution, syneresis of paste or gel and changes in the component of cooked food. The changes occurring during retrogradation include: increased resistant of starch to hydrolysis by amyloytic enzymes, decrease in light transmission of the solutions, inability to form a blue colour complex with iodine, and progressive increase in gel firmness [34]. The intrinsic tendency of starch molecule to entangle with each other by increasing hydrogen bonding caused the retrogradation of the material and resulted in a "push out" of the water molecule which was located inside the starch matrix [44]. A small increase in crystallinity can be observed during retrogradation for potato starch [45]. The content of gelatinization, water content and concentration of other substances (electrolytes or non-electrolytes) can all affect the retrogradation behaviour. Molecular weight of starch from different resources tends to retrograde at a various rate. Whistler and Johnson have shown that the rate of retrogradation is greatest at medium chain length. The motion of the larger molecules is sluggish due to their length. They associate less readily than molecules that undergo rapid Brownian motion, causing a disordering effect [34].

2.1.2 Thermoplastic starch (TPS)

The fundamental motivation for introducing starch into polymer industry is the negative influence generated from plastics accumulation. Remarkable achievements have been reported in several aspects including Granular starch composite [46, 47], starch grafted copolymer [48, 49] and thermoplastic starch blends [50-52].

Thermoplastic starch is a material consisting of relatively homogeneous polymer phase rather than the semicrystalline structure of native starch, which could be achieved via mechanical and thermal processing. The melting temperature (T_m) of native starch is higher than its decomposition temperature and hence plasticizers such as water and other organic small molecules are necessary for the production of

thermoplastic starch. Together with the influence of shear-force and temperature, thermoplastic starch has been successfully prepared [53].

However, the water sensitivity and brittleness of pure TPS strongly limit its application. Furthermore, the time-dependent properties' such as recrystallisation and retrogradation influence the shelf-life of these products. It had been confirmed that incorporating nanofiller (nanoclay to be specific) was one of the most promising methods to tackle this problem as detailed below.

2.2 Na^+-Montmorillonite

The first successful attempt to incorporate nanoclay into polymers was conducted at Toyota Research Centre, Japan where they established the primary practical applications of the clay/polyamide nanocomposites in motor products [19, 54, 55]. Since then, researchers have carried out relevant studies involving both petrol-based polymers [56-59] and biopolymers [60-62]. More specifically, smectite clay is applied in conventional polymer nanocomposite (e.g. montmorillonite; MMT), which could be intercalated or exfoliated within the mother matrix. The aspect ratio and dispersion degree of clay are considered to be the two core issues concerning the high end-product performance [63]. In clay science, there are two types of basic element sheets that attribute to the formation of various layered silicate, namely, tetrahedral (T) sheets and edge-sharing octahedral (O) sheets. Na^+-montmorillonite (MMT), which is comprehensively applied in the polymer/nanocomposite science, is one member of the smecite family with a structure of 2:1 TOT layer with interlayer cations, Figure 2-2. The typical chemical compositions of MMT could be written as $E_{0.33}(M_y^+ \times nH_2O)(Al_{2-y}^{3+}Mg_y^{2+})Si_4^{4+}O_{10}(OH)_2$, where $E_{0.33}$ relates to the 'exchangeable interlayer hydrated cations (Na, Li, Ca) [64].

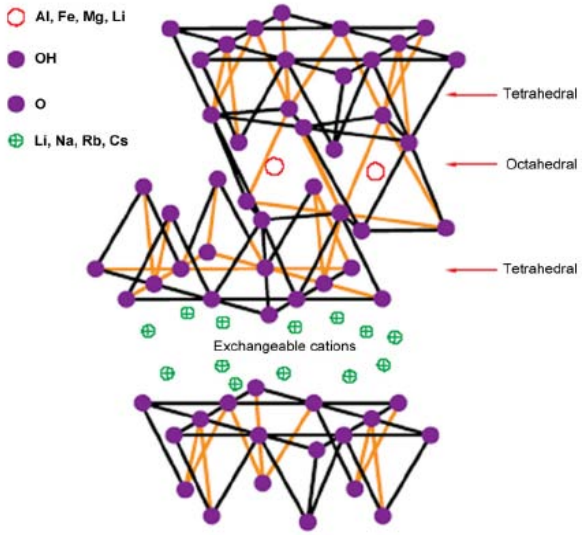

Figure 2-2 The structure of 2:1 layered silicate. Reproduced from [65].

2.3 Starch-based biocomposite

Many work [66-68] have been carried out to overcome the weakness of the TPS product. An effective method is incorporating plasticizers into the starch-water system which can increase the free volume by reducing internal hydrogen bonding between the polymer chains [69-71]. This facilitates starch/plasticizer interaction instead of starch/water interactions and reduces the intermolecular entanglements between biopolymers [70, 72]. Such behaviour is described as plasticization which is portrayed below together with another well-defined phenomenon termed as 'antiplasticization'.

2.3.1 Interactions of starch+water hydrophilic system

2.3.1.1 Plasticization

According the widely-accepted Free-Volume Theory, plasticization could be described as the process of increasing the free volume within the polymeric network by adding small molecules [73]. In terms of starch-based system, it had been proved that glycerol, xylitol and sorbitol are outstanding choices for starch-based polymer due to their positive influence on flexibility [74, 75], water sorption and retention [66, 74, 76]. On the other hand, plasticizers could increase overall biopolymer crystallinity [77] and cause blooming at higher wt%[78].

2.3.1.2 Antiplasticization

It is well known in synthetic polymers that the low molecular weight diluents at low concentrations could amplify rigidity of the polymer-diluents blends by a phenomenon called *antiplasticization.* This phenomenon has been observed in starch-based hydrophilic system as well. The antiplasticization effect by 'water in reduced-moisture food systems' was investigated by Seow *et al.[79]*. They hypothesized that increased modulus and brittleness are similar to antiplasticization by water. Meanwhile, the additive components like sugars and polyols, behave either as antiplasticizers or plasticizers within the system. Specifically, antiplasticization 'threshold' of glycerol and sorbitol have been studied and were determined to be around 12 ~15 wt% and ~25 wt%, respectively [72, 80].

2.3.1.3 Plasticization and Antiplasticization in hydrophilic system

Antiplasticization is a common phenomenon in starch polymer plasticization which usually occurs under low plasticizer concentration and low humidity condition. Meanwhile, the "plasticization threshold" values for different additives that have been reported, usually differing from each other, can be attributed to their unique properties. For instance, the "plasticization threshold" is 12 wt% and 27wt% for sorbitol and glycerol, respectively [79]. Beyond that threshold, additives act like a typical plasticizer, by improving the mechanistic properties, enhancing the mobility and flexibility of the starch chain and increasing water retention in starch matrix [70, 79]. In other words, when the relative humidity is low, at low concentrations, greater number of -OH group from plasticizer interacts with the starch polymer to cause greater chain coalescence which leads to increased polymer crystallinity, "antiplasticization" , but at higher concentrations, they attract water molecules and increase the matrix flexibility [70, 78, 79, 81, 82]. However, they also absorb large quantities of water under greater relative humidity conditions [76, 81]. Shaw *et al.* (2002) indicated the reason that different plasticizers have different effect on starch polymer matrix is because '*the plasticizing effect of polyols can be related to their ability to locate between polymer molecules, bind to water molecules and disturb intermolecular polymer associations'* [83].

2.3.2 Interactions of MMT+modifier (organic molecule, polymer) system

Speaking for clay itself, the well-known interaction mode of clay (more precisely, MMT in the current work) introduces certain 'guest' molecules/polymer chains

between the silicate sheets, forcing apart the gallery. To achieve this goal, modification of clay by organic solvent is a promising method to obtain high gallery spacing clay on the basis of natural properties of clay minerals. Products from Southern clay company could provide MMT with a gallery spacing range from 18.5Å (ternary ammonium salt) to as high as 31.5Å (quaternary ammonium salt.) depending on various modifiers. However, the biggest disadvantage for utilization of most ready organic-modified MMT in starch-biodegradable nanocomposites processing is their high hydrophobicity which is not miscible with starch and result in a microcomposite rather than nanocomposite. With this understanding in mind, the hydrophilic natural MMT (Page 17) became the best candidate in starch-based composite area. Relevant interactions involving MMT are summarized in this section.

2.3.2.1 Hydrophilicity of natural MMT

Natural MMT is a neutral smectite with excellent cation-exchange capacity (CEC) and good swelling properties. The free hydroxyl groups available on the surface of natural montmorillonite clay mineral provide another innovative route for expanding clay's gallery. Thus, by incorporating these hydrophilic nanofillers, starch-based nanocomposites can exhibit dramatically increased attributes. The interaction between the hydroxyl sites and hydrophilic plasticizer can successfully introduce the guest hydrophilic plasticizer molecule between the clay layers (*Chapter 4-6*), for instance, the swelling of montmorillonite after dispersion with water. Moreover, this process is highly dependent on the solvation of interlayer cations and layer charge [84].

2.3.2.2 Clay mineral organic interactions

Clay minerals can react with different types of organic compounds in a particular way, like absorbing organic guest molecules between the layers. In the case of 2:1 clay group, a broader diversity of reactions characteristics are confirmed, which includes grating reactions via silanol and aluminol groups and intercalation of the hydroxyl groups from interlayer [64].

Reaction of 2:1 clay can be achieved by chemical interactions such as hydrogen bonds, ion-dipole interaction, co-ordination bonds, acid-base reactions, charge transfer, and *Van der Waals* forces [64]. Correspondingly, polar molecules such as alcohols, amines, amides, ketones, and aldehydes can form intercalation complexes

with smecite in vapour, liquid as well as solid state. Some large molecules can be introduced by stepwise expansion of the interlayer space as well.

2.3.2.3 Effect of sonication treatment of MMT with water

Utilization of sonication treatment of MMT and water before pre-blended with dry starch had been studied in Dean *et al.*'s article via testing corresponding increase on *basal spacing* of obtained samples [73]. Two types of clays at different ratio with water had been examined. It was found that sonication treatment turned out to only benefit at medium/high clay: water ratio condition which dramatically increased the *basal spacing* from 12.2 Å to 35~40 Å (clay: water= 1:5). However, in the prepared nanocomposites samples, the advantages of ultrasonic treatment could be detected only at a medium (for Na^+-MMT) or high (for Na^+ -FHT) loading scenario. Similar observation was found in our work, whereas pre-treatment of glycerol/sorbitol and MMT by sonication expanded the gallery spacing of MMT to a different extent based on the plasticizer:MMT ratio and increasing plasticizer concentration did not always result in a larger gallery spacing [85, 86].

2.3.2.4 MMT-modified by polymer

From a clay modification point of view, the interaction between starch and MMT in starch-based nanocomposite system could be treated as a process that natural MMT is modified by plasticized starch polymers upon certain preparation conditions. This complex processing might involve a flock of factors, both physical (processing conditions, like heating rate/temperature, shear-force and melting rate) and chemical (starch type/amount, plasticizer type/amount and equilibrium time). Actually, the method of modifying clay minerals via polymer by physical absorption (non-ionic polymer or anionic polymer) or chemical grafting has been widely applied and its applications have seen success in many areas, such as catalysts, adsorbents, in composite materials, and so on [87].

2.3.3 Interactions of starch+plasticizer hydrophilic system

As mentioned in the plasticization section (Page 18), polyols family, especially glycerol, is a commonly used plasticizer for starch-based material investigations. In addition to water/starch interactions (Page 18), the added plasticizer influences the properties and glass-transition temperature of TPS. Researchers are working on exploring the interaction between water/starch/plasticizer to study the moisture

content equilibrated within plasticized starch with different plasticizer [88]. Many empirical/semi empirical equations representing different sorption data have been put forward [10, 14, 89]. Guggenheim-Anderson-deBoer (GAB) model as recommended by the European project group COST 90 on physical properties of foods is the most widely accepted and universal sorption model for most food stuff, e.g. starch, fruit, vegetable, and meat products is also applied in this current study.

Moreover, from an energy equilibrium point of view, within any interaction system, all interactions are aiming to minimizing the system entropy. Therefore, in plasticized starch hydrophilic system, all interactions tend to lower the starch intermolecular entanglements and increase the number of intermolecular interactions of starch, plasticizers, water, etc. The 3-way nature of these interactions (starch-plasticizer, starch-starch, plasticizer-water) also increase the intermolecular interactions; by strengthening plasticizer-biopolymer entities to reduce matrix flexibility and increase T_g. This phenomenon is antiplasticization, where the brittleness and the antiplasticization behaviour are inversely proportional to the concentration of glycerol or sorbitol in starch biopolymers [77, 78].

2.3.3.1 Starch/glycerol (xylitol)/water

In glycerol/water/starch system, a multiphase diagram has been proposed by Godbillot *et al.* [23] as a function of the plasticizer content, highlighting the different interactions taking place [90]. Water vapor adsorption corresponds to the number of hydrophilic sites (hydroxyl groups) in the plasticizer and therefore modified starch films have less adsorption capacity than native or plasticized films. The interaction between the plasticizer and starch chains is due to the hydrogen bonding between starch and plasticizer. For instance, specific sorption sites could be occupied by the plasticizer at low glycerol/moisture conditions. Similarly, the plasticizer might become free when the sorption sites are filled at high relative humidity and glycerol content. Based on these hypothesis, in certain conditions, a phase separation might happen due to the extreme condition, thus generating multiphase structures with rich and poor plasticizer domains [91]. The interesting phenomenon reported in our work is the ‘inversion’ behaviour where higher glycerol loading samples retained significantly lower amount of equilibrium structural water at low a_w values, but as the a_w increased, this relationship between the equilibrium

structural water and the glycerol content was inversed. This finding was attributed to a replacement of immobilised water molecules at a low a_w scenario [92]. Similar finding was found in xylitol-plasticized system [81].

The complex multi-plasticized (glycerol/xylitol/water) starch biopolymer with about 70% amylopectin structure systems were studied by Chaudhary *et al.* by analysing the glass-transition behaviour via using the modified Gordon-Taylor model [93]. When the plasticizer concentration was increased up to 15% and 20% wt, all plasticized samples showed significant reduction in glass-transition temperature suggesting that competitive plasticization existed and occurred at a threshold amount of matrix free water content, due to strong three-way interactions: starches/plasticizer, plasticizer/plasticizer /water and starches/water. Furthermore, the onset temperature for viscous flow behaviour was closely related to the competitive nature of the interactions .

2.3.3.2 Starch/ glycerol (xylitol, sorbitol, and maltitol)/water

Mathew and Dufresne [94] have studied this topic in waxy starch with different plasticizers but fixed concentration of 33%. It was found that T_g was inversely proportional to the moisture content and directly proportional to the molecular weight of the plasticizer. The water resistance of starch and the molecular weight of the plasticizer were directly related to each other and proportional to the total hydroxyl groups. As the molecular weight of the plasticizer increased, the brittleness of the dry system increased. However, the use of high molecular plasticizer allowed good mechanical properties of the moist material to be obtained in terms of both stiffness and elongation at break.

2.3.3.3 Starch/ (glycerol, sorbitol, lactic acid sodium, glycol, urea, ethylene, PEG 200, diethylene glycol, glycerol diacetate)/water

Lourdin *et al.* [95], investigated the ‘Sorption behaviour and calorimetric glass transition on cast starch films plasticized with varying concentrations of different components (glycerol, sorbitol, lactic acid sodium, urea, ethylene glycol, diethylene glycol, PEG 200, glycerol diacetate)’. Precision analysis illustrated that the lowest moisture level was observed in samples conditioned at 57% relative humidity for a plasticizer content of 10–20% (dry basis). ‘Starting from 14.8% of water (as measured in the amorphous starch-water

system), a minimum of 12.7 to 14.4%' can be locked within the sample according to the type of plasticizer added. The general behaviour is universally similar for all components except/glycerol/diacetat; the T_g depended on the type of plasticizer used. Same conclusions are drawn from Chaudhary *et al.*'s work about the glass-rubber transition of glycerol/xylitol-plasticized biopolymer. They reported the tendency of T_g fluctuation from low starch polymer plasticized by glycerol and xylitol at different concentration [96].

2.4 Starch-based Biocomposite with nanoparticles

Upon the addition of nanofiller, new and/or improved properties (gas barrier, mechanical stiffness, thermal stability, transparency, etc.) are possible based on the geometry and nature of the nanofillers incorporated into the polymer matrix [12, 89, 97-99]. Layered silicates form the focal point for starch-based nanocomposite research as the reinforcing phase has very high aspect ratio (100) and versatility [10-15]. This is because 'MMT crystal lattice consists of 1nm thin layers with an octahedral alumina sheet sandwiched between two tetrahedral silica sheets', which can accommodate various polymeric groups for greater stability. As well as the hydrophilic pristine Na^+-montmorillonite clay provide the possibility for interactions between starch and MMT [8, 9]. The preparation of TPS/kaolin hybrids by melt intercalation technique using a twin screw extruder was reported by De carvalho *et al.* briefly [100]. Park *et al.* reported the preparation of TPS/MMT nanocomposites by melt intercalation in detail. It was thought that the polymer chains were able to intercalate into the silicate gallery of pristine MMT due to the strong polar interactions between a small amount of polar hydroxyl group of water in the TPS chain and the silicate layer of the pristine MMT. Similar results were obtained when organic modified layered silicate was incorporated [101]. Respective aqueous suspensions (30 mL) were used to prepare glycerol-plasticized starch/layered compounds composite films at various starch/hectorite ratio. WAXD results revealed the expansion of gallery spacing for hectorite to different extent in Wilhelm's work [102]. It was found that elongation, strength and modulus can be increased simultaneously by addition of a small wt% of clay [103].

2.4.1 Well-defined Morphologies formed in nanocomposites

An explanation to the improvement of mechanical properties (tensile strength, strain to break, Young's modulus) is that the dispersed MMT allows greater reinforcement

of the polymeric matrix, and increases the crystallinity of the matrix [12]. Starch-based nanocomposites can have three types of morphology based on the content of the MMT and the processing conditions intercalated, exfoliated and a combination of intercalation and exfoliations.

Mainly three types of morphologies are well recognized in a polymer/clay blend based on previous researches, intercalation, exfoliation and combination of intercalation and exfoliation [19] , as shown in Figure 2-3.

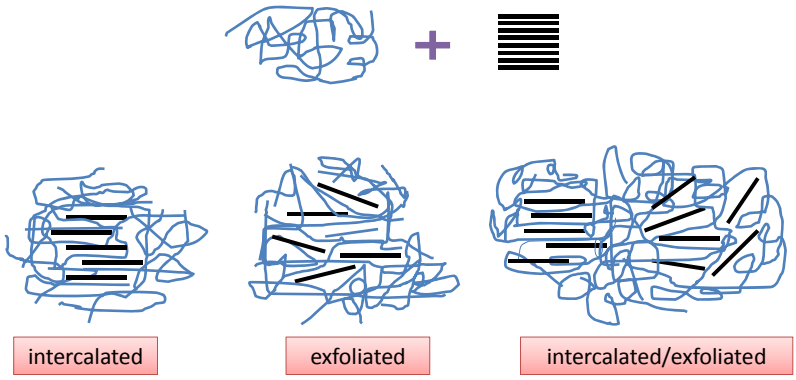

Figure 2-3 Intercalated and exfoliated morphologies for MMT/polymer nanocomposite.

The intercalation or exfoliation is both likely to result from the hydrogen bonding between the clay surfactant and the starch chains. Such morphologies in different types of starch, wheat, potato and corn (maize) with a MMT content ranging from 0 to 9% have been published by many researchers [8, 103-108].

Cyras *et al.* reported that the *basal spacing* shifted to lower angles irrespective of the MMT content. This indicated good intercalation without exfoliation being formed during the preparation. The glycerol or the polymer chains or both could have entered into the silicate layers suggesting strong polar interactions among the hydroxyl groups present in the polymer chain, the glycerol and the silicate layers [98].

Actually, most starch-MMT nanocomposites showed intercalation and exfoliation morphologies due to the uncontrolled factors during processing. Properties of melt-extruded thermoplastic starch/MMT nanocomposites preparation via single screw extrusion from pre-treated MMT/glycerol/starch pulp was reported by Wang *et al.*

[109]. The pre-treatment of applied pulp could be described as this; at first, a glycerol-activated-MMT (AMMT) was obtained by mixing glycerol and MMT (10:3 ratio) at an ultrahigh speed of 9000rpm for 20 min which was then subjected to extrusion with starch/glycerol pulp. Characterization results (WAXD and TEM) suggested a good intercalated morphology had been formed by adding MMT in Park *et al.* [101]. The co-existed morphology had been observed in the Liu *et al.*'s work as well by applied sonicated glycerol/MMT slurry for extrusion processing. It had been reported that due to the pre-treatment the glycerol and MMT interact with starch polymer and the strength of such interactions are greatly dependent on the concentration of both glycerol and MMT [86].

Fully-exfoliated morphology from starch/clay nanocomposites had been reported in the work of Fischer and Fischer [110]. A number of experimental protocols such as the dispersion of MMT clay in water, followed by blending in an extruder at a temperature of 85–105 ^{o}C with a premixed powder of potato starch, glycerol and water were observed. The obtained characterization results proved that the prepared material was fully exfoliated with a reduction in hydrophilicity and improved stiffness, strength and toughness.

2.4.2 Effect of glycerol in starch-MMT nanocomposite

As the most intensively used plasticizer in starch industry, glycerol becomes the dominant component in starch-MMT nanocomposite. The effects of glycerol on physical properties, morphology and structure in starch-MMT nanocomposites have been widely investigated. A comprehensive understanding of the role of glycerol in the starch-based nanocomposite is of significant importance to identify the ternary synergistic interaction. The key aspects from relevant literature are outlined below.

2.4.2.1 Starch-MMT nanocomposite plasticized by only glycerol

A combination of intercalated and exfoliated morphology was observed in Chiou *et al.* 's work and they also pointed out that the increase in glycerol leads to an intercalated rather than exfoliated morphology [103]. Tang *et al.* [60] reported the influence of glycerol on the properties and structure of its bionanocomposites, and the results were compared to two nanocomposites prepared with urea and formamide in the same method. The hindrance effect of glycerol on clay exfoliation was confirmed from the relevant WAXD and TEM

results as well as the mechanical properties for low-glycerol content samples due to the well-known antiplasticization of glycerol. They also concluded that urea and formamide turned out to be another two suitable plasticizers for starch-based nanocomposite production. Another research [111] examined the effect of clay type and content on the physical properties of corn starch nanocomposite via extrusion. Higher B-type crystallinity was observed in glycerol-rich sample and the biodegradation process was enhanced by introducing MMT. As mentioned, glycerol can successfully intercalate into the gallery of MMT, however, a further increase of glycerol concentration did not always enhance the exfoliations degree. It had even been reported to hinder the exfoliate due to the stronger glycerol/glycerol interactions that competed with the starch(glycerol)/MMT interaction [86].

2.4.2.2 Starch-MMT nanocomposite plasticized by mixture of glycerol/other components

Additionally, utilization of mixtures of glycerol/other has also been studied which results in improvements in material properties. Potato starch-based MMT plasticized by glycerol and a urea/ethanolamine mixture was studied [112] where two series of films containing 6 wt % MMT were prepared by a solution/cast process: neat starch, and 20 wt % plasticized starch were used to prepare two series of films. A mixture of intercalated and exfoliated structures was formed by the pristine MMT presented films, whereas an aggregate structure was obtained with organic-MMT presented films. The thermal stability was not significantly influenced by the addition of clays. However, great reduction of oxygen permeability was observed in natural MMT, which was concluded to be related to the high dispersion state of clay.

A broad range of factors including clay cation, glycerol content and mixing mode were taken into account for understanding the dispersion of clay and mechanical properties enhancement in Majdzadeh-Ardakani *et al.* work based on Taguchi experimental design approach [113]. Nanocomposites prepared with MMT modified with citric acid had the highest Young's modulus compared to pristine MMT and organoclay. Dispersion of silicate layers was achieved by combined mechanical and ultrasonic mixing mode and thus the highest Young modulus in nanocomposites. It was also observed that

nanocomposite films with 6% (by weight) of clay loading had the maximum stress strength.

More recently, the impact of plasticizer on the clay (both natural and organic modified) are discussed [114]. Glycerol, sorbitol and polysorb plasticized melt blending starch nanohybrid in the presence of MMT (natural and organic modified), and they have been elaborated by SAXD, water desorption analysis, TGA characterization, DMTA and tensile tests. Intercalated/ aggregated and exfoliated morphologies were obtained respectively. 'Morphological analyses combined with uniaxial tensile tests have shown the negative effect of the sorbitol on the exfoliation extent into such nano-hybrid materials'. Furthermore, 'thermo-mechanical analyses revealed the existence of phase separation between domains rich and without nanofillers induced by the high plasticizer content of the starch formulations'[114].

2.4.2.3 Starch-MMT nanocomposite using higher molecular weight polyols

Compared to glycerol, utilization studies of xylitol and sorbitol as plasticizer in starch-based nanocomposite is less popular. This is because of their relatively larger molecular size and molecular weight which prevent their penetration into the clay gallery. This is one reason why investigations involving sorbitol/xylitol are always presented in combination with other plasticizers like glycerol and formamide.

The authors studied the sorbitol-plasticized nanocomposite system via twin-screw extrusion at different ratio of sorbitol/MMT ratio. The novel step was the pre-treatment of sorbitol with water before mixing the slurry with dry starch power. It had been confirmed that in sorbitol –plasticized system an intercalation/exfoliation co-existed and the basal spacing was found ideally increased upon the increasing of sorbitol concentration. However, the cell packing densities of the crystalline domain are greatly influenced by the sorbitol/sorbitol interactions which altered the final morphologies for different samples [38].

In Ma *et al.* [62], thermoplastic starch/ montmorillonite nanocomposites without organic reactions in the solution was prepared in a two-step protocol. WAXD demonstrated that the interlayer distance of MMT was enlarged by sorbitol during the first step. TPS/MMT nanocomposites were prepared from the modified MMT-sorbitol, formamide and starch in the second step. Intercalations between the layers

of MMT was achieved and confirmed by WAXD and TEM. An increase in MMT content corresponded to better 'thermal stability, tensile strength, Young's modulus and energy break, and a slight decrease of elongation at break'.

Mathew and Dufresne [115] examined the properties and morphology of nanocomposite compared to sorbitol-plasticized waxy maize starch reinforced by tunicin whiskers. They found that the sorbitol-plasticized system exhibited a single glass/rubber transition, and displayed no evidence of transcrystallization of amylopectin on cellulose whisker.

2.4.3 Interaction mechanism of starch-clay bionanocomposites

As discussed above, starch-MMT nanocomposite exhibited excellent properties which are comparable to oil-based polymers. Thus, it is a promising idea to prepare almost tailored-made nanocomposite based on a clear understanding of the synergistic interactions. However, unfortunately, there are few publications that explore the internal synergistic interactions within this complex ternary system, although the phenomenal experimental results are promising.

A key scientific area requiring further investigation is the complex interaction of plasticizers and clay in biopolymeric matrix. Current literature has isolated studies on plasticized starch/MMT and yet no well-known interactions parameters/ mechanism for the system have been developed. However, several publications are focusing on the starch/MMT system to understand the interactions within the complex Starch/MMT/plasticizer system.

2.4.3.1 Starch-MMT-Water interactions

The innovative work from Chaudhary *et al.* [116] investigated the starch chain reorganization behaviour in starch/water/MMT system with clay concentrations from 1.5 wt% to 4 wt %. The influence of MMT on starch crystallinity and the loss of water from the matrix were comprehensively discussed in terms of the mobility of starch chain and its reorganization process. As proposed by the author, from the angle of starch chain mobility, the presence of MMT plates could significantly restrict the starch chain movements. Thus, an extra 10% water molecules could be retained within the matrix. The schematic illustration of this process is depicted in Figure 2-4.

In a starch-MMT-water system, the well dispersed MMT plates or even MMT tactoids can occupy the free volume between starch chains. Under such scenario, the MMT acts like a 'fence or wall' between the starch chain and free water molecules. Therefore, extra amount of free water molecules will be stuck within the starch-MMT polymeric network in a certain period of time.

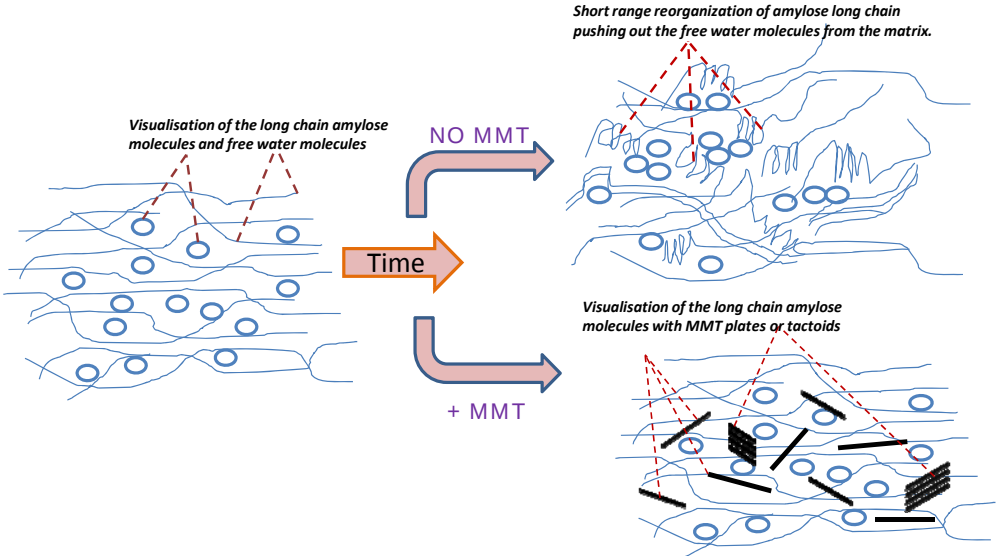

Figure 2-4 MMT particles within starch/water network causing spatial hindrance for starch reorganization. Modified from [105].

The conclusions from starch/water/plasticizer pointed out that the plasticizer (mostly polyols) might be acting in much the same way as water does within the hydrophilic system. The reasonable hypothesis on one aspect of the interactions within the starch/MMT/plasticizer/water system was assumed like this; well dispersed MMT plates or tactoids can restrict the mobility of the plasticizer and starch. Thus the interactions between starch/plasticizer and plasticizer/plasticizers will be greatly influenced by the incorporation of MMT and its corresponding amount used.

2.4.3.2 Role of water in starch-MMT nanocomposite

The influence of water present in the matrix has also been recently investigated. It had been observed in many research that water uptake decreases as the clay content increases [105, 117, 118]. The presence of the dispersed, impermeable large aspect silicate layer reduces the water uptake capacity of polymer-MMT nanocomposites. These layers increase the effective path for diffusion by allowing water to follow a tortuous path through the polymer matrix [106]. Immersion test proves that the clay

platelets behave similar to barriers preventing water to move due to the high aspect ratio which formed a tortuous pathway for a permeate to transverse the nanocomposite [82]. However, presence of glycerol has been shown to hinder the MMT effect on the amount of water uptake and this has been linked to the high hydrophilicity and small size of glycerol [86, 103].

One publication from Chivrac *et al.* [119] examines the correlation between the structure of starch-based nano-biocomposite materials and their moisture barrier properties in detail. 'They characterized the structure via TEM, WAXD and DMA, and evaluated moisture transfer behaviour via permeability measurements and sorption kinetics analysis using dynamic vapour sorption equipment'. The moisture barrier properties of glycerol-plasticized wheat starch materials remain unchanged with the addition of native MMT or MMT modified with cationic starch (OMMT-CS). 'And phase separation with plasticizer rich and carbohydrate rich phases, was observed in the relatively high plasticizer content (23 wt% glycerol) sample'. Thus the authors prospected that the lack of change in crystallinity of the starch-based matrix with the introduction of MMT can be explained by the fact that a preferential pathway for water transfer was created in the matrix instead of MMT platelets. Such phase separation resulted in the MMT being preferentially located in the carbohydrate rich domains. Hence, the very hydrophilic glycerol rich domains where the MMT platelets were almost mostly absent facilitated water transfer. Therefore, even if the high glycerol samples contains an exfoliated morphology, the decline in the moisture barrier for glycerol based starch bio-nanocomposites could be explained by the heterogeneous clay distribution and phase separation.

2.4.3.3 Atomic scale modelling in starch-MMT system

Recently, the application of molecular dynamic modelling had shown its unique strength in understanding nanocomposite interaction [120-122] which is primarily due to the powerful computational capacity of modern supercomputer. Classical force fields and quantum chemical methods in computational chemistry provide a practical approach to evaluate structure and dynamics of the materials on an atomic scale. Combined with classical energy minimization, molecular dynamics, and Monte Carlo techniques, quantum methods provide accurate models of layered materials such as clay minerals, layered double hydroxides, and clay–polymer nanocomposites [122]. Ginzburg *et al.* [121] successfully described the

thermodynamic behaviour of organically modified clays in polymer melt via a “compressible” version of lattice self-consistent field theory (SCFT). The melt consists of the homopolymer matrix and a fraction of end-functionalized “active” chains, each chain having a single “sticker” end-group with strong affinity to the clay surface. The phase map for this system as a function of the melt composition and the strength of the “sticker” adhesion to the clay was then calculated to study the thermodynamic behaviour of the nanohyrid melt.

Based on the approaches on polymer-MMT nanocomposite, even though not starch polymer, it is possible to borrow the relevant or similar ideas for starch-MMT nanocomposite area.

Summary

In summary, the interactions that existed in the starch/plasticizer/MMT were complicated and competed with each other depending on both the physical processing history and the chemical environments. These included starch/water interaction, starch/plasticizer interaction, starch/MMT interaction, plasticizer/ MMT interaction and water/MMT interaction. These interactions can greatly impact the final properties of the material. Although there is some understanding regarding the interaction process, a clear map of the mechanism in this type of material have not been established so far. This thesis aims to fill this knowledge gap by investigating different behaviours of starch-based /MMT nanocomposites plasticized by three polyols (varied based on the number of –OH groups for each plasticizer, namely, glycerol, xylitol and sorbitol).

The innovative aspect of this work is to further investigate the complex interaction within the *TERNARY* system in terms of isolating possible influences by choosing the most representative samples. This is achieved by applying experimental design to maximise the scientific information from our data. Our publication about the interactions within glycerol/starch/MMT and sorbitol/starch/MMT suggested the possible interactions that are responsible for each characterization results [38, 86, 123].

Additionally, the amylose cell for molecular modelling made of 12 glucose monomer units is successfully built. The density and T_g value for dry starch from current simulation is 1.34g/cm^3 and 198^{o}C, respectively which are confirmed to be in accordance with the experimental results in the literature where the experimental results for dry starch density and T_g are around 1.3g/cm^3 and ranges from 170-220 ^{o}C. More detailed simulation results (T_g for starch polymers at different hydration degree) further supports the accuracy of the constructed starch model and calculation protocols (given in the APPENDIX). The calculated results mutually supported the hypothesised interaction map that, at a low-plasticizer loading condition, loosen-soft polymeric network had the tendency to be formed.

Chapter 3

Materials Methodology Characterization

3.1 Materials

3.1.1 Starch

High amylose starch (average DP 690-740, STARCH 6-161) with an amylose percentage around 70% was purchased from Nation Starch U.S; the detailed specifications are shown in Table 3-1.

Table 3-1 Physical properties of starch.

Product code	Starch content	colour	form	moisture	pH
HYLON® VII	≈ 70%	White to off-white	powder	≈11%	≈5

3.1.2 Plasticizers

Plasticizer is the essential component in TPS processing. Three polyols (glycerol, xylitol and sorbitol) are selected in this thesis, based on their different number of hydrophilic activity sites (-OH groups) [94]. Brief introductions for plasticizers selected are cited in the subsequent sections.

3.1.2.1 Glycerol- 3 –OH groups

Glycerol is the most intensively used additive in food and pharmaceutical applications because of its sweet-taste, low toxicity and powerful moisture-retain ability. It is the most favourite and widely used plasticizer in starch-based materials fabrication as well [124].

Glycerol (also known as glycerin, glycerine) is a trihydric polyol compound that is colourless, odourless and syrupy at ambient temperature. Three hydrophilic hydroxyl groups of glycerol ensure its high water-solubility as well as the hygroscopic nature. Food grade glycerol was obtained from Food Dept Melbourne Company (Melbourne,

Vic., Australia). The molecular structure and relevant characteristics of glycerol are shown in Table 3-2.

Table 3-2 Molecular structure and properties of glycerol.

Molecular formula	Molar mass	Density	Melting point	Boiling point
$C_3H_5(OH)_3$	92.09382 g/mol	1.261 g/cm³	17.8 °C (64.2°F)	290°C
Molecular structure*				
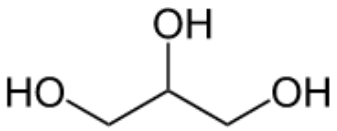		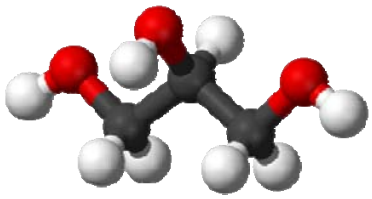		

*molecular structures are obtained from Cambridge Crystallographic Data Centre (CCDC); Colours: carbon atoms are grey, hydrogen-white, and oxygen-red)

3.1.2.2 Xylitol- 5 –OH groups

Xylitol is a sweet-tasting alcohol with the formula $(CHOH)_3(CH2OH)_2$ that can be found in a variety of fruits and vegetables. The most common application of xylitol is as a substitute for glucose (sweetener, in crystal form) in food engineering. Furthermore its antibacterial properties help to diminish the incidence of dental cavities, sinus infection and skin conditions.

This organic compound with 5 –OH groups is also utilized in starch-based materials engineering due to its high hydrophilicity. Food grade xylitol was obtained from Food Dept Melbourne Company (Melbourne, Vic., Australia). The molecular structure and relevant characteristics of glycerol are shown in Table 3-3.

Table 3-3 Molecular structure and properties of xylitol.

Molecular formula	Molar mass	Density	Melting point	Boiling point
$C_6H_{14}O_6$	182.17 g/mol	1.489 g/cm³	95 °C	296 °C
Molecular structure*				
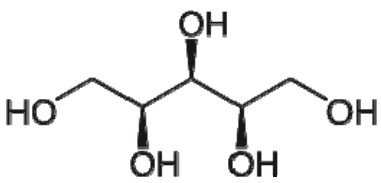		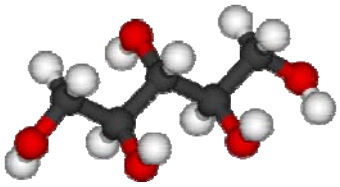		

*molecular structures are obtained from Cambridge Crystallographic Data Centre (CCDC); Colours: carbon atoms are grey, hydrogen-white, and oxygen-red

3.1.2.3 Sorbitol- 6 –OH groups

Sorbitol, classified as a polyhydric alcohol, possesses less sweetness compared to the lower alcohols like glycerol and xylitol. It could be generally obtained by the reduction of glucose via transformation of aldehyde group to hydroxyl group. The application areas of sorbitol and general physical characteristics are similar to those of glycerol.

Sorbitol possesses six groups of –OH making it another excellent candidate as an essential plasticizer in starch-based biodegradable industry. Food grade sorbitol was obtained from Food Dept Melbourne Company (Melbourne, Vic., Australia). The molecular structure and relevant characteristics of glycerol are shown in Table 3-4.

Table 3-4 Molecular structure and properties of sorbitol.

Molecular formula	Molar mass	Density	Melting point	Boiling point
$C_6H_{14}O_6$	182.17 g/mol	1.489 g/cm³	95 °C	242°C
Molecular structure*				
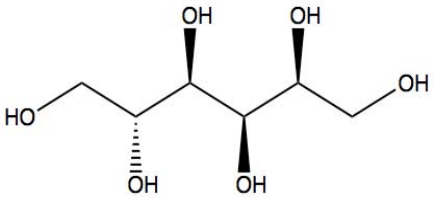		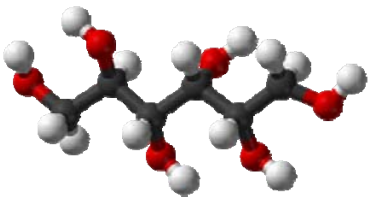		

*molecular structures are obtained from Cambridge Crystallographic Data Centre (CCDC); Colours: carbon atoms are grey, hydrogen-white, and oxygen-red

3.1.3 Na^+-montmorillonite (MMT)

Na^+-montmorillonite (MMT) is the most prevalent one as revealed from the numerous publications. MMT employed in the current research was kindly supplied by NichePlas Ltd. (Sydney, Australia). Typical molecular structure and physical properties are shown in Table 3-5.

Table 3-5 Physical properties of Na^+-montmorillonite.

Product code	Density	colour	form	moisture	d_{001}
Cloisite® Na^+	2.86 g/cc	off-white	powder	≈ 4-9%	11.7Å

3.2 Methodology

3.2.1 Preliminary

With the aim to investigate the influence of plasticizer type and concentration on the performance of starch-based MMT nanocomposites, the individual factors (plasticizer type, plasticizer concentration, and MMT loading) are studied separately. Mixture design with constrained surfaces (extreme vertices design) at full degree design have been employed here [125] for determining the experimental sheet. The detailed formula for specific groups (glycerol, xylitol and sorbitol) of nanocomposites will be listed in the corresponding sections.

Pre-conditioning of dry starch with certain amount of moisture is essential in starch materials extrusion process due to the processing requirement of extrusion [126]. Based on previous research reports, 30-40% moisture content clouding starch turned out to be extremely favourable for extrusion.

Pre-equilibrium starches are prepared by adding corresponding amount of distilled water via a bench top kitchen twin-hook mixer (BEM200 Wizz). Sufficient time (more than 30 minutes) was provided to achieve optimal mixing condition. The powder obtained was placed in a hermetically sealed polyethylene bags for 24 hours to reach equilibrium prior to extrusion fabrication.

3.2.2 Methodology

3.2.2.1 Equipment setup

A lab-scale twin screw co-rotating (SHJ-20, JieYa, China) extruder was used to prepare nanocomposites samples. The extruder is equiped with six heating zones from the feeding copper to the die (namely, zone 1 to zone 5 and die zone) and adjustable screw rotating speed ranges from 12/rpm to 600/rpm as shown in the layout of SHJ-20 (Figure 3-1). The specifications for SHJ-20 are shown in Table 3-6.

Table 3-6 Specifications for SHJ-20.

Model	Screw Diameter(mm)	Depth Of screw Channel (mm)	Ratio of length to diameter	Driving Motor(kW)	Screw Max Speed(rpm)	Output (kg/h)
SHJ-20	21.7	3.85	35	3	600	0.5-15

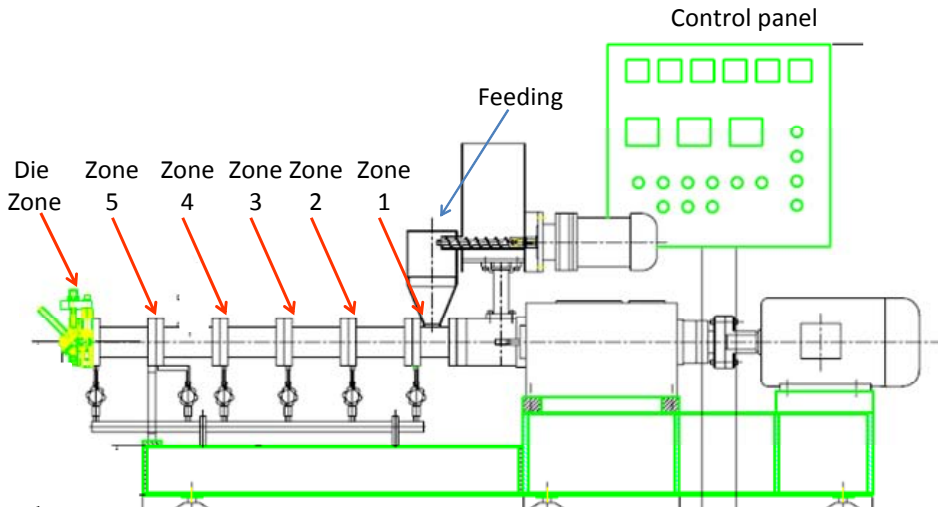

Figure 3-1 The layout drawing of SHJ-20 twin screw co-rotating extruder.

3.2.2.2 Optimization of extrusion processing conditions

The extruder applied in this research is a co-rotating twin screw extruder with five separate heating zones which are responsible for different functions of the screw like surveying (Zone 1 and Zone 2), mixing and compressing (Zone 3 and Zone 4), and plasticizing (Zone 5). Therefore the optimum configuration of the different temperature composition will be a key parameter correlated with the material behaviour. The desired temperature profile for processing should meet the requirement that achieve the highest gelatinization degree of the extrudant. Taking the gelatinization temperature of pure starch (110°C~120°C) as a reference point [127], several temperature profiles (Table 3-7) are examined.

Table 3-7 Temperature profiles tested for extrusion processing optimization.

Profile ID	Heating zones (°C)						Screw speed (rpm)
	Zone 1	Zone 2	Zone 3	Zone 4	Zone 5	Die Temperature	
1	90	115	120	110	85	50	120
2	90	115	120	110	85	50	96
3	90	115	120	110	85	50	72
4	90	115	120	110	85	50	60
5	90	115	125	120	90	50	120
6	90	115	125	120	90	50	96
7	90	115	125	120	90	50	72
8	90	115	125	120	90	50	60
9	90	115	130	110	85	55	120
10	90	115	130	110	85	55	96
11	90	115	130	110	85	55	72
12	90	115	130	110	85	55	60

Subsequently, profile NO 8 (90°C /110°C /125°C /120°C /90°C /50°C from the zone 1 to die zone) was determined to be the best processing condition. The extrudant produced under Profile NO 8 exhibited the maximum gelatinization degree which was evidenced by the WAXD experiment results, Figure 3-2.

As shown in the WAXD results for temperature profiles optimization test, although all other plots are heavily overlapped with each other, profile NO 8 can be recognized to be the lowest curve. Such result indicated that the extrudant produced from profile NO 8 possesses the highest gelatinization degree.

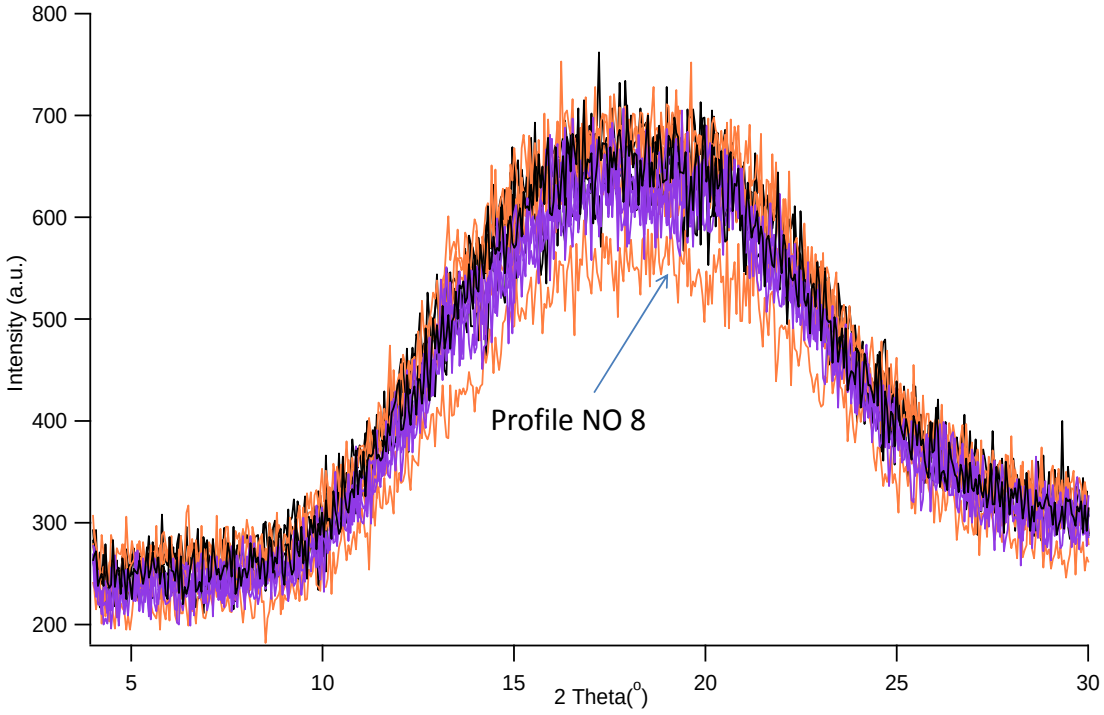

Figure 3-2 X-ray diffraction experiment results for different extrudant corresponding to various tested temperature profiles for extrusion processing parameter optimization purpose.

3.2.2.3 Determination of interval time between two different samples

In order to obtain the representative sample for different formulation during continuous extrusion, interval time between two samples should be precisely calculated to avoid any contamination from the last running sample. The simple method applied here to work out the duration for completely finishing one batch of material was to add certain amount of food dye in the feeding part and monitor the transportation time from feeding copper to die zone.

Based on the optimization extrusion condition that was determined, the interval time was counted as 13 minutes for each batch of material. Aiming to avoid any possible contamination from previous running sample, reference material, PS (without any plasticizer or MMT) was fed and run for 5 minutes for barrel/screw purging purpose before each formula. Furthermore, only samples produced after 8 minutes were collected and used in the actual sample preparation.

3.2.2.4 Sample preparation

Three groups of starch-based biodegradable nanocomposites were prepared according to the optimized extrusion processing condition. The sample nomenclatures used in this work were described with a label such as S105, where S refers to sorbitol (plasticizer type); number 1 indicates 1wt% MMT used; latter two digital numbers "05" refers to the amount of sorbitol (plasticizer amount) within the samples. Pure extruded starch composite is also produced denoted as PS

i. Pure Starch Sample and Starch+MMT samples

Three samples were prepared denoted as PS (Pure Starch Sample), 2 wt % MMT (sample with Starch and 2 wt % MMT) and 4 wt% MMT (sample with Starch and 4 wt % MMT).

ii. Glycerol nanocomposites

Eight samples were prepared according to the experimental sheet in Table 3-8. Prepared nanocomposites could be grouped into four categories with a MMT loading varying from 0% to 3%. Glycerol was diluted in distilled water, mixed with MMT and subjected to 10 minutes sonication. Sonicated solution of glycerol/MMT was added to pre-equilibrium starches just before the extrusion process. The total amount of moisture from pre-equilibrium starches and sonicated solution was adjusted to be 35% in total (weight percentage).

Table 3-8 Detailed formula of glycerol nanocomposite.

Sample ID	G010	G020	G105	G115	G210	G220	G305	G315
MMT (wt %)	0		1		2		3	
Glycerol (wt %)	10	20	5	15	10	20	5	15

iii. Xylitol nanocomposites

Ten samples were prepared at different ratios of MMT/xylitol content from 1:1 to 1:4, as listed in *Table 3-9*. The pre-treated xylitol/MMT slurry was mixed with pre-blended starch for extrusion process.

Table 3-9 Detailed formula of xylitol nanocomposite.

Sample ID	X010	X020	X105	X115	X210	X220	X305	X315	X410	X420
MMT (wt %)	0		1		2		3		4	
Xylitol (wt %)	10	20	5	15	10	20	5	15	10	20

iv. Sorbitol nanocomposites

Ten samples were prepared at different ratios of MMT/sorbitol content from 1:1 to 1:4, as listed in Table 3-10. The pre-treated sorbitol/MMT slurry was mixed with pre-blended starch for extrusion process. The well-mixed starch/sorbitol/MMT was then used for extrusion.

Table 3-10 Detailed formula of sorbitol nanocomposite.

Sample ID	S010	S020	S105	S115	S210	S220	S305	S315	S410	S420
MMT (wt %)	0		1		2		3		4	
Sorbitol (wt %)	10	20	5	15	10	20	5	15	10	20

3.2.2.5 Sample storage

After processing, the nanocomposites ribbons are soft and flexible, named as as-processed ribbons. Two types of sample, vacuum sealed as-processed ribbons and ground nanocomposite powder were stored for different characterization purposes.

i. Vacuum sealed nanocomposite ribbons

In order to avoid the unexpected time-dependent changes which occurred during storage such as aging, recrystallisation of amylopectin and retrogradation; fresh-proceeded starch composite ribbons were cut into 10cm segments and vacuum sealed in plastic bags.

ii. Ground powder samples

A part of nanocomposite ribbons was ground into powder samples for specific characterizations. The soft fresh starch ribbons were clipped into 5mm pellets and subjected for 20 hours oven dried at 70^{o}C. Obtained stiff pellets were ground in a powerful ring mill (Rocklab RingMill).

3.2.2.6 Sorption isotherm measurements in starch/plasticiser/water system

i. Experiment

Four desiccators were used as control humidity chambers for four different relative humidity (RH) values. The desiccators were made of glass and vacuum sealing was used to make the samples hermetically sealed. The prevention of exchange of water between the environment within these controlled humidity chambers is essential in these experiments. Furthermore, it is essential to maintain minimum diffusion path for the water vapour between the surface of the powder and the salt solutions to achieve reasonably shorter equilibration time. Hence, the protocol recommended by COST-90 was used to prepare the standard salt solution. The humidity chamber and all the measurements were taken at 24±0.5^{o}C, in an air-conditioned room. It was ascertained that excess salts remain in the salt (above their solubility) solution even after the completion of the experiments. Around 2 grams of sample was placed on a petri dish in each humidity chamber. The samples were equilibrated for 4 weeks to allow the samples to reach moisture equilibrium. They were taken out and their moisture content was determined immediately. Triplicate tests were conducted and the average values were reported. Regression analysis was completed on the moisture measurement to determine the standard deviation. The standard deviation is reported in the tabulated data. The sample water activity was also cross-checked with Novasina water activity meter (Novasina, Switzerland). Once the moisture content and water activity values of these samples were obtained, sorption isotherms could be determined.

ii. GAB equation evaluation for sorption isotherm results

Several models are available in literature based on different kinetic (mono-layer, multi-layer or condensed film) as well as empirical models. GAB model which is based on the multi-layer kinetic was applied in the current thesis. Corresponding parameters were estimated via a non-linear least square regression routine. The GAB equation is usually presented in the form of equation 3-1 [128]:

$$w = \frac{w_m C K a_w}{(1 - K a_w)(1 - K a_w + C K a_w)} \qquad \text{Eq 3-1}$$

Where w is the moisture content; a_w is the water activity; w_m, C and K are the three parameters characterizing the sorption properties of the material. w_m denotes moisture content corresponding to the 'monomolecular layer' of the whole material surface; K and C depend on the temperature with corresponding molar sorption enthalpies [129].

The equation can be re-arranged as a second degree polynomial formula which we can calculate w_m, C and K as shown below in equation 3-2 [130]:

$$a_w/w = a + ba_w + ca_w^2 \qquad \text{Eq 3-2}$$

Where $a = \frac{1}{w_m CK}$, $b = \frac{(C-2)}{w_m C}$, $c = \frac{K(1-C)}{w_m C}$.

The w_m, C and K can be obtained via regression analysis [131, 132] of the plot of a_w/w *vs.* a_w using experimental points.

3.2.2.7 Plasticizer/MMT interaction experiment

i. Optimization duration (T_{op}) determination

In the first step, the optimization duration *(T_{op})* of sonication treatment was determined before proceeding to main experiments. This was achieved by subjecting the same formula samples for different sonication duration (15 mins, 30 mins, 1 hour and 3 hours) test. The determination of T_{op} was based on comparing the expansion of MMT basal spacing as read from the WAXD results. Glycerol sample with a glycerol:MMT ration of 2:1 was tested.

ii. Plasticizer+MMT sample preparation

MMT and plasticizer were mixed on weight basis at different ratios, see Table 3-11. The plasticizer was dissolved in 100ml distilled water with 15 minutes of continuously stirring. Corresponding amount of MMT (*Table 3-11*) was added dropwise to the pre-prepared solution (plasticizer+water). The obtained slurry was magnetically stirred for 15 minutes before subjecting to sonication treatment at 70 ºC. The sonicated solution was dried in the oven at 130 ºC for 30 hours to remove the

free water. A ring mill was then used to grind the samples to obtain a fine powder (particle size $\approx$ 10 micron).

Table 3-11 Detailed experimental sheet for plasticizer+MMT interaction study.

MMT :Plasticizer ratio	1:1	1:2	1:3	1:4
glycerol	√	√	√	√
xylitol	√	√	√	√
sorbitol	√	√	√	√

3.3 Characterization

Dispersion morphology characterization of incorporated nanoparticles is the most important issue in understanding the synergistic interactions within the nanocomposites. In addition to the routine characterization methods including Wide Angle X-ray Diffraction (WAXD), Fourier Transform Infrared Spectroscopy (FTIR), Differential Scanning Calorimetry (DSC), Proton Nuclear Magnetic Resonance (^{1}H NMR) measurements and Carbon Nuclear Magnetic Resonance (^{13}C NMR); Small Angle X-ray Scattering (SAXS) via synchrotron and Positron Annihilation Lifetime Spectroscopy (PALS) were conducted on representative samples. Specific configurations for experimental condition are expounded as follows.

3.3.1 Moisture Content Measurement (MCM)

The water content in the samples was measured by a moisture meter (CA-100, Mitsubishi, Japan), and the average value from three measurements was recorded. In order to avoid the moisture transfer between the sample and environment, the temperature of the test environment was strictly controlled at 20^{o}C.

3.3.2 Wide Angle X-ray Diffraction (WAXD)

X-ray diffraction has been widely applied in investigations on studying molecular scale dimensions for crystalline materials [133]. Meanwhile X-ray Diffraction is an important method to quantify the intercalated/exfoliated morphology in MMT composites by assessing the characteristic peak of MMT in measured WAXD pattern. More specifically, intercalated morphology is corresponding to the observation that MMT characteristic peak position shifts to a lower 2θ value indicates expansion of basal spacing of MMT to different extent and vice versa. Furthermore, complete disappearance of MMT characteristic peak is considered to be the feature of a fully exfoliation morphology.

WAXD measurements of the prepared samples were performed in Bruker Discover 8 diffractometer operating at 40kV and 40mA with a 2θ range from 3° to 30° at a scanning rate of 0.05 °/second in Physics department of Curtin University. The *basal spacing* of the silicate layered was determined from the Bragg's equation, $\lambda=2d\sin\theta$ (where θ is the diffraction position and λ is the wavelength) [134].

3.3.3 Small Angle X-ray Scattering (SAXS) via Synchrotron

Small Angle X-ray Scattering (SAXS) was carried out at Beamline BL40B2 of Spring-8 synchrotron facility in Sayo, Hyogo, Japan. The light source was a bending magnet and the white X-rays generated were monochromatized using a double crystal monochromator and focused by a 1-m-long rhodium-coated bent-cylinder mirror. The photon flux was 1×10^{11} photons/sec at 12.4 keV with a tunable energy range of 7 keV ~ 18 keV. A high-resolution CCD camera with an imaging plate area (30cm*30cm) detector (RIGAKU R-AXIS IV^{++}) was installed[135].

The beam was monochromatized to a wavelength of 0.1 nm with an object distance of 1151.767mm. All the patterns recorded on CCD camera were calibrated by the diffraction rings from Silver Behenate (AgBH) standard sample. An aluminium filter block was employed to decrease the strength of X-ray and obtain optimized experimental pattern. The measurement time per sample was chosen to eliminate the radiation damage, subsequently determined to be 10 seconds.

3.3.3.1 SAXS profiles extraction

The diffraction profiles were normalized to the beam intensity and corrected considering the empty sample background. The data reduction of obtained 2-D X-ray scattering patterns was proceeded with NIKA macros [136] based on Igor (Wavemetrics, Lake Oswego, Oregon). The 2-D raw SAXS pattern was divided into six vectors and then the averaged Q vector *vs.* intensity plot was recorded for further analysis. Since an automated sample holder was used for data collection, all plots were recorded after the subtraction of background.

3.3.3.2 Size distribution calculation

More valuable information could be drawn from the low Q region of SAXS data plot. Determination of the size distribution is one of the most important steps in understanding the morphology within polymer systems. Size distributions for obtained samples were calculated from the Maximum Entropy Method (MEM) developed by Potton *et al.* [23] for Irena modelling macros [136].

3.3.4 Transmission electron microscopy (TEM)

Transmission electron microscopy (TEM) analysis was used to provide a “visual” confirmation of the morphological information obtained on the platelet dispersion and distribution from the WAXD data which lacks the ability to characterize

disordered intercalated or exfoliated structures due to the absence of scattered intensity peaks for those morphologies [137]. Therefore, TEM analysis, as a visual confirmation, is usually used in conjunction with WAXD data.

TEM was carried out on the samples with MMT to determine the extent of MMT dispersion. TEM was performed on ultra-thin sections at JEM-2100 microscope (JEOL, Tokyo, Japan), operating at an accelerating voltage of 200 kV. Oven-dried ribbon sample was sectioned at room temperature with diamond knife at Leica Ultramicrotome (EM UC7, Tokyo, Japan). The obtained sections, 100nm thin were sandwiched between two 400-mesh copper grids for TEM observation.

3.3.5 Fourier Transform Infrared Spectroscopy (FTIR)

Infrared Spectroscopy is a technique based on vibrations modes of atoms in a molecule and sensitive to the chemical composition environment. The Fourier transform infrared spectra (FTIR) are called as the footprint for bonds and atoms for specific material according to analysis of the corresponding absorption peaks located at different frequencies. Qualitative analysis about bonding formation/breakage can be rapidly drawn from related spectra due to the uniqueness of various bonding and elements. These advantages ensure FTIR as the rapid, economical and non-destructive technique to be used for nanocomposite characterization.

FTIR of all the samples were recorded in PerkinElmer 400 spectrometer using standard accessories in the range of 4000cm^{-1} - 515cm^{-1} for 74 scans.

3.3.6 Differential Scanning Calorimetry (DSC)

Thermal transitions of polymers during heating and cooling cycle are usually studied by Differential Scanning Calorimetry (DSC), a widely used technique that measures the energy required for retaining zero temperature difference between measured sample and the reference [138].

DSC measurement was performed on Perkin Elmer DSC 6000. About 25mg of dried ground sample was placed in an aluminium sample sealed pan. The sample was heated from -50°C to 250°C at a heating rate of 5°C /min, kept at 250°C for 1 minute followed by cooling down to 25°C at 10°C /min. The T_g was taken as the inflection point of the increment of specific heat capacity. T_m was obtained for analysis as well.

3.3.7 Nuclear Magnetic Resonance (NMR)

Dry powder sample of starch nanocomposites were dissolved in DMSO-d_6, which is a popular solvent for starch-based in solution NMR measurement and the treatment of a nanocomposite with DMSO-d_6 does not affect the structural characteristic for starch biopolymer [139] before proceeding to NMR measurement. 0.1gram of powder sample was dissolved in 1ml DMSO- d_6 with 10 minutes of stirring and then kept in oven for two days at 80°C to completely solubilisation of the nanocomposite [140]. The interaction between the plasticizers and the starch biopolymer could be studied via the NMR spectra.

The ^{1}H NMR data was collected from 32 scans on Bruker 500 at 70°C. The chemical shift scale was calibrated using the residual DMSO-d_6 signal at 2.549ppm [141]. The ^{13}C NMR spectra were collected on Bruker 500 at 25°C from 20000 scans. The chemical shift scale was calibrated using the residual DMSO-d_6 signal at 39.52ppm [141].

3.3.8 Positron Annihilation Lifetime Spectroscopy (PALS)

Positron Annihilation Lifetime Spectroscopy (PALS) technique has been applied in polymer science with the aim to understand the free-volume related phenomenon [93, 142-144]. PALS measurements for selected samples were carried out with Beamline 9940 at Centre for antimatter-matter studies (Canberra, Australia).

Positrons were implanted at an energy of 5 keV which ensured that the surface effects were minimized. We used a density of 1.2g/cc to investigate bulk behaviour up to 2000 nm. Each measurement consisted of 1×10^{6} detected annihilation events and took approximately 12 hours of measurement time. A fitting routine convoluted the instrument function spectra with a series of lifetimes to determine the best parameters using the in-house developed program, CAMSFIT V2.1. Two methods, variable and fixed lifetimes, were used for the current study. Fitting variable lifetimes is typically done with 2-5 lifetimes and returns discrete results. A fixed lifetime fit is typically done with 150 lifetimes and is able to return a distribution, usually around the results of the variable lifetime fit.

Chapter 4

Glycerol Plasticized High Amylose Nanocomposites

Chapter Outline

A ternary system involving starch, glycerol and MMT was studied via various characterization techniques such as Wide Angle X-ray Diffraction (WAXD), Fourier Transform Infrared Spectroscopy (FTIR), Differential Scanning Calorimetry (DSC), Water Sorption Isotherm, Proton Nuclear Magnetic Resonance (^{1}H NMR) and Small Angle X-ray Scattering (SAXS) via synchrotron radiation. Three binary systems (starch+MMT, starch+glycerol, glycerol+MMT) were studied separately followed by a complex ternary system (starch+glycerol+MMT) study.

The synergistic interactions within prepared nanocomposites were distinguished from the observed morphologies depending upon the combined effect of glycerol loading and MMT concentration. The observed experimental results could be categorized into three main groups, namely, intermolecular interactions (formation for hydrogen bonds, moisture content in prepared samples and chain/molecular mobility), morphological observations (achievable *basal spacing* of MMT, the growth of lamellar structure as evidenced from the raw 2-D SAXS pattern and SAXS profiles) and crystallization behaviour (T_g, T_m, crystalline domain size distribution and crystallization mechanism/crystal growth rate (analyses via Avrami Equation)). Relevant results are discussed in the corresponding sections below.

4.1 Starch+MMT system

The first binary system studied was the starch+MMT system. The characterization results are categorised into three main sections including intermolecular interactions (4.1.1), morphological observations (4.1.2) and crystallization behaviours (4.1.3).

4.1.1 Intermolecular interactions

4.1.1.1 Moisture Content Measurement (MCM)

The moisture content of the sample can provide important clues about the morphology formed within the composite. These measurements were carried out to correlate the moisture content with the MMT concentration and thus understand the strength of such interactions based on various MMT concentrations [85, 86, 105].

Table 4-1 Moisture content, Basal spacing, Crystallinity, glass-transition temperature (T_g) and melting temperature (T_m) for PS, 2 wt % MMT and 4 wt % MMT.

Sample ID	PS	2 wt % MMT	4 wt % MMT
Moisture (%)	2.22	6.17	5.67
X_c*(%)	7.48	8.23	12.5
T_g (°C)	49.5	60.2	69.0
T_m (°C)	219	211	204
basal spacing (Å)	-	16.53	18.12
Δd** (Å)	-	4.83	6.42

*crystallinity calculated from the method described in Ref [147]

** $\Delta d = d_{samples} - d_{pristine\ MMT}$

As shown in Table 4-1 and based on the well-known tortuous path way theory for water molecules in nanocomposites, the samples with MMT retained higher amount of moisture compared to the PS sample. The moisture content for the 2 wt % MMT, 4 wt % MMT and PS was 6.17%, 5.67 and 2.2%, respectively. The decrease of moisture content observed in 4 wt % MMT sample (5.67%) when compared to 2 wt % MMT sample (6.17%) directly indicated the stronger interactions between starch and MMT at a MMT-rich scenario which resulted in a relatively smaller amount of hydrophilic sites for retaining moisture.

4.1.1.2 Fourier transform infrared spectroscopy (FTIR)

The direct evidence of hydrogen bonding formation was obtained from the FTIR spectra depicted in Figure 4-1.

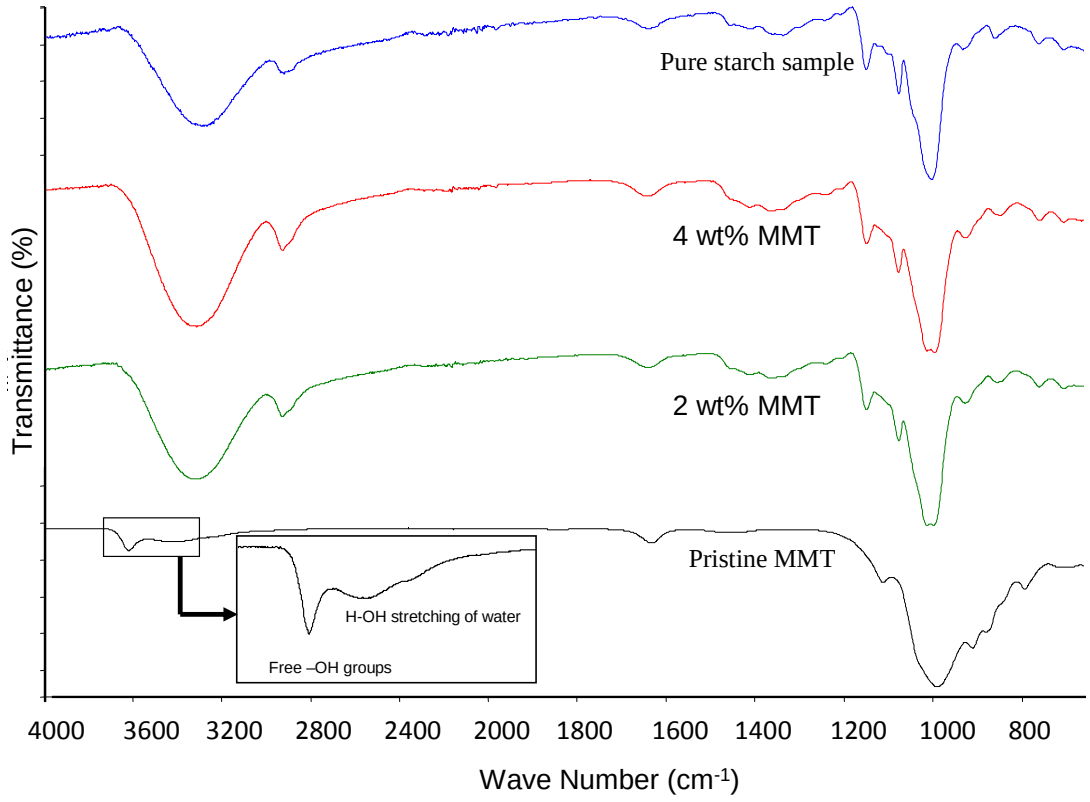

Figure 4-1 FTIR results for PS, pristine MMT, 2 wt % MMT and 4 wt % MMT samples.

As shown in Figure 4-1, the band presenting the free hydroxyl groups in MMT (inset window of Figure 4-1) shifted to a lower wave number after extrusion. This clearly indicated the occurrence of interactions between starch and MMT platelet surface, and a similar finding was reported in Field *et al.*'s work [145]. Furthermore, the disappearance of the broader peak of H-OH stretching of water (inset window in Figure 4-1) around 3234cm^{-1}- 3486cm^{-1} indicated the replacement of free water in the interlayer of pristine MMT by starch chains during the extrusion processing [146] and this corroborated with the WAXD results (Page 51) that the *basal spacing* expanded to different extent in the nanocomposites samples depending on the MMT loading.

4.1.2 Morphological observations

4.1.2.1 Wide Angle X-ray Diffraction (WAXD) results

As revealed in the WAXD patterns, Figure 4-2, the characteristic peak for basal spacing of the MMT (001 peak) shifted to a lower angle to different extent dependent on the loading of MMT, when compared to pristine MMT. Such observations

indicated that the starch chain had intercalated into the gallery of MMT and forced apart the MMT platelets. This was a result of the interaction between the hydrophilic pristine MMT and starch polymer chains since the Δd ($\Delta d = d_{samples} - d_{pristine\ MMT}$) values reasonably agreed with the molecular size of starch fragments (Table 4-1).

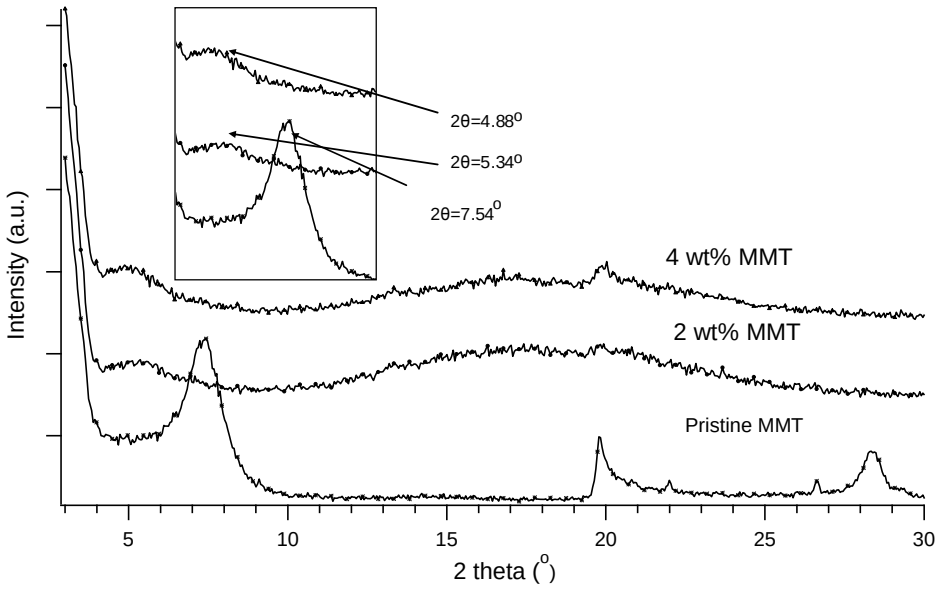

Figure 4-2 WAXD results for Pristine MMT, 2 wt % MMT and 4 wt % MMT samples.

4.1.2.2 Small Angle X-ray Scattering (SAXS)

The growth of lamellar structure upon addition of MMT was evidenced from the raw 2-D SAXS patters of corresponding samples, Figure 4-3.

Greater ellipticity, presenting the electron heterogeneities within the samples (Figure 4-3), was observed in the high-MMT loading samples which indicated the strong interactions between MMT and starch and induced the formation of a more dense and ordered polymeric network. As shown in Figure 4-3, the 2 wt % MMT / 4 wt % MMT samples also showed relatively higher intensities, and these observations supported the argument that the presence of MMT favoured the growth of lamellar morphology within the polymeric network.

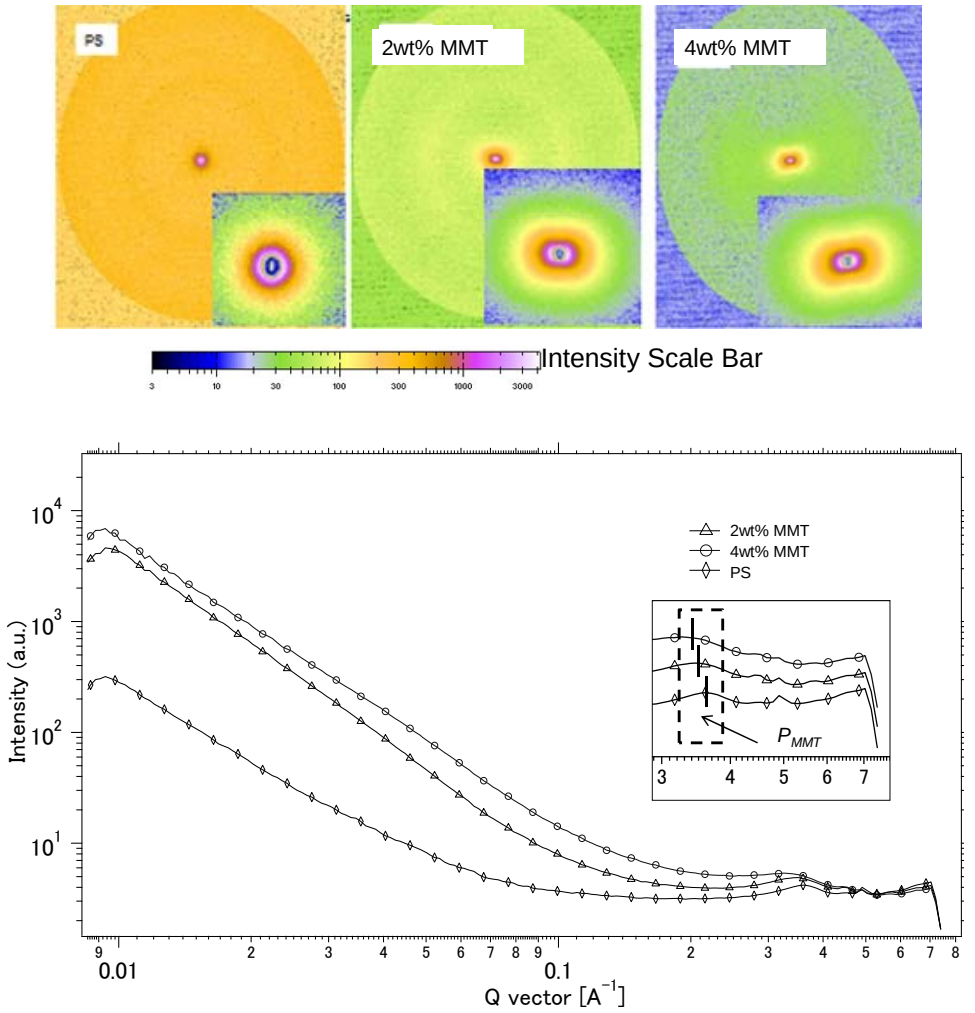

Figure 4-3 Raw 2-D SAXS patterns for PS, 2 wt % MMT and 4 wt % MMT samples and the corresponding SAXS profiles.

The deviation of ellipticity for various samples could be related to the crystallization behaviours within different samples, which will be detailed in the next section (Page 54).

The characteristic peak (as seen in the inset window of Figure 4-2 and Figure 4-3) for the *basal spacing*, denoted as P_{MMT}, shifted to a lower angle which corresponded to an increase in the *basal spacing* after extrusion. P_{MMT} (2 wt % MMT) was allocated in Q=0.423 $Å^{-1}$ (data are shown in the ternary system discussion section, Table 4-7), which indicated that the starch chain successfully penetrated into the gallery of MMT platelets, and such conclusions have been put forward in the literature [60, 103]. This fact mutually supported the case for well intercalated or intercalated/exfoliated systems as evidenced from the WAXD characterization (Page 51).

4.1.3 Crystallization behaviours

4.1.3.1 Crystallinity

From Figure 4-1, the crystallinity values were calculated on the basis of peak fitting procedures that was put forward by Lopez-Rubio *et al*. [147] where they illustrated that this method, widely used for synthetic polymer, was better in reflecting the crystalline content of starch than the traditional two-phase model. The method used took into account irregularities in crystals that are expected to co-exist in semi-crystalline materials and avoid the underestimation (two-phase method did not consider the diffuse scattering from non-perfect crystalline structure) of the crystalline content. *Igor* software package (Wavemetrics, Lake Oswego, Oregon) was used for curve fitting. The fitted coefficients are calculated based on minimized value of *Chi*-square using the Levenberg-Marquardt algorithm. Each fitting procedure was repeated eight times with different initial inputs to check for data reproducibility. As Lopez-Rubio *et al.* [147] suggested, Gaussian shape had been confirmed to reflect the best fitting results even with poor initial guess, and the crystallinity for samples can be calculated as, $X_c = \frac{\sum_{1}^{n} ACi}{At}$, where AC_i is the area under each fitted crystalline peak with index i (please note that the first peak appeared in the WAXD patterns of nanocomposites samples had not been treated as crystalline peak since this peak was the characteristic peak for the *basal spacing* of MMT) and At is the total area under the WAXD pattern. The averaged crystallinity results are shown in Table 4-1.

The well-defined nucleating effect of nanoparticles which had been reported in the literature was observed in the current study. The crystallinity value of 2 wt% MMT and 4 wt% MMT samples was calculated to be 8.23% and 12.5%, respectively, both of them being higher than that of the PS sample (7.48%).

4.1.3.2 Differential Scanning Calorimetry (DSC)

The presence of MMT significantly influenced the crystallization behaviour of starch polymer. Two key parameters, T_g and T_m, were obtained via DSC, Table 4-1. Within expectation, the T_g value for MMT-contained samples increased from 49.5^{o}C (PS) to 60.2^{o}C (2 wt% MMT) and 69^{o}C (4 wt% MMT). Such results highlighted the strong interactions between starch and MMT, thus mutually support the findings in SAXS

measurements (Page 52). The greater ellipticity from the MMT-contained samples which present the formation of a denser polymeric network which could be seen from the high T_g value of corresponding samples. Another evidence was the decrease of T_m value upon increasing MMT, 211^{o}C (2 wt% MMT) and 204 ^{o}C (4 wt% MMT). This was because of the relatively more ordered structure formed in the 4 wt% MMT sample, thus the polymeric chains were slightly easier to break and at a glimmer lower temperature as observed in the DSC measurements.

Other reasons included the reduced crystalline size and the presence of crystal imperfections in the presence of MMT/starch. Interactions from the MMT and starch suppressed the crystallization since the silicate platelet could prevent the starch chains from reorganising. However, it should be noted that the presence of MMT can allow smaller crystalline fractions to grow due to possible nucleating effect and this was manifested by the observed larger crystallinity values for MMT-contained samples (Table 4-1).

The DSC thermograms exhibited typical features of a semi-crystalline polymeric system in terms of the glass transitions and crystallite melting endotherm. Figure 4-4 compared the typical heat flow curve for the PS, 2 wt % MMT and 4 wt % MMT sample, which emphasised the impact of the addition of MMT on the crystalline phase of the bionanocomposites.

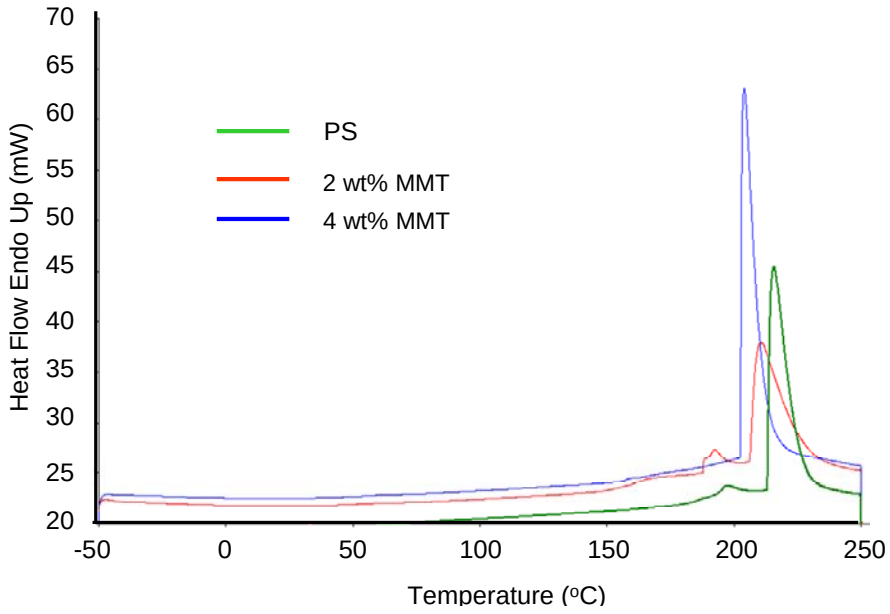

Figure 4-4 DSC endotherm curves for PS, 2 wt %MMT and 4 wt %MMT.

As shown in Figure 4-4, the addition of MMT predominantly affected the packing of the crystalline domain (peak shape changed) by decreasing the T_m of relevant samples. Such observation revealed that the mechanism and crystal development within the samples were significantly affected. This will be further discussed in the following section via Avrami Equation.

4.1.3.3 Avrami Equation analyses based on DSC results

As widely known, in polymer–clay systems, the endotherm peak can provide information on the crystalline phases in the nanocomposites when the clay platelets have nano-scale interactions. To gain an improved understanding of these interactions on the bionanocomposites' crystallization behaviour, the crystallisation process was modelled as a combination of several infinitesimal isothermal steps [24]. The Avrami equation (Eq 4-1), which is widely applied in investigating crystallisation behaviours of polymer systems [24], was employed to study the non-isothermal crystallisation kinetics of the prepared bionanocomposites [137].

$$X_t = \int_{t_0}^{t} \frac{dH_c}{dt} dt \Big/ \int_{t_0}^{t_\infty} \frac{dH_c}{dt} dt \qquad \text{Eq 4-1}$$

All the curves had a partial sigmoid shape, and the analysis of the development of relative crystallinity could be done using $X_t = 1 - \exp(-kt^n)$. A plot of *log[−ln(1 − Xt)] vs. log(t)* could provide *n*, the value depending upon the mechanics of nucleation and on the form of crystal growth, and *k*, a rate constant containing the nucleation and growth parameters. Nearly all samples demonstrated one prominent linear region (Figure 4-5). The value of modelled parameters *n* and *k* is presented in Table 4-2.

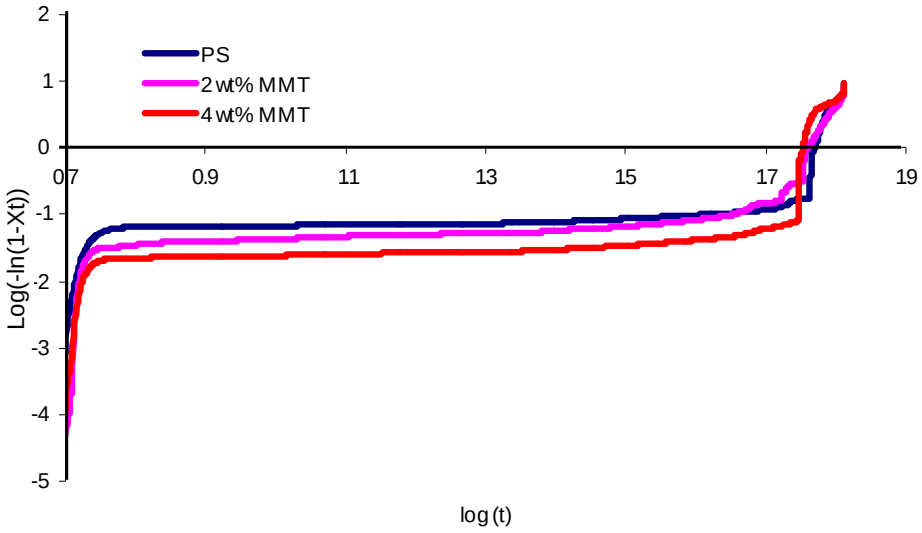

Figure 4-5 Decay of the overall crystallinity based on the non-isothermal crystallization kinetics analyses using the modified Avrami equation for PS, 2 wt % MMT and 4 wt % MMT samples. All plots were corrected for the baseline.

It was shown in Figure 4-5 that the presence of MMT seemed to have no obvious effect on the onset temperature for crystallisation. However, the presence of MMT affected the crystallization mechanism within corresponding samples. As read from Table 4-2, the additions of MMT greatly affected the *n* values (0.48 for PS and 0.85 for 2 wt % MMT and 0.77 for 4 wt % MMT sample), presented the mechanics of nucleation and form of crystal growth, but had little effect on the crystal growth rate parameter *k* since PS, 2 wt % MMT and 4 wt % MMT samples showed a similar *k* value, Table 4-2.

Table 4-2 The exponent n and the factor k obtained for PS, 2 wt % MMT and 4 wt % MMT sample from a non-isothermal crystallization analysis using the modified Avrami equation.

Sample ID	*n*	*k*
PS	0.48	-1.47
2 wt% MMT	0.85	-1.44
2 wt% MMT	0.77	-1.39

This behaviour was within expectation since the addition of MMT provided extra nucleation sites for the starch polymer chains to crystallize in a different form depending on the MMT orientation. However, further increase of MMT did not bring

significant effect on both the *n* and *k* values (comparable *n* and *k* value for 2 wt % MMT and 4 wt % MMT samples).

4.2 Glycerol+MMT system

The interactions between glycerol and MMT were studied by analysing the samples that were prepared at different glycerol/MMT ratio via sonication. FTIR and WAXD had been carried out to characterize the intermolecular interactions and morphological features of this binary system. The experimental results and discussions are presented as follows.

4.2.1 Intermolecular interactions

As revealed from the FTIR result, *Figure 4-6*, the glycerol molecular had successfully intercalated into the 'gallery' of the stack-like MMT via hydrogen bonding which can be proved by the shift, to a lower angle, of free 'OH' groups band vibration (inset window in Figure 4-6) of MMT [148]. The obvious broadening of peaks at 3283 cm^{-1} revealed that glycerol attributed to the increase in the number of oscillation modes, which illustrated the hydrogen bonding interactions between MMT and glycerol [98].

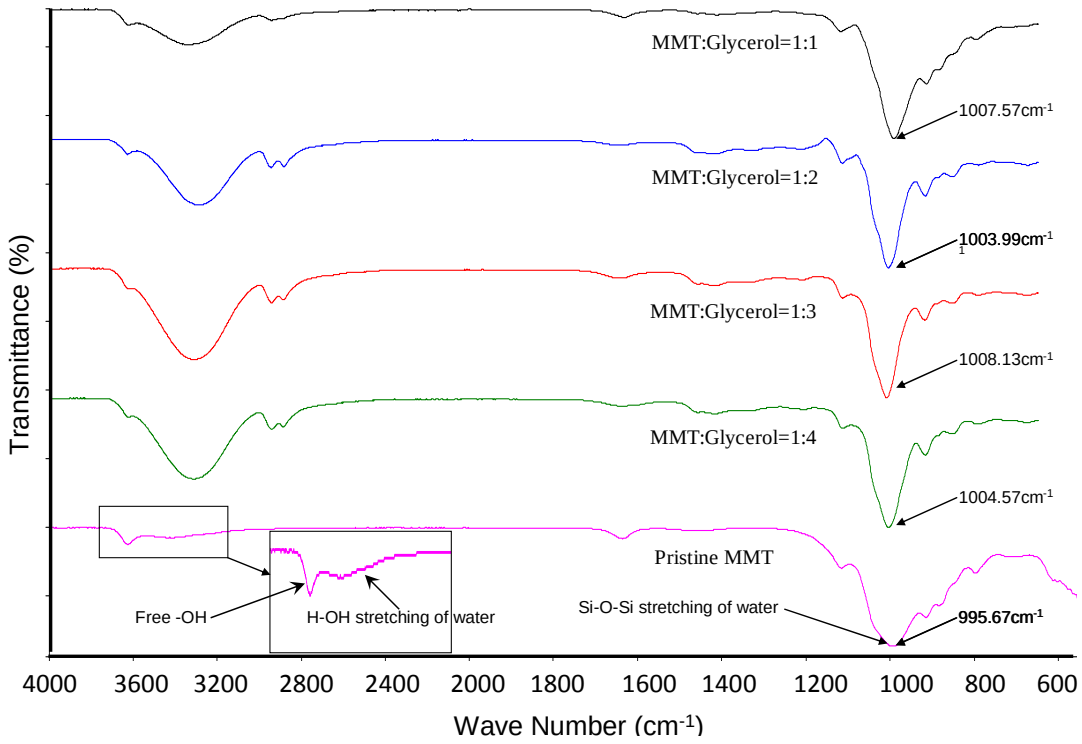

Figure 4-6 FTIR results for MMT: glycerol samples at 1:1, 1:2, 1:3 and 1:4 ratio.

The shift of Si-O-Si vibration peak from 995.67cm^{-1} to a higher frequency after interaction with glycerol showed a decrease in the packing density of the system, which was a characteristic of the expanding MMT's *basal spacing* [149]. Shorter and stronger bonds gave a stretching vibration at higher energy end (shorter wavelength) of IR spectrum. In other words, on the basis of the harmonic oscillator model, it was concluded that the lower the peak frequency, the stronger the interaction [62]. It was observed that the characteristic peak (3200-3300 cm^{-1}) for hydrogen bonds shifted to a smaller frequency in all test samples upon increasing the glycerol amount, which indicated that the interaction between MMT and glycerol became stronger. All peaks excluding free 'OH' peak shifted to a higher frequency than that of MMT or glycerol. This indicated that new hydrogen bonds were formed between the MMT and glycerol [150].

4.2.2 Morphological observations

Comparing the WAXD results of all samples (Figure 4-7), the minimum and maximum value of *basal spacing* occurred in 1:1 MMT: glycerol sample (14.2 Å) and 1:2 MMT: glycerol sample (17.8 Å). The small *basal spacing* value of 1:1 sample could be explained as this; when the glycerol amount was low, that water/MMT interaction was stronger than glycerol/MMT, thus the Δd value of 1:1 sample showed a value comparable to that of the size of water molecules. The value of *basal spacing* showed an inverse proportionality to the glycerol loading except in the 1:1 ratio sample, where MMT:glycerol (1:2 and 1:3) achieved a *basal spacing* of 17.8 Å, but this value decreased to 17.4 Å for 1:4 MMT:glycerol sample.

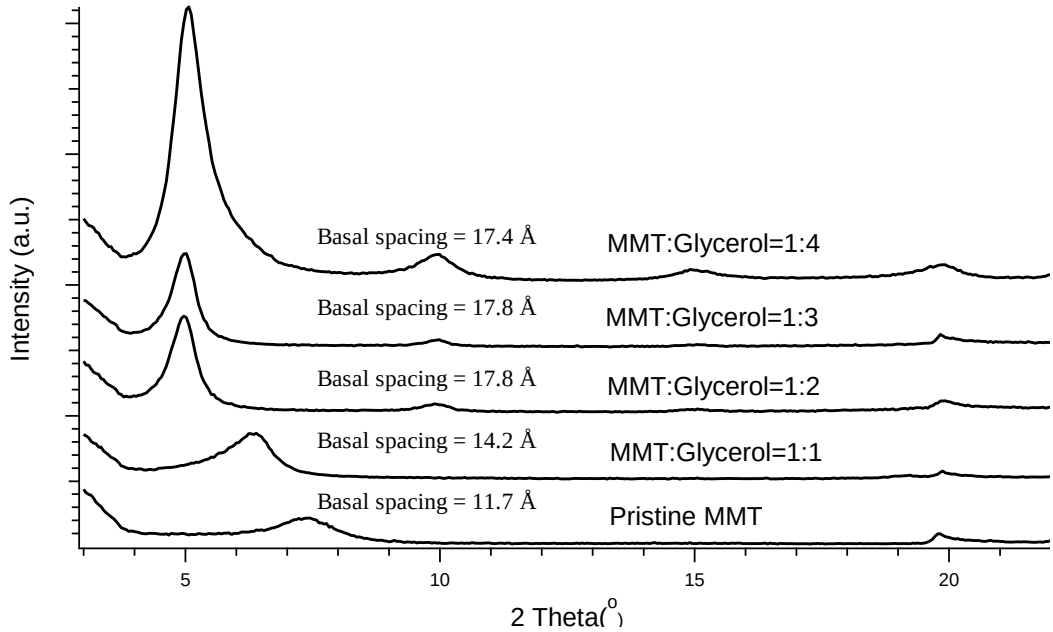

Figure 4-7 WAXD Patterns for MMT: glycerol samples at 1:1, 1:2, 1:3 , 1:4 ratio and Pristine MMT.

The glycerol exhibited some hinderance effect on the 'gallery' expansion of MMT at a higher amount, where the *basal spacing* value decreased as the amount of glycerol increased. This might reflect the competitive interaction characteristic within the hydrophilic system which will be detailed in the ternary system discussion (Page 61).

It can be concluded that the *basal spacing* change (*Δd* value) depended on the molecular size of the plasticizer present. A simple hypothesis can be put forward based on the molecular size, and the extent of *basal spacing* change. For glycerol, *Δd* approximately equalled to the average size of glycerol which meant that the plasticizer molecule had been trapped between two MMT platelets. This could be supported by the fact that all the glycerol samples exhibited similar *Δd* to the glycerol molecule size (except 1:1 sample). Such hypothesis will be further proven in the discussion of xylitol (*Chapter* 5) and sorbitol-plasticized systems (*Chapter* 6).

4.3 Starch+Glycerol system

The last important binary system was the system without nanoparticles, starch+glycerol system. Two samples were produced with 10 wt% and 20 wt% glycerol according to the DOE. The obtained characterization results were presented as follows.

4.3.1 Intermolecular interactions

4.3.1.1 Water Isotherm

Water isotherm is one of the most important and efficient method to study the interactions between starch and glycerol as widely applied in the food engineering industry [151, 152]. Accordingly, the water isotherm for the prepared samples was determined and further mathematically evaluated using GAB model for a better understanding of the interaction behaviours within this binary system.

The discussion here is applicable to the samples that were equilibrated in humidity chambers after the extrusion processing, thus these samples had representative amounts of structural water within the polymer at equilibrium. The experimental results indicated a maximum at m% $\approx$ 0.35 dry basis for PS whereas the GAB empirical analysis (Figure 4-8) showed a maximum at m% $\approx$ 0.282 for the structural water (PS). It can be seen that until $a_w \approx 0.78$, the GAB prediction closely related to the experimental findings; beyond that the deviation was becoming more and more obvious with increasing water activity. This can be attributed to a structural separation of the starch chains and the amylopectin structures which allowed increase in the structural water.

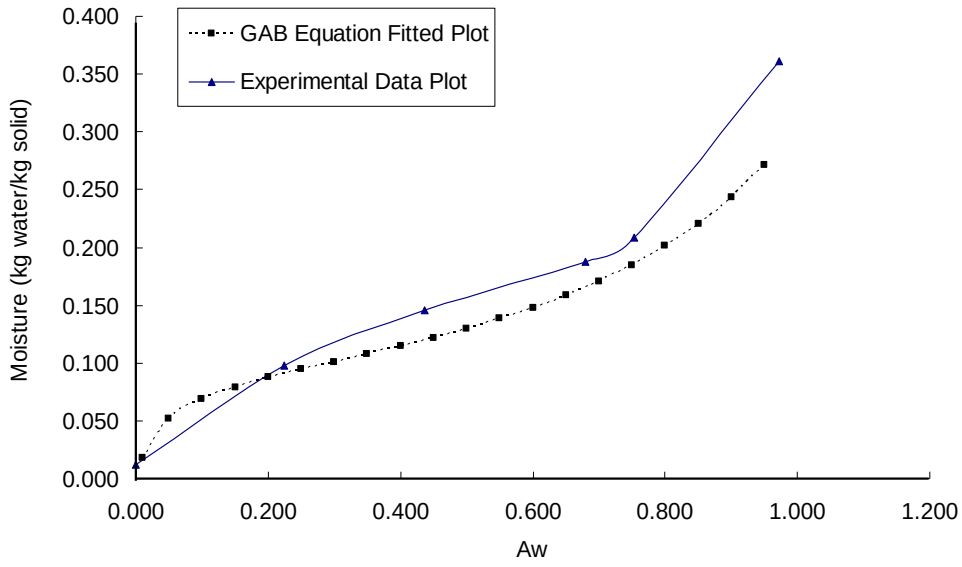

Figure 4-8 Water-sorption isotherm of PS; experimental data and GAB model fitting plot.

An ‘inversion’ phenomenon (Figure 4-9) was observed where higher glycerol loading samples retained lower amount of equilibrium moisture at low a_w values, but as the a_w increased, this relationship between the equilibrium structural water and the glycerol content was inversed. The inversion phenomenon which was due to the hydration effects within different polymers structures, such as linear starch and branched amylopectin has been reported by earlier researchers [153].

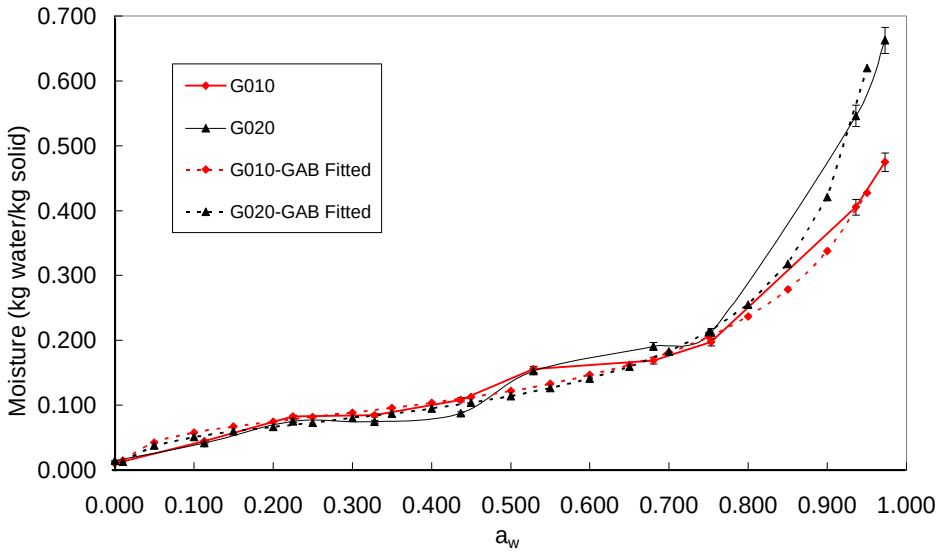

Figure 4-9 Water isotherm results and GAB model fitted plots for G010 and G020.

4.3.1.2 GAB Model for isotherm data

Corresponding parameters of GAB model evaluation are estimated via a non-linear least square regression routine. The GAB equation analysis was completed to understand the isotherm behaviour; relevant results are shown in Table 4-3.

Table 4-3 GAB Fitting Parameters for PS, G010 and G020 (R^2 > 0.88).

Name	w_m	C	K
PS	0.092	46.243	0.669
G010	0.072	28.490	0.878
G020	0.063	26.955	0.946

In Table 4-3, parameter w_m denotes the moisture content value that corresponds to a ‘monomolecular layer’ of water to cover the whole polymer surface. The *K* parameter increased with increasing plasticizer content. This indicated that in terms of the equilibrium between the starch and glycerol, greater glycerol content can be accommodated within the starch matrix by increasing the temperature. The molar

sorption enthalpy values, highlighted by parameter C show that there is no significant effect as glycerol content was increased.

Though the GAB model showed good agreement with the experimental data, it could not account for the region of water activity between 0.5 - 0.7 (inversion region) where the addition of glycerol showed a prominent 'step-change'. A possible reason for this could be the complex ternary interactions among starch-water-plasticizer. Further investigations were carried out to ascertain and understand this behaviour.

4.3.2 Morphological observations

4.3.2.1 Small Angle X-ray Scattering (SAXS)

The growth of lamellar structure upon addition of glycerol was evidenced from the Raw 2-D SAXS diffraction patterns, Figure 4-10. As shown in Figure 4-10, the scattering patterns (shape and the intensity) of the samples were greatly influenced by the presence of glycerol as well. The shape of the scattering pattern changed from circular (PS) to elliptical (G020) similar to the observations found upon MMT addition. The transition from a circular to an elliptical pattern indicated a better defined orientation of the crystalline domains [154]. Such changes in the diffraction pattern reflected the relevant changes at the microstructural level.

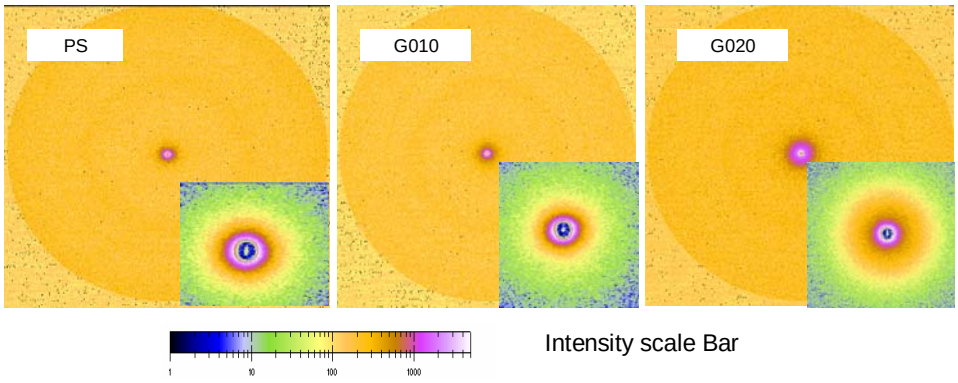

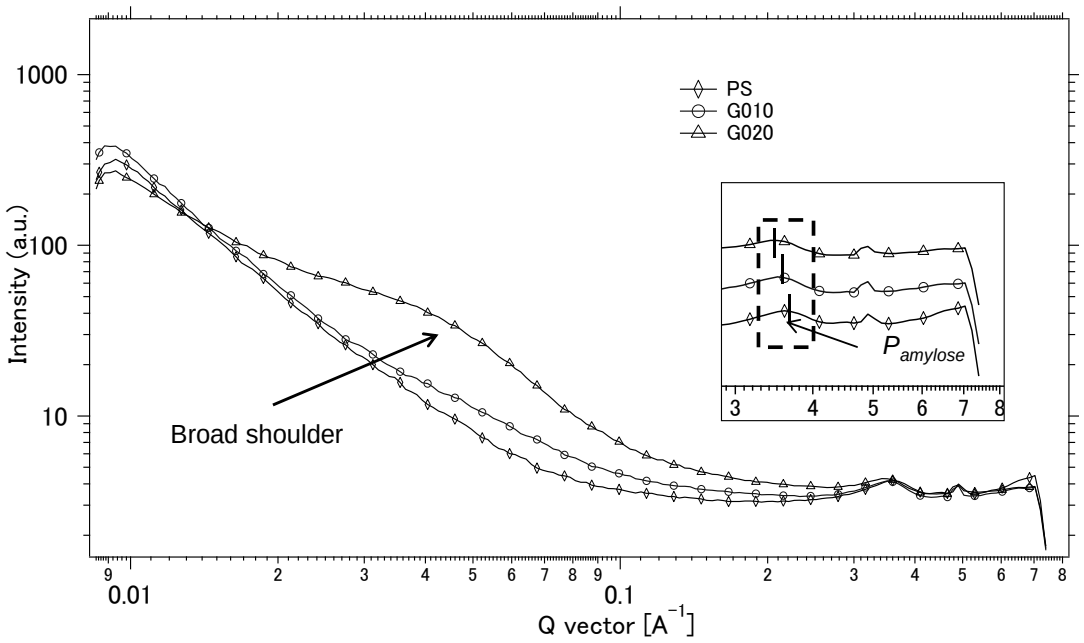

Figure 4-10 The SAXS profiles for PS, G010 and G020 generated from NIKA data processing software.

The scattering intensities from different samples resulted from their inherent electronic density differences [155] and upheld the presence of heterogeneities within the network structure. As shown in Figure 4-10, similar to the finding in starch+MMT system, the G010/G020 samples showed relatively higher intensities, and these observations supported the argument that the presence of glycerol favoured the growth of lamellar morphology within the polymeric network.

The characteristic peak for starch polymer denoted as (P_{starch}) seen from the inset widow of Figure 4-10, decreased (from 0.357 to 0.352 Å^{-1}) with increasing glycerol concentration from 10 wt% to 20 wt%. This shift suggested the formation of increased crystalline order due to the greater starch-glycerol interaction.

Another unique observation for G020 was the 'shoulder' around Q≈0.04-0.05 Å^{-1}, shown in Figure 4-10. However, this structure was observed in all the high moisture samples (Page 80). Such a 'shoulder' typically corresponds to the long periodic structure of processed starch polymer [156] for the samples with higher equilibrium moisture. However, in G020, such glycerol successfully replaced the water molecules in starch/water interactions at high glycerol concentration and contributed to the preservation of the long periodic structure of starch polymer.

4.3.3 Crystallization behaviours

4.3.3.1 Differential Scanning Calorimetry (DSC)

The DSC results, Table 4-4 , indicated that the addition of glycerol undoubtedly decreased the T_g and T_m values. T_g values for glycerol-loaded samples decreased from 49.5 (PS) to 40.7 (G010) and 40.3 (G020).

Table 4-4 glass-transition temperature (T_g) and melting temperature (T_m) for Ps, G010 and G020.

Sample ID	PS	G010	G020
T_g (°C)	49.5	40.7	40.3
T_m (°C)	219	184	171

Such changes were strongly related to the interactions between starch and glycerol which altered the polymeric network. It was suggested that addition of glycerol at a loading less than its antiplasticization 'threshold' value would lead to an even firmer polymeric network and thus increased the T_m in G010 when compared with G020. Meanwhile, the T_g was decreased by the typical plasticization effect from glycerol. Such observations mutually agreed with the obtained SAXS results, Figure 4-10, where the addition of glycerol in favour of the growth of lamellar structure in the sample (scattering patterns changed).

4.3.3.2 Avrami Equation analyses based on DSC

Furthermore, the Avrami equation analyses results as shown in Table 4-5, highlighted the unique behaviour in G020, where both the *n* and *k* value were significantly influenced. Such findings were unlike what we discussed in the starch+MMT system where there was no obvious further effect on *n* of increasing MMT. The manifested the changes in *n* and *k* value of 20 wt% glycerol loaded sample was a direct indicator of the stronger starch/glycerol interactions.

Table 4-5 Exponent n and the factor k obtained from a non-isothermal crystallisation analysis for G010 and G020.

	PS	G010	G020
n	0.48	0.43	0.29
k	-1.47	-1.07	-0.87

4.4 Starch+Glycerol+ MMT nanocomposite system

4.4.1 Intermolecular interactions

4.4.1.1 Moisture Content Measurement

Moisture content measurements can indirectly indicate the strength and direction of interaction between the starch-glycerol and starch-MMT. The moisture content of the prepared samples was presented in Table 4-6.

Table 4-6 Moisture content, basal spacing, crystallinity, glass-transition temperature and T_m for glycerol-plasticized nanocomposites.

Sample ID	G105	G115	G210	G220	G305	G315
Moisture (%)	2.79	1.97	3.31	2.02	4.74	3.15
X_c*(%)	11.39	9.62	9.28	8.08	10.1	6.86
T_g (°C)	44.94	43.5	46.7	44.8	43.2	39.5
T_m (°C)	215	238	146	242	142	186
basal spacing (Å)	16.96	17.92	17.72	17.82	17.52	17.92
Δd** (Å)	5.26	6.22	6.02	6.12	5.82	6.22

*crystallinity calculated from the method described in Ref [147].

** $\Delta d = d_{samples} - d_{pristine\ MMT}$

As shown in Table 4-6, addition of glycerol significantly decreased the moisture content; the moisture content for G200 and G210 was 6.39% and 3.31%, respectively. This decrease was attributed to the strong interactions between glycerol and starch matrix where some immobilized water molecules were replaced by glycerol molecules. Due to relatively stronger starch-glycerol interaction, increasing the glycerol concentration decreased the moisture content regardless of the MMT amount. However, if glycerol concentration was fixed, it was found that the moisture content was proportional to the MMT loading. The high moisture content from the high-MMT samples was considered to be a result of greater resistance for moisture migration due to the well-known tortuous pathway theory for water molecules in nanocomposites.

4.4.1.2 Fourier Transform Infrared Spectroscopy (FTIR)

The FTIR results for glycerol-plasticized nanocomposites are shown in Figure 4-11. The typical saccharide bands region located across 1180cm^{-1} - 953cm^{-1} are often considered as the vibration modes of C-C and C-O stretching and the bending mode

of C-H bonds [157]. These bands turned out to be the most intense in the FTIR-spectrum. Bands at 3300cm^{-1} , 1630cm^{-1} and broader peaks centred around 2200cm^{-1} were typical bands associated with individual biopolymer components in addition to the contributions of the water absorptions [158].

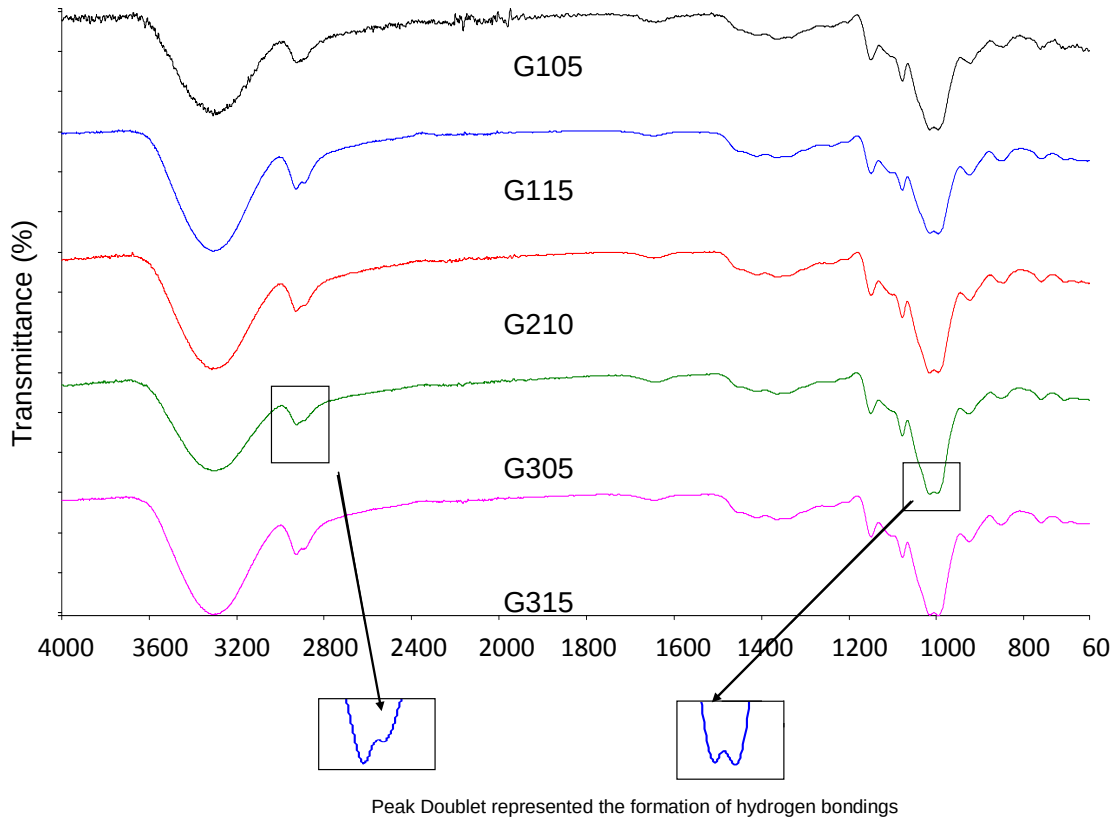

Figure 4-11 FTIR spectra for glycerol-plasticized nanocomposites.

The shift of band 3627cm^{-1}, characteristic band for the free OH group of pristine MMT surface, to a lower frequency, 3302cm^{-1} indicated the occurrence of interactions between starch and MMT platelet surface. Comparing the spectra of pristine MMT (Figure 4-1) and the nanocomposite (*Figure 4-11*), the disappearance of the broader peak of H-OH stretching of water around 3234cm^{-1}- 3486cm^{-1} indicated the replacement of free water in the interlayer of pristine MMT by glycerol/starch during the extrusion processing [146] and this corroborated the WAXD results that the *basal spacing* expanded to different extent in all the nanocomposite samples (Table 4-6).

The presence of new and stronger hydrogen bonding could be evidenced from the double peaks at 2919cm^{-1}-2887cm^{-1} and 999cm^{-1}-992cm^{-1} in the nanocomposites samples when compared with PS [159], inset window of Figure 4-11. The double peak of O-C stretching band at 999cm^{-1}-992cm^{-1} results from bending both 'O' of C-O-H and 'O' of anhydrous glucose ring in starch molecules [160]. Therefore, it could be concluded that the extrusion of native starch to nanocomposite included the formation of hydrogen bonds and ternary interactions in starch/glycerol/MMT system.

4.4.1.3 ^{1}H NMR

The peak intensity of the ^{1}H NMR spectrum was directly related to the mobility of corresponding component. As illustrated in

Figure *4-12*, the peak located in 4.3ppm and 4.1ppm, were assigned to starch and glycerol, respectively. Taking one characteristic peak from each component starch and glycerol spectra denoted as I_{starch} and $I_{glycerol}$. When comparing the spectra from samples contained different amount of glycerol; it is worthy to note the ratio of $I_{glycerol}$ and I_{starch} increasing upon the glycerol concentration. However, $I_{glycerol}$ was unexpectedly observed to be smaller than I_{starch} in G105. This indicated that the mobility of glycerol molecules was unexpected lower than that of starch chains in G105. In other words, the glycerol molecules were strongly 'locked' within a firm polymeric network. And the mobility of glycerol clearly increased when glycerol concentration increased from 5% to 15%. These observations supported the hypothesis that a relatively loose morphology was form in a low plasticizer scenario; such hypothesis will be further discussed in the integrity analyses Chapter (*Chapter 7*).

Meanwhile, unlike the addition of glycerol which resulted in some peak shift to a lower ppm, samples containing only MMT have no effect on the peak position of starch, and the same chemical shifts for PS and 2 wt % MMT were observed, *Figure 4-13*.

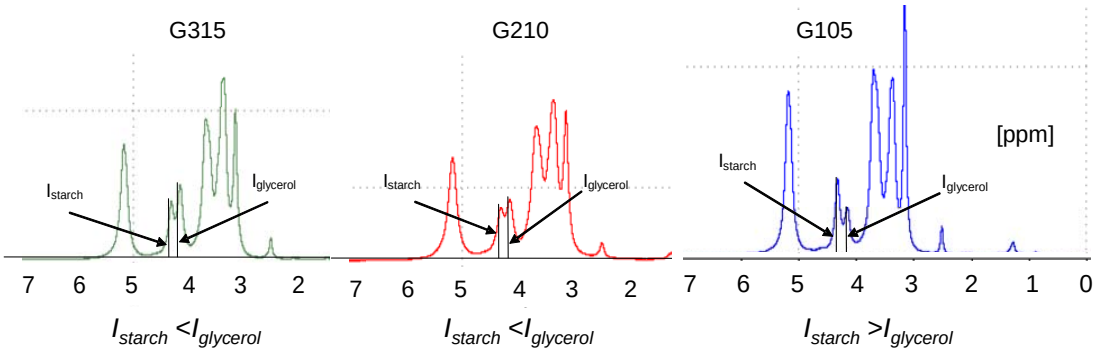

Figure 4-12 ^{1}H NMR spectra for samples with different amount of glycerol in DMSO-d_6 at 70℃.

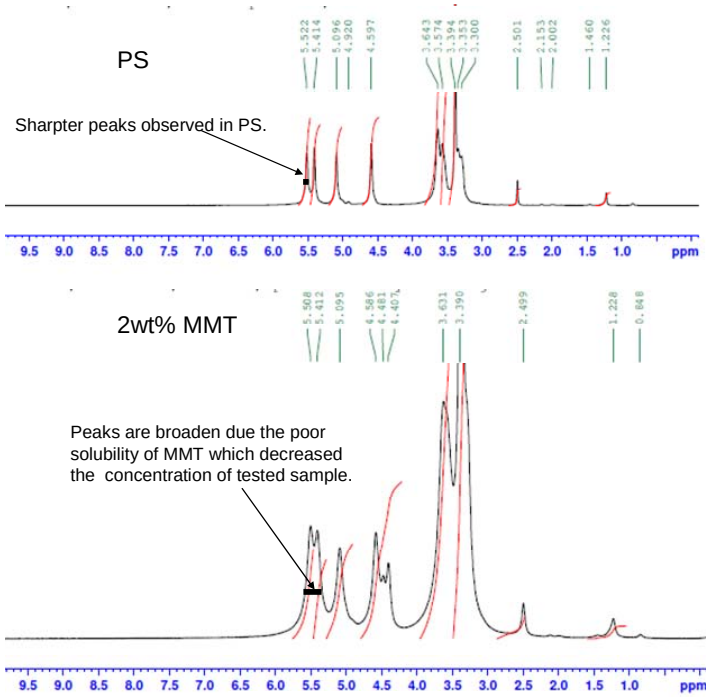

Figure 4-13 ^{1}H NMR spectra for PS and 2 wt % MMT in DMSO-d_6 at 70℃.

4.4.2 Morphology observations

4.4.2.1 Wide Angle X-ray Diffraction (WAXD) and Transmission electron microscopy (TEM)

The WAXD patterns for nanocomposites are shown in Figure 4-14 (a). When compared to the pristine MMT (*basal spacing* value of 11.70 Å), all the nanocomposite samples showed increased *basal spacing* values which was similar to the finding in binary systems. The expansion degree from various composites indicated the glycerol and starch chain had intercalated into the layer of MMT and

forced apart the MMT platelets depending upon the glycerol and MMT interaction. The TEM images for a representative sample (G305) clearly supported the statement that well intercalated composites with a higher ‘gallery spacing’ was achieved, Figure 4-14 (b). The influence of glycerol concentration on expansion of MMT *basal spacing* was revealed based on the loading of MMT, as shown in Table 4-6. Furthermore, the expansions of MMT gallery were mainly attributed to hydrophilic interactions of MMT particles, and the starch/glycerol hydroxyl groups, since the *∆d* values reasonably agree with the molecule size for glycerol/starch fragments (Table 4-6). It can be read from Table 4-6, that the MMT gallery spacing increased upon increasing the glycerol amount, e.g. the *basal spacing* value of G105 and G115 are 16.96 Å and 17.92 Å, respectively.

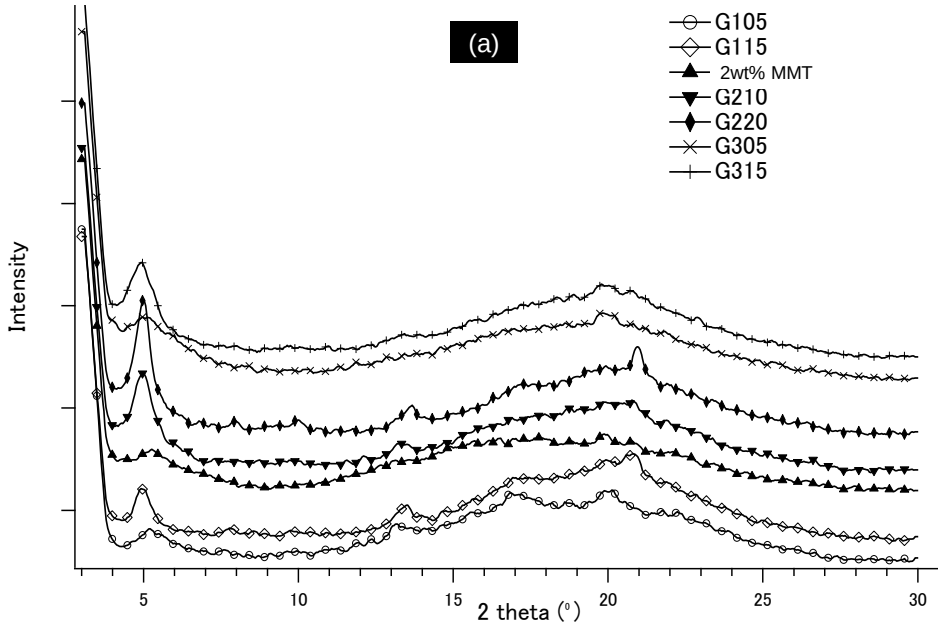

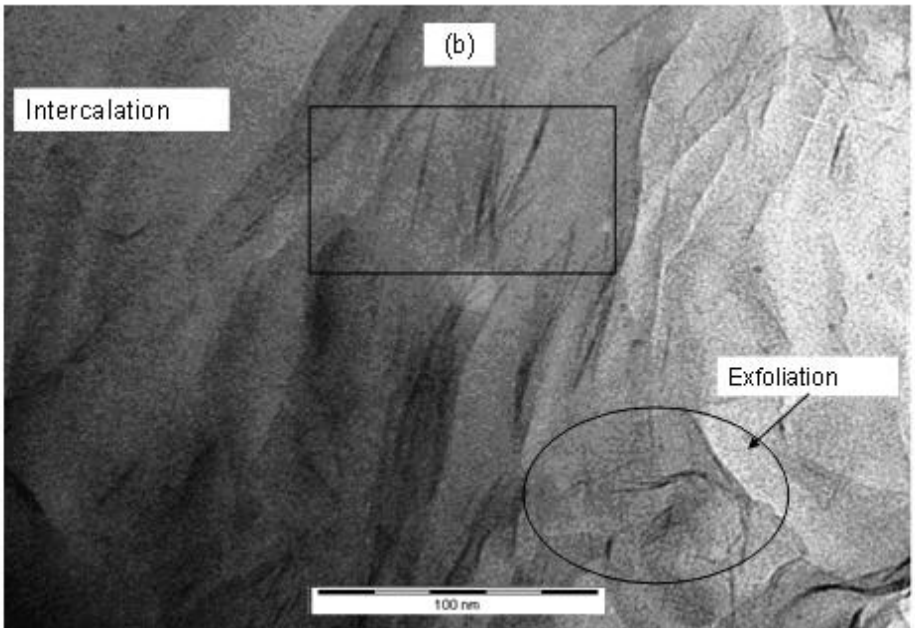

Figure 4-14 (a) WAXD patterns for glycerol-plasticized nanocomposites and (b) TEM images for G305-an intercalation/exfoliation co-existed morphology.

From the WAXD patterns, Figure 4-14 (a), the peak broadening observed with 5 wt% glycerol plasticizer (both G105 and G305) indicated a higher extent of exfoliation morphology in these samples. According to the theory of kinematical scattering, peak broadening is caused by either small crystal size or the presence of large amount of lattice defects [161]. In other words, the amount of free sites in the low-glycerol sample should be higher than the high-glycerol ones due to higher lattice defects. Considering the molecular modelling results (appendix) for glycerol/ starch/water system, the low-glycerol loading sample showed higher free volume. This was solid evidence that more free sites existed in the low glycerol loading samples.

It could be suggested that the broadening of WAXD peaks from the low-glycerol loading sample was primarily a result of relatively weak competitive interaction between glycerol-glycerol (under a scenario that lack of glycerol) and starch-MMT. Furthermore, the peak intensity indicated the total scattering from each plane in the crystal structure and directly related to the distribution of MMT platelets structure [162]. Therefore, lower intensity of low-glycerol sample also suggested a more random distribution of MMT in these samples.

Meanwhile, the WAXD results revealed that the (001) peak for MMT became sharper upon increasing the glycerol amount (Figure 4-14 (a)); which meant the exfoliations were limited. The possible reason for this behaviour could be that the higher glycerol concentration led to a stronger glycerol-glycerol interaction [8] which limited/competed with the MMT-glycerol or MMT-starch interactions, thus enhanced the intercalation rather than exfoliation (as seen by comparing the WAXD patterns for G105 (G305) and G115 (G315). It would be further supported by the DSC results in the following section where G105 (or G305) possessed lower T_m than G115 (or G315). Because a high T_m could result from either more hydrogen bonds formed between relatively low mobility starch and glycerol or a more dense polymeric structure (in this study). Under a glycerol-rich scenario, the enhanced glycerol-glycerol interactions led to the formation of denser polymeric network thus increasing the T_m of the sample.

4.4.2.2 Small Angle X-ray Scattering (SAXS)

The raw 2-D SAXS patterns for the ternary composites samples (starch+glycerol+MMT) are shown in Figure 4-15. Correspondingly, the SAXS profiles are presented in Figure 4-16.

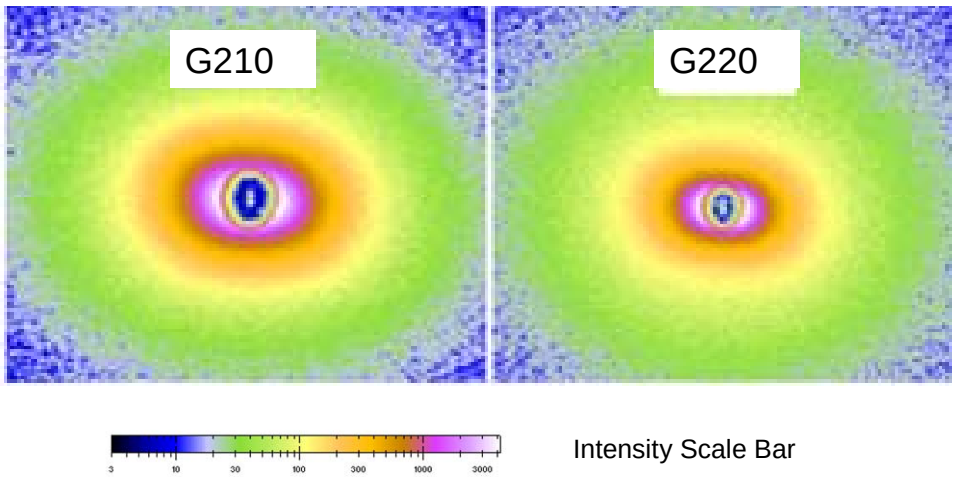

Figure 4-15 Raw 2-D SAXS patterns for selected ternary composites; G210 and G220.

Comparing the raw 2-D SAXS patterns for the binary composites samples (Figure 4-3 and Figure 4-10) and the ternary composites samples (Figure 4-15); no intuitive distinctions can be observed. They shared the similar features such as elliptical shape, and the ellipticity increased upon the increase of MMT or glycerol. These findings

were discussed for the binary composites samples (Page 50 and Page 60). Thus, besides the discussions based on the corresponding SAXS profiles (Figure 4-16 and Table 4-7), further analysis (the size distribution calculation, Page 78) of the ternary composites was carried out to gain a better understanding of the synergistic interactions within the ternary system.

The Bragg peaks occurred at a series of Q values satisfying the relationship of $d_{SAXS} \approx 2\pi/Q$. The corresponding *basal spacing* values and the characteristic peak for MMT are shown in Table 4-7.

Table 4-7 Characteristic peak position profiles and calculated basal spacing for glycerol-plasticized samples.

Sample ID	PS	G010	G020	G105	G115	2 wt %MMT	G210	G220	G305	G315
P_{MMT}	-	-	-	0.35	0.33	0.423	0.33	0.33	0.345	0.325
P_{starch}	0.37	0.352	0.357	All peaks overlapped with P_{MMT}						
d_{SAXS} (Å)				17.9	19.03	14.85	19.03	19.13	18.20	19.32

The characteristic peak for starch polymer structure was assigned to be Q=0.37 Å $^{-1}$ (the inset window in Figure 4-16) which corresponded to the 100 interhelix reflection of the starch polymer and was known to be typical of the B-type crystallinity in starch polymer [163]. Furthermore, these values were very similar to the observation of Lopez-Rubio *et al.*, where they reported the value of extruded high-starch maize starch to be Q=0.375 Å $^{-1}$ [164]. The slight deviation between the two reported values was within expectation because the 100 peak is known to be related to the polymer hydration level [165].

As revealed in Table 4-7, P_{starch} (100 inter-helix distances) shifted to a lower value when the glycerol concentration exceeded 15 wt%, regardless of the MMT loading. These results corroborated the authors' earlier finding that a 'threshold' glycerol loading of ~ 12-15 wt% was related to its plasticization effect [81]. Similar to the observations made by Grubb *et al.*[166], only one peak (an overlapped peak from the *basal spacing* of MMT and 100 inter-helix of starch) was observed (Table 4-7). This finding indicated the presence of short-range order where the MMT hindered the starch/glycerol aggregates to further increase their domain size, which will be further discussed in the size distribution section (Page 78).

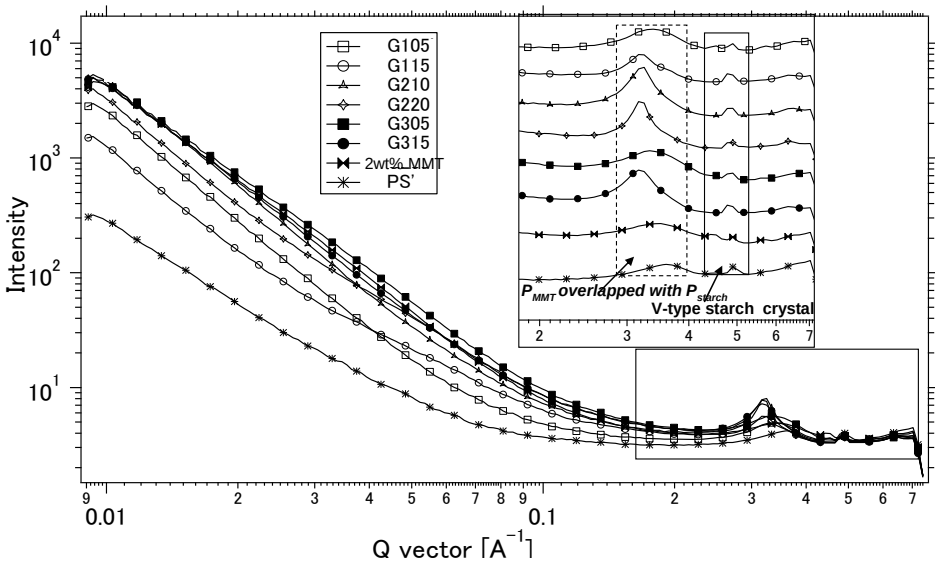

Figure 4-16 SAXS profiles for the PS, starch/glycerol/MMT samples generated from NIKA data processing software.

In addition to the B-type crystals discussed, V-type starch crystals were observed in all the extruded composite samples (the inset window in Figure 4-16). This crystal consisted of the regular packing of an ordered starch single helix, which was defined in the literature with a diameter of 1.3 nm [167] for dehydrated crystal [1, 168]. The V-type crystal peaks were assigned to be 1.28 nm (Q=0.487 Å^{-1}) in the current study.

4.4.3 Crystallization behaviour

4.4.3.1 Crystallinity

As shown in Table 4-6, all the extruded samples showed lower crystallinity values when compared to that of the native high-amylose starch (around 20 wt%) [169]. The interplay of two effects that increasing MMT (enhanced the crystallinity value) and increasing glycerol (decreased the crystallinity) could be distinguished from the crystallinity resulted listed in Table 4-6. The end crystallinity values for different samples were dependent on the concentration of MMT and glycerol (formation of specific morphologies within the samples), respectively.

For instance, in the 5% glycerol loading samples (G105 and G305 with a crystallinity of 11.39% and 10.1%), based on the hypothesis that the glycerol molecules were mainly contributed to the interactions with starch chain, which restricted the mobility of starch chains, its corresponding crystallinity values were higher than that from PS samples (X_c%=9.39%), Table 4-6. However, as the glycerol concentration increased,

its effect of lowering crystallinity values became dominant and thus lowered the crystallinity, such as G315 (X_c%=6.86%) and G220 (X_c%=8.08%). In other words, when the concentration of one component (either MMT or glycerol) was relatively low, the dominant effect on crystallinity value depended on the high-loading component. Such observations further agreed with the argument (put forward in above mentioned binary system studies) that the interactions between starch and glycerol, which contributed to the formation of specific polymeric network of the sample, turned out to be one dominated reason for nanocomposites' crystallinity. However, the crystallinity value for sample G115 (9.62%) was unexpected higher than the pure starch sample as indicated in Table 4-6.

4.4.3.2 Differential Scanning Calorimetry (DSC)

The complex competitive interactions among starch, MMT and glycerol were reflected from the DSC measurement results. Figure 4-17 compared the typical heat flow curve for the PS sample and its bionanocomposites, which emphasises the impact of adding both glycerol and MMT on the crystalline phase of these bionanocomposites.

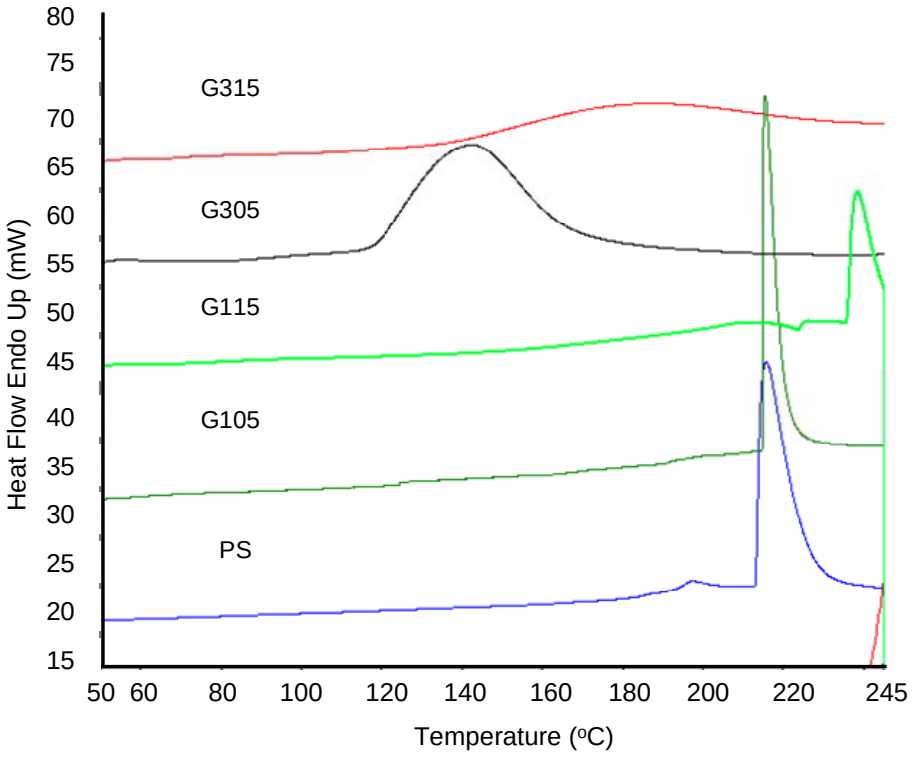

Figure 4-17 DSC heating curves for the selected samples with varying MMT and glycerol contents.

Figure 4-17 demonstrated the complex interactions within the starch/MMT/glycerol hydrophilic system. The variation in the peak (base and height) indicated that the crystallization behaviour was significantly affected by the presence of glycerol and MMT which have already been evidenced in the crystallinity section (Page 74) for binary system. Two main points can be observed in Figure 4-17, first, the presence of low amounts of glycerol (5 wt %) caused the anti-plasticization effect and increased the melting point ($T_{m\text{-G105}} > T_{m\text{-PS}}$), however, the presence of high loading of MMT definitely affecting this behaviour where $T_{m\text{-G305}} < T_{m\text{-PS}}$. Second, an increase (5 wt% to 15 wt %) in the plasticizer content caused a dramatic increase in the melting Figure 4-17. This could be related to the low crystallinity value of 15%-glycerol samples, Table 4-6. The presence of the strong glycerol-MMT interactions at high glycerol concentration enhanced the development of a more tighten and dense polymeric network as evidenced from the WAXD and SAXS results. Thus, in such circumstance, relative larger amount of energy (increased the melting point) was required.

The T_g and T_m value of all the samples are presented in Table 4-6. As mentioned in the binary system discussion, neat extruded sample had the highest T_g value, 49.5°C, and the T_g value for its nanocomposites were smaller than PS which deviated from 39.5°C (G315) to 46.7°C (G220). This behaviour was within expectation, because the mobility of starch chains was significantly improved upon the addition of a plasticizer. And this effect clearly overtook the enforcement effect of MMT (increased the T_g value) in the current case. Once again, it should be clearly enough to emphasize the dominant effect of glycerol/starch interactions that reflected from the well-defined relationship of glycerol loading and T_g value at a fixed MMT concentration. As presented in Table 4-6, the T_g value was decreasing ideally upon the augment of glycerol loading. Besides, the enforcement of adding MMT was revealed as the increase in the T_g value of G210 (46.7°C) than G010 (40.7°C).

The notable aspect was the suppression of ‘anti-plasticization’ behaviour of glycerol composites by addition of MMT which caused an insignificant change in the T_g value [96]. Antiplasticization is well known with lower glycerol concentration because of strong starch-glycerol interaction that limited mobility and increased T_g. Therefore, when comparing the samples with identical glycerol concentration at 5 wt%, increasing the amount of MMT (1 wt% comparing to 3 wt% MMT) slightly

decreased the T_g value. This could be explained by considering that the MMT was able to 'house' glycerol molecules such that the interaction between starch chain and glycerol was reduced and this improved the chain mobility to some extent by hindering the 'antiplasticization' effect of low-glycerol system. The T_g values for G105 and G305 were 44.97°C and 43.2°C, respectively.

4.4.3.3 Avrami Equation analyses based on DSC

The Avrami Equation analyses for ternary system samples were presented in Figure 4-18. The exponent *n* and the factor *k* from Avrami Equation analyses are presented in Table 4-8.

Table 4-8 The exponent n and the factor k obtained from a non-isothermal crystallisation analyses for the glycerol-plasticized nanocomposite samples.

Sample ID	G105	G115	G210	G220	G305	G315
n	0.24	0.28	0.20	0.18	0.22	0.32
k	-0.94	-0.90	-0.63	-0.5	-0.77	-0.35

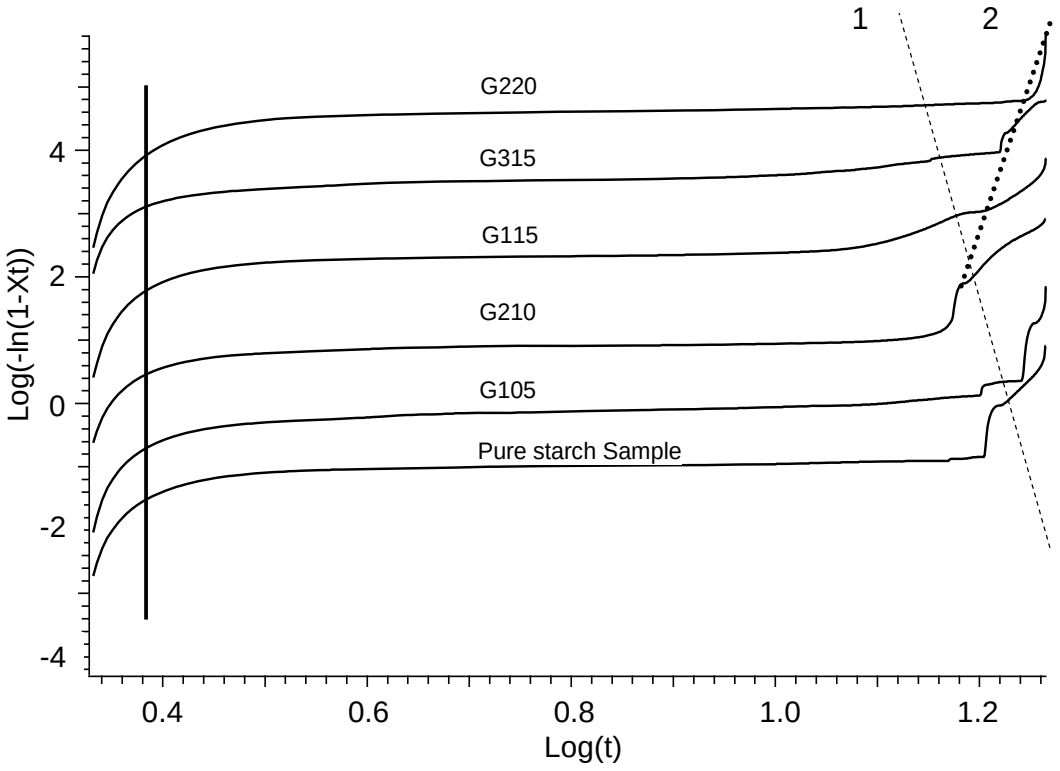

Figure 4-18 Decay of the overall crystallinity based on the non-isothermal crystallisation kinetics analysis using the modified Avrami equation for glycerol-plasticized samples. All plots were corrected for the baseline and offset for clarity.

Two key points are highlighted in Figure 4-18. First, the presence of glycerol and MMT did not seem to influence the onset temperature for crystallisation (shown by the vertical solid line); second, they influenced the presence of heterogeneities within the crystalline domains (shown by the slanted dash line 1 and 2), which was most likely due to the competitive interactions existed in this complex system. Furthermore, change to the slope (dash line 1 and 2) indicated the presence of heterogeneous crystalline domain, due to the typical secondary nucleation. Such behaviour was caused by the rearrangement of smaller imperfect crystals into larger domains, which had been reported previously for other polymer nanocomposites systems as well [170].

Finally, the *n* values for the composite samples were overall lower than that of the PS polymer (*n*=0.48). The next factor *k* (related to the rate of crystal growth), which showed a large variation was considered to be related to the moisture amount which could stroll around within the samples. Because water molecules can facilitate the reorganisation process, the most likely reason for the reduced domain growth rate for G105 (*k*=-0.94) and G115 (*k*=-0.90) sample was the comparatively low moisture content, Table 4-6.

4.4.3.4 Size distribution of the various crystalline domains

The crystallization behaviour of the ternary system was further investigated by analysing the crystalline domain size distribution (Maximum Entropy Method) from obtained SAXS profiles. The variation of shapes of the SAXS profile from different samples indicated the deviation of size distribution of the samples [171]. Based on the theory of SAXS, quantitative analysis could be carried out on the SAXS profiles; the only condition being the presence of heterogeneities in electron density distribution on Nano scale [155].

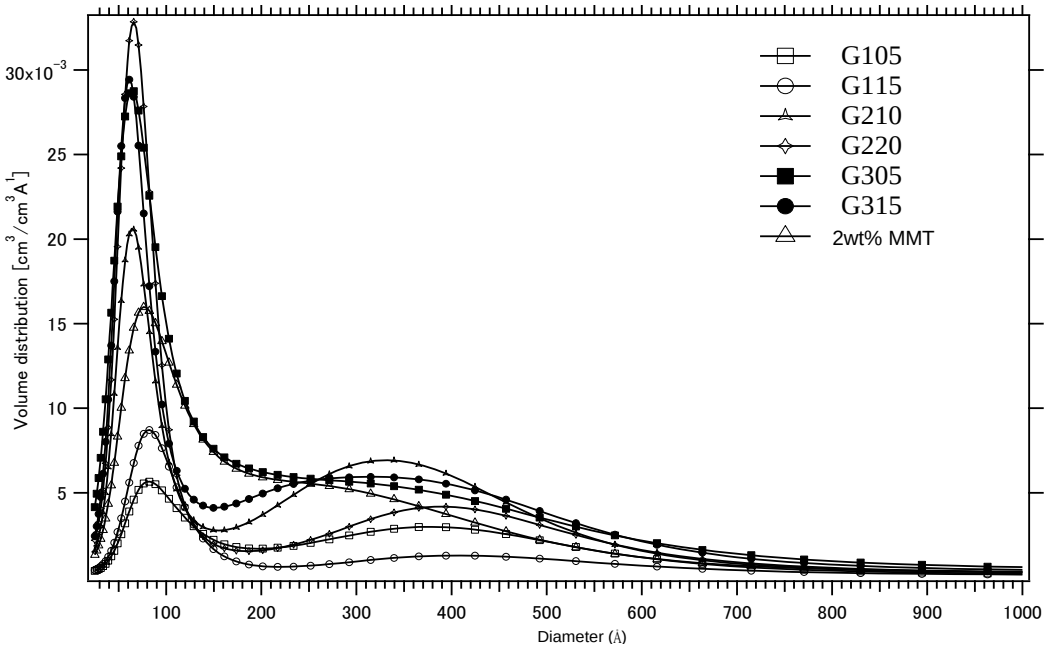

Figure 4-19 Size distribution calculation result for glycerol-plasticized nanocomposites.

Obtained size distribution profile results (method had been described in the Methodology *Chapter, Page 46*) were shown in Table 4-9. Two domains were observed, the diameter of scattering denoted as $\bar{d}_{1-glycerol}$ (around 91.3 Å) and $\bar{d}_{2-glycerol}$ (around 387.9 Å).

Table 4-9 Radius (Å) from the size distribution calculation by the MEM method for glycerol-plasticized samples with both high moisture and low moisture content.

high moisture samples		low moisture samples		
Sample ID	$\bar{d}_{1-hm-glycerol}$*(Å)	Sample ID	$\bar{d}_{1-glycerol}$*(Å)	$\bar{d}_{2-glycerol}$ *(Å)
HG105	95.8	G105	107.4	389.6
HG115	102	G115	97	412.6
HG210	101.3	G210	86.4	369.1
HG220	108.8	G220	78.6	403.8
HG305	96.2	G305	93.5	368.2
HG315	105.9	G315	85.3	384.1

$\bar{d}$ *: mean scatter diameter (Å)

As revealed in Table 4-9, the value of mean scatter diameter for domain one ($\bar{d}_{1-glycerol}$) ranged from 78.6 Å to 107.4 Å for different samples. The mean diameter of domain one was related to the glycerol/MMT loading since the interactions among

starch/MMT/glycerol was influenced by various glycerol/MMT loading. It is observed that glycerol-rich samples had a lower value of scatter diameter ($\bar{d}_{1-glycerol}$) as seen from Table 4-9. It is clear that increasing the glycerol concentration within a 'MMT-rich' environment resulted in a larger degree MMT intercalation (and thus higher *basal spacing* as seen in Table 4-6), and this was reflected by the decreased size in crystalline domain. Such interactions will prevent long-range order in the bionanocomposites matrix. Furthermore, drying process led to the removal of moisture and allowed the rapid retrogradation of starch chains to form a tighter polymeric network [172], and this was proven by the reduced scatter diameter of crystalline domain one when compared to the high moisture content samples (Page 85).

The observations regarding of the two size domains could be correlated to the well-defined retrogradation phenomenon which occurred due to the aggregation of starch chains during aging [173, 174]. The rearrangements of starch chains became dominant upon the drying process and the availability of MMT provided local sites for polymer aggregations, thus led to the formation of larger domains (size around 387 Å ($\bar{d}_{2-glycero}$) as extracted from the SAXS data, *Table 4-9*.

4.5 Role of water molecules indicated from SAXS profiles

In order to further clarify the role of water molecules in this complex system, another set of samples, denoted as HGXX (the prefix H means high moisture) with higher moisture content were subjected to synchrotron test. The role of water molecules was illustrated in terms of comparing the synchrotron results from the samples at different hydration degree.

4.5.1 Moisture content measurement

Moisture content measurement results for the high moisture content samples are shown in Table 4-10. In the high moisture content samples, increasing glycerol concentration retained higher amount of moisture within the matrixes due to the typically plasticization effect of glycerol.

Table 4-10 Characteristic peak position profiles and basal spacing results (d_{SAXS}) of glycerol-plasticized high moisture content samples.

Sample ID	*m%*	*Δm*%*	P_{MMT}	P_{starch}	d_{SAXS} (Å)	Δd_{SAXS} **(Å)
HPS	30.69	28.47		0.36		
H2 wt %MMT	27.17	20.78	0.287	0.355	21.88	7.03
H4 wt %MMT	18.47		0.381	o.36	exfoliated	
HG010	22.24	18.07		0.36		
HG020	28.91	26.26		0.320		
HG105	20.24	17.45	0.317	0.357	19.8	1.9
HG115	26.13	24.16	0.318	0.34	19.74	0.61
HG210	21.97	18.66	0.320	0.357	19.6	0.57
HG220	30.65	28.63	0.320	overlap	19.6	0.67
HG305	26.04	21.3	0.29	0.359	21.66	3.46
HG315	30.08	26.93	0.313	overlap	20.06	0.03

**Δm%=m%* (high moisture content samples) - *m%* (low moisture content samples)

***Δd= d* (high moisture content samples) - *d* (low moisture content samples)

The moisture content data in Table 4-6 and Table 4-10 indicated two key points. First, under a moisture-rich scenario, the presence of glycerol increased the moisture retention within the polymer matrix, regardless of the presence of MMT (analysis of values of *m%* (high moisture) row-wise). This behaviour was expected because the typical hydrophilicity of glycerol attracted and stabilized a greater amount of water molecules. Second, when the same samples were subjected to drying treatment, the difference in the moisture content values (*Δm* %) demonstrated that the samples with 10 wt% or higher amounts of glycerol had lower moisture within the samples (because the *Δm* values were larger). This highlighted the stronger starch-glycerol interaction, which can cause glycerol to replace some of the structure water molecules in the starch polymer matrix. Furthermore, based on the well-known tortuous pathway theory [19, 105] for moisture migration, the high-MMT loading samples were supposed to show relatively higher moisture content. In other words, the moisture migration behaviour was affected by the addition of MMT, which helped retain higher amounts of moisture in the MMT-rich samples.

4.5.2 SAXS results for PS ,starch+glycerol and starch+MMT samples with high moisture content

The raw 2-D SAXS patterns from the selected representative high moisture content samples are shown in Figure 4-20.

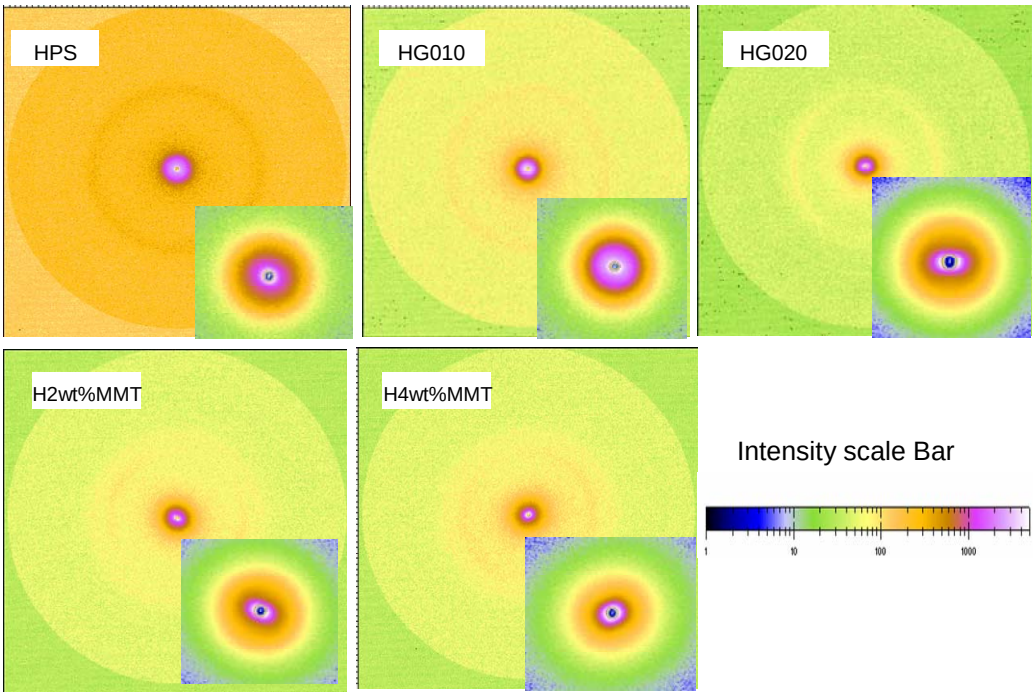

Figure 4-20 Raw 2-D SAXS patterns for PS, starch/glycerol and starch/MMT from high moisture samples.

As shown in Figure 4-20, same as the low moisture content samples, the scattering patterns were greatly influenced by the presence of MMT or glycerol and their respective concentrations. The shape of scattering pattern for HPS changed from circle to ellipse when glycerol concentration reached 20 wt% (however, similar shapes was observed for HPS and HG010). This was different from the observation from the low moisture content samples. Furthermore, the deviation in the ellipticity between G200 and HG200 (and between G400 and HG400) reflected the heterogeneity difference within the lamellar structure that resulted from the removal of water molecules. In the study of Grubb *et al.*, higher intensities of the SAXS profiles were observed for hydrophilic nylon-6 fibres after dehydration [166], which suggested that the lamellar structure can be enhanced by controlled drying (removal of water from the polymer matrix) because the removal of water molecules can allow the polymer structure to coalesce.

The removal of free water from the bionanocomposites samples significantly impacted the polymer-polymer and polymer-glycerol interactions. Removal of the free water led to greater intercalation (decrement of *basal spacing* from 21.88 Å to 14.74 Å for HG200 and G200, respectively) since the water molecules 'trapped'

between MMT and starch polymer and/or in MMT galleries were pushed out. Similar observation was found in the work on the interaction of water with synthetic saponite clay sample, where hydration levels influenced the *basal spacing* [175].

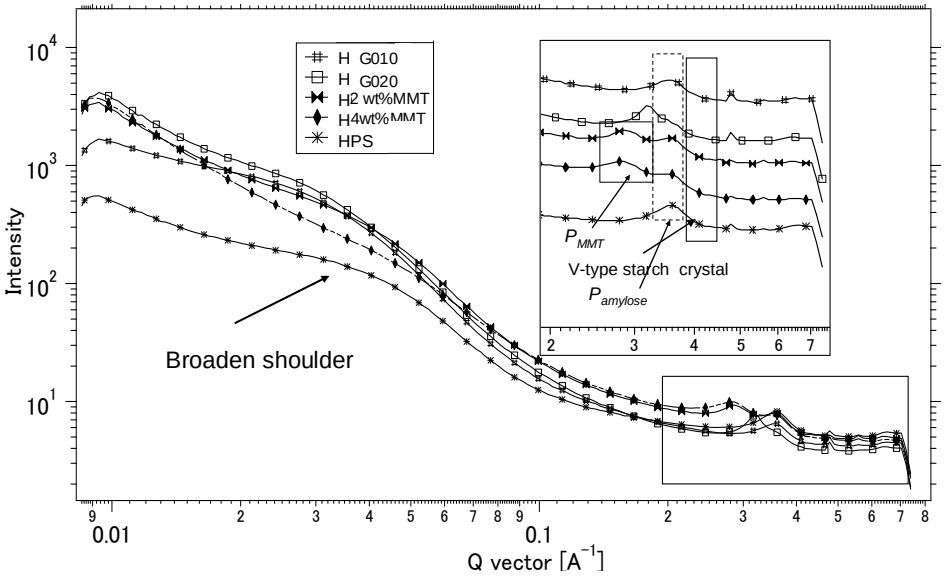

Figure 4-21 SAXS Profiles for PS, starch/glycerol and starch/MMT from high moisture samples.

Together with the SAXS profiles from the high moisture content samples (Figure 4-21), the well-defined 'broaden shoulder' around Q=0.04-0.05 $Å^{-1}$ corresponding to the long periodic structure of processed starch polymer [156] was observed in all the high moisture content samples. Such a 'shoulder' typically corresponded to the long periodic structure of processed starch polymer [156]. For the samples with higher moisture content, such observation typically meant that higher plasticizer concentration (both glycerol and water) allowed larger 3-dimensional periodic growth. Shamai *et al.*[176] had earlier discussed the disappearance of a shoulder in the low moisture content starch samples and how this disappearance reflected the retrogradation behaviour. The typical reorganisation of a polymeric network tended to form different domain sizes, which do not aggregate to form a long-range ordered structure. Thus, in the absence of moisture, this morphology was possible due to the strong starch-glycerol interactions that allowed the glycerol molecules to replace the water molecules at starch-water interaction sites and result in the formation of two different sized crystalline domains (Page 78).

As read from Table 4-10, The 100 interhelix characteristic peak for starch was assigned at Q=0.36 Å $^{-1}$ for the high moisture content sample. Using Bragg's calculation, the interhelix domain showed an increase from 16 Å (PS) to 17.9 Å(HPS), and this result was in agreement with Cleven *et al.*'s work where the diffraction peaks for B-type starch shifted toward greater lattice spacing with increasing hydration degree of the sample [177]. Unlike only tiny difference of P_{starch} observed between HG010 and HG020, P_{starch} shifts from 0.36 (HPS) to 0.32 (HG020) when the glycerol concentration increased 20 wt%, Table 4-10. This dramatically increased interhelix spacing of starch polymer under water-rich scenario, could be reasonably explained by the stronger polymer-water coalesce on top of the plasticization effect from glycerol.

4.5.3 SAXS results of samples starch+glycerol+MMT with high moisture content

The SAXS profiles of high moisture content ternary nanocomposites are shown in

Figure 4-22, and HPS and H2 wt % MMT are included as well.

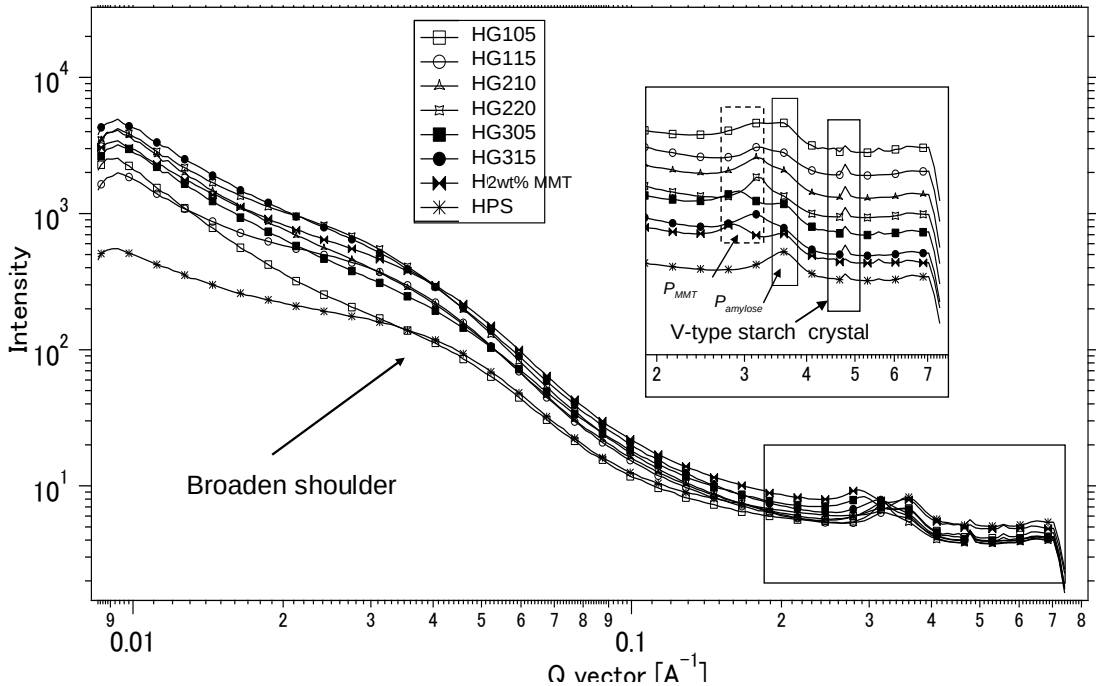

Figure 4-22 SAXS Profiles for PS, starch/glycerol/MMT samples with high moisture content generated from NIKA data processing software.

The size of V-type crystal in the high moisture content sample was assigned to be 1.36nm which was slightly larger than that from the low moisture content samples, as shown in the inset window in

Figure *4-22*. The removal of free water molecules resulted in the disappearance of the broad 'shoulder' (short-range order peaks which appears at Q≈15.5nm) found in the high moisture content samples as well as the change from circular diffraction pattern to elliptic pattern. The drop in moisture content was in accordance with the changes in the SAXS intensity peak which both emphasize the role of water, and similar conclusions are found in Grubb *et al.* work [166].

Unlike the low moisture content samples, where P_{MMT} and P_{starch} were overlapped, two well-separated peaks (from basal distance of MMT and 100 interhelix distances for starch polymer), in the inset window in

Figure *4-22*, were observed in all the high moisture content samples. As compared from the *basal spacing* results, dehydrated (low moisture content) samples possessed a overall smaller *basal spacing* value when compared to the high moisture content samples; for example, 19.8 Å (HG105) and 17.9 Å (G105). This could be attributed to the loss of "trapped" water molecules during drying.

4.5.4 Size distribution of the various crystalline domains

The crystalline size distribution results for high moisture content samples were shown in Figure 4-23. Only one domain ($\bar{d}_{1-hm-glycerol}$) sized around 101.7 Å was observed, Table 4-9.

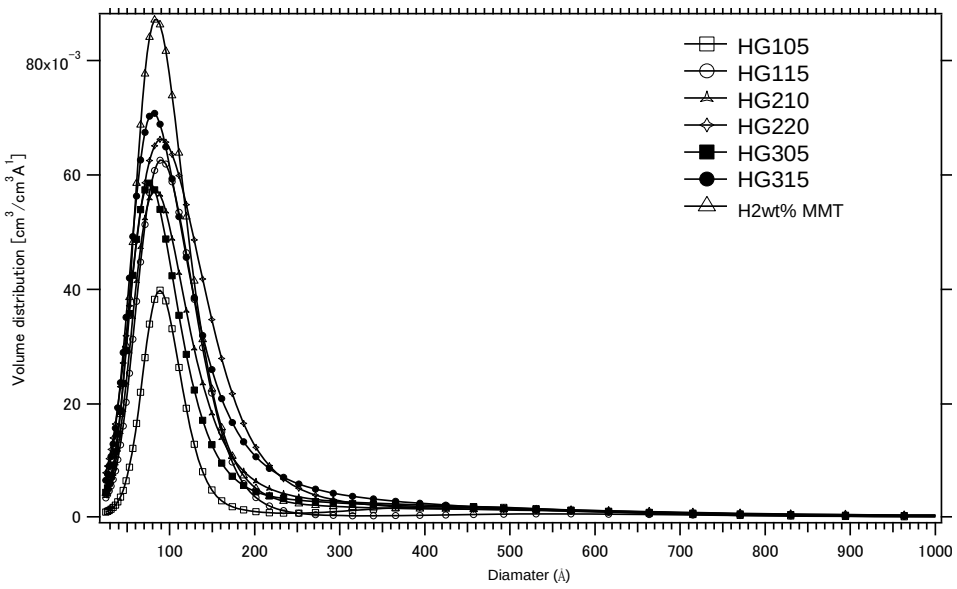

Figure 4-23 Size distribution calculation result of starch/glycerol/MMT nanocomposites for high moisture samples by MEM method.

Mean scatter diameter for crystalline domain ($\bar{d}_{1-hm-glycerol}$) ranged from 95.8 Å to 108.8 Å which was overall larger than that from the low moisture content samples, Table 4-9. The larger domain size for the high moisture content samples indicated that the long-period decreased upon drying, and similar observation were reported in Grubb *et al.'s* work where the periodicity decreased from 10.2nm to 9.8nm in dry Nylon-6 fibres [166]. It is observed that glycerol-rich and high moisture system have a higher value of scatter diameter ($\bar{d}_{1-hm-glycerol}$) due to the stronger glycerol-water interactions which slightly expanded the domain size.

The hypothesis that emergence of the larger domain resulted from the rapid retrogradation of starch chains upon drying was further confirmed by the observation that only one domain was observed in the moisture-rich samples. In the presence of excess water or glycerol (which strongly interacted with the starch polymer), retrogradation was hindered since the interactions from starch/glycerol/water restricted the moisture redistribution, as suggested by Schiraldi *et al.* [178]. The presence of moisture and plasticizer limited the starch-starch interactions and prevented the retrogradation in the high moisture content samples, which prevented the formation of the larger domains ($\bar{d}_{2-glycerol}$ observed in the low moisture content samples).

Summary

The synergistic interaction in the glycerol-plasticized nanocomposite was studied via various characterization methods. The combined influence of glycerol (1-20 wt %) and MMT (1-3 wt %) loading on the characteristics of extruded starch nanocomposites which directly reflected the interaction tendentiousness and strength under different scenarios were studied separately. Important conclusions can be drawn as follows.

1. The glycerol/MMT interaction was the dominating factor for achieving *basal spacing* expansion of MMT. However, this gallery spacing was also significantly influenced by the glycerol/glycerol interactions which will compete with the glycerol/MMT interactions and led to a more intercalated morphology.

2. The strong interaction of starch/glycerol resulted in the decrease in the T_g values within the antiplasticization 'threshold' of glycerol. Furthermore, incorporation of MMT successfully balanced the starch/glycerol interaction and hindered the antiplasticization of glycerol.

3. The interplay of glycerol and MMT within the nanocomposites was reflected from the evaluation results of crystallization behaviour via Avrami Model which highlighted the main effect of MMT lied on modifying the crystallization mechanism rather than crystal growth rate, but glycerol could affect both.

These discussions suggested the polymeric network formation was determined by the system-specific dominate interaction took placed. The analysis also indicated that competitive interactions among starch/glycerol/MMT resulted in different behaviours in terms of the MMT *basal spacing* and the crystalline domain size distribution profile for different samples. More studies which employed xylitol as plasticizer are illustrated in the next Chapter.

Chapter 5

Xylitol Plasticized High Amylose Nanocomposites

Chapter outline

Xylitol, with five hydroxyl groups, was the second plasticizer selected in the current study. Based on the discussions in *Chapter* 4, it can be concluded that one of the core factors influencing the synergistic interactions was the hydrophilicity (the number of –OH) of the plasticizer. In this Chapter the importance of the intrinsic chemistry (crystallization ability and intermolecular hydrogen bonding force) turned out to be another factor that significantly influenced the interactions within the xylitol-plasticized starch system. Furthermore, the molecular size of the plasticizer turned out to be another significant element that contributed to the distinct behaviour in two systems. For instance, the crystallization behaviour of xylitol-plasticized samples was greatly different to that from glycerol-plasticized samples. The crystal growth in xylitol system was disrupted and tended to form smaller crystals with a higher crystallinity value. Such hypothesis was also supported from the high T_m of xylitol-plasticized samples.

The discussion structure in this Chapter followed the same structure presented in the glycerol- plasticized samples Chapter (*Chapter* 4). Different binary systems will be discussed separately (the xylitol+MMT system and starch+xylitol system) followed by investigations into the complex ternary system (starch+xylitol+MMT). Conclusions have been drawn based on the relevant discussions and presented at the end of the chapter.

5.1 Starch+MMT system

This binary system (starch+MMT) had been studied in *Chapter* 4 (glycerol-plasticized system) sections 4.1 (Page 50). Please kindly refer to the indicated section for detailed information.

5.2 Xylitol+MMT system

Similar to glycerol+MMT study, the interactions between xylitol and MMT was carried out via investigation of the samples that were prepared at different xylitol:MMT ratio by sonication. The experimental results including intermolecular interactions (FTIR) and morphological observation (WAXD) are presented as follows.

5.2.1 Intermolecular interactions

Overall, the finding in this section was similar to that from glycerol-plasticized system. The disappearance of free 'OH' groups band vibration (band 3627 cm^{-1}, which indicated the existence of free 'OH' groups) of MMT clearly demonstrated that interactions took place between MMT and the xylitol upon sonication, Figure 5-1. The xylitol molecules penetrated into the 'gallery' of stack-like MMT via hydrogen bonding formation.

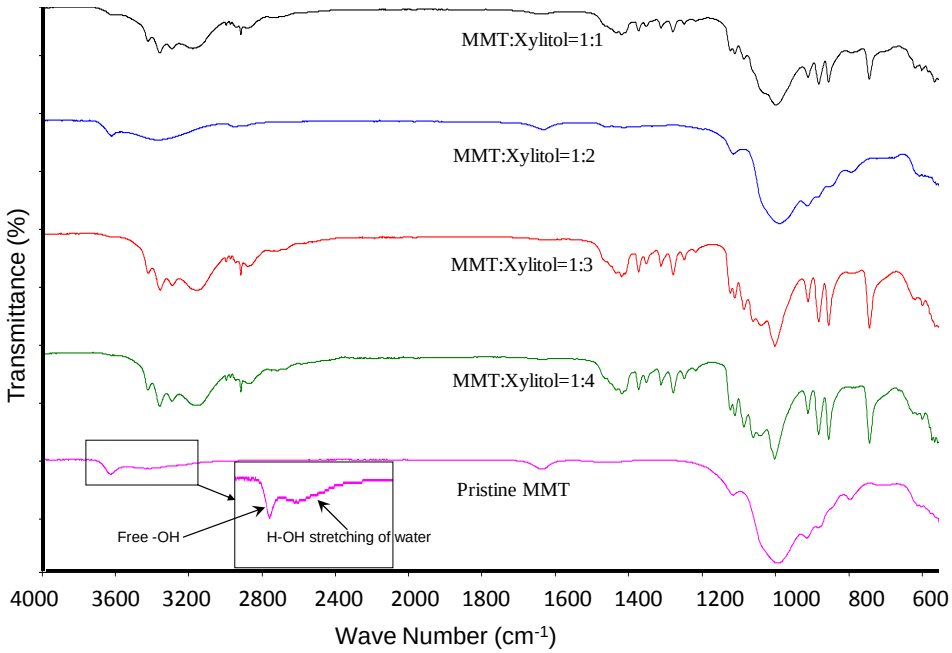

Figure 5-1 FTIR results for MMT: Xylitol samples at 1:1, 1:2, 1:3 and 1:4 ratios.

As mentioned in previous Chapter (Page 66), lower the peak frequency, the stronger the interaction [62], xylitol-plasticized samples showed a generally lower frequency in terms of the –OH band from FTIR spectra, Table 5-1.

Table 5-1 Summary of –OH band for glycerol/xylitol-plasticized samples (cm^{-1})

	1:1	1:2	1:3	1:4
Glycerol	3334.07	3279.22	3312.83	3307.65
Xylitol	3183.45	3168.63	3158.01	3159.56

The observed low frequency of xylitol-plasticized sample clearly presented stronger interactions with MMT via sonication. This was related to the relatively weaker intermolecular hydrogen bonding of xylitol plasticizer due to the low boiling point of xylitol; see the methodology section for relevant parameters for different plasticizers (Page 34). This will be further covered in the discussion of ternary system.

5.2.2 Morphological observations

Comparing the WAXD results of all the prepared samples, Figure 5-2, the value of *basal spacing* for xylitol samples showed an inverse proportionality to the xylitol loading, where an equal loading (1:1) of MMT: xylitol achieved a 18.23 Å *basal spacing*, but this value decreased to 17.77 Å for 1:4 MMT:xylitol sample. In other words, at higher concentrations of xylitol, the increased interaction restricted MMT/xylitol interaction. This was suggested to result from the competed interaction of xylitol/xylitol and xylitol/MMT at a xylitol-rich scenario.

Compared to the results obtained for glycerol-plasticized samples, the low *basal spacing* value of glycerol-plasticized might indicate that when the glycerol loading was low, there was not enough –OH sites for interactions between MMT and glycerol, thus resulting in lower gallery spacing than the xylitol-plasticized samples. This will be further discussed in the ternary system.

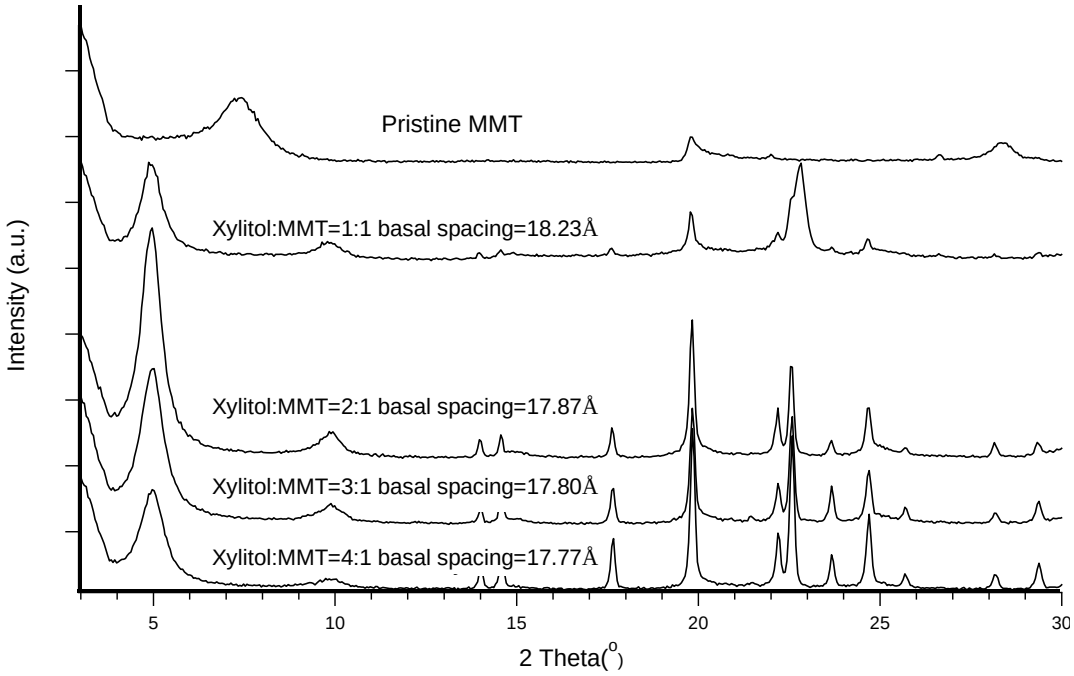

Figure 5-2 WAXD Patterns for MMT:xylitol samples at 1:1, 1:2, 1:3 , 1:4 ratio and Pristine MMT.

5.3 Starch + xylitol system

Two samples were produced with 10 wt% (X010) and 20 wt% (X020) xylitol according to the DOE for studying the interactions within the starch+xylitol system. The obtained characterization results are presented as follows.

5.3.1 Intermolecular interactions

5.3.1.1 Water isotherm

Same method had been applied in the starch+glycerol which include water isotherm, GAB Model evaluation, morphological observation and crystallization behaviour studies.

An 'inversion' phenomenon, defined in the glycerol-plasticized sample section (Page 61), was observed in the xylitol samples as well; where higher xylitol loading samples retained lower amount of moisture at low a_w values. But as the value of a_w increased, the relationship between the moisture content water and the xylitol content was inversed, Figure 5-3. The difference when applying xylitol as the plasticizer was that the inversion point increased to ~ 0.61 instead of 0.55 in glycerol-plasticized samples.

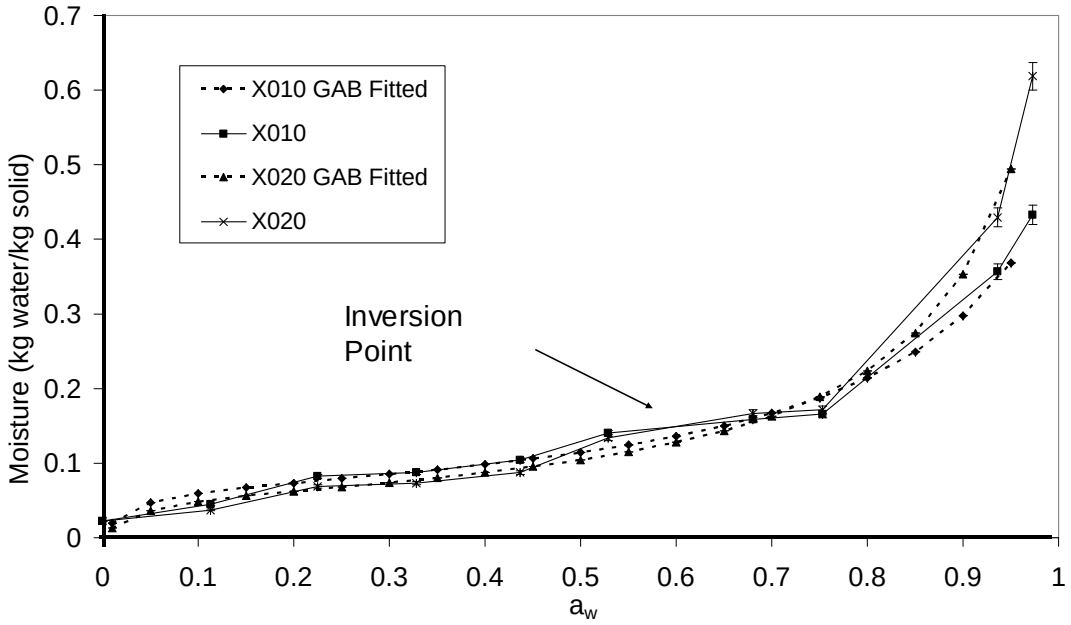

Figure 5-3 Water isotherm experimental results and GAB fitted data for X010 and X020.

5.3.1.2 GAB Model for isotherm data

The GAB equation analysis was completed to understand the isotherm behaviour; relevant results are shown in Table 5-2.

Table 5-2 GAB Fitting Parameters for tested samples. $R^2 > 0.88$.

Name	w_m	C	K
PS	0.092	46.243	0.669
X010	0.068	45.452	0.862
X020	0.058	30.708	0.930

In Table 5-2, parameter w_m denotes the moisture content value that corresponds to a 'monomolecular layer' of water to cover the whole polymer surface. The K parameter increased with increasing plasticizer content. This indicated that in terms of the equilibrium between the polymer and the plasticizer, greater plasticizer content can be accommodated within the polymer matrix by increasing the temperature. The molar sorption enthalpy values, highlighted by parameter C shows that, there is no significant effect as the plasticizer content is increased.

Different to the observations in glycerol-plasticized samples, the GAB model for xylitol-plasticized showed good correlation with the experimental data for the full a_w range. A possible reason for this could be the relative weaker moisture sensitivity of

xylitol (lower hydrophilicity and hydroscopicity) when compared to glycerol. Therefore, the separation of starch and amylopectin at high a_w condition was not that obvious which ensured the good prediction of GAB model on the xylitol-plasticized samples.

5.3.2 Crystallization behaviours

5.3.2.1 Differential Scanning Calorimetry

The DSC results, *Table 5-3*, indicated that the addition of xylitol decreased the T_m value. T_m value for xylitol-plasticized samples decreased from 219(PS) to 209(10% xylitol) and 215 (20% xylitol) due to the typical plasticization effect of xylitol When considering the antiplasticization 'threshold' for xylitol (around 22%) and glycerol (reported to be around 13%), the distinctness of tendencies of the T_m changes could be explained. The sudden decrease of T_m in G020, from 184 to 171, was due to the shift from 'antiplasticization region' to 'plasticization region' of glycerol and the reason for no obvious changes between the T_m value for X010 and X020 was that the xylitol concentration was still within the 'antiplasticization region' of the xylitol plasticizer.

5.3.2.2 Avrami Equation analyses based on DSC

Furthermore, the Avrami equation analyses results for PS, X010 and X020 are shown in *Table 5-3*. It could be read from *Table 5-3*, in the xylitol-plasticized system, that the effect of xylitol on the crystallization behaviour was more impacted on the crystallization mechanism aspect since the *n* parameter was greatly dependent on the xylitol concentration, the *n* parameter for X010 and X020 were 1.038 and 1.508, respectively. The influence of xylitol on the crystallinity of corresponding samples can be further evidenced from the high crystallinity value of high xylitol-loading samples in the ternary system, *Table 5-4*. The unique stronger crystallization ability of xylitol plasticizer will be further discussed together with the glycerol-plasticized samples in the integrity analyses chapter (*chapter 7*). However, the other parameter, *k*, was significantly larger than that of PS. This suggested that the crystal growth rate was larger in the xylitol-plasticized samples.

Table 5-3 Exponent n and the factor k obtained from a non-isothermal crystallisation analysis for the PS, X010 and X020 samples.

Sample	T_m, °C	*n*	*k*
PS	219	0.48	-1.47
X010	209	1.038	-0.21
X020	215	1.508	-0.476

5.4 Starch +Xylitol+MMT nanocomposites system

5.4.1 Intermolecular interactions

5.4.1.1 FTIR results

Several similar findings were observed, Figure 5-4, including the shift of band from 3627cm^{-1} to 3302cm^{-1}; the disappearance of the broad peak of H-OH stretching associated with water around 3234cm^{-1}- 3486cm^{-1} . These observations are corroborated with the WAXD results that the *basal spacing* expanded to different extent in all nanocomposite samples, Table 5-4.

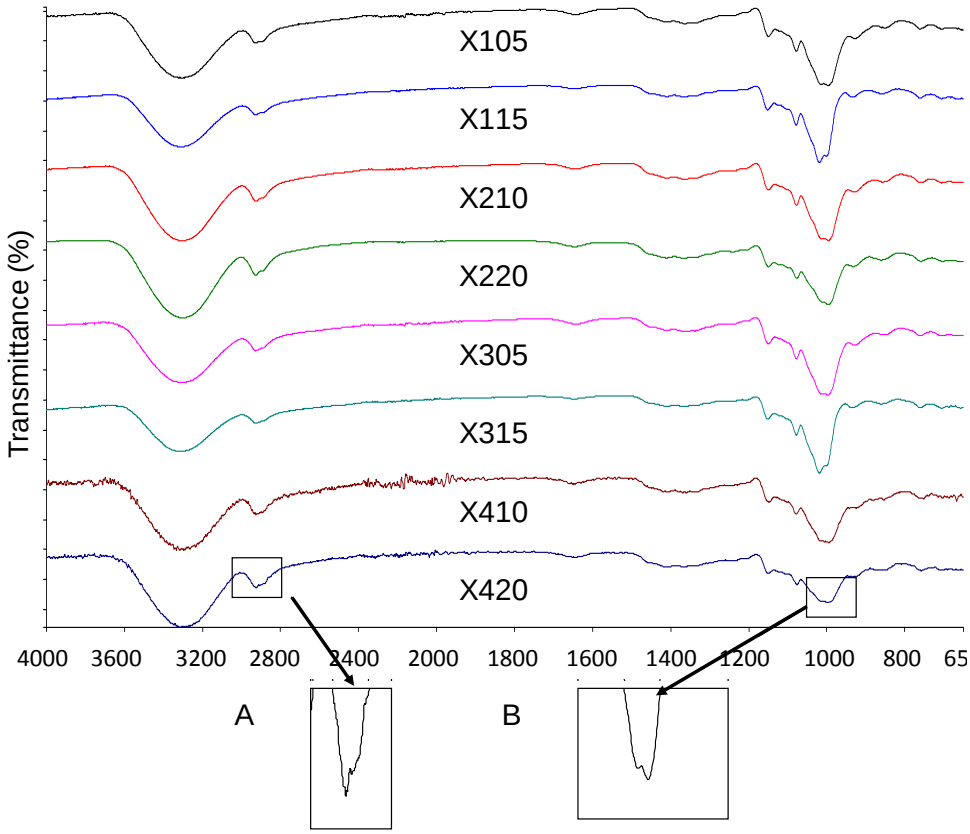

Figure 5-4 FTIR spectra for PS, pristine MMT and xylitol-plasticized nanocomposites.

Furthermore, the presence of new and stronger hydrogen bonding was evidenced from the double peaks at 2919cm^{-1}-2887cm^{-1} (inset window A of Figure 5-4) and 999cm^{-1}-992cm^{-1} (inset window B of Figure 5-4) in nanocomposites samples when compared to PS [159]. Additionally, the double peak of O-C stretching band at 999cm^{-1}-992cm^{-1} resulted from bending both 'O' of C-O-H and 'O' of anhydrous glucose ring in starch molecules [160].

5.4.2 Morphology observations

5.4.2.1 Wide Angle X-ray Diffraction (WAXD) and Transmission Electron Microscopy (TEM)

The WAXD patterns for the prepared samples, in Figure 5-5, showed that the *basal spacing* of all the samples increased to different extents regardless of the MMT content. The *basal spacing* value also suggested that starch and/or xylitol molecules had successfully migrated into the gallery of MMT. This was because the molecule sizes for xylitol/starch fragments reasonably agreed with the *Δd* values observed (Table 5-4).

Table 5-4 Basal spacing, crystallinity, glass-transition temperature (T_g) and melting temperature (T_m) for xylitol-plasticized nanocomposites.

Sample ID	X105	X115	X210	X220	X305	X315	X410	X420
*Xc**(%)	7.05	11.4	13.4	11.26	9.7	9.34	10.09	9.01
T_g (°C)	55.7	49.6	56.25	39.7	58.5	50.6	50.0	48.6
T_m (°C)	218	204	233	237	133	153	213	246
basal spacing (Å)	17.3	18.7	17.6	18.3	17.0	18.7	17.9	17.6

*crystallinity calculated from the method described in Ref [147].

It could be read from Table 5-4 that, the *basal spacing* value increased upon increasing of xylitol and MMT. Correspondingly, X420 possessed the highest *basal spacing* value of 17.85Å due to the hydrophilic starch and xylitol plasticizer. Meanwhile the TEM images for the representative samples (X410 and X420) are shown and it is representative of most of the samples that achieved mixed morphologies. Well intercalated morphologies with a higher 'gallery spacing' were obtained in the current study, Figure 5-5 (b).

The broadening of MMT characteristic peak occurred in all the samples with xylitol concentration less than 10% (X105, X210, X305 and X410). Such observation was

significantly different to what was found in the glycerol-plasticized samples, where the broadening of this peak occured in the 5% plasticizer loading samples only. In other words, in the xylitol samples, the well-recognized crystalline domain can only be observed with a xylitol-plasticized loading larger than 10% instead of 5% in the glycerol-plasticized samples. Such observation could be correlated with the crystallization behaviour that is induced by the intrinsic chemistry of xylitol plasticizer, which will be further discussed in the crystallization mechanism analysis section (Page 102). On the other hand, the sharp peaks presented in the WAXD patterns for the high xylitol loading samples suggested that stronger starch/xylitol interaction became dominant and enhanced the extent of MMT intercalation rather than exfoliation.

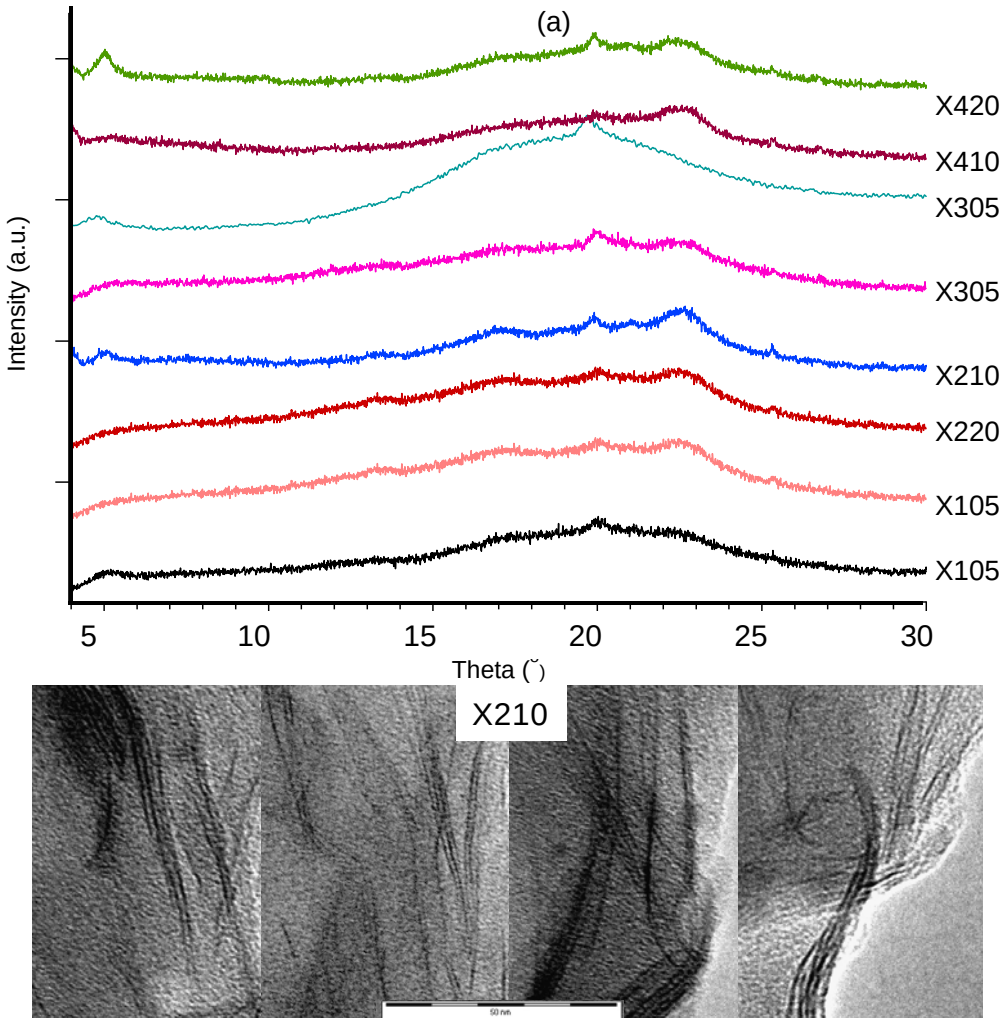

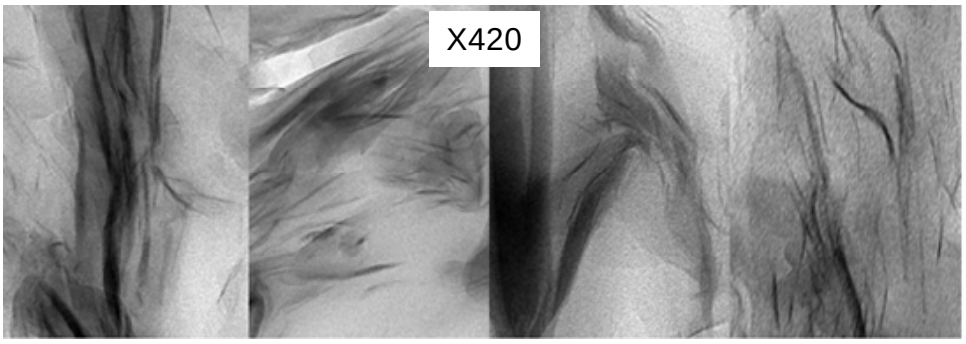

Figure 5-5 (a) WAXD diffractograms for xylitol – plasticized samples; (b) TEM images for X210 and X420.

5.4.2.2 Small Angle X-ray Scattering (SAXS)

The raw 2-D SAXS patterns for the representative xylitol-plasticized composites are shown in Figure 5-6.

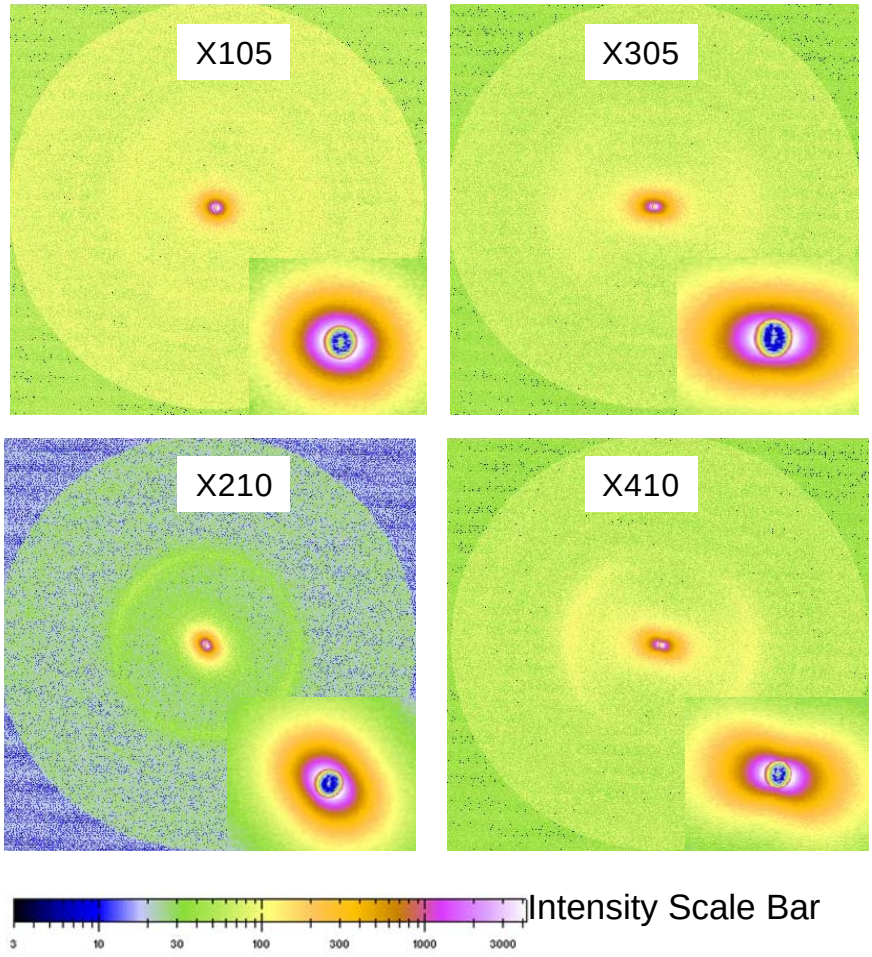

Figure 5-6 Raw 2-D SAXS patterns for X105/X305 and X210/X410.

As shown in Figure 5-6 the scattering patterns (shape and the intensity) of the samples were greatly influenced by varying the loading of MMT or xylitol. The shape of the scattering pattern changed from approximately circular (X105) to obviously elliptical (X410), which reflected the growth of lamellar structure/ crystalline domains distinctness within the composites. Furthermore, the heterogeneity across the polymeric network could be reflected on the scattering intensity from different samples due to the crystalline size differences and their electron-density heterogeneities [155]. The SAXS profiles for the obtained samples are shown in Figure 5-7.

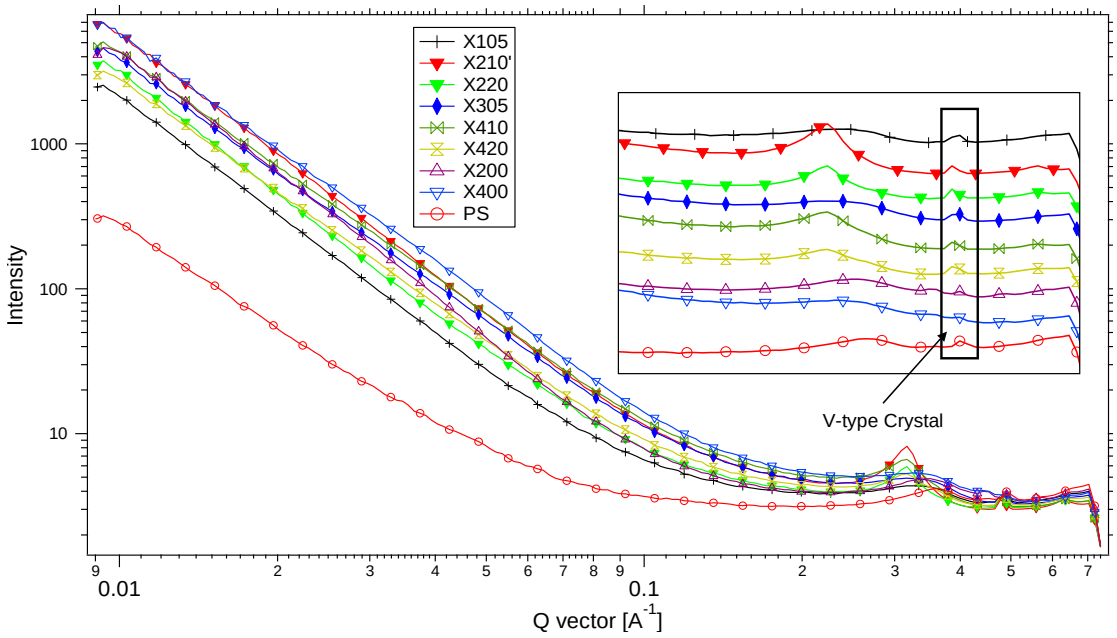

Figure 5-7 SAXS Profiles for xylitol-plasticized samples.

Figure 5-7 showed that higher intensity was observed in the nanocomposite samples as compared to PS, which further supported the argument that the presence of xylitol or MMT favoured the growth of lamellar morphology within the polymeric network. SAXS patterns for the V-type starch crystal was observed in all the extruded starch samples, seen in the inset window of Figure 5-7. The intensity of scattering increased with the MMT loading was attributed to the typical lamellar structure of the MMT, as seen in Figure 5-7 (intensity of X410 was larger than X210 and X305 was larger than X105). Regarding the influence of xylitol (at a fixed MMT loading) concentration on MMTs' *basal spacing* d_{SAXS} , it was observed that the d_{SAXS} value increased upon

increasing xylitol loading except in the 4% MMT samples, where X410 possessed a higher d_{SAXS} than X420 (19.8Å and 19.3Å, respectively).

We also compared the *basal spacing* d_{SAXS} for xylitol-MMT assemblage to that obtained from glycerol-plasticized samples, Table 5-5. As read from Table 5-5, the main tendency of the value of d_{SAXS} was that, the d_{SAXS} of MMT increased upon the concentration of MMT and plasticizer. Furthermore, together with the WAXD results for samples plasticized by different plasticizer, the d_{SAXS} was primarily determined from the molecular size of the plasticizer.

Table 5-5 Comparison of basal spacing (d_{SAXS}) results for glycerol, and xylitol-plasticized samples from SAXS measurements.

Sample ID	105	115	210	220	305	315	410	420
Glycerol	17.9	19.03	19.04	19.13	18.2	19.32		
xylitol	18.8	19.3	19.23	19.8	18.3	19.55	19.8	19.3

5.4.3 Crystallization behaviours

5.4.3.1 Crystallinity

As mentioned in the glycerol Chapter (Page 74), the crystallinity values were dependent on the interplay of two effects: increasing MMT (enhanced the crystallinity value) and increasing plasticizer concentration (decreased the crystallinity). Same principle could be applied in the xylitol-plasticized system as read from the crystallinity results in Table 5-4.

Briefly; all the extruded samples showed a lower crystallinity value compared to that of the native high-starch starch (around 20%) [169], Table 5-4, and influenced by the xylitol concentration. The addition of xylitol decreased the X_c%, e.g., the X_c% decreased from 7.48 % (PS) to 5.3% after adding 20 wt% xylitol (X020). The incorporation of MMT led to a higher crystallinity value regardless of the plasticizer content due to the well-defined nucleating effect of the presence of nanofiller [179, 180]. Meanwhile, the plasticization effect of xylitol was seen from the decrease of X_c% with increasing xylitol concentration at a constant MMT loading (except for the 1% MMT samples). For example, X_c % decreased from 10.09 % to 9.01% for X410

and X420. This trend was also valid for samples with 2 wt% and 3 wt% MMT, as seen in Table 5-4.

Furthermore, considering the crystallinity values from the same-formula samples plasticized by glycerol and xylitol, it was surprise to find that the crystallinity value of xylitol-plasticized sample were significantly higher than that from glycerol-plasticized one. Meanwhile, in WAXD results, the well-recognized crystalline domain can only be observed with a xylitol loading larger than 10% instead of 5% in the glycerol-plasticized samples. This will be discussed in detail in the integrity analysis chapter (*chapter 7*).

These two observations strongly suggested that in xylitol-plasticized system, the crystallization process was significantly different to that of glycerol-plasticized systems. In xylitol-plasticized system, the form of crystal were likely to be smaller (broadened WAXD pattern) but the totally amount of crystal, higher X_c % values, was larger than glycerol-plasticized systems. Such assumption will be further verified in the following Avrami Modelling section (Page 102).

5.4.3.2 Differential Scanning Calorimetry (DSC)

On top of the similar observations found in glycerol plasticizer system, the addition of xylitol also decreased the T_g value for the system. For example, it decreased from 49.5°C to 38.4°C for 20 wt% xylitol (X020). This was due to the plasticizing effect that improved the mobility of the starch polymer chains, as shown in Table 5-4, which was different to the observation in glycerol-plasticized nanocomposite samples where the value of T_m increase upon increasing glycerol amount. The melting point of xylitol-plasticized samples varied depended on the MMT-loading. When the MMT loading was low (less than 2%), T_m value decreased upon increasing xylitol concentration, Figure (a); however, this tendency was inverse in the MMT-rich circumstance, Figure 5-8 (b). No well-defined trend was observed of the value of T_m. For instance, in the 1wt% MMT loading sample, T_m value decreased from 218 °C to 204°C after increasing xylitol to 15%, however this value increased from 130 to 160 °C in the 3wt% MMT loading samples, Table 5-4. Such observation meant that a higher loading of xylitol led to a tighter polymeric network when the MMT amount was larger than 2 wt%. The T_m value for X210/X220 and X410/X420 were 233°C /237°C and 213°C /246°C, respectively.

The rather random and unpredictable T_m value of xylitol-plasticized sample was a vivid evidence of the influence of the unique chemistry of xylitol (stronger crystallization ability and weaker intermolecular hydrogen bond). The xylitol/starch interactions seemed to become even stronger upon the addition of MMT (larger than 2%) which resulted in the high T_m values in the high xylitol loading samples. The above mentioned starch/xylitol interaction and the reduced mobility of the polymer can be further seen in the High MMT-High Plasticiser samples (246°C for X420), which strongly indicated the starch/xylitol and xylitol/MMT interactions.

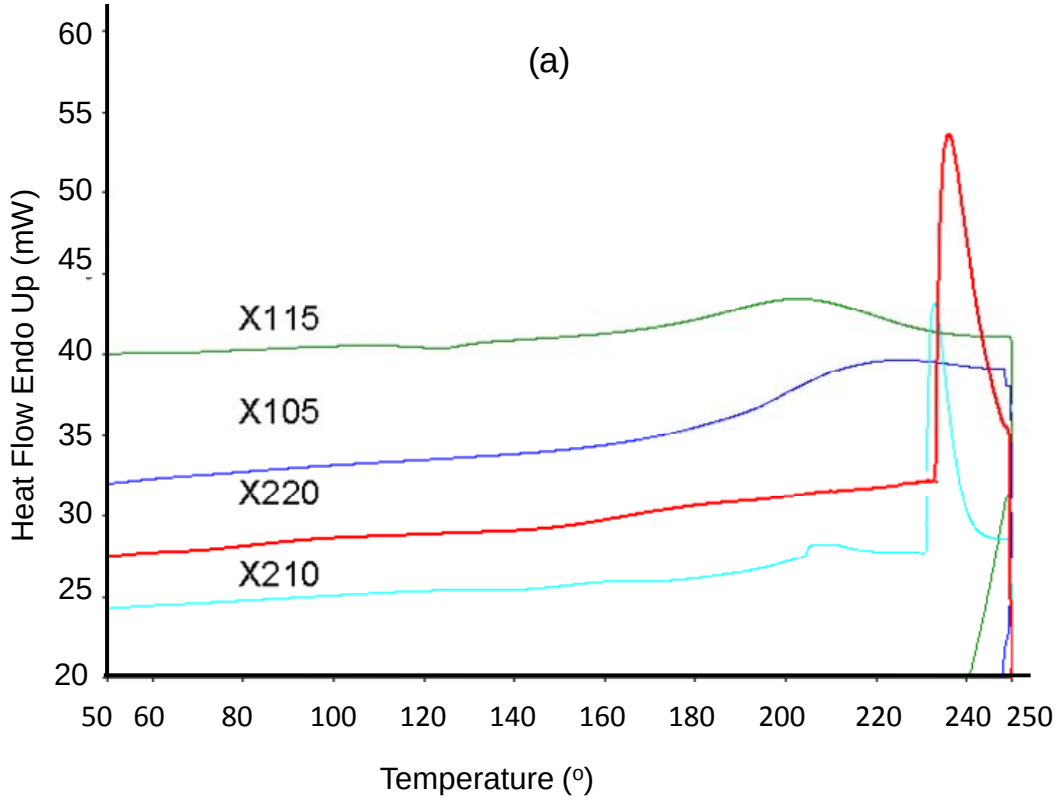

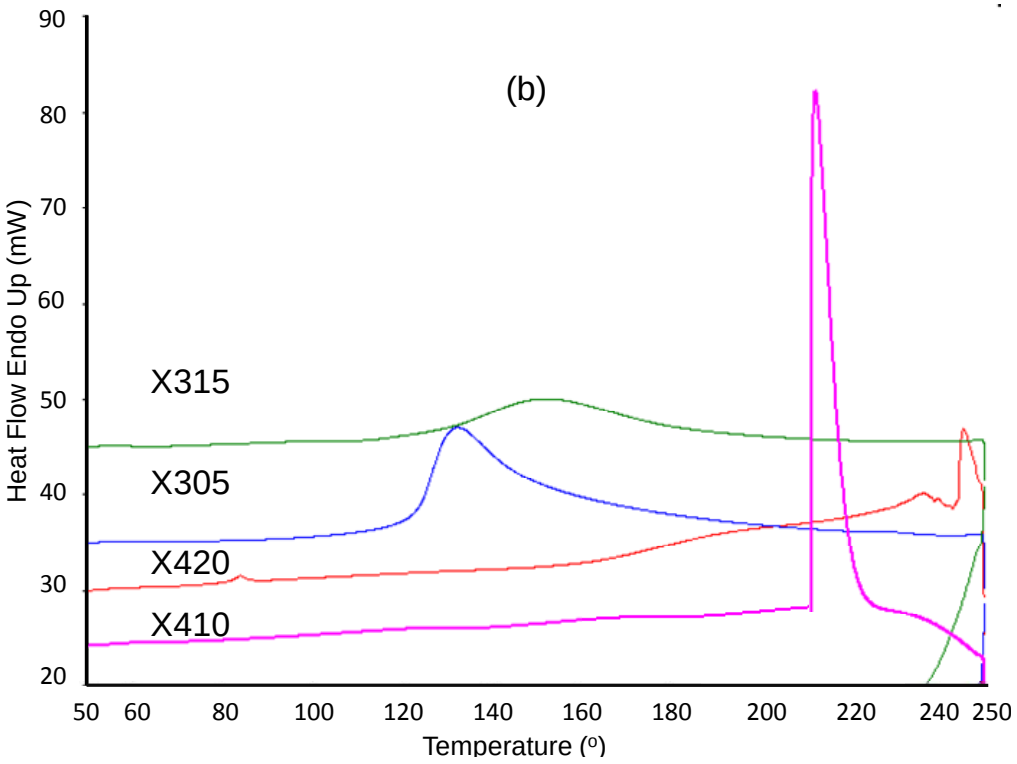

Figure 5-8 DSC heating curves for the xylitol-plasticized samples.

It could be read from Figure 5-8, that the T_m increased upon increasing the xylitol concentration at a MMT-rich scenario as well as the melting enthalpy (the peak width and height). This was different to the observation in glycerol-plasticized system but same to the sorbitol-plasticized system will be discussed (Page 129). Therefore, the argument that the decrease of T_m at a low MMT scenario was related to the antiplasticization 'threshold' of applied plasticizer was confirmed in the xylitol-plasticized system. Since xylitol was reported to possess a higher antiplasticization effect (larger than 20%) than glycerol (~12%), it was within expectation that the T_m value decreased in low MMT samples. Such phenomena will be further discussed in the integrity analyses (based on the type of plasticizers) Chapter (*Chapter* 7).

5.4.3.3 Avrami Equation analyses based on DSC

The Avrami Equation analyses for this ternary system were carried out .Based on the non-isothermal crystallization kinetics analysis; similar to what was mentioned in the glycerol-plasticized sample Chapter (Page 77) the linear regions from crystallization kinetics analyses were distributed over different time-lengths. Meanwhile, the onset temperature was not greatly influenced by either the present of MMT/xylitol or its

relative ratio. The exponent *n* and the factor *k* from Avrami Equation analyses are presented in Table 5-6.

Table 5-6 The exponent n and the factor k obtained from a non-isothermal crystallisation analysis for nanocomposite samples plasticized by xylitol

Sample ID	X105	X115	X210	X220	X305	X315	X410	X420
n	0.71	0.73	052	0.50	2.62	1.42	1.11	0.61
k	-1.21	-1.4	-1.69	-1.32	-4.26	-2.38	-2.91	-1.12

As read from the results from Table 5-6, the *n* values for the composite samples were differed from that of the PS which confirmed the suppressed domain size of the crystalline region. In other words, a relatively random polymeric network formed in xylitol-plasticized composite samples when compared to glycerol-plasticized samples. It was notable to compare the *n* value from xylitol-plasticized samples and the glycerol-plasticized (Table 4-8) samples; the *n* value extracted from the xylitol samples was obviously lower than that from glycerol-plasticized samples. Based on the concept that *n* parameter presented the mechanism of crystal formation, the larger *n* values (from glycerol-plasticized samples) presented a different crystalline mechanism when compared with the xylitol-plasticized samples. And this was in fair conformity with the results obtained in the morphological observation section (Page 95). The next parameter *k* (related to the rate of crystal growth) was smaller than that of glycerol-plasticized samples. Variation among different samples ranged from -0.85(X115) to -3.59(X410) and no obvious tendency was observed.

5.4.3.4 Size distribution of the various crystalline domains

The size distribution profile results are shown in Figure 5-9. Two domains were observed in all the samples, where the diameters of scatters were denoted as $\overline{d}_{1-xylitiol}$(around 104.1Å, domain 1) and $\overline{d}_{2-xylitol}$(around 350.5Å, domain 2), Table 5-7. Further, as per common knowledge, the presence of MMT provided local sites for polymer aggregation and led to the formation of the larger domains. The re-aggregation of certain number of silicate layers into ordered domains during drying, which gave rise to the appearance of extra crystalline domain could further support he observation that two domains were found in the dehydrated samples .

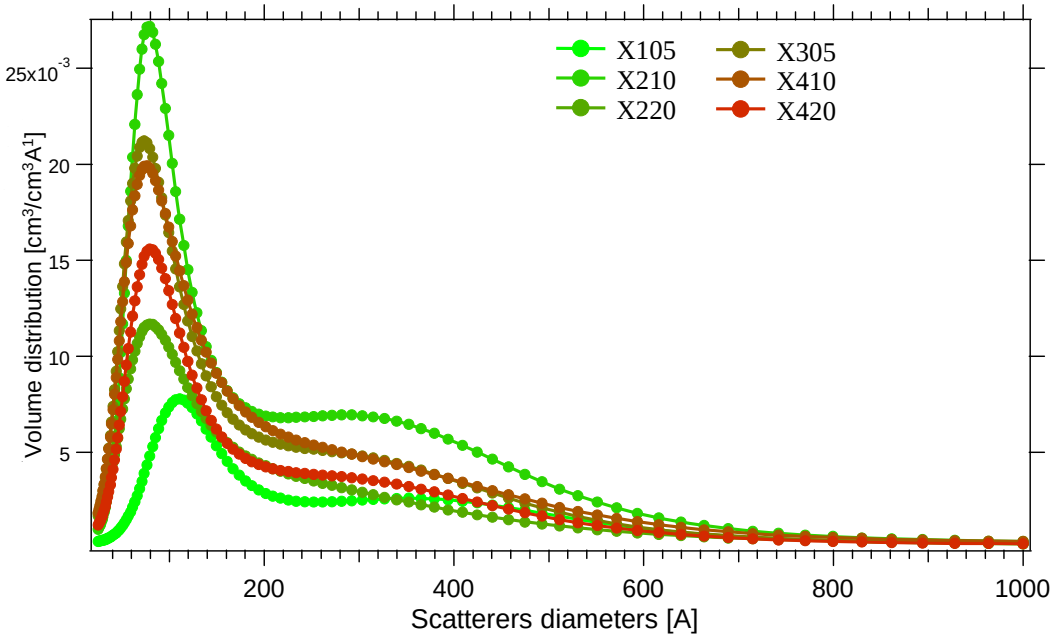

Figure 5-9 Size distribution calculation result for starch/xylitol/MMT nanocomposites.

As shown in Table 5-7, the mean scatter diameter for $\bar{d}_{1-xylitiol}$ ranged from 95.3Å to 119.4Å. The value of $\bar{d}_{1-xylitiol}$ decreased with increasing xylitol amount. In addition, under a 'MMT-rich' environment, a higher xylitol concentration resulted in an increased starch-xylitol interaction, and limited the overall MMT intercalation. Such interactions were supposed to limit long-range order in the bionanocomposites matrix [172]. Furthermore, the MMT/xylitol interactions led to the formation of small crystalline domains due to the nucleating effect of MMT. Additionally, this was reflected in the reduced scatter diameter with changing xylitol concentrations.

Table 5-7 Radius values (Å) from size distribution calculated by MEM method for xylitol-plasticized low moisture content samples.

Sample ID	$\bar{d}_{1-xylitiol}$*(Å)	$\bar{d}_{2-xylitol}$*(Å)
X105	119.3	357.7
X210	98.3	364.1
X220	95.1	345.1
X305	101.2	350.1
X410	106.3	348.1
X420	104.3	338.6

* $\bar{d}$: mean scatter diameter (Å)

The impact of modifying the MMT with the xylitol-plasticizer was observed in domain size difference of xylitol-plasticized sample and the glycerol-plasticized samples. It could be read from Table 5-7 that $\overline{d}_{1-xylitol}$ of xylitol-plasticized samples are higher than glycerol-plasticized $\overline{d}_{1-glycerol}$, however , $\overline{d}_{2-xylitol}$ from xylitol sample turned out to be smaller than $\overline{d}_{2-glycerol}$. This was because the high molecular mobility of the glycerol present in the polymeric network occupied more free cavities and induced the formation of relatively larger crystalline domain.

5.5 Role of water molecules indicated from SAXS profiles

Another set of samples, denoted as HGXX (the prefix H means high moisture) with higher moisture content was subjected to synchrotron test. The role of water molecules within this ternary system was illustrated in terms of comparing the SAXS results from the samples with different moisture content.

Table 5-8 SAXS characterization results extracted from NIKA Diffraction data processing software and Radius (Å) from size distribution calculated by MEM method for xylitol-plasticized samples .

Sample ID	SAXS profiles			Size distribution results
	P_{MMT} (nm^{-1})	P_{starch} (nm^{-1})	d_{SAXS} (Å)	$\overline{d}_{1-hm-xylitol}$ (Å)
X105	0.293	036	21.43	93.6
X210	0.301	0.37	20.86	96.6
X220	0.301	0.361	20.86	84.3
X305	0.309	overlapped	20.32	94.7
X410	0.292	0.69	21.5	95.2
X420	-	0.37	exfoliated	94.6

5.5.1 SAXS results of starch+xylitol+MMT samples with high moisture content

The raw 2-D SAXS patterns from the selected representative high moisture content samples are shown in Figure 5-10. SAXS profiles of high moisture content nanocomposites are shown in Figure 5-11.

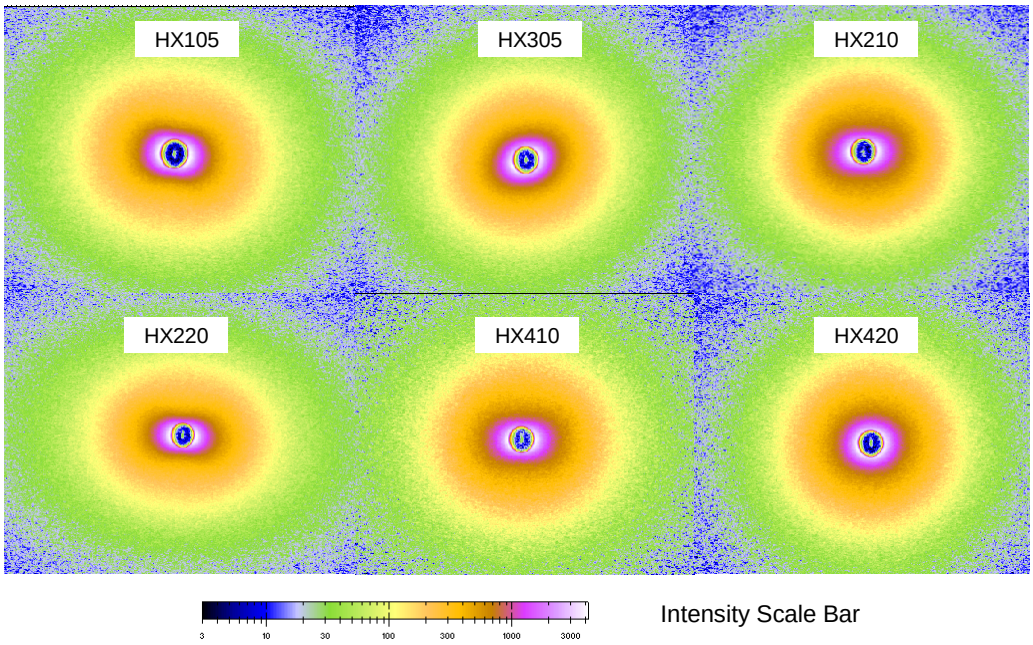

Figure 5-10 Raw 2-D SAXS patterns for selected xylitol-plasticized samples at high moisture content.

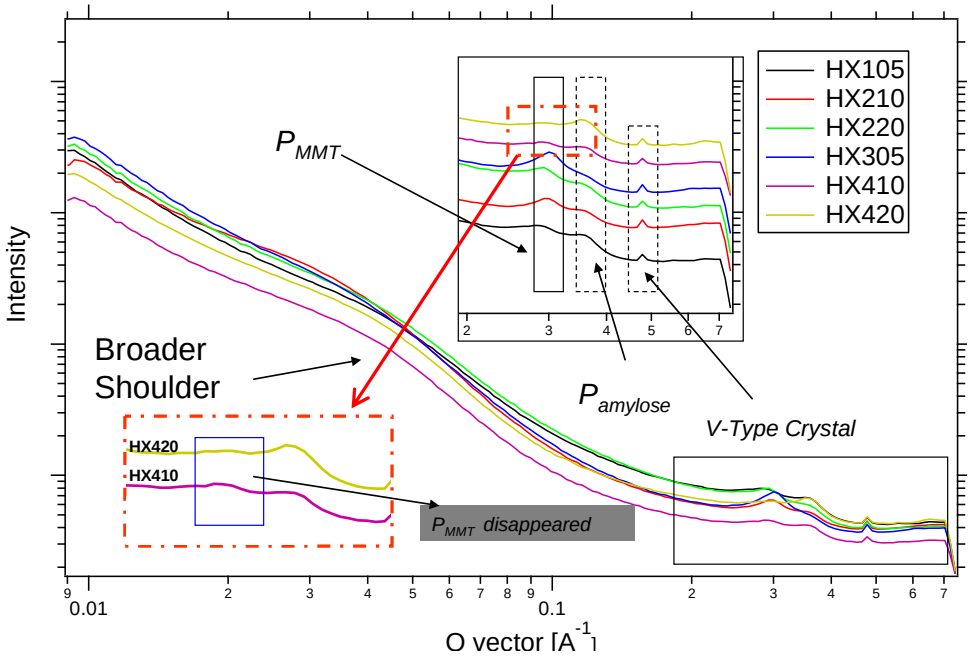

Figure 5-11 SAXS Profiles for PS, starch/xylitol/MMT samples with high moisture content generated from NIKA data processing software.

Together with the SAXS profiles from the high moisture content samples (Figure 5-11 the well-defined 'broader shoulder' around Q=0.04-0.05 Å^{-1} corresponding to the long periodic structure of processed starch polymer [156] was observed.

Meanwhile, similar observations such as larger *basal spacing* (observed to be larger than glycerol-plasticized samples, but smaller than sorbitol-plasticized samples, Table 5-8) and two well separate characteristic peaks for starch and MMT were noticed in this system.

The most significant specific behavior of the xylitol-plasticized high moisture sample was that in 4% MMT samples, a fully exfoliated morphology was obtained upon hydration , inset window of Figure 5-11. This notable finding indirectly indicated that the water molecules were of great importance and contributed to the synergistic interactions. As discussed in the glycerol -plasticized systems, the importance of water molecules mostly lay on its ability to scroll within the polymeric network and balance the heterogeneity. The morphology of the xylitol-plasticized system featured as smaller crystal size and it could be concluded that the optimized results of the balancing effect of water molecule occurred in 4% MMT xylitol-plasticized samples (fully exfoliated morphology).

In xylitol-plasticized system, the interaction of xylitol/starch in the presence of moisture was relatively stronger than xylitol/starch interaction due to weaker intermolecular hydrogen bond force of xylitol crystal. Furthermore, when the MMT concentration was high enough, 4 wt% in the current study, on top of the *bridge effect* (bridging role for fulfilling the cavities within the polymeric network) (Page 139) of water molecules, the relative stronger water/starch interaction probably resulted in the redistribution of the MMT platelets and led to the formation of a fully exfoliated morphology which has been illustrated in Figure 5-12 by the disappearance of the characteristic of MMT.

5.5.2 Size distribution of the various crystalline domains

The size distribution profile results for high moisture samples are shown in Figure 5-12. Only one domain ($\bar{d}_{1-hm-xylitol}$) sized around 93.2 Å which was significantly smaller than $\bar{d}_{1-hm-glycerol}$ (101.7Å) and $\bar{d}_{1-hm-sorbitol}$ (97.8 Å) (in next chapter, Page 132), was observed in the high moisture samples.

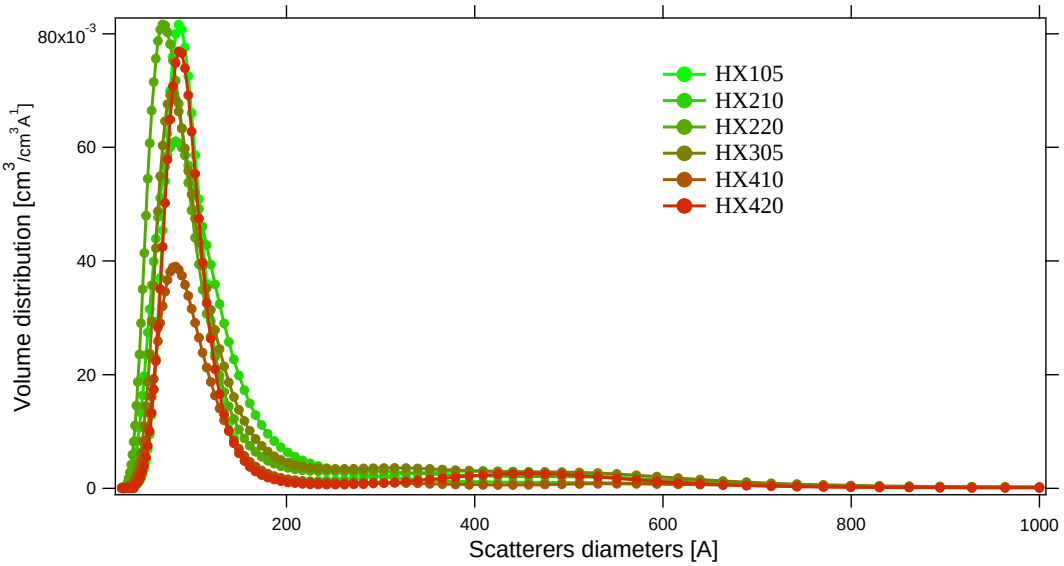

Figure 5-12 Size distribution calculation result of starch/xylitol/MMT nanocomposites with high moisture samples by MEM method.

Mean scatter diameter for $\bar{d}_{1-hm-xylitol}$ ranged from 84.3 Å to 96.6 Å which was unexpectedly smaller than that from the low moisture content samples. Exactly opposite findings were observed in the glycerol and sorbitol-plasticized system (in next chapter, Page139), where the crystalline domain size for the high moisture content samples was larger than the low moisture ones as the 'trapped' water molecules slightly expanded the crystalline domain. However, the introduction of water molecules in the xylitol-plasticized system further enhanced the obstruction of crystallization process and decreased the crystalline domain size. It was believed that the excess water molecule provided certain extent of lubricant for the competitive interactions between xylitol-MMT crystals rather than involving in the crystallization growth (the case in glycerol and sorbitol-plasticized samples).

Summary

The synergistic interaction in xylitol-plasticized nanocomposite was studied via various characterization methods. The combined influence of xylitol (1-20 wt %) /MMT (1-4 wt %) loading on the characteristics of extruded xylitol-plasticized starch nanocomposites was analysed.

Important conclusions that were drawn are as follows.

1. Based on the results from WAXD, it could be further concluded that the achievable *basal spacing* of MMT was determined from the molecular size of the plasticizer. Interactions between starch and MMT were evidenced from corresponding FTIR spectra as well as the formation of hydrogen bonds.

2. These two observations (high X_c% and broadening of WAXD patterns) strongly suggested that in xylitol-plasticized system, the crystallization process was significantly different to that of glycerol-plasticized systems. In xylitol-plasticized system, the form of crystal were likely to be smaller (broadened WAXD pattern) but the total amount of crystal, higher *Xc* % values, was larger than glycerol-plasticized sample.

3. Two domains sized at approximately 93.7Å (larger than glycerol/sorbitol sample) and 350Å (smaller than glycerol samples) were found in the low moisture samples. These observations resulted from the strong crystallization ability and weaker intermolecular hydrogen bonding strength of xylitol plasticizer.

4. A fully exfoliated morphology was observed in HX410 and HX420. This observation was believed to result from the redistribution of MMT platelets at a high MMT loading caused by the relatively stronger water/starch interaction which competed with xylitol/starch interaction in the presence of excess moisture content.

5.

Chapter 6

Sorbitol Plasticized High Amylose Nanocomposites

Chapter Outline

Supplementary experiments (^{13}C NMR) were carried out on sorbitol-plasticized system to provide supporting evidence in the relevant discussion.

The discussion arrangement structure in this Chapter is similar to that of the glycerol and xylitol chapter, except that the starch+MMT *system* will not be repeated in this Chapter. Different binary systems (the sorbitol+MMT system and starch+sorbitol system) would be discussed separately followed by investigations into the complex ternary system (starch+sorbitol+MMT). Conclusions have been drawn based on the presented discussions.

6.1 Starch+MMT system

The system had been studied in *Chapter 4* (Glycerol-plasticized High amylose nanocomposites), sections 4.1 (Page 50). Please kindly refer to the indicated section for detailed information.

6.2 Sorbitol+MMT system

The interaction between sorbitol and MMT was analysed by investigating the samples that were prepared with different sorbitol: MMT ratio by sonication. FTIR and WAXD were performed to characterize the intermolecular interactions and morphological features of this binary system. The experimental results and discussions are presented as follows.

6.2.1 Intermolecular interactions

Similar to the glycerol/MMT hydrophilic system, the disappearance of free 'OH' groups band vibration (band 3627 cm^{-1} indicated the existence of plenty of free 'OH' groups) of MMT [148] clearly indicated that the interactions took place between MMT and sorbitol upon sonication. It was reasonable to assume from the FTIR spectra that the sorbitol molecules were penetrated into the 'gallery' of stack-like MMT via hydrogen bonding.

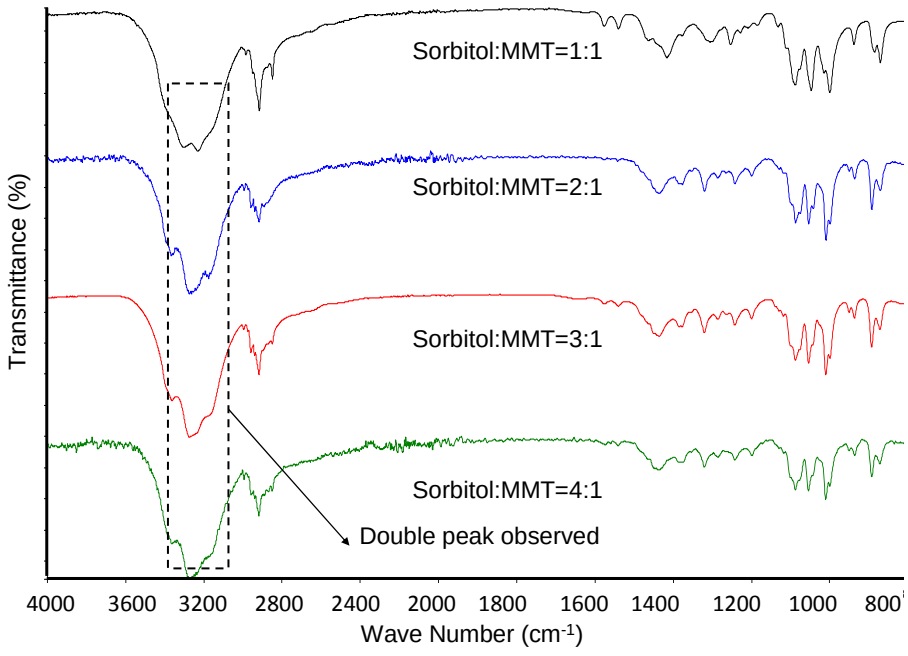

Figure 6-1 FTIR results for MMT: sorbitol samples at 1:1, 1:2, 1:3 and 1:4 ratio.

On top of the similar findings, different to what found in glycerol/xylitol-plasticized samples, the double peak observed in – 3270 cm^{-1} was noticed in only sorbitol-plasticized samples. These observation suggested that the interaction between sorbitol and MMT was stronger than those from glycerol/xylitol-plasticized system, which was due to the larger number of hydroxyls groups presented in sorbitol (-6-OHs). Further discussions are presented in the ternary system discussion (Page 118).

6.2.2 Morphological observations

Comparing the WAXD results of all the prepared sorbitol-plasticized samples, the minimum and maximum value of *basal spacing* occurred in the 1:1 MMT: sorbitol sample (17.84 Å) and 1:4 MMT: sorbitol sample (18.14 Å), Figure 6-2. The value of *basal spacing* showed an ideal direct proportionality to the sorbitol loading.

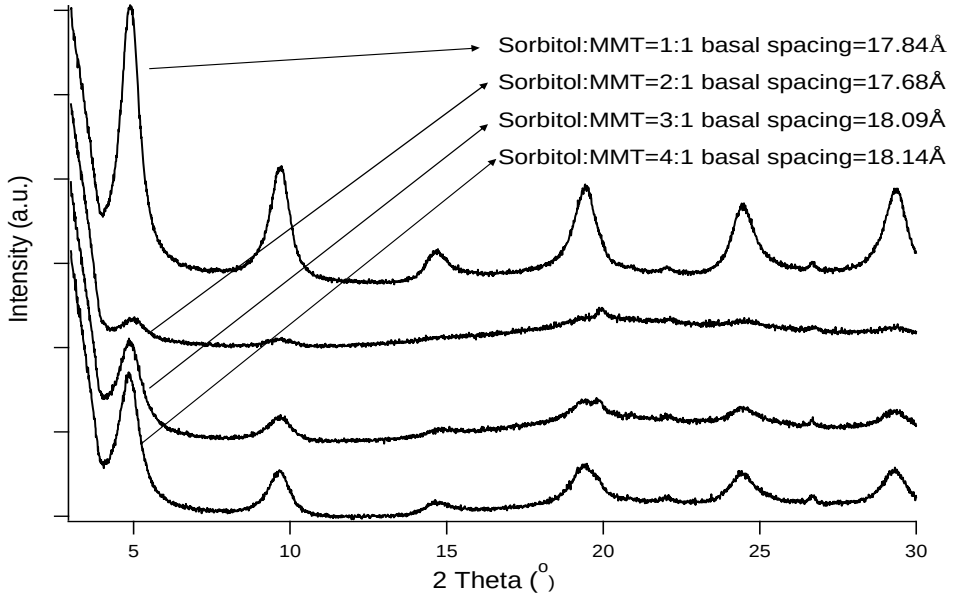

Figure 6-2 WAXD Patterns for MMT: Sorbitol samples at 1:1, 1:2, 1:3 and 1:4 ratio.

The hinderance effect of plasticizer on the 'gallery' expansion of MMT at a higher amount was not so obvious in the sorbitol-plasticized system, where *basal spacing* value increased as the amount of sorbitol increased. This was contrary to that of the glycerol-plasticized samples. As shown in Figure 6-2, the largest basal spacing occurred in 1:4 (MMT: Sorbitol) samples (18.14Å).

The hypothesis that the expansion of the gallery was mostly dependent on the molecular size of the plasticizer could be confirmed by the larger *basal spacing* of sorbitol samples since sorbitol had a larger molecular size than glycerol. For sorbitol,

Δd equalled the average size of sorbitol which meant the sorbitol molecule had been trapped between two MMT platelets. This could be supported from the fact that the glycerol samples exhibited similar *Δd* to glycerol's molecule size, except 1:1 (MMT: glycerol) sample. However, it was found that the *basal spacing* for xylitol turned out to be higher than both glycerol and sorbitol-plasticized samples. Molecular symmetry could be the reason to this observation, since the conformation of 'trapped' xylitol was dependent on its intrinsic molecular symmetry.

6.3 Starch+Sorbitol system

The final binary system studied was the starch+sorbitol system that was devoid of nanoparticles. Two samples were produced with 10 wt% and 20 wt% sorbitol according to the DOE. The obtained characterization results are presented as follows.

6.3.1 Intermolecular interactions

6.3.1.1 Water Isotherm

Water isotherm, shown in Figure 6-3, was used to investigate the interactions between starch and sorbitol.

An 'inversion' phenomenon was observed in the sorbitol-plasticized samples , where higher sorbitol loading samples retained lower amount of equilibrium moisture at low a_w values; but as the a_w increased, this relationship between the equilibrium moisture content and the sorbitol content was inverse . However, it is important to note that the equilibrium moisture content for sorbitol-plasticized samples were overall lower than that from glycerol-plasticized samples. For example, the equilibrium moisture content of G010 and S010 at a a_w value of ~0.328 was 0.083 and 0.073 kg water/kg solid. This could be due to the low hygroscopicity of sorbitol to retain moisture molecules when acting as a plasticizer. The relatively weaker plasticization ability of sorbitol (when compared to glycerol) had been illustrated in Chivrac *et al.* 's work [114]. Furthermore, this inversion happened at comparable a_w value of ~0.56 compared to that of ~0.55 for glycerol- plasticized samples.

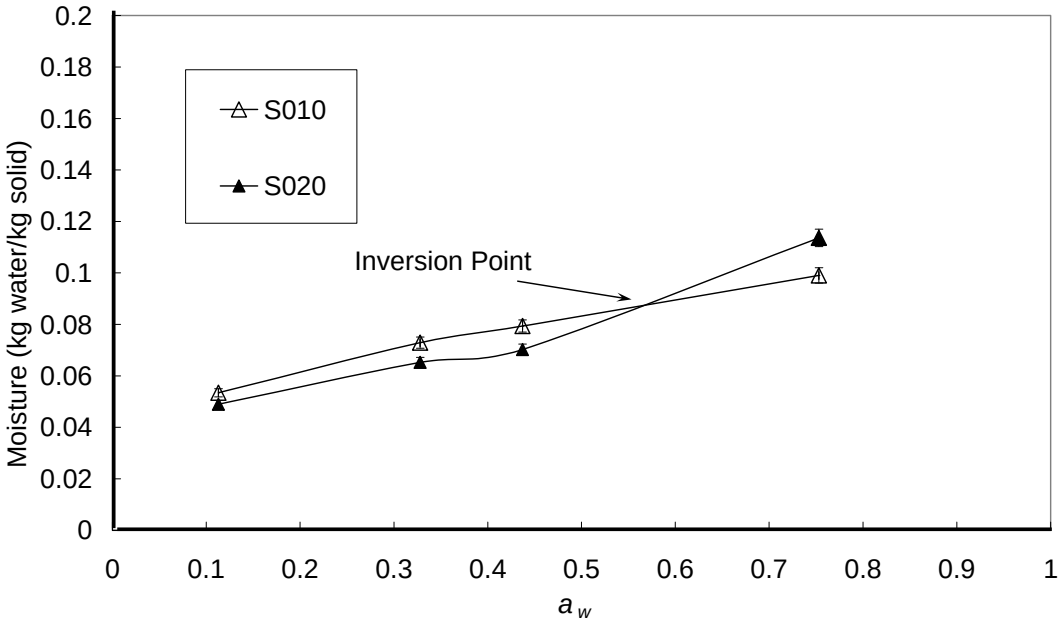

Figure 6-3 Water isotherm experimental results and GAB fitted data for S010 and S020

6.3.1.2 GAB Model for isotherm data

The GAB equation analysis was completed to understand the isotherm behaviour; relevant results are shown in Table 6-1.

Table 6-1 GAB Fitting Parameters for sorbitol-plasticized samples, $R^2 > 0.88$

Name	w_m	*C*	*K*
PS	0.092	46.243	0.669
S010	0.040	21.370	0.899
S020	0.037	30.830	0.935

In Table 6-1, parameter w_m (denotes the moisture content of the whole polymer surface) was obviously overall smaller than that of glycerol/xylitol-plasticized samples which highlighted the negative effect of sorbitol when concerning the plasticization effect. In other words, less amount of moisture could be retained due to the plasticization effect of sorbitol. The molar sorption enthalpy values, represented by parameter *C* increased upon the increasing of sorbitol concentration. this indicated that in terms of the equilibrium conformation of the polymer and the plasticizer, greater energy exchange occurred in the case of higher-sorbitol loading samples .

6.3.2 Morphological observations

6.3.2.1 SAXS

The 2-D SAXS patterns and the SAXS profiles for PS, S010 and S020 are shown in Figure 6-4. The shape of the scattering pattern changed from circular (PS) to elliptical (G020) with the addition of 20 wt% glycerol in glycerol-plasticized samples. However, in sorbitol-plasticized samples, the addition of 20% sorbitol did not progressively change the shape of the scattering pattern. Negligible differences were observed in S010 and S020 in terms of the ellipticity of the scattering pattern. Such observation indicated that the polymeric network order of S020 was lower than that of G020 as reflected from the higher ellipticity of G020. We noted that both glycerol and sorbitol had almost exactly the same number of hydroxyl groups per unit mass of plasticizer, 3/92 ~ 6/182 ~0.033 gmol OH/g plasticizer, and also their molecular diameters are very similar at ~6.4 Å. However, their molecular lengths, as measured by the number of carbon atoms (C), are different: 3 C for glycerol compared to 6 C for sorbitol. Thus, it was within expectation to obtain a relatively more non-uniformed polymeric network in sorbitol system when compared to the glycerol system as shown by the higher ellipticity in G020. The trend of interhelix spacing changes upon increasing sorbitol concentration. This will be discussed in the following section with further evidence about the effect of molecular length on the final polymeric structure formed.

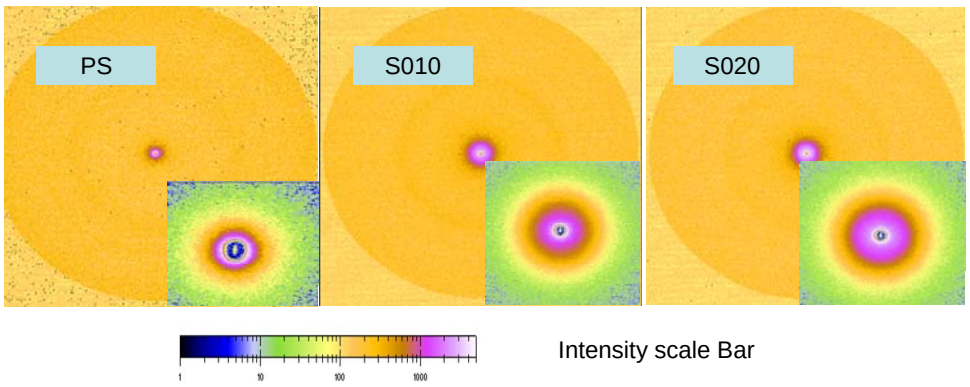

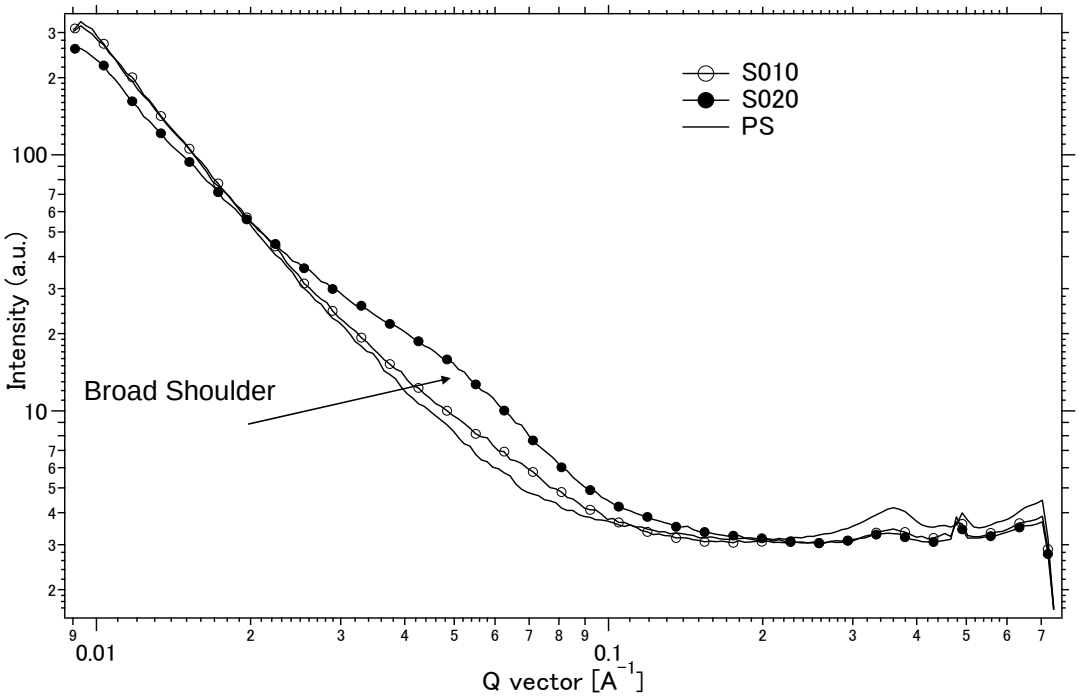

Figure 6-4 The SAXS profiles for PS, S010 and S020 generated from NIKA data processing software.

As shown in Figure 6-4, similar to the glycerol-plasticized system, the S010/S020 samples showed relatively higher intensities, and these observations further indicated that strong interactions took place and reflected the presence of heterogeneities within the network structure. In other words, the addition of sorbitol promoted the growth of lamellar structure within the samples.

Table 6-2 SAXS characterization results for PS, S010 and S020.

Sample ID	Moisture (%)	P_{MMT} (nm^{-1})	P_{starch} (nm^{-1})
PS	2.2	-	0.368
S010	2.71	-	0.358
S020	2.14	-	0.355

The characteristic peak of extruded starch denoted as P_{starch} in Table 6-2 was a reflection of B-type crystalline morphology and this peak was found to decline upon the addition of sorbitol, as seen in Figure 6-2. This was due to the higher amount of sorbitol "hosted" by the starch and was again indicative of the strong starch-sorbitol interactions. Meanwhile, contrary to the findings in glycerol-plasticized system where the P_{starch} increased (from 0.352 to 0.357), in Table 6-2, with increasing

sorbitol concentration from 10 wt% to 20 wt%, the P_{starch} for S010 and S020 decreased from Q=0.358 Å $^{-1}$ to Q=0.355 Å^{-1} (indicating greater starch-sorbitol interaction), respectively. The P_{starch} also shifted to a lower Q value indicating an enlarged interhelix spacing, confirming the sorbitol molecules were "held" tightly within the starch network after equilibrating the samples at low moisture content environment. Such observation was well related to consideration of molecular length from different plasticizer.

The unique observation for G020 (the 'shoulder' around Q=0.04-0.05 Å^{-1}) was also observed in S020, shown in Figure 6-4. This observation typically meant that, as suggested in Section 4.3.2 (Page 63), the sorbitol successfully replaced water in starch-water interactions at high sorbitol concentration and contributed to the preservation of the long periodic structure of starch polymer, which was similar to the finding from glycerol-plasticized system.

6.3.3 Crystallization behaviours

6.3.3.1 Differential Scanning Calorimetry

The DSC results, Table 6-3, indicated that the addition of sorbitol undoubtedly decreased the T_g value and no obvious effect was seen on the T_m value, Table 6-3, which was different from the observation made in glycerol-plasticized system. T_g value for sorbitol-loaded samples decreased from 49.5 (PS) to 45.7 (10% sorbitol) and 25.8 (20% sorbitol) due to the typical plasticization effect of sorbitol, Table 6-3. When considering the antiplasticization 'threshold' for sorbitol (reported to be around 27%) and glycerol (reported to be around 13%), the distinctness of tendencies of the T_m changes could be explained. The sudden decrease of T_m in G020, from 184 to 171, was due to the transition from 'antiplasticization region' to the 'plasticization region' of glycerol. The reason for no obvious changes between the T_m value for S010 and S020 was that the sorbitol concentration was still within the 'antiplasticization region' of sorbitol plasticizer.

Finally, two melting endotherms were observed in S020 samples indicating the phase separation within the corresponding composite. The first T_m is ascribed to be the sorbitol-rich phase and the second T_m to the low-sorbitol or MMT-rich domain. Such phase separation of domains either with or without nanofillers induced by high plasticizer content of starch formulation could further explain the interesting

moisture measurement and crystallinity behaviour .This will be discussed later and similar results have been published by other researchers [62, 114].

6.3.3.2 Avrami Equation analyses based on DSC

Furthermore, the Avrami equation analyses results for PS, S010 and S020 are shown in Table 6-3. It could be read from Table 6-3, in the sorbitol-plasticized system, the crystallization behaviour was more unpredictable and the evaluated crystallization behaviour related parameters, *n* and *k*, were distributed randomly. More data from ternary system will be discussed later to provide a better interpretation for the crystallization behaviour of this complex system.

Table 6-3 Exponent n and the factor k obtained from a non-isothermal crystallisation analysis for the PS, S010 and S020 samples.

Sample	T_g, °C	T_m, °C	*n*	*k*
PS	49.5		0.48	-1.47
S010	45.73	239	0.56	-6.24
S020	25.75	236	0.68	-0.96

6.4 Starch+Sorbitol+MMT nanocomposite system

6.4.1 Intermolecular interactions

6.4.1.1 Moisture Content Measurement

Moisture content measurements results for the prepared sorbitol-plasticized samples are presented in Table 6-4.

Table 6-4 Moisture content, basal spacing, crystallinity, glass-transition temperature (T_g) and melting temperature (T_m) for sorbitol-plasticized samples.

Sample ID	Moisture (%) (S.D. =1%)	*Basal spacing* (Å)	*Xc**(%) (S.D. =2%)	T_g (°C)	T_m (°C)
S105	2.38	exfoliated	4.50	49.6	217
S115	4.83	18.044	3.73	47.5	214
S210	3.23	18.189	4.01	47.73	233
S220	4.53	18.044	6.11	31.25	240
S305	3.52	17.544	7.81	53.4	211
S315	2.53	18.179	4.32	50.4	236
S410	2.45	18.572	8.28	55.5	218
S420	2.07	18.638	6.56	33.83	198

$\Delta d = d_{sample} - d_{pristine\ MMT}$

*crystallinity calculated from the method described in Ref [147].

As shown in Table 6-4, similar to the observations found in glycerol-plasticized system, the addition of sorbitol decreased the moisture content; the moisture content for S200 and S210 was decreased to 6.19% and 3.23%, respectively. This reduction was a consequence of the strong interaction between sorbitol and starch matrix where the water molecules within the polymer structure were replaced by sorbitol molecules. The data shown in Table 6-4 indicated a complex interaction among starch, sorbitol and the MMT depending upon their relative concentrations. It was important to remember that moisture content varies based on the active –OH sites available in the system. Two prominent tendencies were observed based on the moisture content values. Samples showed higher moisture content for increased sorbitol amount and this is a well-known plasticization effect due to the hydrophilic plasticizer. However, as the MMT content was increased, sorbitol could interact with the MMT, and this competed with relatively stronger starch-sorbitol interaction, thereby decreasing the moisture content. Interestingly, if sorbitol concentration was fixed, it was found that the moisture content was inversely proportional to the MMT loading except for S105 and S305. The high moisture content from low MMT content samples was believed to be a result of a lower proportion of sorbitol, thereby reinforcing sorbitol's typical plasticization effect. Meanwhile the unexpected results of S105 and S305 indicated the formation of different morphology within the low-plasticizer loading samples. This will be detailed in the Integrity Analyses Chapter (*Chapter 7*).

6.4.1.2 FTIR results

The FTIR results for the sorbitol-plasticized nanocomposites are shown in Figure 6-5. First, the vibration modes of C-C and C-O stretching and the bending mode of C-H bonds which was considered to be the typical saccharide bands turned out to be the most intense in the FTIR-spectra. Secondly, the formation of hydrogen bonds between sorbitol/MMT and starch/MMT was proved by the shift of the band 3627cm^{-1} (characteristic band for the free OH group of pristine MMT surface) to a lower frequency, 3302cm^{-1}. And finally the presence of new and stronger hydrogen bonds could be evidenced from the double peaks at 2919cm^{-1}-2887cm^{-1} and 999cm^{-1}-992cm^{-1} in the nanocomposites samples when compared with PS [159]. The double peak of O-C stretching band at 999cm^{-1}-992cm^{-1} results from bending both 'O' of C-O-H and 'O' of anhydrous glucose ring in starch molecules [160].

The FTIR spectra revealed the polymeric network of starch/sorbitol, starch/MMT, and sorbitol/MMT interactions. Integrity analysis and other characterization results are discussed in the later sections.

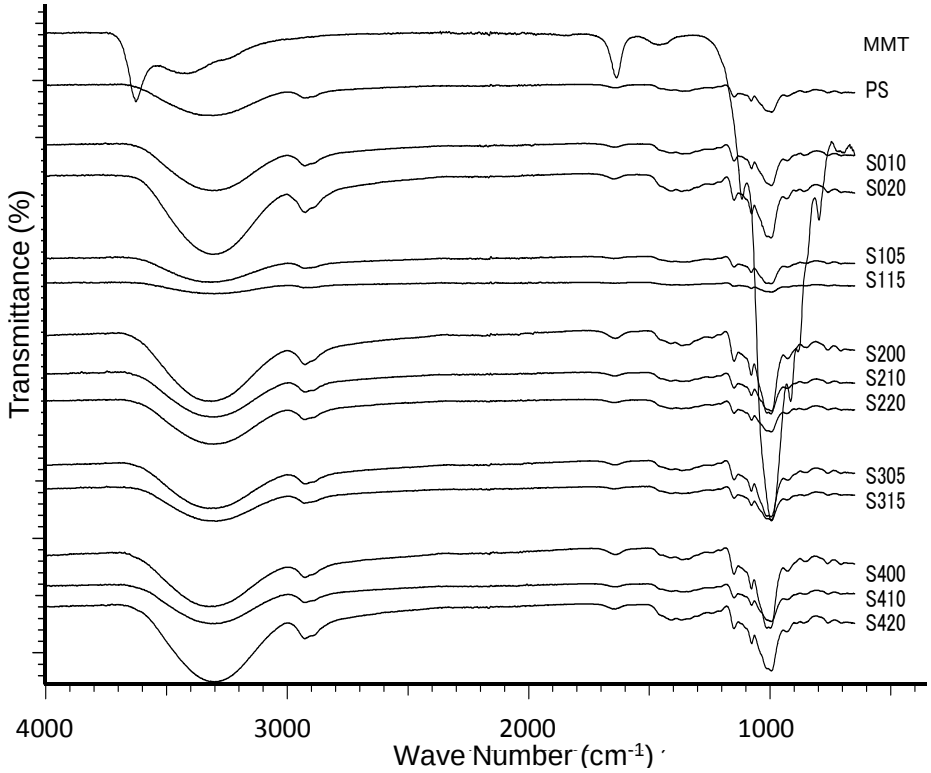

Figure 6-5 FTIR spectra for PS, pristine MMT and sorbitol-plasticized nanocomposites.

6.4.1.3 ^{13}C NMR results

^{13}C NMR measurements were carried out to clarify the intermolecular interactions. The characteristic peaks for sorbitol and starch were shown in Figure 6-6. Selecting two separate peaks (number 6 for sorbitol and number 6 for starch as shown *Figure 6-6* from sorbitol and starch spectrum, denoted as $I_{sorbitol}$ and I_{starch}, the relative ratio of peak intensity $\Delta I = (I_{sorbitol\text{-}6}/I_{starch\text{-}6})$ can be determined. Mobility of sorbitol was clearly higher than that for starch chains, and depending on the initial ratio of starch/sorbitol. The carbon mobility of sorbitol was significantly higher than that of starch chains. This could be attributed to the sorbitol's smaller molecular size. The relative ratio between sorbitol peak and starch peak was dependent on the initial ratio of sorbitol/starch and also influenced by the interaction between starch/sorbitol which restricted the molecular movement.

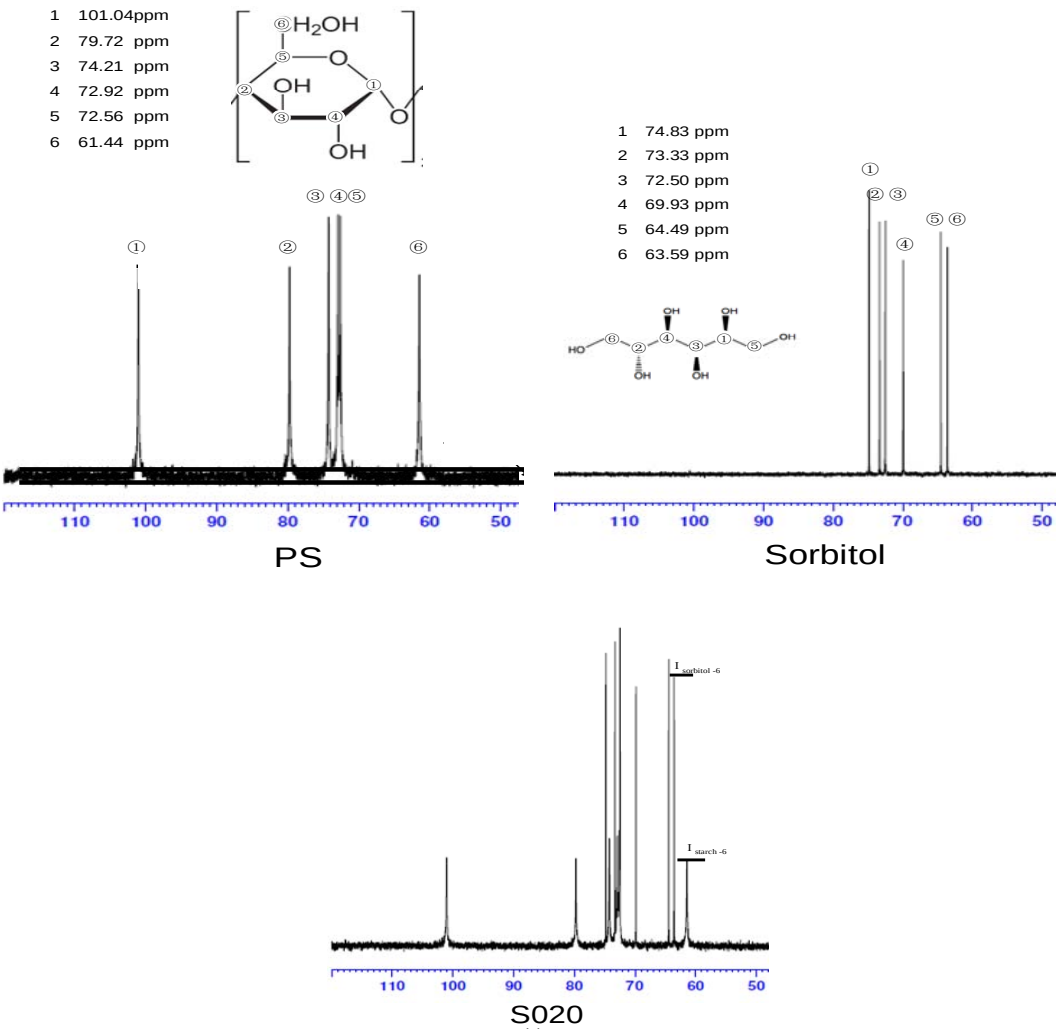

Figure 6-6 ^{13}C spectra for PS, Sorbitol and S020.

This relationship could be reflected from the *ΔI* values for different samples, as shown in Table 6-5. As seen from Table 6-5, *ΔI* values increased with the sorbitol amount, except S105, regardless of the MMT concentration which was attributed to greater proportion of high mobility sorbitol molecules. Also, increasing the MMT within samples with identical sorbitol resulted in higher *ΔI* value due to stronger interaction between starch chains and MMT that influenced the starch concentration; however the highest *ΔI* values came from S315 rather than S420.

Table 6-5 $\Delta I = (I_{sorbitol\text{-}6}/I_{starch\text{-}6})$ for sorbitol-plasticized nanocomposite as determined from ^{13}C spectra.

Sample ID	ΔI
S105	0.648
S305	1.037
S210	1.691
S410	1.732
S115	2.658
S315	3.067
S220	2.687
S420	2.703

In Table 6-5, ΔI values increased with the higher loading of MMT when the sorbitol concentration was fixed. Furthermore, it was interesting to note that a different behaviour was observed when comparing spectra for S105 and S115, where the mobility of sorbitol was unexpectedly lower than the long chain starch, as shown in Figure 6-7.

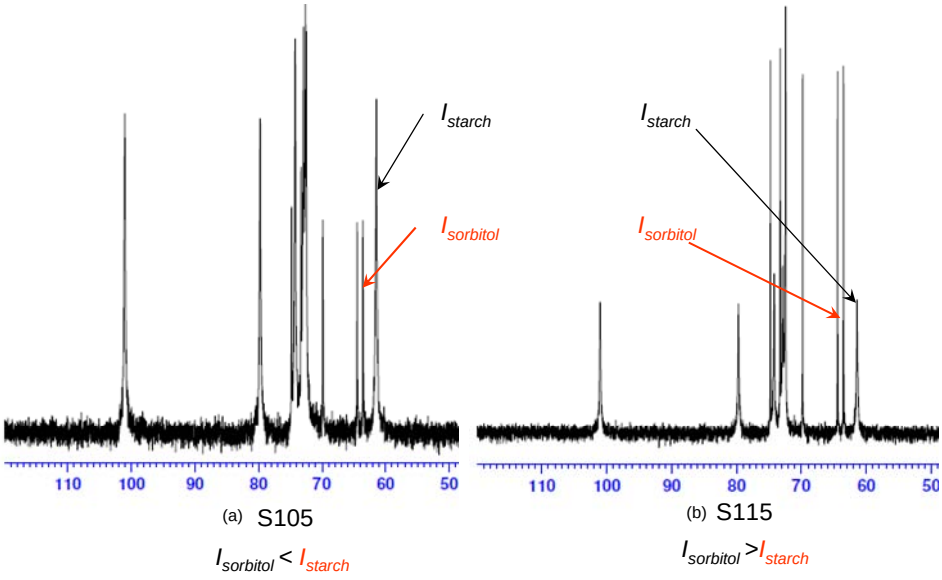

Figure 6-7 ^{13}C spectra for S105 (loosen-soft polymeric network. and S115 (tighten-firm polymeric network).

The observation that lower mobility of sorbitol component when comparing to starch chains in S105 was believed to be due to the low concentration of both MMT and sorbitol. At higher sorbitol concentrations (S115), the sorbitol molecules shows higher mobility than that from starch chains which might be attributed to the higher loading of sorbitol. The high concentration of sorbitol results in an over-saturated polymeric structure in terms of sorbitol molecules mobility. This was corroborated by diffraction measurements that WAXD patterns for S105 showed that greater

exfoliation morphologies existed for these samples. The diffraction peak from S115 was obviously sharper than that from S105 indicating a higher packing density from S115 sample.

6.4.2 Morphology observations

6.4.2.1 WAXD and TEM

The WAXD patterns in Figure 6-8 (a) show that all the nanocomposites samples exhibited an increase in the *basal spacing* regardless of the MMT content, similar to the glycerol/xylitol-plasticized system. The *basal spacing* values also suggested that starch and/or sorbitol molecules had migrated into the gallery of MMT, and this suggestion was based on the molecule sizes for sorbitol/starch fragments that reasonably agree with the Δd values (Table 6-4).

It could be read from Table 6-4 that *basal spacing* increased with sorbitol and MMT concentration. Correspondingly, S420, the sample with highest amount of sorbitol and MMT imposed the highest *basal spacing* value of 18.64 Å. This was attributed to the overall interaction between the hydrophilic starch and sorbitol plasticizer, which can facilitate the polymer to penetrate into the hydrophilic MMT gallery. These basal spacing values of sorbitol-plasticized samples were overall higher than those of glycerol-plasticized samples, Table 4-6 and Table 6-4, and were believed to be due to the relatively larger molecular size of sorbitol.

From the WAXD patterns, it was seen that 5% sorbitol samples showed highest degree of MMT's exfoliation which reflected as a broaden peak in the WAXD pattern. According to the theory of kinematical scattering, peak broaden is caused by either reduced crystal size or the presence of large defects [161]. The broadened peaks for 5% sorbitol (in S105 and S305) strongly indicated that greater starch/MMT interaction had been achieved by using sorbitol as the modifier for MMT.

On the other hand, the sharp peaks for higher sorbitol amounts suggested that the stronger starch/sorbitol interaction became dominant and reduced the amount of MMT intercalation. It could be assumed that 5% sorbitol acted like a 'threshold' for further expansion/ exfoliation of MMT. In other words, 5% sorbitol will be the optimum concentration for MMT expansion/exfoliation when exfoliation was the

only factor to be considered. This was manifested by the obviously broaden peaks found in samples with 5% plasticizer when compared to other specimens.

TEM image for representative samples (S305, S220 and S315) with intercalated/exfoliated mixed morphologies are shown in Figure 6-8 (b). A high degree of exfoliation was observed in S105 sample, and this was a likely effect of high polymer and plasticizer to MMT ratio, which provided proportionally higher polymer free –OH groups to interact with the MMT. It is thought that the stabilization of sorbitol in natural MMT attracted greater starch chains due to their inherent hydrophilicity and improves polymer/MMT interaction during extrusion processing. Such observations were similar to that found in glycerol-plasticized samples, which means that 5% plasticizer loading was the critical point in the formation of certain polymeric network. This would be detailed in the Integrity Analyses Chapter (*Chapter 7*).

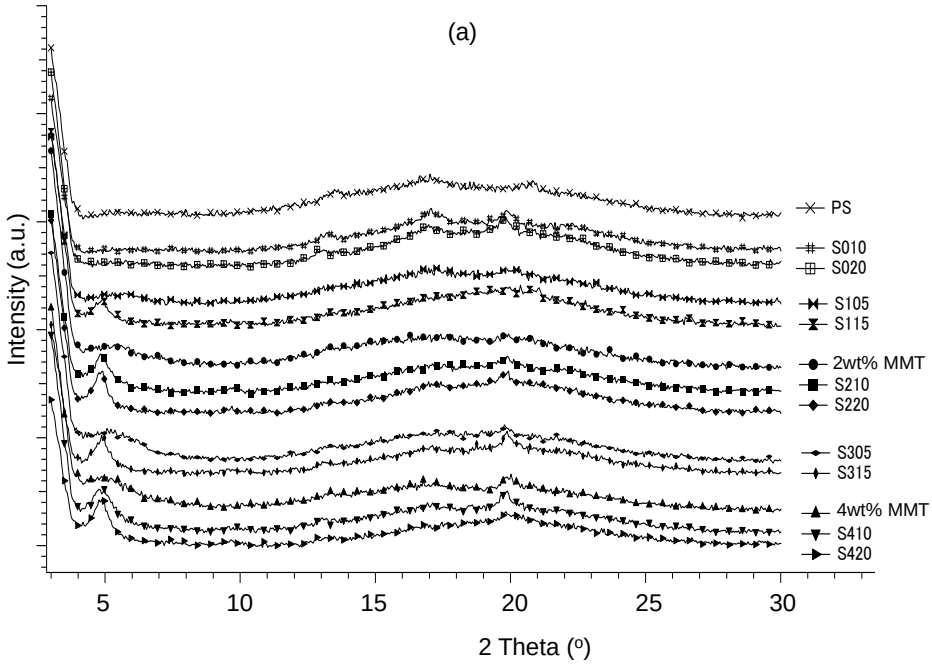

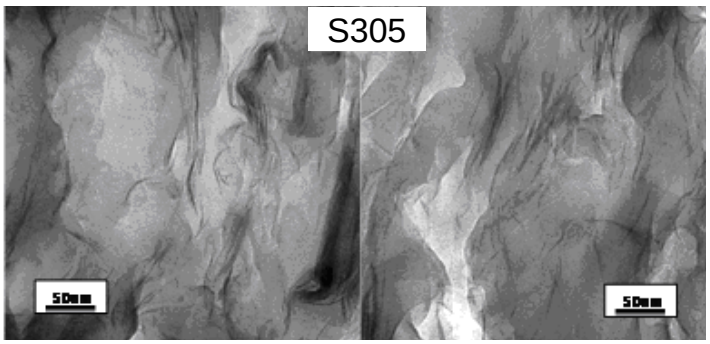

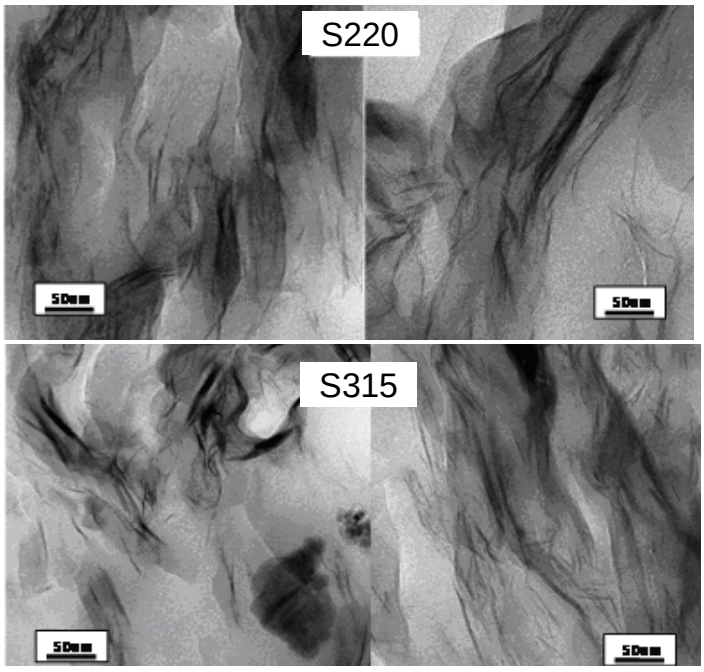

Figure 6-8 (a) WAXD patterns for sorbitol-plasticized nanocomposites and (b) TEM images for S305, S315 and S220.

6.4.2.2 Small Angle X-ray Scattering (SAXS)

The raw 2-D SAXS patterns for the ternary composites samples (starch+sorbitol+MMT) are shown in Figure 6-9. The SAXS profiles for all the sorbitol-plasticized samples are presented in

Figure *6-10*.

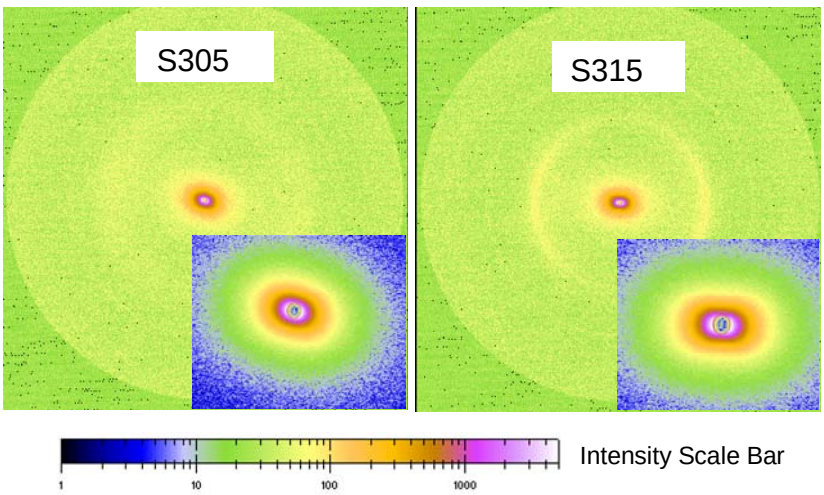

Figure 6-9 Raw 2-D SAXS patterns for selected ternary composites; S305, S315

Similar to the glycerol-plasticizer systems, there was no intuitive distinction that could be observed between the raw SAXS patterns for the binary composites samples (Figure 6-4) and the ternary composites samples (Figure 6-9). They shared the

common features such as elliptical shape, and the ellipticity increased upon the increasing of MMT. The crystalline domain size distribution calculation of the ternary composites was carried out to gain a better understanding of the synergistic interactions.

The corresponding *basal spacing (d_{SAXS})* values and the characteristic peak for starch and MMT are shown in Table 6-6.

Table 6-6 Characteristic peak position profiles and calculated basal spacing for sorbitol-plasticized samples.

Sample ID	Moisture (%)	P_{MMT} (nm^{-1})	P_{starch} (nm^{-1})	d_{SAXS} (Å)
S105	2.38	0.423	0.358	Exfoliated
S115	4.83	0.315	-	19.9
S210	3.23	0.317	-	19.8
S220	4.53	0.310		20.3
S305	3.52	0.422	0.36	Exfoliated
S315	2.53	0.311	-	20.2
S410	2.45	0.309	-	20.3
S420	2.07	0.302	-	20.8

The presence of peak overlapping of basal distance of MMT and 100 interhelix of polymer and the absence of well-defined peaks in low moisture content samples (when compared to the high moisture samples which will be discussed in the 'role of water' section, Page 135) indicated the presence of short-range order where the MMT prevented starch-sorbitol to form large domain structures. This is typical of moisture sensitive polymer upon drying as reported by other researchers [156, 166]. Heterogeneities reflected from the intensity of scattering were not only related to the presence of MMT but also to their concentration. As expected the intensity of scattering increased with the MMT loading.

From SAXS profiles,

Figure *6-10*, the sharp *d001* in low moisture content samples strongly indicate closely packed structures of starch-MMT and starch-sorbitol assemblages. Since removal of water is similar to aging, it has been suggested that a closely packed starch network is an indication of lower polymer chain mobility [172]. And this was

mutually supported from the observed the high T_m value for high sorbitol concentration samples.

As shown in Table 6-6, the *basal spacing* for different samples was overall larger than that from glycerol-plasticized nanocomposites. For instance, the d_{SAXS} value for G210 and S210 are 19.03 Å and 19.81 Å, respectively. Similar results are obtained in G220/S220, G410/S410, G420/S420. Such phenomena clearly indicated that the expansion degree of the MMT gallery was related to the size of the plasticizer incorporated in the complex system. Another convincing evidence could be drawn when comparing the 100 interhelix value for G020 (17.6 Å) and S020 (17.7 Å) when the plasticizer amount was high enough.

Together with the result in Table 5-5 (d_{SAXS} for glycerol and xylitol-plasticized samples), It was noticed that the d_{SAXS} from the xylitol-plasticized samples was overall larger than that from the glycerol-plasticized nanocomposites but smaller than that from sorbitol-plasticized samples. For instance, the d_{SAXS} value for G210 and X210 are 19.03Å and 19.23Å, respectively. On the other hand, the d_{SAXS} value for X210 and S210 are 19.23Å and 19.8Å, respectively. Similar results were obtained in G220/X220, G410/S410 and G420/S420. Such finding clearly indicated that the expansion degree of the MMT gallery was mostly related to the molecular size of the plasticizer incorporated into the complex system. This will be further discussed in the integrity analyses Chapter (*Chapter* 7).

In addition to the B-type crystals discussed in the previous sections, SAXS pattern for V-type starch crystals were also observed in all the sorbitol-plasticized extruded composite samples, same as the findings from glycerol/xylitol-plasticized system.

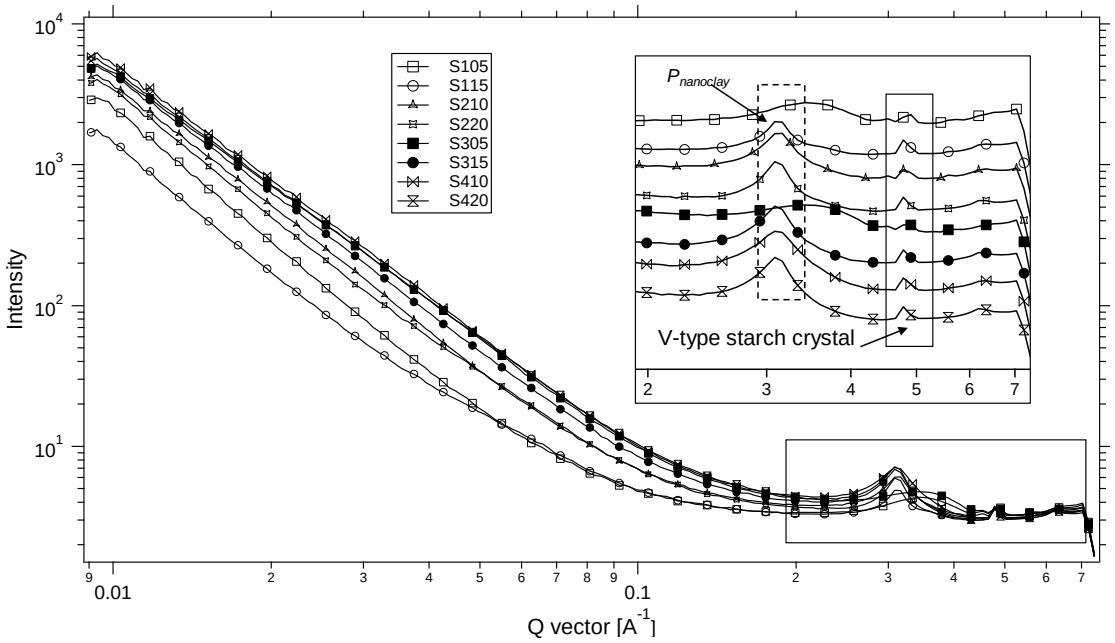

Figure 6-10 SAXS profiles for the PS, starch/sorbitol/MMT samples generated from NIKA data processing software.

6.4.3 Crystallization behaviours

6.4.3.1 Crystallinity

As mentioned in the glycerol-plasticized sample Chapter, the crystallinity values were dependent on the interplay of two effects: increasing MMT (enhanced the crystallinity value) and increasing glycerol (decreased the crystallinity). Same principle could be applied in the sorbitol-plasticized system as read from the crystallinity results in Table 6-4.

Briefly; addition of sorbitol dramatically decreased the crystallinity, e.g., crystallinity decreased from 7.48 % (PS) to 5.28% after adding 10% sorbitol to starch polymer. Incorporation of MMT led to a higher crystallinity regardless of the plasticizer content, and this was a result of the nucleating effect of the nanofiller [179, 180]. Meanwhile the plasticization effect of sorbitol was seen from the decrease of crystallinity with increasing sorbitol concentration for constant MMT content (except for 2% MMT samples). For example, X_c% decreased from 8.28% to 6.56% for S410 and S420. This trend was valid for samples with 1% and 3% MMT samples, as seen in Table 6-4.

Furthermore, considering the crystallinity values from the same-formula samples plasticized with glycerol and sorbitol, it can be concluded that the sorbitol, with larger quantity of hydroxyl groups presented, showed a stronger suppression effect on the MMT's nucleating ability. The evidences were outlined in terms of two scenarios, the low-plasticizer loading scenario and the high-plasticizer loading scenario. When the plasticizer concentration was low, the nucleating effect (increasing the $X_c\%$) of MMT became the dominant factor after the elimination of the plasticization effect of plasticizer (decreasing the $X_c\%$). Under such scenario, hydroxyl groups present in the plasticizer positively suppressed MMT's nucleation effect, which was in correlation with the experimental results indicated in Table 6-4, for e.g. the $X_c\%$ for G305 and S305 was 10.1% and 7.84%, respectively and similar findings for G105 (11.39) / S105 (4.5%) were noticed. Thus under a high plasticizer scenario, the $X_c\%$ value for relevant glycerol-plasticizer sample was supposed to be lower than that of the sorbitol-plasticized sample, and this was in accordance with the experimental data where the $X_c\%$ for G315 and S315 was 6.86% and 4.32%, respectively. Similar findings for G115 (9.62) / S115 (3.73%), G210 (9.28) / S210 (4.10%) and G220 (8.08) / S220 (6.11%) were noticed.

6.4.3.2 Differential Scanning Calorimetry

The addition of sorbitol decreased the T_g value for the system, and increasing the sorbitol concentration led to a higher T_m value (except 1wt% MMT samples), Table 6-4. Once again, it was important to emphasize the dominant effect of sorbitol-starch interactions that was dependent on sorbitol loading and T_g value at a fixed MMT concentration. As presented in Table 6-4 , the T_g value was decreasing ideally upon the augment of sorbitol loading. Figure 6-11 compared the typical heat flow curve for starch polymer and its sorbitol-plasticized bionanocomposites. The figure outlined the impact of addition of MMT/sorbitol on the crystalline phase and the T_m value of the bionanocomposites.

Similar to what found in glycerol-plasticized samples, the variation in peak width and height indicated that the crystallization behaviour was significantly affected by the presence of sorbitol due to the molecular level interactions within the starch polymer matrix. This indication can be evidenced from the SAXS data and TEM images in the morphological observation section (Page 95).

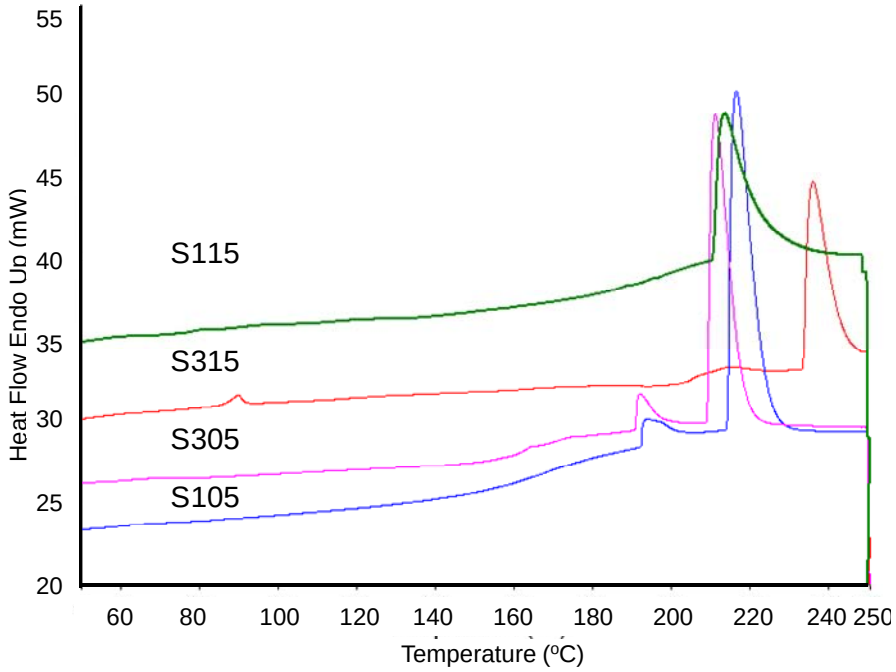

Figure 6-11 DSC heating curves for the selected samples with varying MMT and sorbitol contents.

It could be read from Figure 6-11 that the T_m increased upon increasing the sorbitol concentration, even though the melting enthalpy remained comparable (comparable peak height and width), except for 1 wt% MMT samples. This meant that the crystalline packing became narrower and the crystalline domains exhibited difference in its diffraction patterns due to secondary domains (Figure 6-9 and

Figure *6-10* showed scattering patterns have varied intensities and sharpness).

The different behavior of 1 wt% MMT samples was believed to be resulted from the fact that sorbitol had a higher antiplasticization 'threshold'(~ 27% wt) [69]. Such antiplasticization behaviour was typically attributed to the stronger sorbitol/starch domains which formed as a result of the greater hydroxyl dependent linkages between the sorbitol and the starch. In other words, when the MMT loading was low, the interaction of starch/sorbitol (antiplasticization) dominated the formation of relevant morphology and affected the polymer rearrangement process, thus $T_{m\text{-S105}} > T_{m\text{-S115}}$.

6.4.3.3 Avrami Equation analyses based on DSC

The Avrami Equation analyses for this ternary system were presented in Figure 6-12.

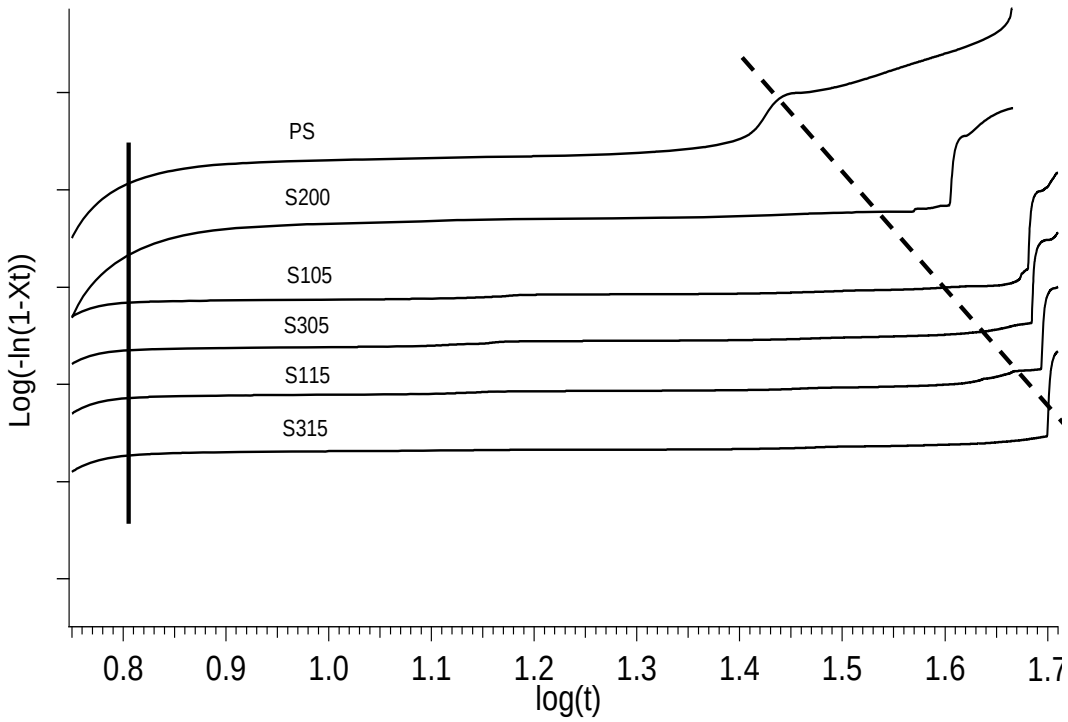

Figure 6-12 Decay of the overall crystallinity based on the non-isothermal crystallisation kinetics analysis using the modified Avrami equation for sorbitol-plasticized samples. All plots were corrected for the baseline and offset for clarity.

Based on the non-isothermal crystallization kinetics analysis, Figure 6-12, nearly all the samples demonstrated one prominent linear region. This linearity reflected a large scale homogeneous domain formed by the starch/MMT intercalated regions. Further, the small changes in the slope (Figure 6-12, region near the dashed line) indicated the presence of a small fraction of heterogeneous crystalline domain, and such heterogeneity was due to the typical secondary nucleation, similar to what is mentioned in the glycerol-plasticized sample Chapter. Such behaviour arose from the smaller imperfect crystals rearranging to form larger domains, and this behaviour depended upon the crystal size and aging time, and have been reported previously in other polymer nanocomposite systems [170]. Meanwhile, same as what previously observed in the glycerol system (Page 77), the onset temperature was not influenced by either the present of MMT/sorbitol or its relative ratio. The exponent *n* and the factor *k* from Avrami Equation analyses are presented in Table 6-7.

Table 6-7 The exponent n and the factor k obtained from a non-isothermal crystallisation analysis for the sorbitol-plasticized nanocomposite samples.

Sample ID	S105	S115	S210	S220	S305	S315	S410	S420
n	0.76	0.26	0.20	1.35	0.36	0.31	0.17	0.57
k	-1.25	-0.61	-0.78	-2.91	-1.27	-0.81	-0.76	-2.53

It was notable to compare the *n* value from glycerol-plasticized samples (*Chapter* 4, section 4.4.3) and the sorbitol-plasticized samples, the *n* values for the sorbitol-plasticized samples were overall slightly larger than from the glycerol-plasticized samples. Because a higher *n* (sorbitol-plasticized samples) compared to *n* (glycerol-plasticized samples) indicate the heterogeneous nucleation and suppressed domain size of the crystalline region. Therefore, the larger *n* values (from sorbitol-plasticized samples) presented a smaller crystalline domain when compared with the glycerol-plasticized samples. And this was in fair agreed with the results obtained in the size distribution section; see the next section (Page 132).

The next parameter *k* (related to the rate of crystal growth) showed a significant variation among different samples ranged from -0.61 (S115) to -2.91 (S220) and no obvious tendency was observed. This value was overall smaller than that from glycerol-plasticized samples indicating a slower crystal growth rate in sorbitol-plasticized samples. It could be assumed as the starch chain mobility contributed the unpredictable changes in this term. More specifically, the small *k* value found for the high sorbitol content samples (S020=-2.91 and S420=-2.53) and the glycerol-plasticized (better plasticization effect) samples ($k_{glycerol}$ values were overall larger than $k_{sorbitol}$ values.) further suggested that higher crystal growth rate can be obtained from a higher chain mobility system.

6.4.3.4 Size distribution of the various crystalline domains

The size distribution calculation results are shown in Figure 6-13. Two well-defined domains were observed, where the diameters of scatters were denoted as $\bar{d}_{1-sorbitol}$ (around 95 Å) and $\bar{d}_{2-sorbitol}$ (around 310 Å).

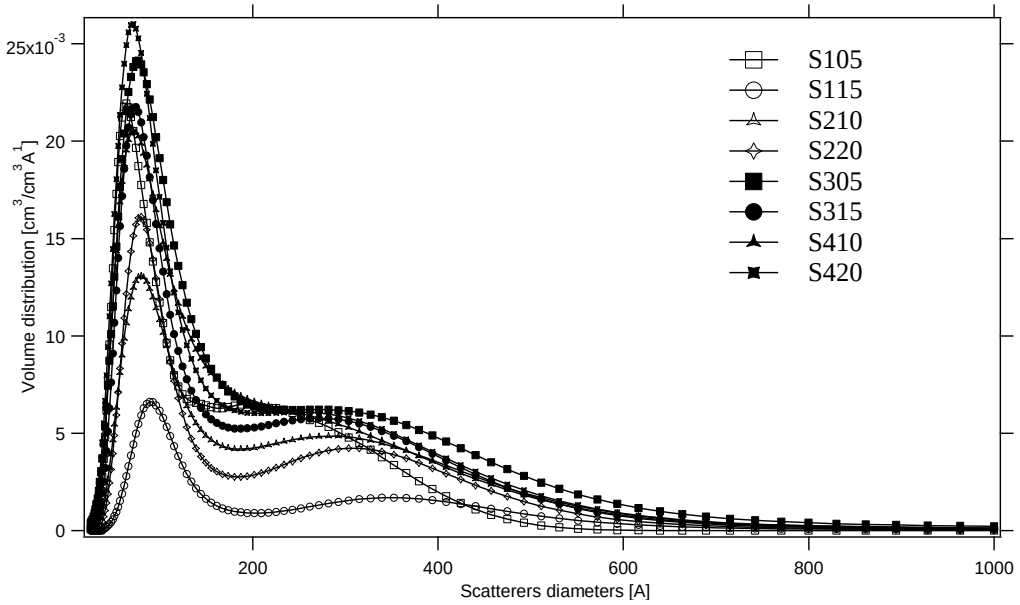

Figure 6-13 Size distribution calculation result for sorbitol-plasticized nanocomposites.

The quantitative results of size distribution within these samples are tabulated in Table 6-9, where the normalized residuals for all the fittings were within ±1Å, suggesting a fairly good fitting. The mean diameter was related to the sorbitol/MMT loading due to their strong interactions and the value of $\bar{d}_{1-sorbitol}$ decreased with increasing the sorbitol amount. However, no well-defendable tendency can be observed for the other domain ($\bar{d}_{2-sorbitol}$). The observations regarding of the two size domains could be correlated to the retrogradation phenomenon which occurred due to the aggregation of starch chain during aging [173, 174], as suggested in the glycerol Chapter (Page 78). The rearrangements of starch chains become dominant upon the drying process and the availability of MMT provided local sites for polymer aggregations, thus lead to the formation of larger size crystalline domains ($\bar{d}_{2-sorbitol}$).

Table 6-8 Radius values (Å) from size distribution calculated by MEM method for both the high and low moisture content samples.

Sample ID	S105	S115	S210	S220	S305	S315	S410	S420
$\bar{d}_{1-sorbitol}$ *(Å)	80	101.9	94	92.5	98.6	97.9	99.5	96
$\bar{d}_{2-sorbitol}$ *(Å)	275.7	351.4	333.1	311.9	309.1	301.5	296.6	308.4
$\bar{d}_{1-hm-sorbitol}$	94.1	104	99.3	102	93	97.7	95.4	97

* $\bar{d}$: mean scatter diameter (Å)

The impact of modifying the MMT with the sorbitol plasticizer was seen in the limited long-range order achieved by the bionanocomposites matrix. This behaviour was due to the typical interactions within 'MMT-rich' matrix [172] attribute to the smectic hindrances associated with the platelet type structure. However, in this study, it was interesting to note that the starch-MMT interactions were comparatively stronger with low sorbitol amounts, which led to higher degree exfoliation morphology. This was reflected in the reduced scatter diameter upon changing the sorbitol concentration as indicated by the size distribution results (Table 6-8). Furthermore, this behavior was also seen in the representative TEM images (Page 123), and they were the visual representation of MMT intercalation at both low sorbitol and high sorbitol concentration to compare the impact of excess plasticizer.

When comparing the size distribution for glycerol-plasticized samples (Table 4-9) and sorbitol-plasticized samples (Table 6-8), it could be observed that the average value $\bar{d}_{1-glycerol}$ (~ 91 Å) was overall smaller than that $\bar{d}_{1-sorbitol}$ (~93 Å). However, the average value of $\bar{d}_{2-glycerol}$ (~ 387Å) was significantly larger than that from $\bar{d}_{2-sorbitol}$ (~ 310Å). These information irradiated the speculation that the formation of $\bar{d}_1$ was more dependent on the plasticizer type applied, whereas the formation of d_2 was based more on the morphology that resulted from the starch/plasticizer interactions. Such hypothesis will be further discussed in the integrity analyses Chapter (*Chapter 7*).

6.5 Role of water molecules indicated from SAXS profiles

Similarly, another set of sorbitol-plasticized samples, denoted as HSXX (the prefix H means high moisture) with higher moisture content was subjected to synchrotron analysis. The role of water molecules within this ternary system was illustrated in terms of comparing the synchrotron results from the samples with different moisture content.

6.5.1 Moisture content Measurement

Moisture content measurements for the high moisture content samples are shown in Table 6-9. In the high moisture content samples, increasing sorbitol concentration decreased the amount of moisture within the samples. This observation was exactly opposite to the tendency found in the glycerol-plasticized samples (Page 80).

Table 6-9 Characteristic peak position profiles and calculated basal spacing for sorbitol-plasticized samples with high moisture content.

Sample ID	Moisture (%)	Δm%	P_{MMT} (Å $^{-1}$)	P_{starch} (Å $^{-1}$)	d_{SAXS} (Å)	Δd_{SAXS} (Å)
HPS	30.69	28.49	-	0.36	-	
HS010	26.23	23.52	-	0.36	-	
HS020	16.68	14.54	-	0.36	-	
HS105	30.32	27.94	0.292	0.363	21.50	-
HS115	17.31	12.48	0.3	0.360	20.90	6.344
HS210	28.46	25.23	0.295	shoulder	21.28	6.489
HS220	21.93	17.4	0.302	shoulder	20.79	6.344
HS305	27.59	24.07	0.304	shoulder	20.66	5.844
HS315	22.98	20.45	0.295	shoulder	21.29	5.479
HS410	25.93	23.48	0.290	shoulder	21.66	6.872
HS420	15.61	13.54	0.295	shoulder	21.29	6.938

The moisture content data in Table 6-4 (low moisture content samples) and Table 6-9 (high moisture content samples) indicated two key points.

First, under a moisture-rich scenario, the increase of sorbitol strengthened the interactions of sorbitol/sorbitol and sorbitol/starch and competed with the sorbitol/water interaction to ‘squeeze out’, to some extent, the water molecules from the polymeric network. The larger domain size for $\overline{d}_{1-hm-sorbitol}$ directly supported such idea. Secondly, when the same samples were subjected to drying treatment, the

difference in the equilibrium moisture content values (*Δm* %) demonstrated that the samples with 10 wt% or higher amounts of sorbitol retained lower equilibrium moisture within the samples (because the *Δm*% values were smaller). This highlighted the negative plasticization effect of sorbitol when compared with glycerol, which generated a hindrance effect in terms of reducing the plasticization effect of sorbitol upon increasing the concentration.

6.5.2 SAXS results for PS, starch+sorbitol and starch+MMT samples with high moisture content

The raw 2-D SAXS patterns from the selected representative high moisture samples are shown in Figure 6-14.

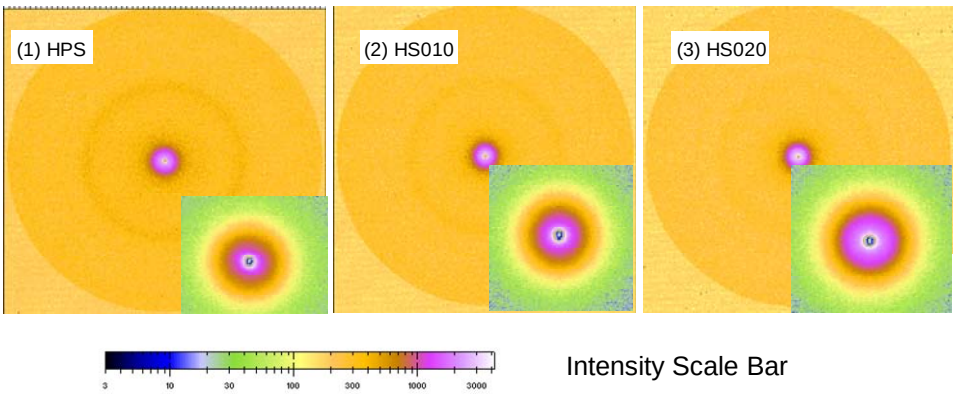

Figure 6-14 Raw 2-D SAXS patterns for PS, HS010 and HS020.

As shown in Figure 6-14, the addition of sorbitol did not induce a direct intuitive change on the diffraction pattern of corresponding samples. Meanwhile, unlike the observation obtained in glycerol-plasticized sample (elliptical shape in HG020), diffraction patterns for HPS, HS010 and HS020 exhibited similar features as seen in Figure 6-14. In terms of the influence of MMT, which had been portrayed in section 4.5.2 (Page 81), the removal of moisture, was in favour of the growth of lamellar structure within the samples.

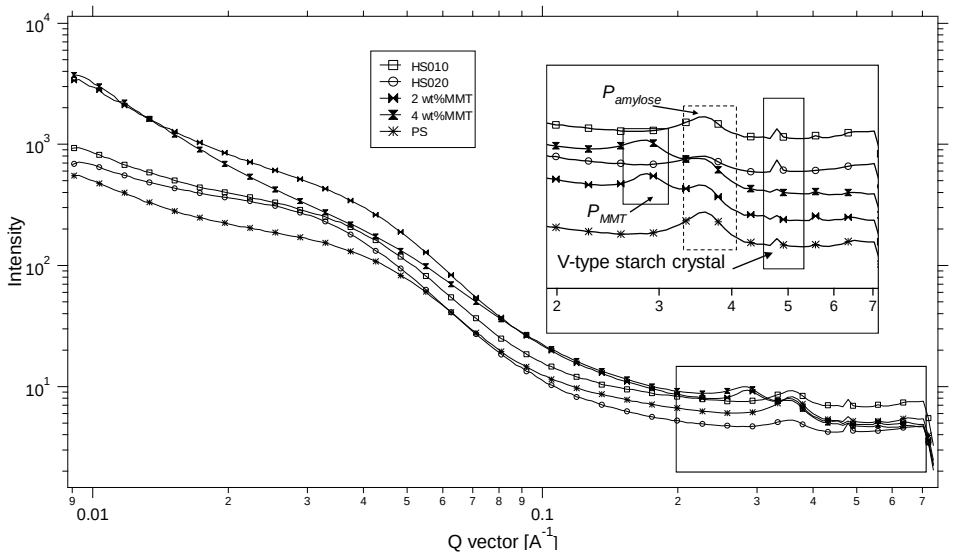

Figure 6-15 SAXS Profiles for PS, starch/sorbitol and starch/MMT from high moisture samples.

The SAXS profiles from the high moisture content samples (Figure 6-15) revealed the well-defined 'broaden shoulder' around Q≈0.04-0.05 $Å^{-1}$ corresponding to the long periodic structure of processed starch polymer [156]. Such a 'shoulder' typically corresponds to the long periodic structure of processed starch polymer [156] and for the samples with higher equilibrium moisture, which typically meant that greater plasticizer (both sorbitol and water) quantities allowed larger 3-dimensional periodic growth. Shamai *et al.*[176] had earlier discussed such observation was the reflection of the retrogradation behaviour (section 4.5.2, Page 81).

As read from Table 6-9, unlike the obvious shift of P_{starch} occurred in HG020 (from 0.36 (HPS) to 0.32 (HG020)), the characteristic peak for starch did not shift upon the addition of sorbitol which indicated the glycerol-starch interaction was stronger than the sorbitol-starch interaction. Thus, the glycerol molecules could replace the water molecules within the starch matrix but not from the sorbitol-plasticized system.

6.5.3 SAXS results of starch+sorbitol+MMT with high moisture content

SAXS profiles of high moisture content sorbitol-plasticized nanocomposites are shown in Figure 6-16.

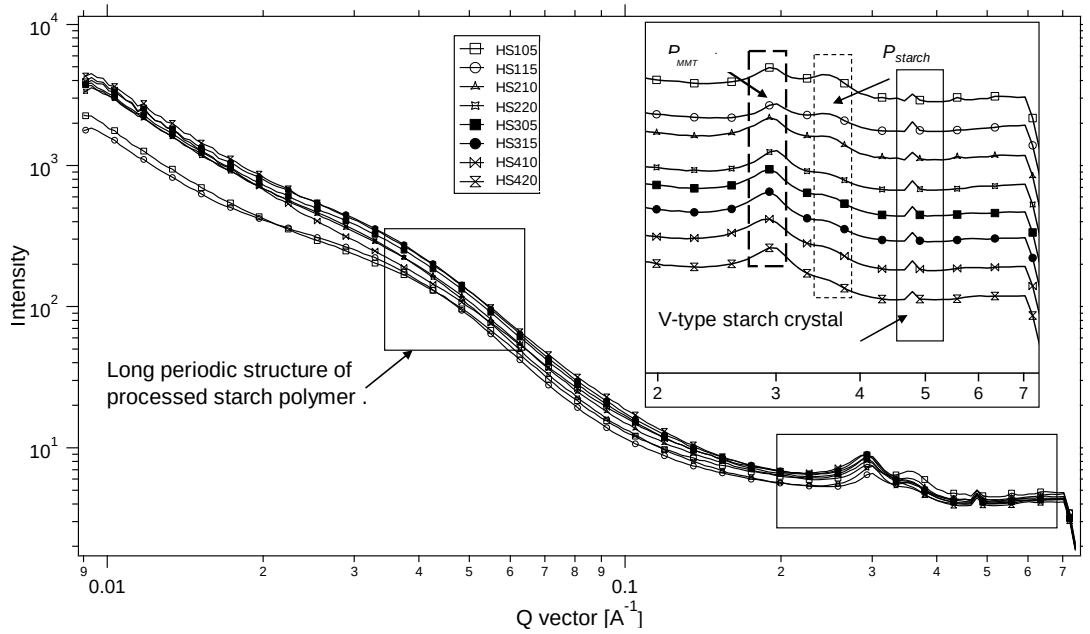

Figure 6-16 SAXS Profiles for PS, starch/sorbitol/MMT samples with high moisture content generated from NIKA data processing software.

The role of water could be evidenced from the changes of tendencies related to *basal spacing* (d_{SAXS}) value in two sets of samples. Some researchers [8] have reported that increasing sorbitol amount could lead to a small reduction in the *basal spacing* (d_{SAXS}) value and the reason for this was the stronger interaction of water-sorbitol competing with *basal spacing* (d_{SAXS}) value water-MMT interaction. We found that this was true for high humid conditions where the sample moisture content was not limiting, for example, for 2 wt% MMT samples, the *basal spacing* reduced from 21.28 Å to 20.79Å, as the sorbitol was doubled (from 10% to 20%), and from 21.15 Å to 20.29 Å for 4% MMT samples. But for low moisture content samples, we note that no dominant trend exists because water played a significant role as it could interact with both sorbitol and MMT and excess plasticizer could also interact with polymer chains. The deviation in *basal spacing* (d_{SAXS}) value from high moisture content and low moisture content sample (denoted as Δd in Table 6-9*)* decreased with sorbitol concentration irrespective of the MMT loading.

Two well-separate peaks (from *basal spacing* of MMT and 100 interhelix distances for starch polymer) were observed in all the high moisture content samples. As compared to the *basal spacing* (d_{SAXS}) result of glycerol and sorbitol-plasticized

samples, sorbitol samples showed larger *basal spacing* attributed to its relatively larger molecules size (compared to glycerol).

6.5.4 Size distribution of the various crystalline domains

The size distribution profile results for high moisture content samples were shown in Figure 6-17. Only one domain ($\overline{d}_{1-hm-sorbitol}$) sized around 97.8 Å (smaller than the glycerol-plasticized sample but larger than that of xylitol-plasticized sample) was observed in the high moisture content samples.

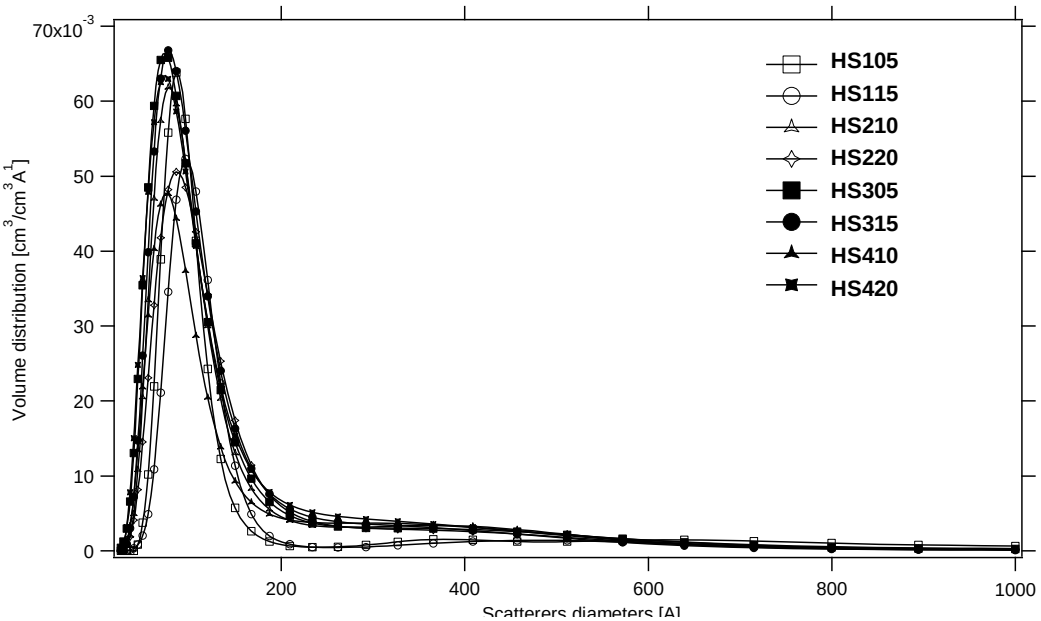

Figure 6-17 Size distribution calculation result for starch/sorbitol/MMT nanocomposites from high moisture samples by MEM method.

Mean scatter diameter for $\overline{d}_{1-hm-sorbitol}$ ranged from 93 Å to 104 Å for the high moisture samples which was overall larger than that $\overline{d}_{1-sorbitol}$ which had been suggested to be due to the decrease of long-period order upon dehydration, Table 6-8. Also, the hypothesis that the emergence of the larger domain resulted from the rapid retrogradation of starch chains upon drying was further confirmed by the observation that only one domain was observed in the moisture-rich samples. In the presence of excess water or sorbitol (which strongly interacted with the starch polymer), retrogradation was hindered as the interactions from starch/sorbitol/water restricted the moisture redistribution, as suggested by Schiraldi *et al.* [178]. The presence of moisture and plasticizer limited the starch/starch interactions and prevented the

retrogradation in the high moisture samples, which prevented the new formation of the larger domains.

There was no obvious size difference between the crystalline domain size from both glycerol and sorbitol-plasticized samples in the presence of excess moisture since the surplus water molecule were playing a bridging role for fulfilling the cavities within the polymeric network and balancing the molecular interactions within the hydrophilic environment via water/plasticizer, water/starch and water/MMT starch biopolymer system.

It could be read from the size distribution calculation results from three plasticizers (Table 4-9,Table 5-7 and Table 6-8) that $\bar{d}_{1-xylitol}$ of xylitol-plasticized samples are higher than both glycerol and sorbitol samples, however , the size value of $\bar{d}_{2-xylitol}$ was fine following the assumption that '$\bar{d}_{2-xylitol}$ depended more on the morphology resulting from the starch/plasticizer interactions'. Since the molecular mobility of xylitol was larger than sorbitol and smaller than glycerol, $\bar{d}_{2-xylitol}$ from xylitol sample turned out to be smaller than glycerol samples but larger than those sorbitol samples. This was because the high molecular mobility of the plasticized present in the polymeric network occupied more free cavities and induced the formation of relatively larger crystalline domain.

Summary

The synergistic interactions in sorbitol-plasticized nanocomposite were studied via various characterization methods. The combined influence of sorbitol (1-20 wt %) / MMT (1-4 wt %) on the characteristics of extruded starch nanocomposites was studied in detail.

Important conclusions can be drawn as follows.

1. Exfoliation process of MMT was dominated by the concentration of sorbitol (sorbitol/sorbitol interactions) which competed with the sorbitol/MMT interactions.

2. It was concluded that the crystallinity value was a result of the interplay of two effects: increasing the MMT (enhanced the crystallinity value) and increasing sorbitol (decreasing the crystallinity). Thus, different tendencies were found with various formula samples.

3. The sorbitol, with larger quantity of hydroxyl groups, showed a stronger suppression effect on the MMT's nucleating ability.

4. Two *domains* sized at approximately 93Å and 300Å (significantly smaller than glycerol samples) were found in the low moisture content samples. These information irradiated the speculation that the formation of $\overline{d}_1$ was more dependent on the plasticizer type applied, whereas the formation of $\overline{d}_2$ was based more on the morphology that resulted from the starch/plasticizer interactions.

The number of –OH groups presented in the plasticizer did significantly influence the morphology formed within the relevant composites such as achievable *basal spacing* of MMT and the crystalline domain distribution. The unique polymeric network of low –plasticizer loading samples was further studied. A clearer map of synergistic interactions influenced by plasticiser type and concentration was drawn in the next Integrity Analyses Chapter (Page142).

Chapter 7

Integrity analysis And Synergistic Interactions

Chapter outline

Based on the discussion in previous Chapters, the distinctness observed in samples prepared from different plasticizer indicated that the interactions within the starch/plasticizer/MMT system were greatly dependent on the plasticizer used. The *basal spacing* for different nanocomposites determined the size of plasticizer as sorbitol-plasticized samples possessed the highest *basal spacing* value at a comparable formula. However, the crystallization behaviour was altered by the crystallization ability of the plasticizer applied.

The interactions in a given scenario are a combined *physical-chemical process* caused by the competitive interplay of different components (type and loading). The physical factors included the molecular size and molecular structure of the plasticizer. Hydrophilicity-number of hydroxyl groups, crystal features and intermolecular hydrogen bond strength are the chemical characteristics that affected the crystallization behaviour along with water molecules.

The synergistic interactions within the hydrophilic system were summarized as a three stages process, named as *unsaturated relatively loose-soft polymeric network* (stage one), *competitive relatively tighten-firm polymeric network* (stage two) and *saturated phase separation polymeric network* (stage three).

7.1 Physical factors dominating interactions

Physical factors discussed in this section include molecular size and symmetry of the applied plasticizers. Based on the previous study (*Chapter 4 to Chapter 6*), it could be confirmed that the exfoliation process of MMT was more dependent on the physical aspects of the plasticizer in specific system. For instance, the basal spacing of glycerol, xylitol and sorbitol was directly related to their molecular size order where $d_{\text{-sorbitol}} > d_{\text{-xylitol}} > d_{\text{-glycerol}}$. Similar tendency was observed in the SAXS results as well.

7.1.1 Effect of plasticizer molecular size

7.1.1.1 Achievable basal spacing for MMT

As discussed in the previous Chapters (*Chapter 4 to Chapter 6*), the influence of the molecular size can be ascertained from the achievable *basal spacing* for the plasticized samples Table 7-1.

Table 7-1 Basal spacing (Å) for samples plasticized by different plasticizer from WAXD result.

Sample ID	105	115	210	220	305	315	410	420
Glycerol	16.9	17.9	17.7	17.8	17.5	17.9		
Xylitol	17.3	16.6	17.5	18.2	17.0	18.2	17.9	17.7
Sorbitol	-	18.0	18.2	18.1	17.5	18.2	18.6	18.8

Samples with at least 15% plasticizer were used for the study as the xylitol-plasticized samples with less than 10 wt% failed to show well-defined crystalline peaks. The xylitol/sorbitol-plasticized samples possessed overall higher *basal spacing* compared to glycerol-plasticized samples due to their bigger molecular size. Similarly, such tendencies were observed with *basal spacing* extracted from the SAXS results. However, it is worth to mention that further increase in plasticizer amount enhanced the interactions within plasticizer/plasticizer rather than with other component. These observations highlighted the hypothesis that stronger plasticizer/plasticizer interactions that resulted from increase of plasticizer would compete with plasticizer/MMT interaction hindering the exfoliation process of MMT. The molecular size of applied plasticizer also affected the crystallization process and impacted the morphologies formed.

7.1.1.2 Domain Size distribution

Direct evidence closely related to the molecular size of those plasticizers was the size distribution results calculated from the SAXS profiles of different samples.

The size distribution profiles for different samples further supported the assertion that smaller molecule size could be the contributing factor to the observed strong interactions between plasticizer and starch/MMT. As revealed in Table 7-2 for domain 2, glycerol-plasticized samples had a higher value than xylitol/sorbitol-plasticized samples. As discussed in the previous Chapters, the formation of domain 2 could be a result of plasticizer/starch interaction. Thus, stronger interactions occurred due to the smaller size of glycerol and larger crystalline domains formed, as shown in Table 7-2.

Table 7-2 Size distribution (Å) results for samples plasticized by different plasticizer.

Sample ID	Glycerol		Xylitol		Sorbitol	
	Domain 1	Domain 2	Domain 1	Domain 2	Domain 1	Domain 2
105	107.4	389.6	119.35	375.3	80	275.7
115	97	412.6			101.9	351.4
210	86.4	369.1	98.26	364.1	94	333.1
220	78.6	403.8	95.07	345.1	92.5	311.9
305	93.5	368.2	101.02	350.8	98.6	309.1
315	85.3	384.1			97.9	301.5
410			106.34	348.1	99.5	296.6
420			104.29	338.6	96	308.4

The SAXS measurement profiles further supported that molecular size of plasticizers turned out to be a non-ignorable factor that influences the crystallization process within this system, as shown in Figure 7-1 (105,305).

The sharp peaks in glycerol-plasticized samples indicated a tighter polymeric network due to the strong interactions between starch/MMT and glycerol plasticizer. Glycerol occupied more hydrophilic sites due to their high molecular mobility and strong hydrogen bonds formation. This resulted in large size secondary domains in glycerol samples.

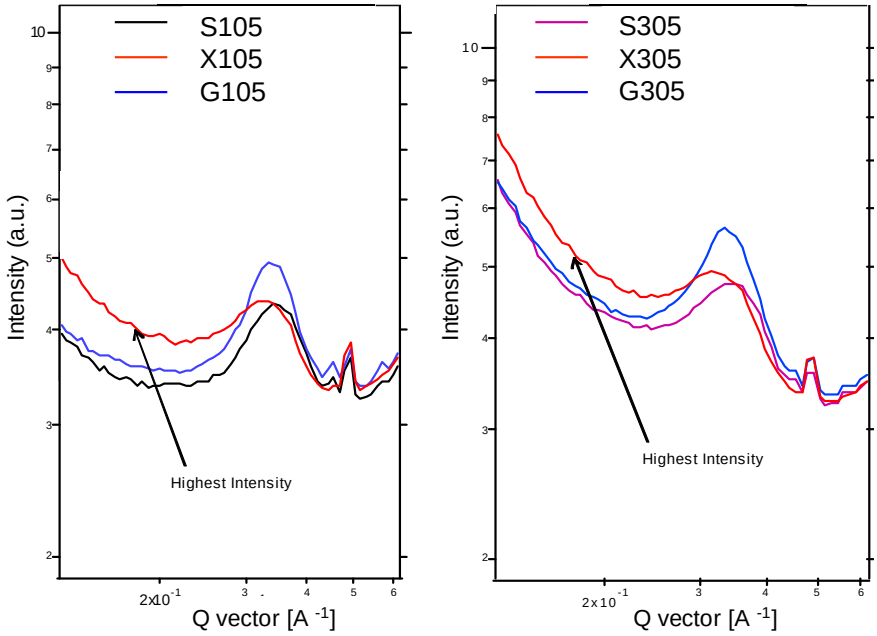

Figure 7-1 SAXS profiles for 105 and 305 system plasticized by different plasticizer.

7.1.2 Effect of plasticizer molecular symmetry

As shown in Figure 7-2, the broadened WAXD peak in 5% glycerol/sorbitol samples represented a high dispersion MMT polymeric network in the sample. In other words, the higher packing density was formed within samples at a higher plasticizer concentration.

Upon further increasing the plasticizer amount, stronger interactions were introduced between the plasticizer and more hydroxyl groups from plasticizer eased starch/plasticizer interaction, thereby forming a more saturated polymeric network. Interactions between MMT and starch and/or plasticizers were promoted to some extent as seen from the enlarged *basal spacing* value for higher plasticizer samples. However, the stronger interaction within plasticizer competitively hindered the further exfoliation of MMT at such high plasticizer loading (sharpen of WAXD peaks) [85, 86].

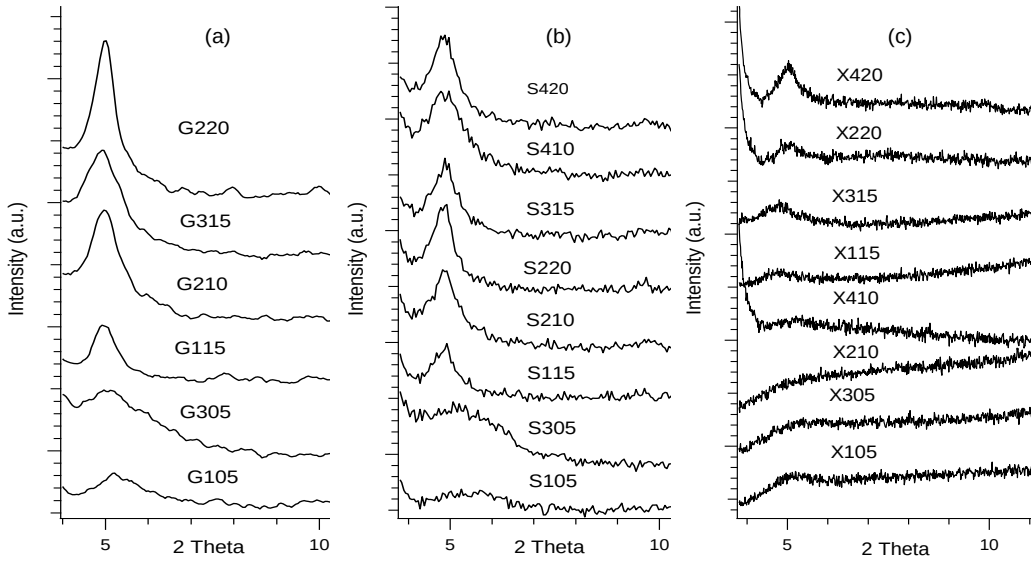

Figure 7-2 WAXD patterns for samples plasticized by different plasticizer.

It has been previously reported that glycerol-sorbitol-plasticized samples possessed similar tendencies in terms of the changes in the WAXD shape and intensity for different samples, where 5% was considered as the critical point led to two different polymeric networks. However, the corresponding value in xylitol-plasticized increased to 10%. The phenomenon that no hindrance effect on MMT exfoliation was observed in xylitol -plasticized samples till 10% could be interpreted from the molecular symmetrical structure of xylitol, see section 3.1.2 (Page 34).

According to the packing coefficient theory, morphotropic changes associated with a loss of symmetry are accompanied by an increase in the packing density [181]. Hence it was acceptable to conclude that plasticizers with less symmetry (glycerol and sorbitol) form a higher packing density theme. Based on the above mentioned hypothesis, it is within expectation to detect well-defined crystal peaks in glycerol/sorbitol-plasticized samples at a lower concentration (5%) compared to xylitol samples (10%). Under the same condition, the samples plasticized by glycerol and sorbitol formed a relatively firmer polymeric network than xylitol. The concentration for observing a well-defined morphology depended on the plasticizers' molecular symmetry.

7.2 Intrinsic Chemistry factors dominating interactions

Chemistry of different plasticizers discussed in this section includes *crystallization ability*, *crystal structure* and the i*ntermolecular forces* (the strength of intermolecular

hydrogen bonds). It had already been presented in the previous Chapters that samples prepared from plasticizer with similar molecular physical properties (molecular size and molecular structure) exhibited significant distinctness in crystallization behaviour. The intrinsic chemistry of different plasticizers dominated the chemical aspect-related interaction (crystallization) within the nanocomposites. The relevant evidences could be extracted from the thermal analysis including glass-transition temperature, T_m, crystalline domain distribution evaluation results and crystallization process modelling results (from Avrami equation).

7.2.1 Crystallinity

Crystallinity of specific sample could reveal the effect of plasticizer on the crystallization process of obtained composite [182]. As shown in Table 7-3, the crystallinity values for xylitol samples are overall higher than that of glycerol/sorbitol-plasticized samples.

Table 7-3 Comparison of crystallinity value for samples plasticized by different plasticizer.

Sample ID	Crystallinity (%)		
	glycerol	xylitol	sorbitol
105	11.39	7.05	4.5
115	9.62	11.4	3.73
210	9.28	13.4	4.01
220	8.08	11.26	6.11
305	10.1	11.7	7.81
315	6.86	9.8	4.32
410		12.26	8.28
420		10.1	6.56

The WAXD results of xylitol samples displayed broader diffraction peaks suggesting the presence of small crystals in high quantity compared to glycerol/sorbitol samples. This was due to the stronger crystalline ability and weaker intermolecular hydrogen bonds (as reflected from the lower boiling point) in xylitol. The higher crystallinity reflected the superior crystalline ability of xylitol compared to glycerol or sorbitol. A phenomenal supportive experiment was carried out (Figure 7-3) where the prepared samples (3.2.2.7) were exposed to the atmosphere for 2 weeks. As shown in Figure 7-3, large amount of crystals were formed on the surface of the xylitol samples compared to glycerol contained samples. The crystallization behaviour the growth

rate of crystals in xylitol will be detailed in the Avrami Equation evaluation section (Page 150).

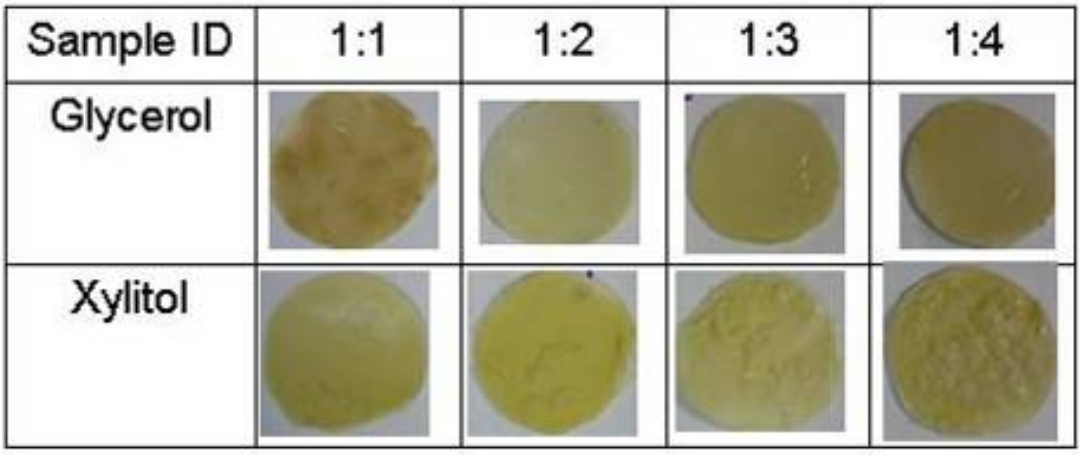

Figure 7-3 Comparison of crystallization growth for samples plasticized by different plasticizer.

The large crystalline domains (Domain 1) of xylitol-plasticized samples were compared to that of glycerol and sorbitol-plasticized samples. It was observed that the intermolecular hydrogen bonds of xylitol plasticizer were weaker than glycerol/sorbitol plasticizer. High crystallinity of xylitol prevented the formation of large single crystals and facilitated easy interruption of the crystallization process. Hence relatively larger domain sizes (domain 1 in Table 7-2) and loose polymeric network (Figure 7-2) were observed in xylitol-plasticized samples.

Therefore it could be concluded that the polymeric morphology of xylitol-plasticized samples featured small single crystals grouped into slightly large domain sizes in high volumes. This was due to the unique intrinsic chemistry of xylitol and was confirmed by volume distribution results; Figure 7-4 (a)-(b).Samples 105 and 210 of xylitol showed higher crystal volumes than glycerol/sorbitol plasticizer. Nevertheless such influences became insignificant on addition of plasticizer and/or MMT, Figure 7-4 (c)-(d).

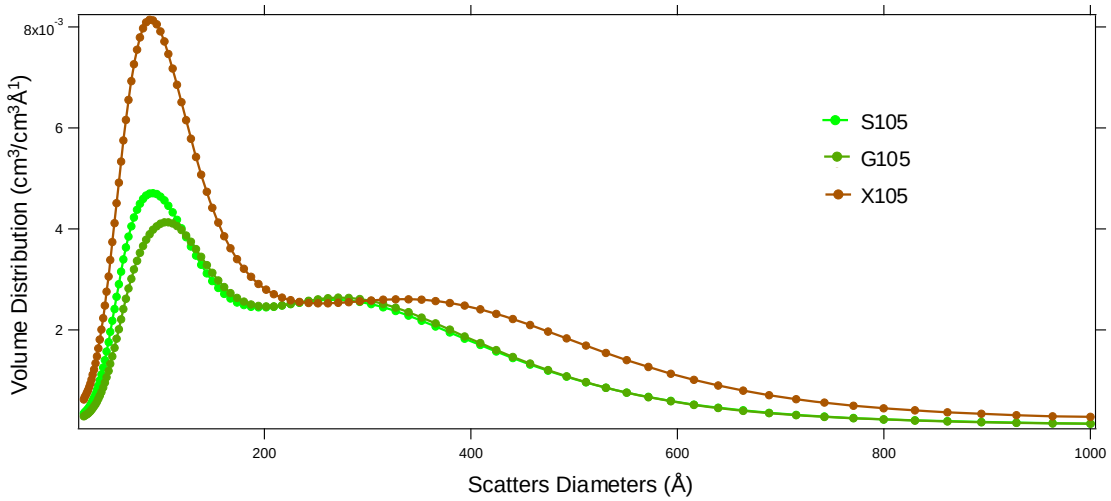
8x10-3
6
4
2
Volume Distribution (cm3/cm3Å1)
S105
G105
X105
200
400
600
800
1000
Scatters Diameters (Å)

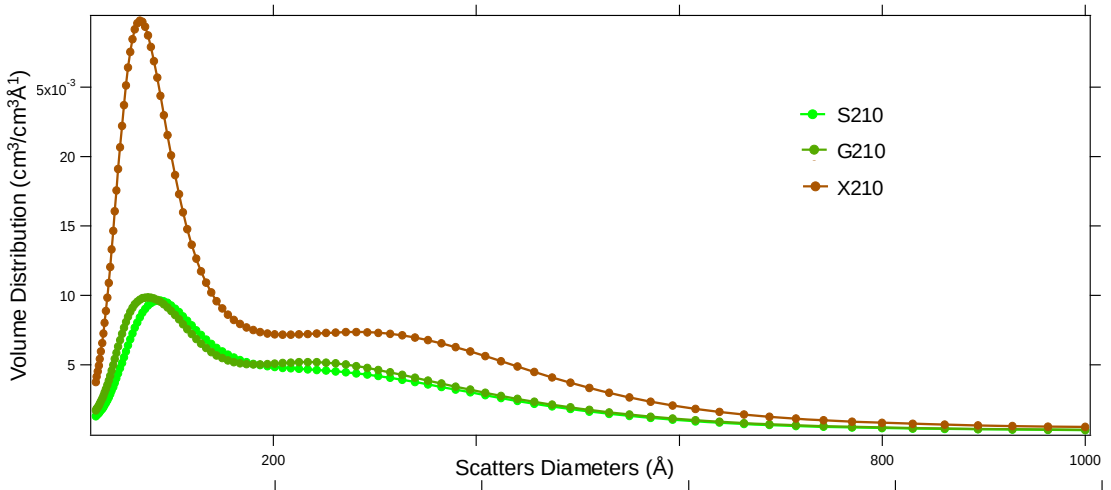
5x10-3
20
15
10
5
Volume Distribution (cm3/cm3Å1)
S210
G210
X210
200
800
1000
Scatters Diameters (Å)

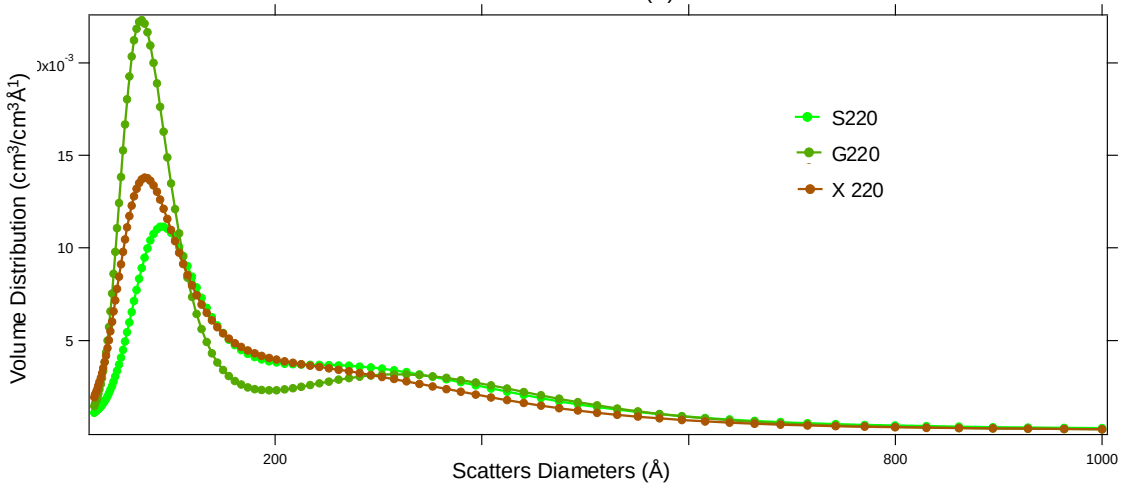
)x10-3
15
10
5
Volume Distribution (cm3/cm3Å1)
S220
G220
X 220
200
800
1000
Scatters Diameters (Å)

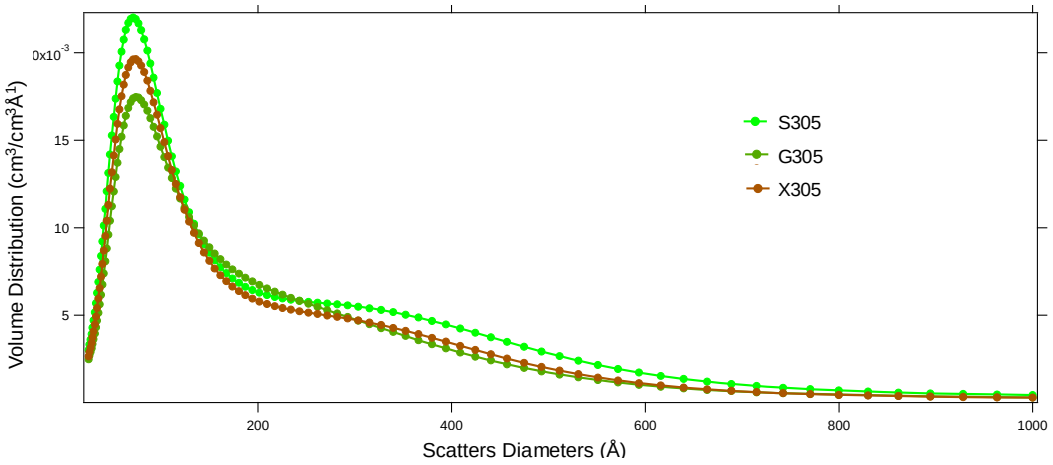

Figure 7-4 Size distributions of selected samples, (a) 105, (b) 210, (c) 220 (d) 305 system.

Glycerol-plasticized composite showed higher crystallinity than sorbitol samples. This was based on the assumption that small glycerol molecules formed highly ordered morphology than sorbitol. This increased the overall crystallinity of relevant materials resulting in stronger glycerol/MMT interactions.

The SAXS measurement results further supported the above assumption as shown in Figure 7-1. It should be clearly observed that xylitol-plasticized samples possessed higher intensity when compared to glycerol and sorbitol-plasticized samples. This indicated a higher degree of heterogeneous morphology within xylitol-plasticized samples and larger amount of crystals tended to grow in xylitol-plasticized samples. This was finely correlated with the finding that high scattering intensity was observed in the SAXS profiles.

7.2.2 Crystallization Behaviours (mechanism and growth) via *Avrami* Equation

Adequate considerations should be given to the effect of interplay of both the plasticizer and MMT as they would have mutually influence during the crystallization process. Furthermore, the nanoparticles (MMT) greatly modified the interaction tendency and strength at the same time. For example, the crystallinity values for the samples showed direct proportion to the MMT loading. Therefore, in the following discussions, the presented arguments are always referred to certain scenarios including high-MMT (HM), low-MMT (LM), high-plasticizer (HP), and low-plasticizer (LP) themes.

7.2.2.1 Thermal characterization via DSC

Figure 7-5 compared the calculated plot for non-isothermal crystallization kinetics analyses using modified Avrami equation under various scenarios. The variation in the onset temperature and second nucleation characteristic shift indicated that the crystallization behaviour was significantly affected by the type of plasticizers and MMT.

As revealed in the Figure 7-5 the typical secondary nucleation characteristic shift for xylitol-plasticized samples (in all the presented scenarios) tended to be more obvious (well defined second nucleation range), however, this phenomenon was not predominately observed in glycerol/sorbitol-plasticized samples. Such behaviour arose from smaller imperfect crystals rearranging to form larger domains, and this had been reported previously for other polymer nanocomposites systems [170]. This was mutually supported by the higher crystallinity values observed in xylitol-plasticized samples.

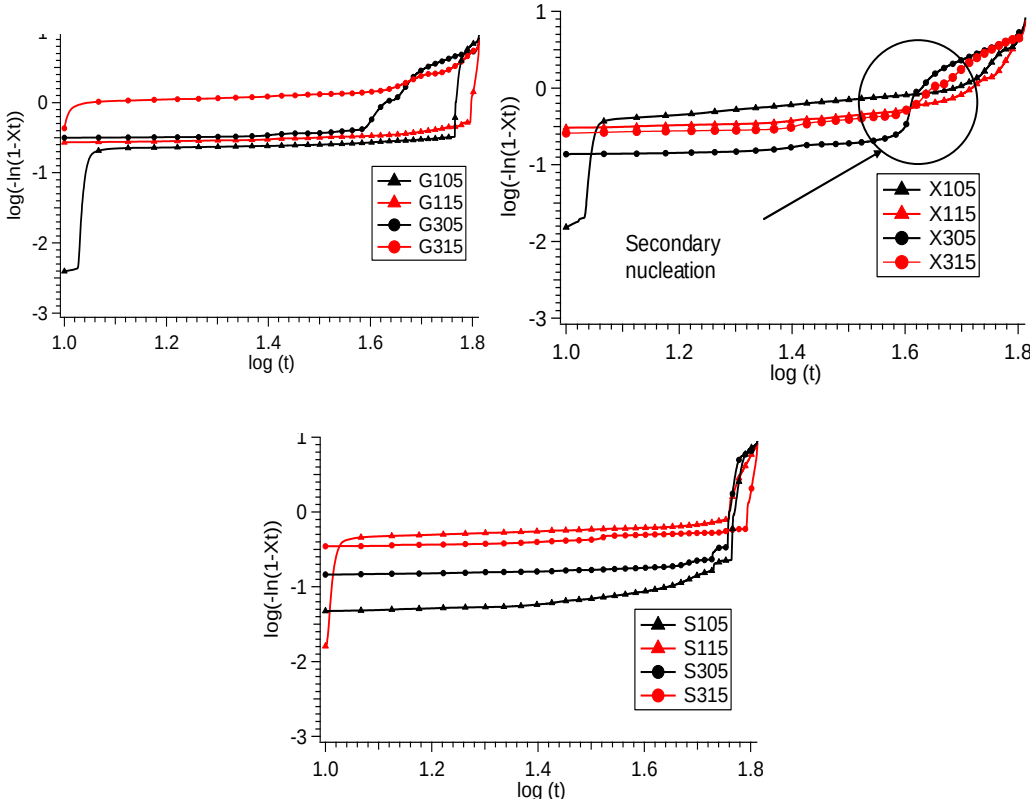

Figure 7-5 Decay of overall crystallinity based on non-isothermal crystallization kinetics using modified Avrami equation for samples plasticized by different plasticizer. All plots were corrected for the baseline.

As mentioned, Figure 7-5 showed that the linear region of the starch crystallization kinetics that highlighted the nucleation mechanism showed significant deviation upon the type of plasticizer (compare X105 to G105 and S105) [183]. The comparison *Avrami* graphs of samples prepared from different plasticizer at the same formula was presented in Figure 7-6. The crystallization parameters extracted from the *Avrami* evaluation detailed the influence of plasticizer intrinsic chemistry on both the mechanism of crystallization and growth of crystalline domain. For a quantitative evaluation of the crystallization process, the crystal formation parameter *n* and crystal growth parameter *k* are presented in *Table 7-4*.

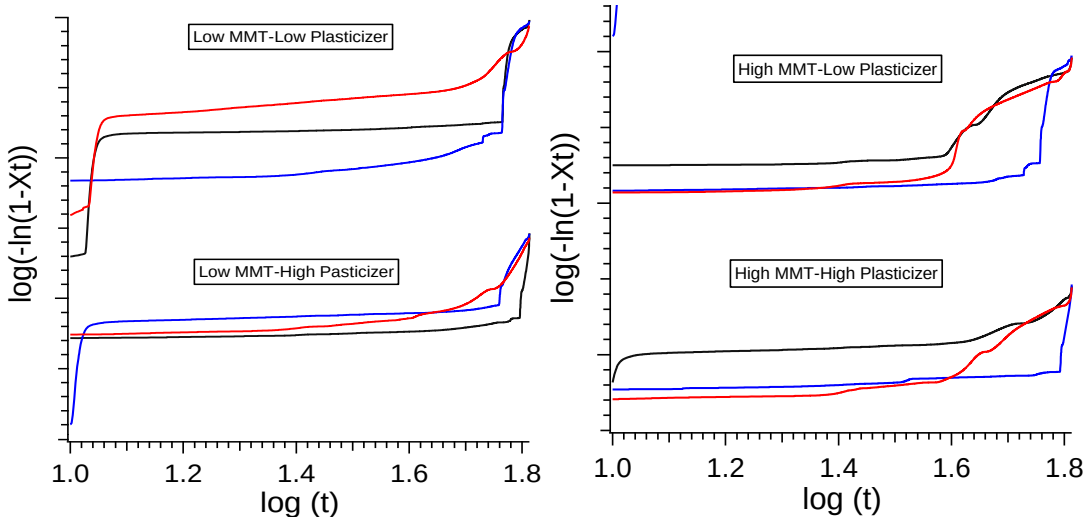

Figure 7-6 Comparison Avrami graphs of samples prepared from different plasticizer at the same formula.

Finally, an analysis of the two model parameters, namely, *n* and *k* which related to crystallization process, for samples with different plasticizer revealed two interesting points, Table 7-4 and Figure 7-7.

As shown in Table 7-4, the values of *n* for glycerol samples were comparable to the *n* value of sorbitol samples; however both of them were very much lower than that value of xylitol samples irrespective of the plasticizer concentration or MMT loading. Meanwhile, similar tendency was observed in terms of the crystal growth parameter *k*. Since a higher *n* (xylitol samples) compared to *n* (glycerol and sorbitol) indicated heterogeneous nucleation and suppressed the size of the crystals, this behaviour was expected for xylitol samples based on the morphological discussion. The unique stronger crystallization ability and weaker intermolecular hydrogen bonding strength

of xylitol led to overall higher randomness of crystalline domains thus suppressing the crystalline size. This has been mutually supported from the SAXS and WAXD profile for different plasticizer samples (*Chapter* 6).

Table 7-4 The exponent n and the factor k obtained from a non-isothermal crystallization analysis for samples plasticized by different plasticizer.

Sample ID	Glycerol		Xylitol		Sorbitol	
	n	*k*	*n*	*k*	*n*	*k*
105	0.24	-0.94	0.71	-1.21	0.76	-2.25
115	0.28	-0.90	0.73	-1.40	0.26	-0.61
210	0.20	-0.63	0.52	-1.69	0.20	-0.78
220	0.18	-0.5	0.50	-1.32	1.35	-2.91
305	0.22	-0.77	2.62	-4.26	0.36	-1.27
315	0.32	-0.35	1.42	-2.38	0.31	-0.81
410			1.11	-2.91	0.17	-0.76
420			0.61	-1.12	0.57	-1.53

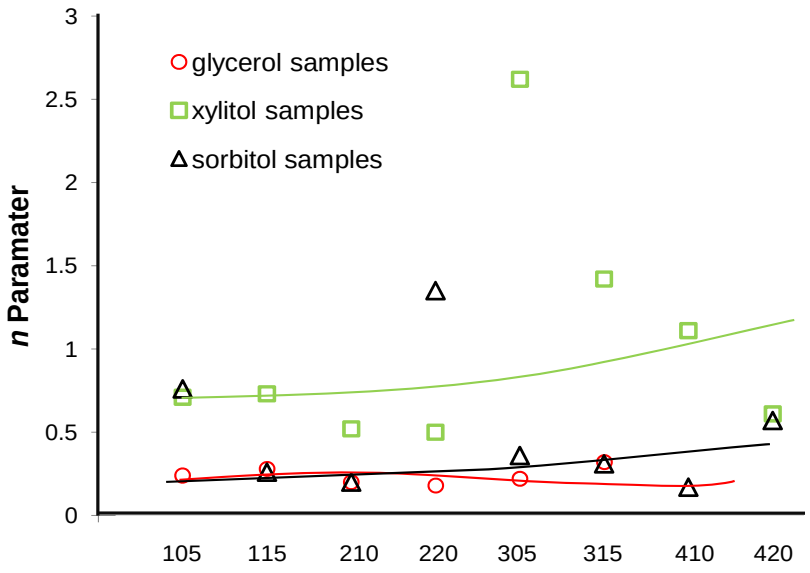

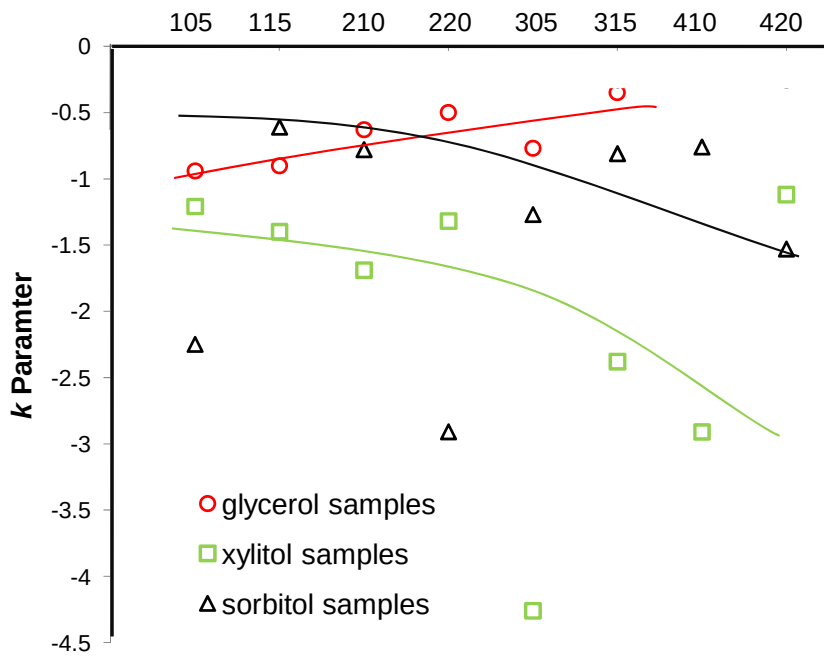

Figure 7-7 Comparison of parameter n and k extracted from modified Avrami equation. The x-axis represents the concentration of MMT and plasticizer only, without their prefix letter for plasticizer.

It is well-known that in polymer system, parameter *k* represents the constant for crystalline growth rate [184]. A higher *k* of glycerol samples indicated its rapid crystalline growth rate compared to xylitol and sorbitol samples, except the low-MMT sorbitol samples (S105 and S115). This was due to the small molecular size and high hydrophilicity of glycerol. Highly ordered crystalline domains could be formed faster than those samples plasticized by larger molecules (xylitol and sorbitol). This was because smaller glycerol molecules could travel among starch/MMT network faster and ensured the appearance of larger crystalline domain. The size distribution results show further evidence that glycerol sample was able to form larger crystalline domains than the others. Additionally, prominent plasticization effect of glycerol as proven in lots of researches was also playing a positive role in facilitating the mobility of starch polymer chains to reorganize into larger size domain as shown in *Table 7-3*. Glycerol-plasticized sample had a larger domain size when compared to xylitol/sorbitol-plasticized samples.

7.3 Physical-chemical interplay dominating interactions

The interactions existing in this complex were not only dependent on either the physical or chemical aspects of the plasticizer/polymer but also a combined effect of

them. In order words, in most circumstances, the interactions result from the interplay of both physical and chemical process. The final properties (characterization results) of different samples (different plasticizer type and loading) were determined by the combined consequence of the interaction strength of physical chemical-factors. A vivid picture of this hypothesis can be evidenced from the glass-transition temperatures analyses for the prepared samples, Table 7-5.

Glass-transition is one of the most important parameters to study polymer behaviour in the polymer science. As indicated in the literature review *Chapter*, the glass-transition temperature presented a physical state transformation, from a low chain mobile glass state to a high chain mobile rubber state. The polymer chains as well as the plasticizer within the material were able to move and this temperature depended on both the physical properties (chain length /molecular size) and the chemistry particularity (intrinsic chemistry) of the components.

Table 7-5 Comparison of glass-transition temperature (T_g)values for different samples.

Sample ID	T_g (˚C)		
	glycerol	xylitol	sorbitol
105	44.9	55.7	49.6
115	43.5	49.6	47.5
210	46.7	56.25	47.73
220	34.8	39.7	31.25
305	43.2	58.5	53.4
315	39.5	50.6	50.4
410		50.1	55.5
420		48.6	33.83
average	42.1	51.1	46.1

On one hand, similar to the tendency in crystallinity values, glass-transition temperature (T_g) for different samples followed a descending order where xylitol-plasticized samples < glycerol-plasticized <sorbitol-plasticized samples. Since larger amount of crystals were present in xylitol-plasticized samples due to its unique chemical properties, the higher T_g value of xylitol-plasticized samples were believed to be from the extra thermal energy required for those more crystals. Meanwhile, the effect of molecular size of the plasticizers (physical factor) was revealed from the higher T_g value for the samples plasticized by larger plasticizers (xylitol and sorbitol)

compared to the samples plasticized by the relatively smaller plasticizer (glycerol) as shown in *Table 7-5*.

7.4 Role of moisture molecules

The water molecules are believed to affect the interactions among starch/plasticizer/MMT to some extent since water was the core component for fabrication of starch-based bionanocomposites. In this study, as indicated in the methodology section (Page 37), 35%wt water had been added to the raw materials before extrusion. The effect of hydration on different plasticizer behaviour was important for understanding the synergistic interactions occurring in these bionanocomposites.

Considering the importance of moisture for starch based green packing materials, another set of samples had been produced without oven drying treatment (as-proceeded ribbons). The averaged moisture content of these set of samples was around 20% which was much higher than those oven-dried samples. SAXS and DSC measurements had been carried out for studying the role of moisture on the synergistic interactions within the hydrophilic system, Table 7-6.

Table 7-6 The exponent n and the factor k obtained from a non-isothermal crystallization analysis for the high moisture nanocomposites samples.

Sample ID	Glycerol		Xylitol		Sorbitol	
	n	*k*	*n*	*k*	*n*	*k*
H105	0.29	-1.1	0.53	-1.97	0.22	-1.56
H115	0.26	-1.08	0.44	-1.65	0.24	-1.55
H210	0.28	-1.03	0.21	-1.25	0.44	-1.54
H220	0.24	-1.15	0.30	-1.28	0.19	-1.42
H305	1.1	-1.93	0.32	-1.42	0.25	-1.57
H315	0.21	-1.37	0.47	-1.87	0.15	-1.36
H410			0.65	-2.4	0.18	-1.4
H420			0.34	-1.26	0.18	-1.49

As shown in the Table 7-6 and Figure 7-8, all samples showed comparable *n* and *k* values, which meant that the presence of moisture modified the interactions amongst starch/MMT/plasticizer and balanced the effect that was induced from physical-chemical aspects of different plasticizer (different *n* and *k* value). A possible explanation was that under a moisture rich scenario, the excess moisture molecules act like the major plasticizer and induce interactions with starch/MMT to form a more uniform polymeric network. Since the water molecules could penetrate into the cavity between the starch chains, which was inaccessible by larger plasticizers, it

occupied the voids in the polymeric network. In other words, the presence of rich moisture molecules significantly influenced the mechanism of crystallization and rate of crystal growth.

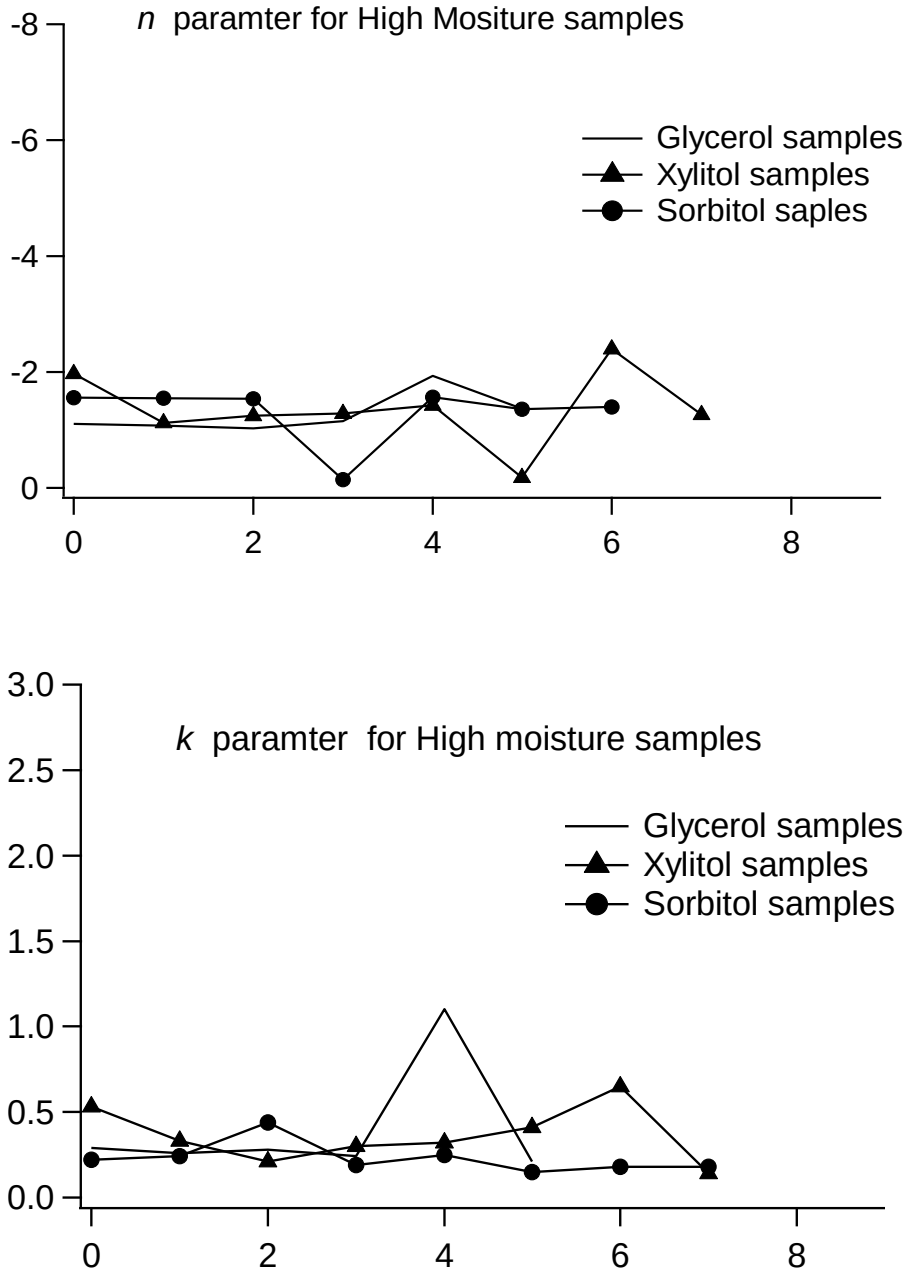

Figure 7-8 Comparison of parameter n and k extracted from modified Avrami equation for the high moisture samples.

7.5 Synergistic interaction maps

Based on the above discussion, the preventative map of the synergistic interactions within this complexity hydrophilic polymeric system could be described as a three stage process as below:

7.5.1 Stage one (*unsaturated relatively loosen-soft polymeric network*)

When the plasticizer and MMT concentration were both relatively low, not all the available interaction sites are occupied. The interaction of starch/plasticizer and interaction starch/MMT can take place without competing with each other. Therefore, higher degree of exfoliation of MMT was observed in this scenario (105 and 305 samples) together with a relatively higher glass-transition temperature due to the antiplasticization effect of low plasticizer loading.

A graphical representation of the *unsaturated relatively loosen-soft polymeric network* is given in Figure 7-9.

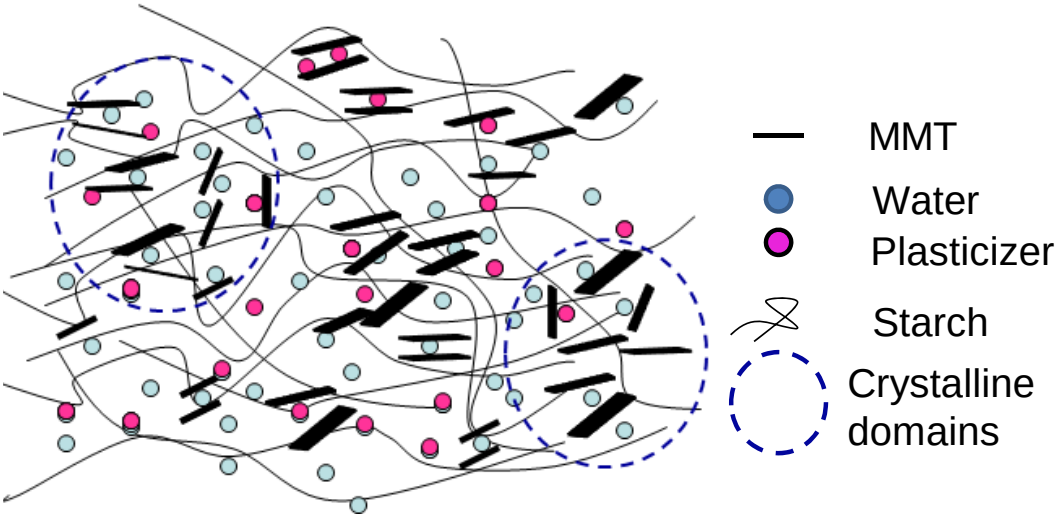

Figure 7-9 Schematic diagram of the unsaturated relatively loosen-soft polymeric network.

Direct evidences for this stage were the broad peaks from WAXD patterns and SAXS profiles from corresponding samples. Besides, under such scenario, though loosen and soft polymeric network was present due to the well-known antiplasticization effect at low loading of plasticizer. In other words, the MMT and plasticizer molecules were firmly ‘locked’ in this situation which had been supported by the high glass-transition temperature value of corresponding samples. Meanwhile,

the loosen characteristic of this morphology could be directly evidenced from the analyses of the melting point for low-plasticizer samples, Table. As shown in Table 7-7, the melting point value for low-plasticizer samples were lower than that of high-plasticizer samples, which indicated that a loosened network required less energy to be melted.

Table 7-7 Comparison of melting temperature (T_m) values for different samples.

Sample ID	T_m (˚C)		
	glycerol	xylitol	sorbitol
105	215	185	207
115	238	204	214
210	176	233	233
220	242	237	240
305	142	133	211
315	186	153	236
410		213	218
420		246	198

Solid supporting results for formation of different polymeric networks can be obtained from the NMR results (^{1}H NMR for the glycerol samples (*Chapter* 4) and ^{13}C for the sorbitol samples(*Chapter* 5)) of selected samples, where low-plasticizer loading samples showed a specific lower molecular mobility (plasticizer) indicating that the plasticizer molecules were firmly 'held' within the polymeric network.

7.5.2 Stage two (*competitive relatively tighten-firm polymeric network*)

A tighter polymeric network was formed upon increasing the plasticizer concentration since the stronger plasticizer/plasticizer interaction was competing with the starch/MMT interaction which hindered the exfoliation of MMT in this circumstance. Therefore, an overall tighter polymeric network was formed when the plasticizer concentration was high enough. Meanwhile, as a result of the relative higher amount of plasticizer present, the overall chain mobility was restricted when compared to that in stage one, which was termed as 'firm' in this circumstance. A graphical representation of the *competitive relatively tighten-firm network* was given in

Figure *7-10*. The solid evidence was the high melting point for high-plasticizer samples as shown in Table 7-7, where larger amount of energy was required in a tighten-firm polymeric network.

The straight evidence of the formation of an *unsaturated relatively loosen-soft polymeric network* in low plasticizer system and a *competitive relatively tighten-firm polymeric network* in higher plasticizer system can be confirmed from the PALS measurement results for selected sorbitol-plasticized samples, Table 7-8. A more uniform void distribution was observed in 5% sorbitol samples. However, two types of well-defined voids were found in high (10% and 20%) sorbitol loading samples. Such observations strongly supported the prospect morphology formation under specific conditions.

Table 7-8 PALS measurement results for representative samples.

Sample ID	Lifetime(ns)	Void Radius (nm)	Weight (%)	Lifetime(ns)	Void Radius (nm)	Weight (%)
S305	1.37	0.22	3.27	1.67	0.25	11.80
S210	1.29	0.21	14.70	8.65	0.61	4.30
S420	1.78	0.26	12.19	7.8	060	2.93

Short lifetime components have been converted to pore radius using the Tao-Eldrup model.
Long lifetime components have converted using the Rectangular Tao-Eldrup model.

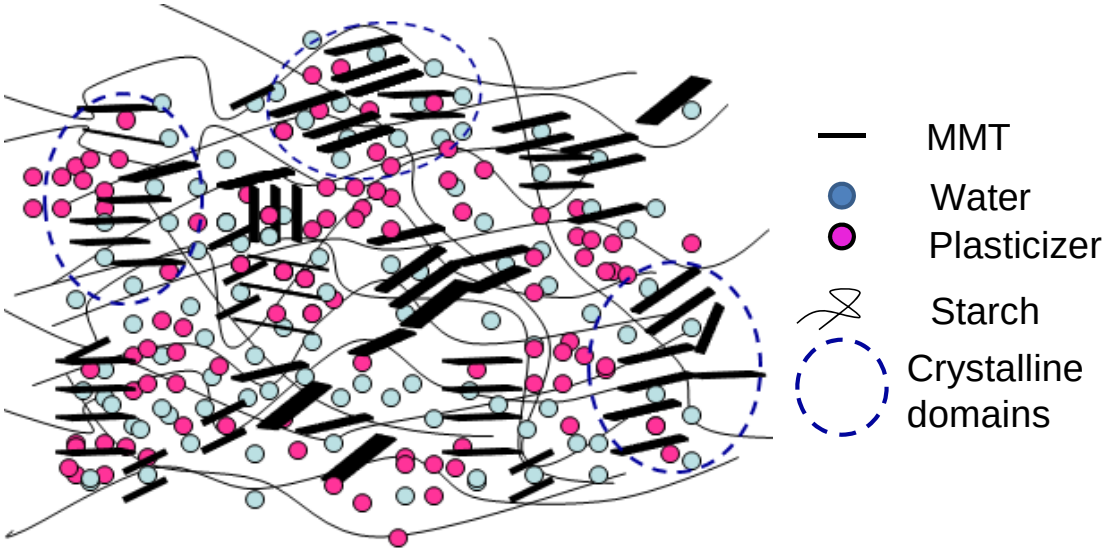

Figure 7-10 Schematic diagram of the competitive relatively tighten-firm polymeric network.

Simultaneously, interactions involving MMT (starch/MMT, plasticizer/MMT, and MMT/MMT) contributed to the observed distinctness of samples from various formulas.

a. Increasing either plasticizer or MMT loading resulted in a higher *basal spacing*.

b. Increasing the plasticizer enhanced the starch/plasticizer interaction and replaced the water molecules which decreased the moisture content within the samples. However, this phenomenon was affected by the molecular hydrophilicity of the plasticizer and balanced by the addition of MMT which tended to hold higher amount of moisture within the matrixes.

c. A competition of plasticizer/starch interaction (decreasing the crystallinity value) and plasticizer/MMT interaction (increasing the crystallinity value) was evidenced from the crystallinity values from different samples. Due to the high affinity between starch and plasticizer (plasticization effect), the well-known nucleation effect of MMT was suppressed to a large extent at a high plasticizer scenario. Because the main tendency found in the crystallinity value was described as decreasing steadily upon the increase of plasticizer concentration regardless of the MMT loading, except in the 1%MMT Xylitol samples.

d. The effect of competitive forces (resulting from crystal growth) was proven to become dominant at a high xylitol level due to its strong crystallization ability. As a result, it had been assumed that xylitol-plasticized samples were intended to produce a high crystalline value polymeric network with smaller crystals compared to that of glycerol/sorbitol morphologies. This had been supported by the larger domain size, high crystallinity and unique n parameter (crystal formation mechanism parameter extracted from Avrami equation) values when compared to the corresponding parameters to that of glycerol/sorbitol-plasticized samples, as well as the relatively low crystallization enthalpy value for xylitol-plasticized samples.

7.5.3 Stage three (*saturated phase separation polymeric network*)

Further increasing the plasticizer concentration resulted in the phase separation of several samples (with 20% plasticizer loading) due to the stronger interactions

between plasticizers as evidenced from the thermal endotherm of high sorbitol-loading samples.

Summary

Comparison analysis had been carried out across different type of plasticizer used in the current work, glycerol, sorbitol and xylitol. Main factors considered from both physical (molecular size of the plasticizer, molecular structure of the plasticizer), intrinsic chemistry aspects (hydrophilicity-number of hydroxyl groups, crystal features, crystallization ability, intermolecular hydrogen ponds strength) were taken into consideration. Important conclusions are indicated as follows:

1. Physical aspects of the plasticizer were the dominant factors influencing the overall polymeric network order, cell packing density as well as the rate constant *k* (extracted via modified *Avrami* equation) containing the crystal growth parameters. The achievable *basal spacing* and the formation of larger crystalline domains (resulting from the retrogradation of starch polymer) was obviously dependent on the molecular size of the used plasticizers.

2. Analyses of the crystallization behaviour for samples suggested that intrinsic chemistry of plasticizer was the primary factor that determined the crystallization behaviour. As proven by the finding that no sharp crystalline peak was observed until 10% plasticizer in xylitol samples as well the mechanism of nucleation and crystal form parameter *n* via Avrami equation and high X_c%.

3. The presence of excess moisture successfully modified the interactions amongst starch/ MMT/plasticizer and balanced the effect induced from different plasticizers. Water molecules were acting like typical plasticizer and occupied most of the small vacates between starch polymers throughout the polymeric network, which were too small for the larger plasticizers. Thus uniformed the morphological characteristic for corresponding samples.

4. A three stage process was introduced to describe the synergistic interactions within this hydrophilic system. The process involved *unsaturated relatively loosen-soft polymeric network (5% plasticizer); competitive relatively tighten-firm polymeric network (larger than 5% but less than 20%)* and *saturated phase separation polymeric network (20%).*

Chapter 8

Conclusions and Recommendations

8.1 Conclusions

Based on the previous discussions, the complex interactions existing in the polymeric system were dependent on several main factors including type of the plasticizer (hydrophilicity, size, molecular symmetry, intermolecular hydrogen bonds strength, and crystallization ability), and the relative ratio of plasticizer and MMT. These factors could affect the synergistic interactions to different extent. These interactions included starch/plasticizer interactions, plasticizer/plasticizer interactions, starch/MMT interactions, plasticizer/ MMT interactions, and MMT/MMT interactions. Apparently, stronger affinity of plasticizer determined that the interaction between starch and plasticizer was the primary interaction within the system; this was followed by plasticizer/plasticizer interactions, starch/MMT interactions and plasticizer/ MMT interactions.

8.1.1 General regularities

Several regularities can be drawn as below:

1. The major starch polymer chain is a mother network presented with larger amount of activity sites available for the interactions (starch+plasticizer and starch+MMT). The interaction of starch/plasticizer is stronger than the interaction of starch/MMT. The interaction of plasticizer/plasticizer is stronger than the interaction of starch/MMT.
2. The increase of certain component enhanced the interaction within that component first, and then improved the interaction related to another component that possessed a higher hydrophilicity and/or more similar molecular structure. For example, the interactions of MMT and plasticiser will be enhanced upon increasing the MMT loading. Though the MMT/MMT inactions were improved, the high hydrophilicity of plasticizer ensured a stronger interaction of plasticizer/MMT which overtook the MMT/MMT (intended to agglomerate the MMT plate together) interaction, therefore an expansion of *basal spacing* was observed in the high plasticiser loading samples.

3. The crystallization process was dominantly influenced by the intrinsic chemistry (crystallization ability and intermolecular hydrogen bond strength) of the applied plasticizer. The xylitol-plasticized samples showed highest crystallinity and the crystallization mechanism was confirmed to be significantly different from that of glycerol/sorbitol samples. Meanwhile, the molecular size of the plasticizer was another important factor that affected the crystalline domain formation where the crystalline domain size of glycerol samples was overall larger than xylitol and sorbitol-plasticized samples.
4. The final morphology of the nanocomposites was determined from the interplay of the different interactions.

8.1.2 Synergistic interaction maps

The interaction process was divided into three stages according to the concentration of plasticizer used. And the existence of morphology 'threshold' was confirmed to differ in defend systems. The morphology 'threshold' was described as the critical plasticizer concentration for the formation of either a *loosen-soft* polymeric network (within the 'threshold') or *tighten-firm* polymeric network (beyond the 'threshold'). Specifically, the 'threshold' value for glycerol, xylitol and sorbitol-plasticized systems was proven to be 5%, 10% and 5%, respectively.

- Within the 'threshold': *a relatively unsaturated loosen-soft polymeric network was formed and the starch/plasticizer interaction and starch/MMT interaction can take place without interfering with each other too much.*

- Beyond the 'threshold': *a relatively saturated tighten-firm polymeric network was formed and the stronger plasticizer/plasticizer interactions significantly alter/affect the MMT exfoliation process and crystallization behaviour of the corresponding sample. The three-way interactions competed mutually.*

Furthermore, the high 'threshold' of xylitol plasticizer resulted from the unique intrinsic chemistry features including stronger crystallization ability and weaker intermolecular hydrogen bonds when compared to that of glycerol and sorbitol.

8.1.3 Role of water molecule

Based on the importance of water molecule in the starch-related material manufacture process, the studies on water molecule revealed some significant effects in the investigated system. The presence of excess moisture successfully modified

the interactions amongst starch/ MMT/plasticizer. Water molecules were acting like typical plasticizer and occupied most of the small spaces between starch polymers throughout the polymeric network, which were too small for the larger plasticizers. Thus the morphological characteristic for corresponding samples as proved by the results indicates that only one crystalline domain was defined in the high moisture samples.

The plasticization effect of molecules was confirmed from the molecular modelling results as well where significant drop of glass-transition temperature was observed in high hydration (11.3%) samples. The glass-transition temperature for starch fragments at different hydration was calculated as 186(anhydrous), 137(5.4%), 63(8.35%) and 42(11.3%), respectively.

8.2 Recommendations

Below are the recommended future works from this study:

1. The time-dependent changes occurred in starch-based materials is one of the most significant areas inducing unexpected effects on the properties of obtained material. Mature strategies had not been well developed yet. The results obtained in this study were not sufficient for covering all the internal behavioural changes upon material ageing. Further work is recommended in this aspect. More experiments and characterizations upon ageing are necessary to be carried out to monitor the changes happening at a macro-structural level.

2. The second important future work recommended is the validation of proposed hypothesis via molecular modelling. Accurate model is necessary for such validation. As indicated in *Chapter* four (interaction of glycerol/starch/water had been simulated via molecular modelling), initial trial work had been done in this research and the promising preliminary results strongly supported the possibility of the applicability of molecular modelling in this area.

3. Considering the application of these materials, studies on the mechanical and physical properties data of obtained materialist will be another batch of validation data of great interest. It is worth to relate the internal interactions within the materials of more mechanical properties and physical properties data. Such relationship can provide direct relationship of the micro-scale changes and bulk properties.

REFERENCES

1. Van Soest, J.J.G. and P. Essers, *Influence of amylose-amylopectin ratio on properties of extruded starch plastic sheets.* Journal of Macromolecular Science, Part A, 1997. **34**(9): p. 1665-1689.
2. Dufresne, A., D. Dupeyre, and M.R. Vignon, *Cellulose microfibrils from potato tuber cells: processing and characterization of starch-cellulose microfibril composites.* Journal of Applied Polymer Science, 2000. **76**(14): p. 2080-2092.
3. Averous, L., *Cellulose-based biocomposites: Comparison of different multiphasic systems.* Composite Interfaces, 2007. **7**(9): p. 787-805.
4. Dufresne, A. and M.R. Vignon, *Improvement of starch film performances using cellulose microfibrils.* Macromolecules, 1998. **31**(8): p. 2693-2696.
5. Wollerdorfer, M. and H. Bader, *Influence of natural fibres on the mechanical properties of biodegradable polymers.* Industrial Crops and Products, 1998. **8**(2): p. 105-112.
6. Funke, U., W. Bergthaller, and M.G. Lindhauer, *Processing and characterization of biodegradable products based on starch.* Polymer Degradation and Stability, 1998. **59**(1-3): p. 293-296.
7. Curvelo, A.A.S., A.J.F. De Carvalho, and J.A.M. Agnelli, *Thermoplastic starch-cellulosic fibers composites: preliminary results.* Carbohydrate Polymers, 2001. **45**(2): p. 183-188.
8. McGlashan, S.A. and P.J. Halley, *Preparation and characterisation of biodegradable starch-based nanocomposite materials.* Polymer International, 2003. **52**(11): p. 1767-1773.
9. Tjong, S.C., *Structural and mechanical properties of polymer nanocomposites.* Materials Science and Engineering: R: Reports, 2006. **53**(3-4): p. 73-197.
10. Follain, N., et al., *Quaternary starch based blends: Influence of a fourth component addition to the starch/water/glycerol system.* Carbohydrate Polymers, 2006. **63**(3): p. 400-407.
11. Kampeerapappun, P., et al., *Preparation of cassava starch/montmorillonite composite film.* Carbohydrate Polymers, 2007. **67**(2): p. 155-163.
12. Zhang, Q.-X., et al., *Preparation and crystalline morphology of biodegradable starch/clay nanocomposites.* Polymer, 2007. **48**(24): p. 7193-7200.
13. Xiong, H., et al., *The structure and properties of a starch-based biodegradable film.* Carbohydrate Polymers, 2008. **71**(2): p. 263-268.
14. Namazi, H., M. Mosadegh, and A. Dadkhah, *New intercalated layer silicate nanocomposites based on synthesized starch-g-PCL prepared via solution intercalation and in situ polymerization methods: As a comparative study.* Carbohydrate Polymers, 2009. **75**(4): p. 665-669.
15. Wang, N., et al., *Effect of citric acid and processing on the performance of thermoplastic starch/montmorillonite nanocomposites.* Carbohydrate Polymers, 2009. **76**(1): p. 68-73.
16. Alexandre, M. and P. Dubois, *Polymer-layered silicate nanocomposites: preparation, properties and uses of a new class of materials.* Materials Science and Engineering: R: Reports, 2000. **28**(1-2): p. 1-63.
17. Biswas, M. and S. Ray, *Recent progress in synthesis and evaluation of polymer-montmorillonite nanocomposites.* New polymerization techniques and synthetic methodologies, 2001: p. 167-221.

18. LeBaron, P.C., Z. Wang, and T.J. Pinnavaia, *Polymer-layered silicate nanocomposites: an overview*. Applied Clay Science, 1999. **15**(1-2): p. 11-29.
19. Sinha Ray, S. and M. Okamoto, *Polymer/layered silicate nanocomposites: a review from preparation to processing.* Progress in Polymer Science, 2003. **28**(11): p. 1539-1641.
20. Park, J.H. and S.C. Jana, *Mechanism of Exfoliation of Nanoclay Particles in Epoxy- Clay Nanocomposites.* Macromolecules, 2003. **36**(8): p. 2758-2768.
21. Kashiwagi, T. and R. Harris, *Flame retardant mechanism of polyamide 6-clay nanocomposites* 1*. Polymer, 2004. **45**(3): p. 881-891.
22. Wang, K., et al., *Epoxy nanocomposites with highly exfoliated clay: mechanical properties and fracture mechanisms.* Macromolecules, 2005. **38**(3): p. 788-800.
23. Potton, J.A., G.J. Daniell, and B.D. Rainford, *A new method for the determination of particle size distributions from small-angle neutron scattering measurements.* Journal of Applied Crystallography, 1988. **21**(6): p. 891-897.
24. Lee, S.W., et al., *Synthesis and non-isothermal crystallization behaviors of poly(ethylene isophthalate-co-terephthalate)s.* Polymer, 1999. **40**(25): p. 7137-7146.
25. Imberty, A., et al., *Recent advances in knowledge of starch structure.* Starch-Stärke, 1991. **43**(10): p. 375-384.
26. Ophardt, C., *Virtual chembook*, E. College, Editor. 2003: Chicago.
27. French, A.D. and V.G. Murphy, *Computer modeling in the study of starch.* Cereal Foods World, 1977. **22**(2): p. 61.
28. Hsein-Chih, H.W. and A. Sarko, *The double-helical molecular structure of crystalline B-amylose.* Carbohydrate Research, 1978. **61**(1): p. 7-25.
29. Hsien-Chih, H.W. and A. Sarko, *The double-helical molecular structure of crystalline a-amylose.* Carbohydrate Research, 1978. **61**(1): p. 27-40.
30. Karel, M., et al., *The glassy state in foods*. 1993, Nottingham University Press Loughborough. p. 13.
31. Sears, J.K., J.R. Darby, and Knovel, *The technology of plasticizers*. 1982: Wiley New York.
32. Aiken, W., et al., *Creep behavior of plasticized vinylite VYNW.* Journal of Polymer Science, 1947. **2**(2): p. 178-198.
33. Moorshead, T., *Advances in PVC Compounding and Processing*, ed. M.K. Sons. 1962.
34. Williams, M.L., R.F. Landel, and J.D. Ferry, *The temperature dependence of relaxation mechanisms in amorphous polymers and other glass-forming liquids.* Journal of the American Chemical Society, 1955. **77**(14): p. 3701-3707.
35. Boyer, R.F., *The relation of transition temperatures to chemical structure in high polymers.* Rubber Chemistry and Technology, 1963. **36**: p. 1303.
36. Gidley, M.J. and P.V. Bulpin, *Aggregation of amylose in aqueous systems: the effect of chain length on phase behavior and aggregation kinetics.* Macromolecules, 1989. **22**(1): p. 341-346.
37. Tester, R.F. and W.R. Morrison, *Swelling and gelatinization of cereal starches. I. Effects of amylopectin, amylose, and lipids.* Cereal Chemistry, 1990. **67**(6): p. 551-557.

38. Cooke, D. and M.J. Gidley, *Loss of crystalline and molecular order during starch gelatinisation: origin of the enthalpic transition.* Carbohydrate Research, 1992. **227**(5): p. 103-112.
39. Biliaderis, C.G. and B.O. Juliano, *Thermal and mechanical properties of concentrated rice starch gels of varying composition.* Food Chemistry, 1993. **48**(3): p. 243-250.
40. Siljeström, M., et al., *Effects on polysaccharides during baking and storage of bread-in vitro and in vivo studies.* Cereal Chemistry, 1988. **65**(1): p. 1-8.
41. Boyer, R.F., E. Baer, and A. Hiltner, *Concerning gelation effects in atactic polystyrene solutions.* Macromolecules, 1985. **18**(3): p. 427-434.
42. Clark, A.H., et al., *Rheological studies of aqueous amylose gels: The effect of chain length and concentration on gel modulus.* Macromolecules, 1989. **22**(1): p. 346-351.
43. French, D., *Starch and its Derivatives.* Journal of the American Chemical Society, 1955. **77**(9): p. 2664-2665.
44. Hallberg, L.M. and P. Chinachoti, *A fresh perspective on staling: The significance of starch recrystallization on the firming of bread.* Journal of food science, 2002. **67**(3): p. 1092-1096.
45. Primo-Martin, C., et al., *Crystallinity changes in wheat starch during the bread-making process: Starch crystallinity in the bread crust.* Journal of Cereal Science, 2007. **45**(2): p. 219-226.
46. Endres, H.J. and A. Pries, *Mechanische Eigenschaften stärkegefüllter Polymerverbunde.* Starch-Stärke, 1995. **47**(10): p. 384-393.
47. Nielsen, L.E., *Mechanical properties of polymers and composites. Volumes 1 & 2(Book)*. Vol. 2. 1974, New York: Marcel Dekker Inc. 386-414.
48. A. A. Berlin, E. A. Penskaya, and G.I. Volkova, *Mechanicochemical conversion and block copolymerization by freezing of starch solutions.* Journal of Polymer Science, 1962. **56**(164): p. 477–484.
49. Bagley, E.B., et al., *Composite compositions from graft polymerized rigid fillers*. 1977, US Patent 4 026 849.
50. Fanta, G.F., C.L. Swanson, and R.L. Shogren, *Starch-poly (ethylene-co-acrylic acid) composite films. Effect of processing conditions on morphology and properties.* Journal of Applied Polymer Science, 1992. **44**(11): p. 2037-2042.
51. Otey, F.H., et al., *Starch-based film for degradable agricultural mulch.* Industrial & Engineering Chemistry Product Research and Development, 1974. **13**(1): p. 90-92.
52. Jasberg, B., et al., *Mixing Polyethylene-Poly (ethylene-co-acrylic acid) Copolymer-Starch Formulations for Blown Films.* Journal of Polymer Materials, 1992. **9**(1-2): p. 153-153.
53. Stepto, R.F.T., *Thermoplastic starch and drug delivery capsules.* Polymer International, 1997. **43**(2): p. 155-158.
54. Kaya, E., M. Tano lu, and S. Okur, *Layered clay/epoxy nanocomposites: Thermomechanical, flame retardancy, and optical properties.* Journal of Applied Polymer Science, 2008. **109**(2): p. 834-840.
55. Sarwar, M.I., S. Zulfiqar, and Z. Ahmad, *Polyamide-silica nanocomposites: mechanical, morphological and thermomechanical investigations.* Polymer International, 2008. **57**(2): p. 292-296.
56. Haraguchi, K. and T. Takehisa, *Nanocomposite hydrogels: A unique organic-inorganic network structure with extraordinary mechanical, optical, and*

swelling/de-swelling properties. Advanced materials, 2002. **14**(16): p. 1120-1124.
57. Ma, J., et al., *A novel method for preparation of disorderly exfoliated epoxy/clay nanocomposite.* Chemistry of materials, 2004. **16**(5): p. 757-759.
58. Maiti, P., et al., *New polylactide/layered silicate nanocomposites: role of organoclays.* Chemistry of materials, 2002. **14**(11): p. 4654-4661.
59. Messersmith, P.B. and E.P. Giannelis, *Synthesis and characterization of layered silicate-epoxy nanocomposites.* Chemistry of materials, 1994. **6**(10): p. 1719-1725.
60. Tang, X., S. Alavi, and T.J. Herald, *Effects of plasticizers on the structure and properties of starch-clay nanocomposite films.* Carbohydrate Polymers, 2008. **74**(3): p. 552-558.
61. Vigui, J., S. Molina Boisseau, and A. Dufresne, *Processing and characterization of waxy maize starch films plasticized by sorbitol and reinforced with starch nanocrystals.* Macromolecular bioscience, 2007. **7**(11): p. 1206-1216.
62. Ma, X., J. Yu, and N. Wang, *Production of Thermoplastic Starch/MMT Sorbitol Nanocomposites by Dual Melt Extrusion Processing.* Macromolecular Materials and Engineering, 2007. **292**(6): p. 723-728.
63. Fornes, T.D., D.L. Hunter, and D.R. Paul, *Effect of sodium montmorillonite source on nylon 6/clay nanocomposites.* Polymer, 2004. **45**(7): p. 2321-2331.
64. Bergaya, F., B.K.G. Theng, and G. Lagaly, *Handbook of clay science*. 2006: Elsevier Science Ltd.
65. Beyer, G., *Nanocomposites: a new class of flame retardants for polymers.* Plastics, Additives and Compounding, 2002. **4**(10): p. 22-28.
66. Bader, H.G. and D. Göritz, *Investigations on High Amylose Corn Starch Films. Part 2: Water Vapor Sorption.* Starch - Stärke, 1994. **46**(7): p. 249-252.
67. Mali, S., et al., *Microstructural characterization of yam starch films.* Carbohydrate Polymers, 2002. **50**(4): p. 379-386.
68. Mali, S., et al., *Barrier, mechanical and optical properties of plasticized yam starch films.* Carbohydrate Polymers, 2004. **56**(2): p. 129-135.
69. Gaudin, S., et al., *Plasticisation and Mobility in Starch-Sorbitol Films.* Journal of Cereal Science, 1999. **29**(3): p. 273-284.
70. Chang, Y.P., K.A. Abd, and C.C. Seow, *Interactive plasticizing-antiplasticizing effects of water and glycerol on the tensile properties of tapioca starch films.* Food Hydrocolloids, 2006. **20**(1): p. 1-8.
71. Pittia, P. and G. Sacchetti, *Antiplasticization effect of water in amorphous foods. A review.* Food Chemistry, 2008. **106**(4): p. 1417-1427.
72. Gaudin, S., et al., *Antiplasticisation and oxygen permeability of starch-sorbitol films.* Carbohydrate Polymers, 2000. **43**(1): p. 33-37.
73. Dean, K., L. Yu, and D.Y. Wu, *Preparation and characterization of melt-extruded thermoplastic starch/clay nanocomposites.* Composites Science and Technology, 2007. **67**(3-4): p. 413-421.
74. Park, H.J. and M.S. Chinnan, *Gas and water vapor barrier properties of edible films from protein and cellulosic materials.* Journal of Food Engineering, 1995. **25**(4): p. 497-507.
75. Päivi, M., et al., *Effect of glycerol on behaviour of amylose and amylopectin films.* Carbohydrate Polymers, 2002. **50**(4): p. 355-361.

76. Mali, S., et al., *Water sorption and mechanical properties of cassava starch films and their relation to plasticizing effect.* Carbohydrate Polymers, 2005. **60**(3): p. 283-289.
77. Smits, A.L.M., et al., *Interaction between dry starch and plasticisers glycerol or ethylene glycol, measured by differential scanning calorimetry and solid state NMR spectroscopy.* Carbohydrate polymers, 2003. **53**(4): p. 409-416.
78. Bozdemir, O.A. and M. Tutas, *Plasticiser effect on water vapour permeability properties of Locust bean gum-based edible films.* Turkish Journal of Chemistry, 2003. **27**(6): p. 773-782.
79. Seow, C.C., P.B. Cheah, and Y.P. Chang, *Antiplasticization by Water in Reduced-Moisture Food Systems.* Journal of Food Science, 1999. **64**(4): p. 576-581.
80. Lourdin, D., H. Bizot, and P. Colonna, *"Antiplasticization" in starch-glycerol films?* Journal of Applied Polymer Science, 1997. **63**(8): p. 1047-1053.
81. Chaudhary, D.S., H. Liu, and B. Adhikari, *Influence of Branching and Plasticiser on Water Activity in Starch Biopolymer*, in *30th Australasian Polymer* 2008: Melbourne, Victoria, Australia. p. 151.
82. Kalambur, S.B. and S.S.H. Rizvi, *Starch-based nanocomposites by reactive extrusion processing.* Polymer International, 2004. **53**(10): p. 1413-1416.
83. Shaw, N.B., et al., *Physical Properties of WPI Films Plasticized with Glycerol, Xylitol, or Sorbitol.* Journal of Food Science, 2002. **67**(1): p. 164-167.
84. Varma, R., *Clay and clay-supported reagents in organic synthesis.* Tetrahedron, 2002. **58**(7): p. 1235-1255.
85. Liu, H., D. Chaudhary, and M.O. Tadé *Preparation and characterization of sorbitol modified nanoclay with high amylose bionanocomposites.* Carbohydrate Polymers, 2011. **85**(1): p. 97-104.
86. Liu, H., et al., *Glycerol/starch/Na+-montmorillonite nanocomposites: A XRD; FTIR; DSC and 1H NMR study.* Carbohydrate Polymers, 2011. **83**(4): p. 1591-1597.
87. Liu, P., *Polymer modified clay minerals: A review.* Applied Clay Science, 2007. **38**(1-2): p. 64-76.
88. Müller, C.M.O., F. Yamashita, and J.B. Laurindo, *Evaluation of the effects of glycerol and sorbitol concentration and water activity on the water barrier properties of cassava starch films through a solubility approach.* Carbohydrate Polymers, 2008. **72**(1): p. 82-87.
89. Huang, M.F., J.G. Yu, and X.F. Ma, *Studies on the properties of montmorillonite-reinforced thermoplastic starch composites.* Polymer, 2004. **45**(20): p. 7017-7023.
90. Godbillot, L., et al., *Analysis of water binding in starch plasticized films.* Food Chemistry, 2006. **96**(3): p. 380-386.
91. Lourdin, D., S.G. Ring, and P. Colonna, *Study of plasticizer-oligomer and plasticizer-polymer interactions by dielectric analysis: maltose-glycerol and amylose-glycerol-water systems.* Carbohydrate Research, 1998. **306**(4): p. 551-558.
92. Liu, H., et al. *Reduced RH influence on starch structure with different Plasticizer for biodegradable packaging*. in *International Symposium on Recent Developments and Applications in Polymer Nanostructured-Materials*. 2009. Melbourne, Australia.

93. Chaudhary, D.S., B.P. Adhikari, and S. Kasapis, *Glass transition behaviour of plasticized starch biopolymer system-a modified Gordon-Taylor approach.* Food Hydrocolloids, 2011. **25**(1): p. 114-121.
94. Mathew, A.P. and A. Dufresne, *Plasticized waxy maize starch: Effect of polyols and relative humidity on material properties.* Biomacromolecules, 2002. **3**(5): p. 1101-1108.
95. Lourdin, D., et al., *Influence of equilibrium relative humidity and plasticizer concentration on the water content and glass transition of starch materials.* Polymer, 1997. **38**(21): p. 5401-5406.
96. Chaudhary, D. and B. Adhikari, *Glass-Rubber Transition of Plasticised Starch Biopolymer Affected by Relative Humidity.* In *CHEMECA* 27-30 September 2009:(ID:406) Perth , Australia.
97. Cao , X., et al., *Green composites reinforced with hemp nanocrystals in plasticized starch.* Journal of Applied Polymer Science, 2008. **109**(6): p. 3804-3810.
98. Cyras, V.P., et al., *Physical and mechanical properties of thermoplastic starch/montmorillonite nanocomposite films.* Carbohydrate Polymers, 2008. **73**(1): p. 55-63.
99. Jitendra, K.P. and P.S. Raj, *Green Nanocomposites from Renewable Resources: Effect of Plasticizer on the Structure and Material Properties of Clay-filled Starch.* STARCH - stärke, 2005. **57**(1): p. 8-15.
100. De Carvalho, A.J.F., A.A.S. Curvelo, and J.A.M. Agnelli, *A first insight on composites of thermoplastic starch and kaolin.* Carbohydrate Polymers, 2001. **45**(2): p. 189-194.
101. Park, H.-M., et al., *Preparation and Properties of Biodegradable Thermoplastic Starch/Clay Hybrids.* Macromolecular Materials and Engineering, 2002. **287**(8): p. 553-558.
102. Wilhelm, H.M., et al., *The influence of layered compounds on the properties of starch/layered compound composites.* Polymer International, 2003. **52**(6): p. 1035-1044.
103. Chiou, B.S., et al., *Extruded starch-nanoclay nanocomposites: Effects of glycerol and nanoclay concentration.* Polymer Engineering and Science, 2007. **47**(11): p. 1898-1904.
104. Cao, X., et al., *Preparation and properties of plasticized starch/multiwalled carbon nanotubes composites.* Journal of Applied Polymer Science, 2007. **106**(2): p. 1431-1437.
105. Chaudhary, D.S., *Understanding amylose crystallinity in starch-clay nanocomposites.* Journal of Polymer Science Part B: Polymer Physics, 2008. **46**(10): p. 979-987.
106. Margarita, M., M. Juana E., and R.-G. Francisco J., *Nanocomposites from plasticized high-amylopectin, normal and high-amylose maize starches.* Polymer Engineering & Science, 2008. **48**(7): p. 1261-1267.
107. Pérez, C.J., et al., *Water uptake behavior of layered silicate/starch-polycaprolactone blend nanocomposites.* Polymer International, 2008. **57**(2): p. 247-253.
108. Xiaofei, M., Y. Jiugao, and F. Jin, *Urea and formamide as a mixed plasticizer for thermoplastic starch.* Polymer International, 2004. **53**(11): p. 1780-1785.
109. Wang, X., et al., *Impact of Pre Processing of Montmorillonite on the Properties of Melt Extruded Thermoplastic Starch/Montmorillonite Nanocomposites.* Starch Stärke, 2009. **61**(9): p. 489-494.

110. Fischer, H., *Polymer nanocomposites: from fundamental research to specific applications.* Materials Science and Engineering: C, 2003. **23**(6-8): p. 763-772.
111. Magalhães, N.F. and C.T. Andrade, *Thermoplastic corn starch/clay hybrids: Effect of clay type and content on physical properties.* Carbohydrate Polymers, 2009. **75**(4): p. 712-718.
112. Yang, K.K., X.L. Wang, and Y.Z. Wang, *Progress in nanocomposite of biodegradable polymer.* Journal of Industrial and Engineering Chemistry, 2007. **13**(4): p. 485-500.
113. Majdzadeh-Ardakani, K., A.H. Navarchian, and F. Sadeghi, *Optimization of mechanical properties of thermoplastic starch/clay nanocomposites.* Carbohydrate Polymers, 2010. **79**(3): p. 547-554.
114. Chivrac, F., et al., *Starch-based nano-biocomposites: Plasticizer impact on the montmorillonite exfoliation process.* Carbohydrate Polymers, 2010. **79**(4): p. 941-947.
115. Mathew, A.P. and A. Dufresne, *Morphological investigation of nanocomposites from sorbitol plasticized starch and tunicin whiskers.* Biomacromolecules, 2002. **3**(3): p. 609-617.
116. Chaudhary, D.S. and B.P. Adhikari, *Understanding polymeric amylose retrogradation in presence of additives.* Journal of Applied Polymer Science, 2010. **115**(5): p. 2703-2709.
117. Chen, J., et al., *Structural characterization and properties of starch/konjac glucomannan blend films.* Carbohydrate Polymers, 2008. **74**(4): p. 946-952.
118. Leonardo, d.V.-M., et al., *Capillary zone electrophoretic determination of cytochrome c in mitochondrial extracts and cytosolic fractions: Application to a digitalis intoxication study.* Talanta, 2008. **74**(4): p. 478-488.
119. Chivrac, F., et al., *How does water diffuse in starch/montmorillonite nano-biocomposite materials?* Carbohydrate Polymers, 2010. **82**(1): p. 128-135.
120. Katti, D. and K. Katti, *Simulation Based Design Of Polymer Clay Nanocomposites Using Multiscale Modeling: An Overview*. Nanostructured Materials and Nanotechnology III. 2009: Wiley-American Ceramic Society. 27.
121. Ginzburg, V., et al., *Thermodynamics of Polymer- Clay Nanocomposites Revisited: Compressible Self-Consistent Field Theory Modeling of Melt-Intercalated Organoclays.* Macromolecules, 2009. **42**(22): p. 9089-9095.
122. Cygan, R., et al., *Molecular models and simulations of layered materials.* Journal of Materials Chemistry, 2009. **19**(17): p. 2470-2481.
123. Liu, H. and D. Chaudhary, *The Moisture Migration Behavior of Plasticized Starch Biopolymer.* Drying Technology, 2011. **29**(3): p. 278-285.
124. Róz, A.L.D., et al., *The effect of plasticizers on thermoplastic starch compositions obtained by melt processing.* Carbohydrate Polymers, 2006. **63**(3): p. 417-424.
125. Cornell, J., *Experiments with mixtures: designs, models, and the analysis of mixture data*. 2002: Wiley New York.
126. Wiedmann, W. and E. Strobel, *Compounding of Thermoplastic Starch with Twin screw Extruders.* Starch Stärke, 1991. **43**(4): p. 138-145.
127. Biliaderis, C. and T. VOSE, *Starch gelatinization phenomena studied by differential scanning calorimetry.* Journal of food science, 1980. **45**(6): p. 1669-1674.

128. Blahovec, J. and S. Yanniotis, *GAB generalized equation for sorption phenomena.* Food and Bioprocess Technology, 2008. **1**(1): p. 82-90.
129. Van den Berg, C., *Description of water activity of foods for engineering purposes by means of the GAB model of sorption.* Engineering and food, 1984. **1**: p. 311-321.
130. Schar, W. and M. Ruegg, *The evaluation of G. A. B. constants from water vapour sorption data.* Lebensmittel-Wissenschaft und -Technologie, 1985. **18**(4): p. 225-229.
131. Lewicki, P.P., *The applicability of the GAB model to food water sorption isotherms.* International Journal of Food Science & Technology, 1997. **32**(6): p. 553-557.
132. Chen, C., *Moisture sorption isotherms of pea seeds.* Journal of Food Engineering, 2003. **58**(1): p. 45-51.
133. Kickelbick, G. and E. Corporation, *Hybrid materials: synthesis, characterization, and applications*. 2007: Wiley-vch Weinheim.
134. Bond, W., *Precision lattice constant determination.* Acta Crystallographica, 1960. **13**(10): p. 814-818.
135. Inoue, K., et al. *Present status of BL40B2 and BL40XU at SPring-8 (Beamlines for small angle X-ray scattering).* in *Eighth International Conference on Synchrotron Radiation Instrumentation*. 2004. California.
136. Ilavsky, J. and P. Jemian, *Irena: tool suite for modeling and analysis of small-angle scattering.* Journal of Applied Crystallography, 2009. **42**(2): p. 347-353.
137. Chaudhary, D.S., et al., *Clay intercalation and influence on crystallinity of EVA-based clay nanocomposites.* Thermochimica Acta, 2005. **433**(1-2): p. 187-195.
138. Höhne, G., W. Hemminger, and H. Flammersheim, *Differential scanning calorimetry*. 2003: Springer Verlag.
139. Fournaris, K.G., et al., *Clay- Polyvinylpyridine Nanocomposites.* Chemistry of materials, 1999. **11**(9): p. 2372-2381.
140. Schmitz, S., et al., *Assessment of the Extent of Starch Dissolution in Dimethyl Sulfoxide by 1H NMR Spectroscopy.* Macromolecular bioscience, 2008. **9**(5): p. 506-514.
141. Hoffman, R.E., et al., *High-resolution NMR.* Journal of Magnetic Resonance, 2008. **194**(2): p. 295-299.
142. Dong, A.W., et al., *Positron Annihilation Lifetime Spectroscopy (PALS) as a Characterization Technique for Nanostructured Self-Assembled Amphiphile Systems.* The Journal of Physical Chemistry B, 2008. **113**(1): p. 84-91.
143. Dlubek, G., et al., *Positron annihilation lifetime spectroscopy (PALS) for interdiffusion studies in disperse blends of compatible polymers: a quantitative analysis.* Macromolecules, 2002. **35**(16): p. 6313-6323.
144. Dlubek, G., et al., *Effect of free volume and temperature on the structural relaxation in polymethylphenylsiloxane: A positron lifetime and pressure-volume-temperature study.* The Journal of chemical physics, 2007. **126**(2): p. 024906.
145. Field, L.D., S. Sternhell, and J.R. Kalman, *Organic structures from spectra.* Journal of Chemical Education, 2002. **79**(11).
146. Xu, Y., J. Zhou, and M.A. Hanna, *Melt-Intercalated Starch Acetate Nanocomposite Foams as Affected by Type of Organoclay 1.* Cereal Chemistry, 2005. **82**(1): p. 105-110.

147. Lopez-Rubio, A., et al., *A novel approach for calculating starch crystallinity and its correlation with double helix content: A combined XRD and NMR study.* Biopolymers, 2008. **89**(9): p. 761-768.
148. Field, L.D., S. Sternhell, and J.R. Kalman, *Organic structures from spectra*. 2002: Wiley New York.
149. Pandey, J.K. and R.P. Singh, *Green nanocomposites from renewable resources: Effect of plasticizer on the structure and material properties of clay-filled starch.* Starch/Starke, 2005. **57**(1): p. 8-15.
150. García, N. L., et al., *Physico-Mechanical Properties of Biodegradable Starch Nanocomposites.* Macromolecular Materials Engineering 2009. **294**(3).
151. Peng, G., et al., *Modeling of water sorption isotherm for corn starch.* Journal of Food Engineering, 2007. **80**(2): p. 562-567.
152. Al-Muhtaseb, A., W. McMinn, and T. Magee, *Water sorption isotherms of starch powders:: Part 1: mathematical description of experimental data.* Journal of Food Engineering, 2004. **61**(3): p. 297-307.
153. Han, J.H., *Innovations in Food Packaging*. 2005, Academic Press.
154. Eslami, H., M. Grmela, and M. Bousmina, *Structure and rheology correlation in polymer nanocomposites*. 2009, Society of Plastics Engineers: Newtown.
155. Chu, B. and B.S. Hsiao, *Small-angle x-ray scattering of polymers.* Chemical Reviews 2001. **101**(6): p. 1727-1762.
156. Lemke, H., et al., *Structural processes during starch granule hydration by synchrotron radiation microdiffraction.* Biomacromolecules, 2004. **5**(4): p. 1316-1324.
157. Mousia, Z., et al., *FTIR microspectroscopy study of composition fluctuations in extruded amylopectin-gelatin blends.* Biopolymers, 2001. **62**(4): p. 208-218.
158. Souza, R.C.R. and C.T. Andrade, *Investigation of the gelatinization and extrusion processes of corn starch.* Advances in Polymer Technology, 2002. **21**(1): p. 17-24.
159. Ding, Q.B., et al., *The effect of extrusion conditions on the functional and physical properties of wheat-based expanded snacks.* Journal of Food Engineering, 2006. **73**(2): p. 142-148.
160. Pushpadass, H.A., D.B. Marx, and M.A. Hanna, *Effects of Extrusion Temperature and Plasticizers on the Physical and Functional Properties of Starch Films.* Starch-St rke, 2008. **60**(10): p. 527-538.
161. Ungar, T., *Microstructural parameters from X-ray diffraction peak broadening.* Scripta materialia, 2004. **51**(8): p. 777-781.
162. Connolly, J.R., *Introduction quantitative X-ray diffraction methods*. 2003.
163. Sarko, A. and H.C.H. Wu, *The crystal structures of A-, B-and C-polymorphs of amylose and starch.* Starch-Stärke, 1978. **30**(3): p. 73-78.
164. Lopez-Rubio, A., A. Htoon, and E.P. Gilbert, *Influence of extrusion and digestion on the nanostructure of high-amylose maize starch.* Biomacromolecules, 2007. **8**(5): p. 1564-1572.
165. Buleon, A., et al., *Evolution of crystallinity and specific gravity of potato starch versus water ad-and desorption.* Starch-Stärke, 1982. **34**(11): p. 361-366.
166. Grubb, D.T. and N.S. Murthy, *Real-Time X-ray Study of Nylon-6 Fibers during Dehydration: Equatorial Small-Angle Scattering is Due to Surface Refraction.* Macromolecules, 2009. **43**(2): p. 1016-1027.

167. Murphy, V.G., B. Zaslow, and A.D. French, *The structure of V amylose dehydrate: A combined X-ray and stereochemical approach.* Biopolymers, 1975. **14**(7): p. 1487-1501.
168. Pushpadass, H.A. and M.A. Hanna, *Age-induced changes in the microstructure and selected properties of extruded starch films plasticized with glycerol and stearic acid.* Industrial & Engineering Chemistry Research, 2009. **48**(18): p. 8457-8463.
169. Cheetham, N.W.H. and L. Tao, *Variation in crystalline type with amylose content in maize starch granules: an X-ray powder diffraction study.* Carbohydrate polymers, 1998. **36**(4): p. 277-284.
170. Li, Y., et al., *Isothermal and nonisothermal crystallization kinetics of partially melting nylon 10 12.* Journal of Applied Polymer Science, 2003. **88**(5): p. 1311-1319.
171. Pikus, S., *Small-Angle X-Ray Scattering (SAXS) Studies of the Structure of Starch and Starch Products.* Fibres & Textiles In Eastern Europe 2005. **13**(53): p. 82-86.
172. Vodovotz, Y. and P. Chinachoti, *Glassy- Rubbery Transition and Recrystallization during Aging of Wheat Starch Gels.* Journal of Agricultural and Food Chemistry, 1998. **46**(2): p. 446-453.
173. Farhat, I.A., J.M.V. Blanshard, and J.R. Mitchell, *The retrogradation of waxy maize starch extrudates: Effects of storage temperature and water content.* Biopolymers, 2000. **53**(5): p. 411-422.
174. Hoover, R., *Starch retrogradation.* Food Reviews International, 1995. **11**(2): p. 331-346.
175. Rinnert, E., et al., *Hydration of a synthetic clay with tetrahedral charges: a multidisciplinary experimental and numerical study.* The Journal of Physical Chemistry B, 2005. **109**(49): p. 23745-23759.
176. Shamai, K., E. Shimoni, and H. Bianco-Peled, *Small angle X-ray scattering of resistant starch type III.* Biomacromolecules, 2004. **5**(1): p. 219-223.
177. Cleven, R., C. Van den Berg, and L. Van Der Plas, *Crystal structure of hydrated potato starch.* Starch/Stärke, 1978. **30**(7): p. 223-228.
178. Schiraldi, A., L. Piazza, and M. Riva, *Bread staling: a calorimetric approach.* Cereal Chemistry, 1996. **73**(1): p. 32-39.
179. Misra, R.D.K., et al., *Hierarchical structures and phase nucleation and growth during pressure-induced crystallization of polypropylene containing dispersion of nanoclay: The impact on physical and mechanical properties.* Materials Science and Engineering: A, 2010. **527**(9): p. 2163-2181.
180. Yuan, Q., et al., *Nanoparticle Interface Driven Microstructural Evolution and Crystalline Phases of Polypropylene: The Effect of Nanoclay Content on Structure and Physical Properties.* Materials Science and Engineering: A, 2010. **527**(21-22): p. 6002-6011.
181. Kitaigorodsky, A.I., *Molecular Crystals and Molecules: Physical Chemistry* 1973: Academic Press.
182. Chaudhary, D., *Competitive plasticization in ternary plasticized starch biopolymer system.* Journal of Applied Polymer Science, 2010. **118**(1): p. 486-495.
183. Ozawa, T., *Kinetics of non-isothermal crystallization.* Polymer, 1971. **12**(3): p. 150-158.

184. Dangaran, K. and J. Krochta, *Kinetics of sucrose crystallization in whey protein films.* Journal of Agricultural and Food Chemistry, 2006. **54**(19): p. 7152-7158.
185. Levitt, M., *Detailed molecular model for transfer ribonucleic acid.* Nature, 1969. **224**(5221): p. 759-763.
186. Berendsen, H.J.C., et al., *Molecular dynamics with coupling to an external bath.* The Journal of Chemical Physics, 1984. **81**(8): p. 3684-3690.
187. Rosenbluth, M.N. and A.W. Rosenbluth, *Monte Carlo calculation of the average extension of molecular chains.* Journal of Chemical Physics, 1955. **23**(2): p. 356-362.
188. Ding, H.Q., N. Karasawa, and W.A. Goddard Iii, *Atomic level simulations on a million particles: The cell multipole method for Coulomb and London nonbond interactions.* The Journal of Chemical Physics, 1992. **97**(6): p. 4309-4316.
189. Metatla, N. and A. Soldera, *Computation of densities, bulk moduli and glass transition temperatures of vinylic polymers from atomistic simulation.* Molecular Simulation, 2006. **32**(14): p. 1187-1193.
190. Hofmann, D., et al., *Molecular modelling of amorphous membrane polymers.* Polymer, 1997. **38**(25): p. 6145-6155.
191. Hofmann, D., et al., *Molecular simulation of small molecule diffusion and solution in dense amorphous polysiloxanes and polyimides.* Computational and Theoretical Polymer Science, 2000. **10**(5): p. 419-436.
192. Hofmann, D., et al., *Detailed-atomistic molecular modeling of small molecule diffusion and solution processes in polymeric membrane materials.* Macromolecular Theory and Simulations, 2000. **9**(6): p. 293-327.
193. Dudowicz, J., K.F. Freed, and J.F. Douglas, *The glass transition temperature of polymer melts.* Journal of Physical Chemistry B-Condensed Phase, 2005. **109**(45): p. 21285-21292.
194. Bennemann, C., W. Paul, and K. Binder, *Molecular-dynamics simulations of the thermal glass transition in polymer melts: α-relaxation behavior.* Physical Review E, 1998. **57**(1): p. 843-851.
195. Fried, J.R. and P. Ren, *Molecular simulation of the glass transition of polyphosphazenes.* Computational and Theoretical Polymer Science, 1999. **9**(2): p. 111-116.
196. Hopfinger, A.J., et al., *Molecular modeling of polymers. IV. Estimation of glass transition temperatures This is the fourth paper from an on-going series of investigations dealing with the applications of computational chemistry to predict properties of polymers.* Journal of Polymer Science Part B: Polymer Physics, 1988. **26**(10): p. 2007-2028.
197. Paul, W., *Molecular dynamics simulations of the glass transition in polymer melts.* Polymer, 2004. **45**(11): p. 3901-3905.
198. Rigby, D. and R.J. Roe, *Molecular dynamics simulation of polymer liquid and glass. I. Glass transition.* The Journal of Chemical Physics, 1987. **87**(12): p. 7285.
199. Prathab, B. and T.M. Aminabhavi, *Molecular modeling study on surface, thermal, mechanical and gas diffusion properties of chitosan.* Journal of Polymer Science Part B: Polymer Physics, 2007. **45**(11): p. 1260-1270.
200. Orford, P.D., et al., *Effect of water as a diluent on the glass transition behaviour of malto-oligosaccharides, amylose and amylopectin.* International journal of biological macromolecules, 1989. **11**(2): p. 91-96.

201. Liu, H., et al., *Interactions of hydrophilic plasticizer molecules with amorphous starch biopolymer- an investigation into the glass transition and the water activity behaviour*. Journal of Polymer Science Part B: Polymer Physics, 2011. **In press**.

Every reasonable effort has been made to acknowledge the owners of copyright material. I would be pleased to hear from any copyright owner who has been omitted or incorrectly acknowledged.

APPENDIX

1. Molecular Dynamic Modelling in amylose/(glycerol)/water system

This is an attempt to investigate the interactions in amylose/water (at different hydration) and amylose/water/glycerol (at different glycerol concentration) system via Molecular modelling. Molecular dynamics (MD) simulations had been employed in this computational work with a three dimensional periodic condense phase. The equilibrium structure which showed good similarity to the amylose polymer in terms of density value, (1.33g/cm^3 from calculation and 1.4g/cm^3 from experiments) had been built. The built atomic amylose fragments was further applied in the calculation of glass-transition temperature (T_g) temperature from MD simulation (NPT ensemble), by analysis the specific volume as a function of temperature. Both the density and the estimated T_g values were agreed with experimental data. The value of T_g for amylose fragment from different input density was 168-174 ^{o}C which was good agree with the average values of experimental data for dry starch (181 ^{o}C), this indicated the simulations protocol developed in the present work was able to generate accurate results for amylose fragments simulations. Results for estimation of T_g from hydrated amylose fragment and glycerol -plasticized system had been presented. The work presented in this section was only tip of the iceberg for the entire interactions in starch/MMT/plasticizer system. Even so, the exciting results reported here would point out a new route for understanding the fundamental map of the starch-based nanocomposite in the future.

Key words: molecular dynamics, amylose fragments, glass transition temperature, free volume.

2. Molecular structure of amylose, glycerol and water

Amylose is an essential linear section of the starch molecule consisting of alpha 1-4 linked glucose units, Figure 1. The amylose fragment, water and glycerol molecules used were obtained from Cambridge Crystallographic Data Centre (CCDC) without any further modification.

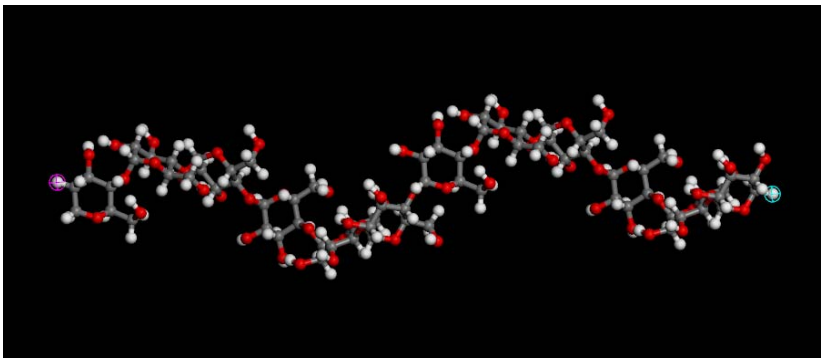

Figure 1 structure of amylose modified from Cambridge structural database (This model shows 36 glucose units, forming a single helical structure. Colours: carbon atoms are grey, hydrogen-white, and oxygen-red)

3. Simulation method

Simulation of amylose fragments was performed via the Materials Studio 4.4 software from Accelrys, San, Diego, on a Core2-based PC. Amorphous cell and Discover modules were used to build amylose cell and implemented the MD calculation by employing COMPASS (condensed-phased optimized molecular potentials for atomistic simulation studied) forcefield. Steepest descent approach followed by the conjugate gradient method with a convergence level of 0.01 kcal/mol/A has been applied in the minimization step [185]. Berendsen temperature fluctuations control method [186] had been employed in all calculation stages, same as pressure control. Considering the accuracy of simulation atom-based cut-off was used although it is such as computationally expensive.

i. Amorphous cell built

The system construction method used within Amorphous Cell incorporates an algorithm developed by Theodorou and Suter and the Meirovitch's scanning method which based on Rosenbluth and Rosenbluth’s publication. A single chain was packed into a cubic cell with the periodic boundary conditions. The edge length of the cubic cell was determined based on the input density of the polymer; an experimental bulk

amylose density, 1.3g/cm^3 and assumed density 0.58g/cm^3 was used here to ensure the equilibrium protocols employed was accurate enough to generate a correct equilibrium density between built cell and bulk polymer properties. With PBC, a molecular system had been built had the same density as that of the real system and then repeated in the space, in such way the real system can be correctly simulated by a molecular model with fewer atoms, a representative amorphous cell of amylose is shown in Figure 2 [187].

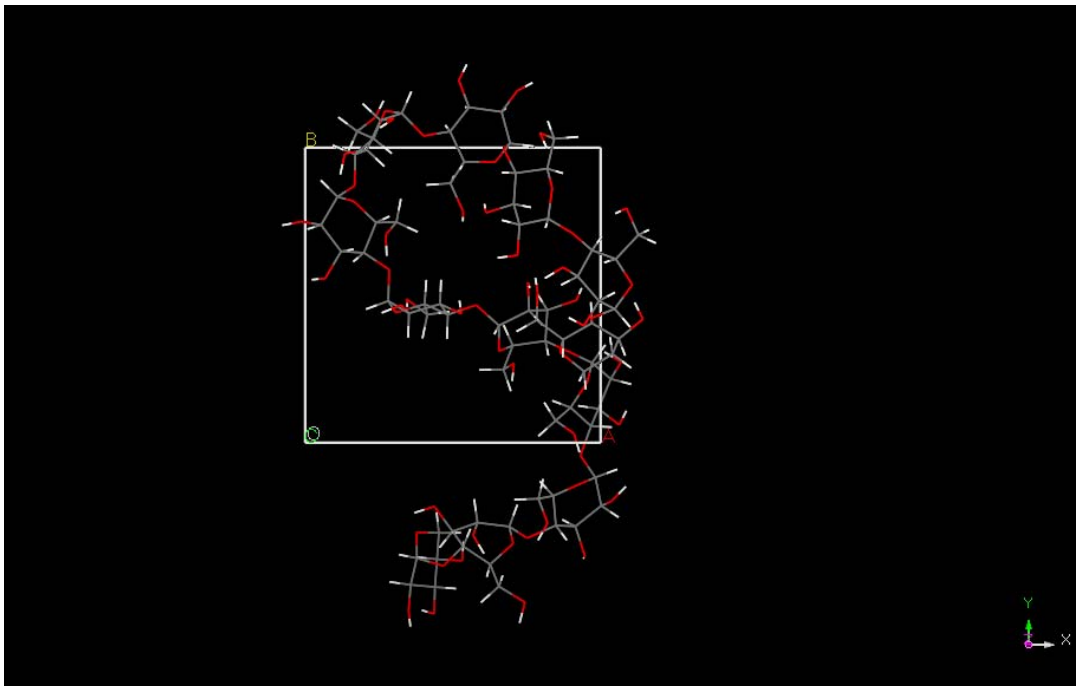

Figure 2. Amorphous model of amylose (this amorphous cell showed a single chain with 12 monomers packing in a cubic cell. Colours: carbon atoms are grey, hydrogen-white, and oxygen-red)

The amorphous cell for hydrated/plasticized amylose system was built via adding corresponding number of water/glycerol molecules to the amylose fragment system, Table1. Determination of molecular number of water/glycerol was based on the experimental data from our previous work.

Table 1 amorphous cell glass-transition temperature (T_g) simulation schedule

T_g simulation						
	Hydrated cell				Plasticized cell	
	0%	5.4%	8.35%	11.3%	GHA5	GHA15
Amylose monomers	12	12	12	12	12	10
Water	0	6	10	14	5	4
glycerol	–	–	–	–	1	3

ii. Relaxation of the amorphous cell

As reading from the output file of the amorphous cell construction job, the initial potential energy is very huge attributed to the non-bond interactions between the atoms of the fragment chain. Therefore, appropriate relaxation protocol required for the initial generated structure. Electrostatic interactions were explicitly considered by the charge-equilibrium method of Rappe and Goddard [188], Berendsen method was used for temperature and pressure control. An annealing-like relaxation procedure was applied on this stage, Table 2.

Table 2 Amorphous cell relaxation sheet

	Heating									Cooling	
Protocol	Tem	50K	100K	150K	200K	250K	300K	350K	400K	350K	300K
A	time	50ps at each temperature									
B	time	100ps at each temperature									

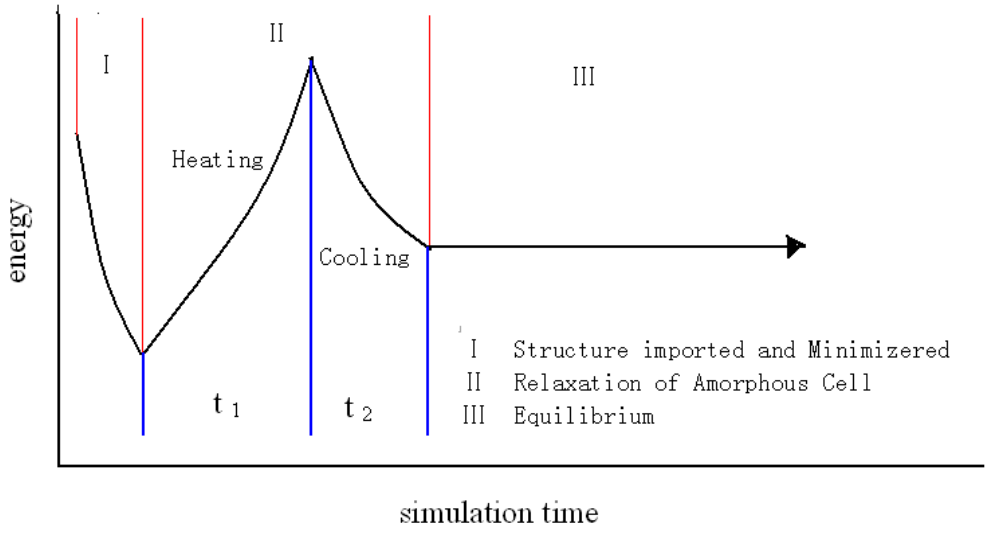

Figure 2 amorphous cell relaxation schematic

1. 5000 steps Minimization with steepest descent approach followed by the conjugate gradient method with a convergence level of 0.01 kcal/mol/Å.
2. Annealing-like strategy was applied; the whole process was carried out at an interval of each 50 K simulated for 50ps/100ps in both heating and cooling stages. Maximum temperature was fixed at 400K, amorphous cell with 12, 24 and 36 glucose monomers were calculated separately.
3. Final equilibrate running with NPT ensemble of 5 ns at 300K with the snapshots of density being save every 0.1 ps.

The final energy of minimized amorphous was used in all characteristic calculations as presented below.

iii. Equilibrium Density calculation

Since the relaxation time for MD simulation is relative lower comparing to polymer relaxing times, the proposed procedure to get optimized configurations could not be ascertained [189]. Accordingly, generation of the initial configurations is of the major importance since they determined the final properties. It had been pointed out that by Hoffmann *et al.* an extensive equilibrium procedure based on the serious of MD simulation by using Amorphous cell codes can exhibit an excellent agreement with experimental density, however, the biggest backward is the CPU time demanding [190-192]. Another approach put forward by Metatla and Soldera is consisting of a simulated annealing process followed by a uniform hydrostatic compression procedure [189]. The latter method will be used in present work.

Amorphous cell are constructed following the method described in the Amorphous buildt section followed by relaxation (Page 183). Density calculations will be carried for the cell from both protocol A and B, Table 2. Density *vs* simulation time plot were recorded for the whole simulation duration. The results discussion will be mainly based on the outcome from single chain simulation single together with one twin chain calculation as a comparison.

iv. Thermal properties

Glass-transition temperature *(T_g)* is one of the most important and basic properties of polymer whose magnitude directly related to the physical of bulk polymers and its thermal properties [193]. Understanding the nature of the glass transition is a challenge problem of materials science and physics. Plenty of experimental techniques are developed for this issue. Meanwhile, several researchers had successfully simulated the T_g of some polymers by the specific volume at constant pressure versus the temperature variation. This can be considered as an essential ingredient in the extension of the Lindemann criterion to the 'softening transformation' in glass-forming liquids, generated by MD simulations [193-198]. Same theory is used for calculation of T_g values of amylose fragments by MD simulation.

NPT ensemble is employed in the specific volume calculation with the software package named DISCOVER from Materials Studio, this method had been investigated earlier by Fried and Ren who elucidated that NPT ensemble simulation is valid for estimation of specific volume [195]. Atom –based cut off at 9.5 Å and tailed correction had been applied for all the bonds and non-bond interactions, respectively [199]. Amorphous cells are simulated at series of temperatures (50K-550K) above or below the T_g, after equilibrium completed. Once the density reached equilibrium, the production simulation duration was determined as the time for corresponding cell achieving equilibrium. T_g can be obtained from the plot of specific volume and temperature.

8.2.1.1 Results and discussions

v. Cell relaxation and equilibrium

Equilibrium state of the amorphous is considered as the density of the system reach a plateau value. Initially 5ns production time is applied for all density simulation. The density calculation results were shown in Figure 3.

It can be read from the density calculation result that, all the models established exhibited a density value within 1.28 g/cm^3~1.35 g/cm^3 regardless how many monomers included, which have a good agreement with the experimental data of amylose's theoretical density valued at 1.34 g/cm^3 . It can be deduced, from a physical view, that the amorphous cell built provided an accurate presentation of amylose/Maltodextrin biopolymer. Furthermore, model constructed from 12 monomers with type A relaxing protocol possessed the most similar density value when comparing to the other modes.

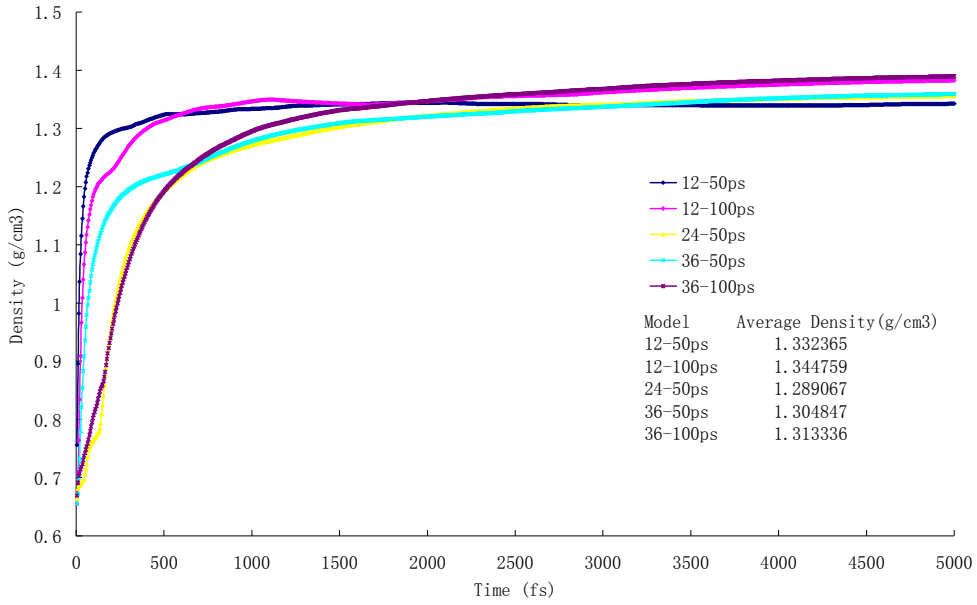

Figure 3 density calculation results for amorphous cell with different numbers of glucose monomer

Equilibrium time for each system increased as the number of monomers increasing due to the number of atoms involved in the simulation. From a modelling point, on the basis of all the models built, simulation time will be another factor should be taken into consideration, the quicker the better. Obviously, the model with 12 monomers subjected to relaxation A protocol with 50ps at each temperature was the best candidate since shortest time required for the cell to reach equilibrium with a accurate density value (1.332365 g/cm^3), Figure 3.

vi. Glass transition temperature (T_g)

Pure amylose fragment

It had been generally accepted that the T_g can be associated with the accompanying slow decrease in free volume and hence in specific volume (inverse of density), which is a direct symbol for polymer chain mobility and interactions within the system. The T_g value was determined from the specific volume versus the simulation temperature, this approach was proposed by Rigby and Roe [198], and had been applied in other work [199].

With the consideration of different hydration scenario, full simulation sheet and simulation results can be read from Table 3. NPT ensembles had been performed at different temperatures. The equilibrium time for the specific volume calculation is determined according to the simulation temperature as the equilibrium rate for

different systems is various depending on the simulation temperature, 1~2 ns production time at each temperature was followed after the equilibrium.

Table 3 Simulation density for different scenario and T_g estimation

	Hydrated amylose fragments				Glycerol-Plasticized	
T (K)	anhydrous	5.4%	8.35%	11.3%	5%	15%
200	1.4154	1.4222	1.4095	1.4039	1.2987	1.3635
225	1.4078		1.4712	1.4036	1.2703	1.3764
250	1.4150	1.4463	1.4896	1.3424	1.3313	1.4025
275	1.413		1.4923	1.3439	1.3603	1.3851
300	1.3976	1.4283	1.478	1.3305	1.3635	1.3753
325	1.3934	1.4327	1.4136	1.2234	1.3526	1.3608
350	1.3868	1.4289	1.3818	1.2304	1.3686	1.3064
375	1.3818	1.4489	1.2834	1.1314	1.3641	1.286
400	1.3755	1.4465	1.1524	0.8654	1.3178	1.265
425	1.3796	1.4214			1.282	
450	1.3638	1.4293			1.1987	
475	1.3513	1.424				
500	1.3564	1.4068				
525	1.351	1.3853				
550	1.3303					

The specific volume was obtained by reciprocal of density which was calculated by the equilibrium amorphous cell with 4ns NPT ensemble via Discover Dynamics. Linear regression method was applied in the fitting of simulated data, the T_g value of each condition was read from the cross point of the fitting curve. The volume-temperature *(V-T)* curve obtained for amylose/Maltodextrin is shown in Figure 4.

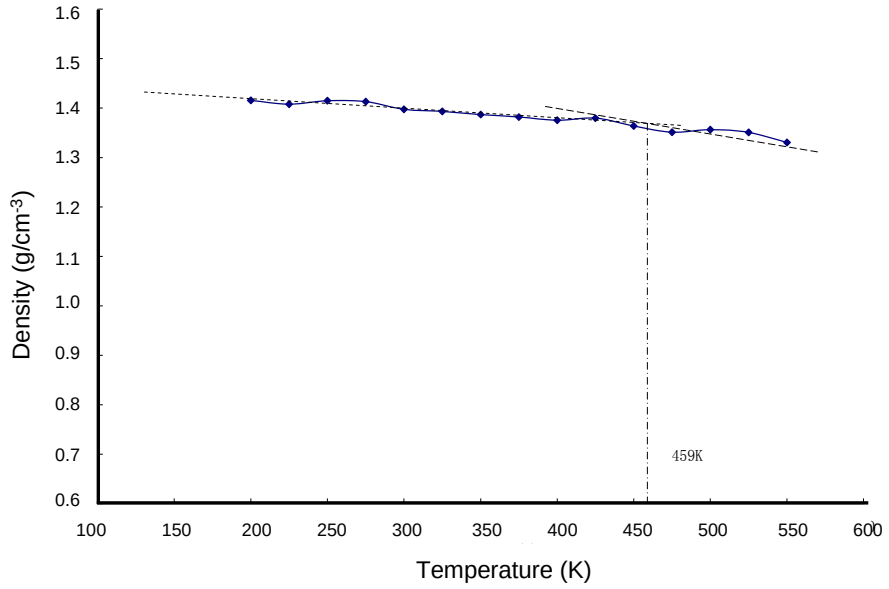

Figure 4 Specific volume vs the simulation temperature for pure amylose fragment

The plot can be divided into two stages according to different status of the cell. The first stage, 200K-300K, was the equilibrium process. The simulated amorphous cell reached its equilibrium and a right density that agreed with the experimental data was obtained. After that the amorphous cell began to behaviour like a real polymer. With different input density the equilibrium process which upto 300K showed different density tendency. When the input density was lower than theoretical value, the batch density increased upon the temperature (Figure 4). While the temperature increased to 300K (27°C) the generally experimental temperature, correct density obtained from the simulation result. We can read from the plot that obviously glass transmission phenomenon had been observed as the density kept nearly constant (the linear regression fitting line in dash line), although bit of fluctuation occurred and then decreasing gradually after certain temperature , that's where is the glass transmission temperature, 459K (186 °C) in this work, figure 4. This is generally agree with experimental values, where the experimental data for dry starch had been estimated with the value of 440K (167 °C) [200] .

Further simulation on the amylose fragments at different hydration degree had been carried out with the aim to built a accurate model for the predicition of T_g for amylose-based systems. Same method had been appiled in all calculations.

Hydrated amylose fragment

In order to have a better validation of the simulation results, amorphous cells at different hydration degree according to the experimental works, 5.4 %, 8.35% and 11.3%, were simulated. Same protocol had been employed and the simulation results were shown in Figure 5 (a) -(c).

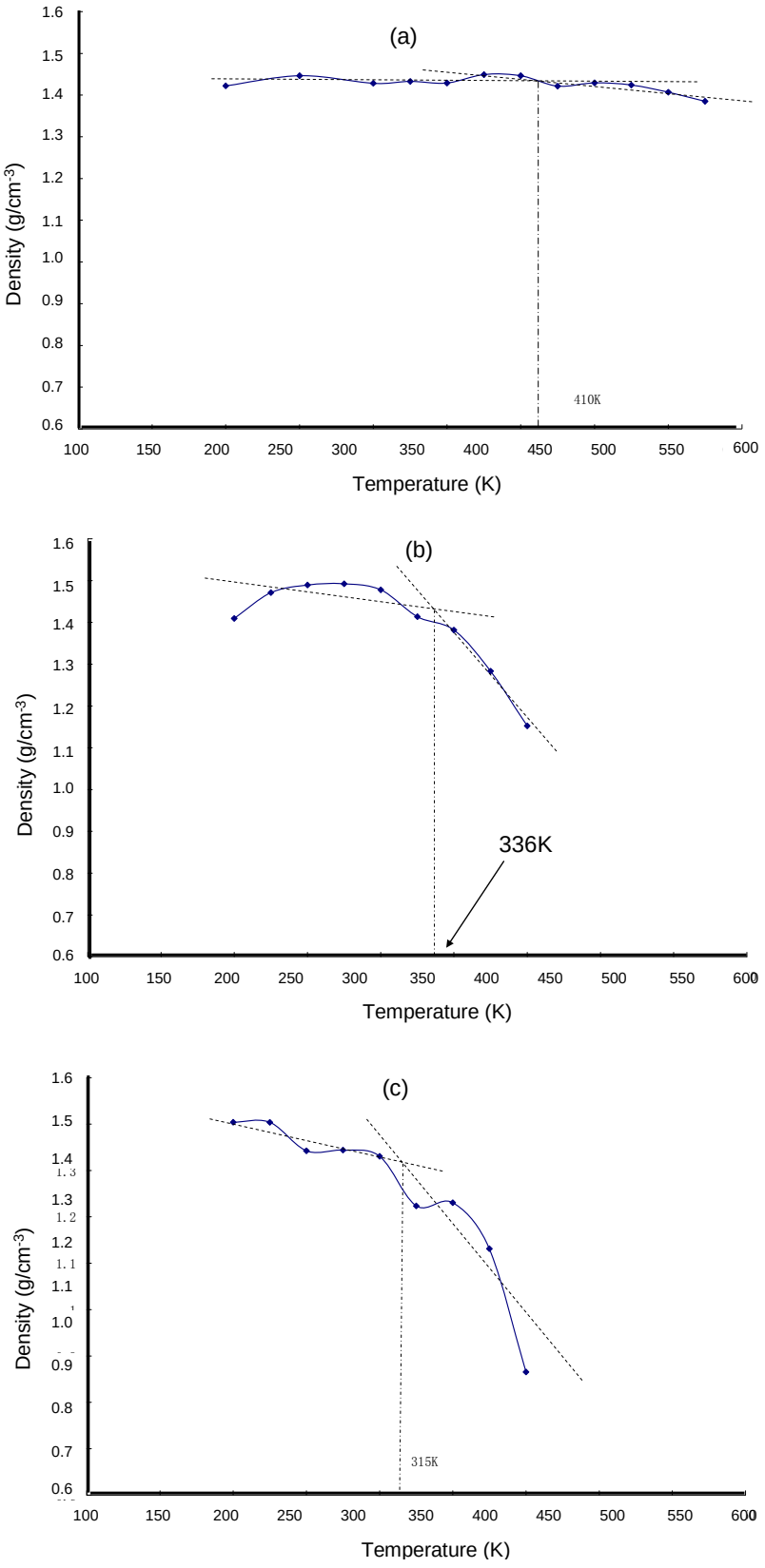

Figure 5 T_g estimation results for hydration amylose fragment (a) 5.4% hydration (b)8.35% hydration (c)11.3% hydration

The T_g of anhydrous amylose cannot be determined experimentally due to the thermal decomposition of starch; maltodextrin had been chosen as a reference for the evaluation of the simulation results. As observed from the simulation results, Figure 5, the T_g was greatly influenced by the moisture content within the system. In other words, the interactions between amylose chain and water molecules were differ from others depending on the amount of water presented. When comparing the plot from 5.4% hydration system and that from 11.3% hydration system, the dramatic increase in free volume in the latter system manifestly indicated a stronger amylose polymer/water interactions occurrence. On the other hand, the 'plateau'-like V-T plot of anhydrous amylose fragment and 5.4% hydration condition could be a straight indication of the firmly coalesces morphology of amylose fragment molecules.

Obviously the T_g decreased as the water concentration increased due to the plasticization effect. Furthermore, it could be noticed from the comparison of simulation data with experimental works, the simulation T_g were generally agree with the experimental data excepted 5.4% hydration model, this was consistent with the investigation from Frank *et al.* [200].

Table 4 Simulated and experimenta values of the T_g values at different hydration levels

	anhyderous	5.4%	8.35%	11.3%	5%	15%
$T_{g\ S}$	186	137	63	42	79.5	67
$T_{g\ E}$	167[200],200[200]	87[200]	52[200]	39.5[200],41[200]	69.5	62
$T_{g\ SR}$	204[200]	113[200]	64[200]	39[200]		

$T_{g\ S}$: T_g value from present simulation
$T_{g\ E}$: T_g from experiment data
$T_{g\ SR}$: T_g value from reference MD simulation work

Another observation that provided important clue for understanding the interactions in amylose/water system was the density tendency from different hydration level. As shown in table 2, density value simulated from low water concentration cells (anhydrous or 5.4%) possessed an overall higher value of density comparing to 11.3% cell. This phenomenon could be explained from the well-known antiplasticization effect of low amount plasticizer. The limit amount of water molecules could strongly interact with the amylose polymer, thus the water

molecules occupied the free space between/among amylose fragments which led to a tighter polymeric network within the system.

8.2.1.2 Glycerol-plasticized amylose fragment

T_g value from simulations, Table 3, turned out to be higher than the LA experimental data which agree with the conclusion from Bizot *et al.* that linear chains appeared to favour chain-chain interactions and branched molecules displayed a lower T_g value due to chain end effects, as well as flexibility of branching points [200]. This indicating that the present protocol for T_g values calculation can be applied to starch/plasticizer/water ternary system without losing much accuracy.

The *V-T* plots for the glycerol-plasticized systems are shown in Figure 5. Within expectation, the T_g value decreased upon the increasing of glycerol content. Similarly, the non-'plateau'-like plot indicated the complicated interactions that occurred within the system. The simple conclusions drawn from starch/water binary system that 'antiplasticization' led to a higher cell density and 'plateau'-like plot shape cannot straight applied in the glycerol-plasticized scenario since the competing plasticization effect from both glycerol and water [201]. The combined effect of antiplasticization and completing plasticization from glycerol and water might be the cause for density decrease in 5% glycerol/amylose/water condition. However, such hypothesis was still crudeness and required more future validation.

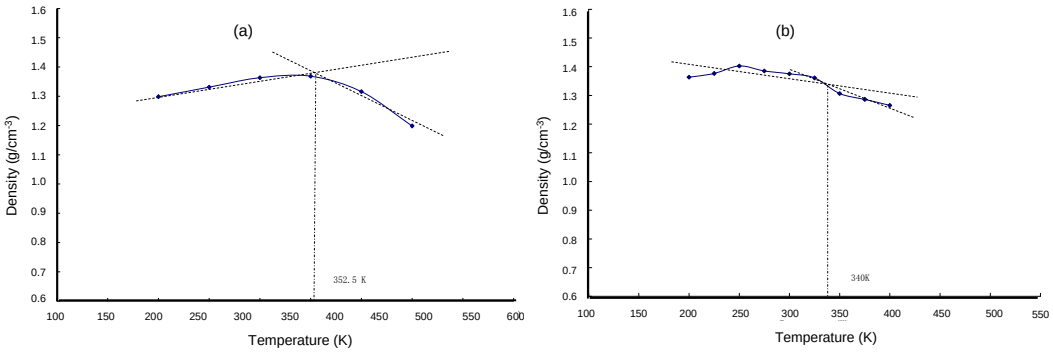

Figure 5 T_g estimation results for glycerol-plasticized amylose fragment (a)5% glycerol (b)15% glycerol

8.2.1.3 Conclusion

An atomic model of amylose fragments had been successfully built in the present work with COMPASS forcefield. The density results from the 12 monomers amorphous cell subjecting for 5ns equilibrium simulation, 1.33 g/cm^2, exhibited

excellence agreement with the theoretical density value for the amylose polymer. The protocol for T_g calculation developed was confirmed to be able to predict an accurate T_g for hydrated amylose system. Overall equilibrium densities for the cells at low hydration degree were higher than that of high hydration degree cells. This was interpreted to be attributing to the strong water-amylose interaction that decreased the free volume and tightening the polymeric network within the amylose chain when the hydration degree was relative low. The estimated T_g for amylose fragment at different hydration level was agreed with the experimental data except 5.4% model. Quality conclusion was putting forward to the glycerol-plasticized system that the decrease of T_g was proposal to the concentration of glycerol and moisture content. Antiplasticization phenomenon was correlated to the overall high density value from the low hydration systems based on the fact that stronger amylose-plasticizer (antiplasticization) would result in a higher packing density (from the entangled amylose and plasticizers) within the simulation cell.